

Donor-acceptor polymers for organic solar cells

Dissertation

Von der Universität Bayreuth
zur Erlangung des Grades eines
Doktors der Naturwissenschaften (Dr. rer. nat.)
genehmigte Abhandlung

von

Christina Saller

geboren in Tirschenreuth

1. Gutachter: Prof. Dr. Peter Strohrriegl

2. Gutachterin: Prof. Dr. Anna Köhler

Tag der Einreichung: 27.06.2018

Tag des Kolloquiums: 16.10.2018

Die vorliegende Arbeit wurde in der Zeit vom Juli 2013 bis Juni 2018 am Lehrstuhl für Makromolekulare Chemie I der Universität Bayreuth unter der Betreuung von Prof. Dr. Peter Strohriegl angefertigt.

Amtierender Direktor der Graduiertenschule: Prof. Dr. Dirk Schüler

Datum der Einreichung der Dissertation: 27.06.2018

Datum des wissenschaftlichen Kolloquiums: 16.10.2018

Prüfungsausschuss:

Erster Gutachter: Prof. Dr. Peter Strohriegl

Zweite Gutachterin: Prof. Dr. Anna Köhler

Drittprüfer: Prof. Dr. Carlo Unverzagt

Vorsitzender: Prof. Dr. Markus Retsch

Für meine Familie

*„Alles ist möglich, vorausgesetzt,
dass es genügend unvernünftig ist.“*

Niels Bohr

Table of contents

1. Summary	1
Zusammenfassung	3
2. Introduction	5
2.1 Solar energy conversion	5
2.2 Operating mode of organic solar cells	9
2.3 Solar cell characteristics	10
2.4 Geometries of organic solar cells	13
2.4.1 FHJ solar cells	14
2.4.2 BHJ solar cells	17
2.4.3 Mixed FHJ-BHJ solar cells	20
2.4.4 Tandem solar cells	22
2.5 Design strategies for conjugated polymers as electron donor materials	26
2.6 General synthetic strategies for conjugated polymers	31
2.7 Polycarbazoles as materials for organic solar cells	32
2.8 Polycyclopentadithiophenes as materials for organic solar cells	36
2.9 Stabilization of organic solar cells via crosslinking	40
2.10 Triarylamine as hole conducting comonomers	50
References	51
3. Objective of the thesis	62
4. Overview of the thesis	65
4.1 Crosslinkable low bandgap polymers	69
4.1.1 Organic solar cells with crosslinked polymeric exciton blocking layer	69
4.1.2 Optimized synthetic procedures for PCDTBT and PCPDTBT	73
4.2 Low bandgap copolymers	79
4.2.1 Role of intrinsic photogeneration in single layer and bilayer solar cells with C ₆₀ and PCBM	81
4.2.2 Monomolecular and bimolecular recombination of electron–hole pairs at the interface of a bilayer organic solar cell	84
4.2.3 A facile method for the investigation of temperature-dependant C ₆₀ diffusion in conjugated polymers	87
4.3 Individual contributions to joint publications	94
5. Organic solar cells with crosslinked polymeric exciton blocking layer	98
6. Role of intrinsic photogeneration in single layer and bilayer solar cells with C ₆₀ and PCBM	108
7. Monomolecular and bimolecular recombination of electron–hole pairs at the interface of a bilayer organic solar cell	124
8. Facile method for the investigation of temperature-dependant C ₆₀ diffusion in conjugated polymers	141
Appendix A: Optimized synthetic procedures for PCDTBTOx and PCPDTBTOx	171
Appendix B: Patternable conjugated polymers for organic solar cells	184
Appendix C: Crosslinkable low bandgap polymers for organic solar cells	195
Appendix D: Crosslinked semiconductor polymers for photovoltaic applications	207
List of publications	218
Danksagung	220
Erklärung	222

1. Summary

Photovoltaics present an interesting option for the energy production using renewable sources. As the sun provides inexhaustible amounts of energy, the global energy consumption could in principle be covered by electricity from solar cells. Organic solar cells present a promising alternative to inorganic devices, although the lower efficiencies and the lack of long-term stability hinder the commercialization so far. In bulk heterojunction solar cells, the efficiency decrease arises from the diffusion of small molecule acceptors. Furthermore, the deposition of a second material on top of a first layer leads to the damage of underlying layers in multilayer devices as well as the dissolution of nanostructured morphologies. For an efficient improvement of organic solar cells, the device degradation has to be extensively studied and strategies for the fabrication of long-term stable devices have to be deduced. Crosslinking is a versatile option to achieve increased stability. The diffusion of small acceptor molecules in bulk heterojunction solar cells can be limited by deploying a crosslinked donor polymer matrix. The insolubility of a crosslinked polymer layer or interface structure allows the deposition of a second layer on top without damage of the underlying device. In addition, the understanding and improvement of organic photovoltaic devices require extensive studies on both charge carrier generation and recombination processes at the donor-acceptor interface of the active layer.

This thesis deals with the modification of the well-established low bandgap polymers PCDTBT and PCPDTBT that are applied as donor materials in organic planar heterojunction solar cells. By this means, contributions to both optimized device fabrication as well as basic investigations were achieved. The synthetic modifications are classified into two parts. On the one hand, PCDTBT and PCPDTBT derivatives bearing crosslinkable units at the side chains of the donor monomers were realized. Oxetane was selected as the crosslinkable group because of its compatibility with the Suzuki coupling reaction and the possibility to initiate the crosslinking reaction by acid vapour. On the other hand, the polymer backbone of PCDTBT was modified with triphenyldiamine moieties exhibiting good hole transport properties. Furthermore, the attachment of aliphatic spacers to the acceptor moiety received a series of copolymers exhibiting different characteristics.

Besides the chemical, thermal, optical and electronic characterisation of the synthesized polymers, the modifications of the polymers were evaluated. This included studies about the polymer properties in dependence of the crosslinking process and conditions as well as investigations about the variation of the polymer characteristics due to the incorporation of the additional donor monomer and the aliphatic sidechains at the acceptor units.

One part of this thesis deals with a first three-layer device realized by solution processing due to the application of a crosslinked and insoluble polymer interlayer that allows the spin coating of the donor polymer on top. An increased external quantum efficiency as well as a higher efficiency of 1.8% compared to the bilayer reference cells with 1.6% efficiency were achieved with the three-layer cell due to the exciton blocking effect of the interlayer.

1. Summary

The low bandgap copolymer series realized by the incorporation of an additional comonomer and aliphatic spacers in the PCDTBT structure was used to conduct fundamental investigations. The PCDTBT modified with triphenyldiamine moieties was chosen for the evaluation of the intrinsic contribution of the acceptors C_{60} and PCBM to the overall photocurrent. EQE measurements of single layer cells in dependence of the excitation energy revealed that the delocalization of the excitons and thus the intrinsic dissociation of both acceptors was enhanced with increasing photon energy.

In a further study, the monomolecular and bimolecular recombination mechanisms in organic solar cells were addressed by the use of the PCDTBT-based donor polymer with triphenyldiamine units and aliphatic spacers at the acceptor monomer. Current-voltage characteristics showed that the fill factor decreased with increasing donor layer thickness at low light intensities due to geminate recombination. Higher light intensities induced non-geminate recombination that became higher for increasing layer thickness and was responsible for the further decreasing fill factor.

A further aspect of this work was the investigation of the diffusion behaviour of C_{60} through different polymers with and without additional triphenyldiamine unit and aliphatic sidechains using a novel bilayer setup. A crosslinked polyfluorene was used to verify the novel bilayer setup in comparison to previously used three-layer samples. Temperature dependent photoluminescence measurements showed that fullerene diffusion occurs already below the glass transition temperature because of the local motion of sidechains that allows the diffusion of the small molecule acceptor.

In conclusion, this work contributes to both fundamental research topics covering photogeneration and charge carrier recombination and device fabrication studies towards the optimization of organic solar cells with respect to long-term stability. Different donor polymers were thus synthesized with modifications to the basic polymer structures of PCDTBT and PCPDTBT like the introduction of the crosslinking ability or the incorporation of an additional comonomer and aliphatic spacers.

Zusammenfassung

Die Photovoltaik stellt eine interessante Möglichkeit für die Energieproduktion aus erneuerbaren Quellen dar. Da die Sonne unerschöpfliche Energiemengen liefert, könnte der weltweite Stromverbrauch prinzipiell mit Strom aus Solarzellen produziert werden. Organische Solarzellen stellen eine vielversprechende Alternative zu anorganischen Solarzellen dar, obwohl die geringeren Effizienzen und die mangelnde Langzeitstabilität bisher die Kommerzialisierung erschweren. In Bulk-Heterojunction-Solarzellen ist die Abnahme der Effizienz auf die Diffusion niedermolekularer Akzeptormoleküle zurückzuführen. Weiterhin führt bei Mehrschichtzellen das Aufbringen eines zweiten Materials auf eine erste Schicht zur Schädigung der darunterliegenden Schichten sowie zur Auflösung von nanostrukturierte Morphologien. Für eine effiziente Verbesserung von organischen Solarzellen muss die Degradation der Zelle intensiv untersucht und daraus Strategien für die Herstellung von langzeitstabilen Solarzellen abgeleitet werden. Vernetzung stellt eine vielfältige Möglichkeit dar, um eine erhöhte Stabilität zu erreichen. Die Diffusion von kleinen Akzeptormolekülen in Bulk-Heterojunction-Solarzellen kann eingeschränkt werden, wenn eine vernetzte Polymermatrix eingesetzt wird. Die Unlöslichkeit einer vernetzten Polymerschicht oder Grenzflächenstruktur erlaubt das Aufbringen einer zweiten Schicht ohne Schädigung des darunterliegenden Bauteils. Darüber hinaus erfordern das Verständnis und die Verbesserung von organischer Photovoltaik intensive Studien sowohl über die Ladungsträgergenerierung als auch über die Rekombinationsprozesse an der Donor-Akzeptor-Grenzfläche der aktiven Schicht.

Diese Arbeit beschäftigt sich mit der Modifikation der bekannten Low-Bandgap-Polymere PCDTBT und PCPDTBT, die als Donormaterialien in organischen Planar-Heterojunction-Solarzellen eingesetzt werden. Auf diese Weise konnten Beiträge zur Optimierung der Herstellung von Solarzellen als auch zu grundlegenden Forschungsthemen erzielt werden. Die synthetischen Modifikationen sind in zwei Teile gegliedert. Zum einen wurden Derivate von PCDTBT und PCPDTBT realisiert, die vernetzbare Einheiten an den Seitenketten der Donormonomere tragen. Oxetan wurde aufgrund seiner Kompatibilität mit der Suzuki-Kupplungsreaktion und der Möglichkeit, die Vernetzungsreaktion mittels Säuredampf zu initiieren, als vernetzbare Gruppe gewählt. Zum anderen wurde das Polymerrückgrad von PCDTBT mit Triphenylamineinheiten, welche gute Lochtransporteigenschaften aufweisen, modifiziert. Weiterhin stand durch die Anbringung von aliphatischen Seitenketten an die Akzeptoreinheit eine Serie von Copolymeren mit verschiedenen Eigenschaften zur Verfügung.

Neben der chemischen, thermischen, optischen und elektronischen Charakterisierung der synthetisierten Polymere wurden die Modifikationen der Polymere bewertet. Dies beinhaltete sowohl Studien über die Polymereigenschaften in Abhängigkeit vom Vernetzungsprozess und den Bedingungen als auch Untersuchungen über die Variation der Polymereigenschaften durch die Einarbeitung des zusätzlichen Donormonomers und der aliphatischen Seitenketten an den Akzeptoreinheiten.

Ein Teil dieser Arbeit beschäftigt sich mit einer ersten Dreischichtzelle, die mittels Lösungsprozessen realisiert wurde. Durch den Einsatz einer vernetzten und unlöslichen Polymerschicht konnte darauf das Donorpolymer aus Lösung aufgebracht werden. Durch den Excitonen-blockierenden Effekt der Zwischenschicht wurde mit den Dreischichtzellen im Vergleich zu den Zweischicht-Referenzzellen mit 1,6 % Effizienz eine erhöhte externe Quanteneffizienz sowie eine höhere Energieeffizienz von 1,8 % erreicht.

Die Serie von Low-Bandgap-Copolymeren, die durch das Einfügen eines zusätzlichen Comonomers und aliphatischer Seitenketten in die PCDTBT-Struktur realisiert wurde, wurde für grundlegende Untersuchungen verwendet. Das modifizierte PCDTBT mit Triphenylamineinheiten wurde für die Evaluierung der intrinsischen Beiträge der Akzeptoren C₆₀ und PCBM zum Gesamtphotostrom ausgesucht. EQE-Messungen der Einschichtzellen in Abhängigkeit von der Anregungsenergie zeigten, dass sich die Delokalisation der Excitonen und damit die intrinsische Dissoziation der beiden Akzeptoren mit steigender Photonenenergie erhöhte.

Eine weitere Studie befasste sich mit den monomolekularen und bimolekularen Rekombinationsmechanismen in organischen Solarzellen. Dafür wurde das PCDTBT-basierte Polymer mit Triphenylamineinheiten und aliphatischen Seitenketten am Akzeptormonomer eingesetzt. Strom-Spannungskennlinien zeigten, dass der Füllfaktor mit steigender Donorschichtdicke bei niedrigen Lichtintensitäten aufgrund geminaler Rekombination abnahm. Bei höheren Lichtintensitäten trat nicht-geminale Rekombination ein, die mit steigender Schichtdicke anstieg und für die weitere Abnahme des Füllfaktors verantwortlich war.

Ein weiterer Aspekt dieser Arbeit war die Untersuchung des Diffusionsverhaltens von C₆₀ in verschiedenen Polymeren mit und ohne zusätzliche Triphenyldiamineinheit und aliphatischen Seitenketten mit Hilfe eines neuen Zweischichtaufbaus. Ein vernetztes Polyfluoren wurde verwendet, um den neuen Zweischichtaufbau im Vergleich zu vorher eingesetzten Dreischichtproben zu verifizieren. Temperaturabhängige Photolumineszenzmessungen ergaben, dass die Fullerediffusion bereits unterhalb der Glasübergangstemperatur auftritt, da die lokale Bewegung der Seitenketten die Diffusion des niedermolekularen Akzeptors ermöglicht.

Zusammenfassend trägt diese Arbeit sowohl zu grundlegenden Forschungsthemen wie der Photogenerierung und Ladungsträgerrekombination als auch zu Studien über Solarzellenherstellung für die Optimierung von Solarzellen hinsichtlich der Langzeitstabilität bei. Dafür wurden verschiedene Donorpolymere synthetisiert, die Modifikationen der Grundstruktur der Polymere PCDTBT und PCPDTBT wie die Einführung der Vernetzungsfähigkeit oder das Einfügen eines zusätzlichen Comonomers und aliphatischer Seitenketten beinhalteten.

2. Introduction

The global energy demand will drastically rise in the coming years, leading to fundamental questions about the production of energy and the consequences related to the use of the energy sources.^[1] At this moment, the worldwide energy consumption is about 12 TW per year. Still over three quarters of the total energy production are supplied by non-renewable sources today whereas renewable energy sources only cover around 20%.^[2] One possibility for using a clean, sustainable, and renewable energy source is photovoltaics.^[3] Besides further natural resources like wind, hydropower, and geothermal energy, the sun possesses the potential to deliver the highest contribution to renewable energies because one hour of sunshine is sufficient to meet the global demand for energy for a whole year.^[4,4] Of course, not all of the solar energy can be converted. However, assuming that photovoltaic devices can be deployed on 2% of the land area and these devices have an efficiency of 12% to convert solar light to energy, 67 TW can be achieved. This is more than three times of the current worldwide energy consumption.^[1] Consequently, photovoltaics can meet the increasing global demand for low-cost, available and sustainable energy, which is of vital importance for the quality of life as well as for the evolution of global economy and the protection of the environment.^[3,4] Furthermore, using solar energy can help to reduce serious environmental problems like global warming due to high carbon dioxide emission. This is caused by the production and burning of fossil fuels such as coal, oil, and gas as they are still the most frequently used energy source of our time. Moreover, the availability of fossil fuels is limited in comparison to the unlimited solar energy. Photovoltaics is thus predestined for a promising, long-term solution of the energy problem.^[5-7]

2.1 Solar energy conversion

Solar technology is based on both solar heat and the direct conversion of sunlight in electricity by means of the photovoltaic effect.^[8] The first observation of this effect was made by A. E. Becquerel in 1839. When shining light on a silver chloride electrode in an electrolytic solution, a light induced voltage occurred.^[9] In 1883, C. E. Fritts built the first solar cell from selenium wafers exhibiting a power conversion efficiency (PCE) of about 1%.^[10] Modern semiconductor solar cells comprise a barrier formed by a junction between a p-type and a n-type material. R. S. Ohl received the patent for this geometry in 1946.^[11] An optimized silicon solar cell by D. M. Chapin, C. S. Fuller and G. L. Pearson from Bell Laboratories achieved an efficiency of around 6% in 1954.^[12] Silicon presents a suitable material for solar cells as it is one of the most abundant elements of the earth crust. In addition, silicon causes no environmental problems.^[13] Today, an efficiency of over 26% can be reached by monocrystalline silicon solar cells. This is realized by only using the back sides for contacting.^[14,15] As the production of monocrystalline silicon is expensive, polycrystalline silicon was investigated for the application in solar cells since the 1970s to reduce costs. Since polycrystalline silicon exhibits an increased charge carrier recombination due to grain boundaries and a higher contamination in comparison to

monocrystalline material, the efficiency of polycrystalline solar cells is lower than the PCE of monocrystalline cells.^[13] Thus, an efficiency of almost 22% is achieved for polycrystalline silicon solar cells.^[16] Both types of silicon solar cells represent the first generation of photovoltaics. A further approach towards the reduction of costs has been pursued with the second generation of solar cells.^[17] These comprise thin film devices with a low-cost and partially flexible substrate like glass, stainless steel, aluminium, or polymer foil onto which the semiconductor is deposited.^[5,18] In the case of silicon, amorphous material is frequently used.^[2] An efficiency of over 10% was confirmed for such solar cells.^[19] Besides silicon, also other semiconductors like copper indium diselenide (CIS) and copper indium gallium diselenide (CIGS) and cadmium telluride are applied.^[18] In 2016, the Centre for Solar Energy and Hydrogen Research Baden-Württemberg presented a CIGS thin film solar cell with an efficiency of 22.6%.^[20] A further interesting research aspect is the change of the geometry towards 3D solar cells that can enhance the efficiency by increasing the light absorption in the solar cell.^[21] First results were maintained covering carbon nanotubes with cadmium telluride.^[22]

Nevertheless, only a small part of the energy production is managed by photovoltaics up to now. This can be basically ascribed to the high costs of the production technologies that are needed for the silicon-based solar cells. The development of a third solar cell generation is thus stimulated. A potential alternative to silicon devices are organic solar cells (OSCs) made from organic materials that feature the possibility of solution processing. By this means, the application of lightweight, large-area, and flexible substrates is enabled.^[3,4,6,17,23] The first investigations concerning organic photovoltaics was made with the dye classes of porphyrins and phthalocyanines. These materials are easy to synthesize, form metal complexes and exhibit a strong colour as well as good semiconducting properties in crystalline films prepared by vacuum sublimation.^[24] In 1958, D. Kearns and M. Calvin observed a photovoltage of 200 mV when measuring magnesium phthalocyanine between two glass electrodes.^[25] G. M. Delacote noticed a rectification effect of copper phthalocyanine between different metals.^[26] Furthermore, also dyes such as methylene blue and photosynthetic pigments like carotenes and chlorophylls were used for the fabrication of simple solar cells. However, the PCE of those cells containing only one dye remained below a value of 0.1%.^[24,27] Besides dyes and small organic molecules, also functional semiconducting polymers are applied in organic photovoltaics.^[3,28–30] These conjugated polymers combine the optoelectronic properties of semiconductors and the mechanical properties of polymers, including the advantages with respect to the processing.^[31] The electron delocalization within these polymers is responsible for the good stability, high charge carrier mobility, and strong absorption and emission, respectively, in the UV-Vis range. The ability to transport different charge carriers is realized by doping, that is a partial oxidation or reduction of the otherwise isolating polymers.^[32] In addition, the solubility and the melting behaviour can be positively influenced by the insertion of relatively long and flexible side chains.^[33] The first organic molecule in which photoconductivity was noticed by A. Pochettino^[34] and M. Volmer^[35] was anthracene.

In 1977, electrical conductivity was detected for the first time in doped polyacetylene. A. J. Heeger, A. G. MacDiarmid and H. Shirakawa were awarded the Nobel prize in chemistry for this discovery in the year 2000.^[28,36] In 1982, polyacetylene was applied as active material in a solar cell with aluminium and graphite electrodes by B. R. Weinberger.^[37] However, the low stability of polyacetylene in air due to the uptake of oxygen already at room temperature and the insolubility in organic solvents limited the utilization of this polymer in organic electronics. New synthetic routes towards substituted polyacetylenes that are rather difficult to synthesize allowed the realization of some derivatives stabilized due to their substitution pattern.^[38-40] Nevertheless, the research concentrated on the development of various derivatives of polythiophenes^[32,41] and poly(*p*-phenylenevinylenes (PPVs)).^[4,23,42] In 1986, different polythiophene derivatives were investigated by S. Glenis.^[43] PPV was applied in solar cells for by S. Karg for the first time in 1993.^[44] In simple solar cells, only low efficiencies were achieved with derivatives of these material classes.^[4,24] For solving this problem, C. W. Tang introduced the concept of the heterojunction from a donor to an acceptor material in 1986. On the basis of a flat heterojunction (FHJ) solar cell, he was able to reach a PCE of 1% by the use of copper phthalocyanine and a perylene derivative.^[45] M. Hiramoto improved this solar cell via the insertion of a layer consisting of a mixture of two dyes. A perylene derivative and phthalocyanine was applied for this layer and deposited by cosublimation.^[46,47] The mixture of the active materials result in a bulk heterojunction (BHJ) geometry.^[4,48,49] In 1993, buckminsterfullerene was used as acceptor material for the first time by N. S. Sariciftci.^[50,51] Today, C₆₀ is the most frequently applied acceptor material in heterojunction solar cells.^[24,52,53] While N. S. Sariciftci built a solar cell with a FHJ geometry,^[50,51] G. Yu realized a BHJ solar cell comprising a PPV derivative and C₆₀.^[54,55] The first all-polymer solar cell, in which the active layer is formed by a mixture of two polymers, was independently developed by the groups of A. J. Heeger^[56] and R. H. Friend,^[57] both cells reached a PCE of 1%. Furthermore, polyfluorenes^[58] and poly(2,7-carbazoles)^[59] in combination with different comonomers are used as organic semiconductors. Besides organic solar cells,^[60-63] further applications of organic semiconductors are organic light-emitting diodes (OLEDs)^[64,65] and organic field-effect transistors (OFETs).^[66,67]

The field of third generation photovoltaics also implement dye-sensitised solar cells (DSSCs) which also known as Grätzel cells and exhibit high efficiencies.^[2,4,68] DSSCs consist of a mesoporous film made of a semiconductor with a wide bandgap like titanium dioxide. This film is covered with a monolayer of a dye. The dye as well as the titanium dioxide is enclosed by an electrolyte or hole transporting material (HTM). When the device is exposed to light, an electron can be transferred from the excited dye to the conduction band of the titanium dioxide. This electron migrates through the inorganic semiconductor towards the anode. The electrolyte regenerates the dye and transports the positive charge towards the cathode. The electrons reaching the cathode through the circuit recondition the electrolyte in turn.^[4,69] The first DSSC was presented by B. O'Regan and M. Grätzel in 1991 and consisted titanium dioxide layer and a ruthenium complex.^[70] As a HTM, a liquid electrolyte like a I⁻/I₃⁻ redox couple in volatile organic

solvents such as acetonitrile is frequently applied. This ensures high efficiencies, but the long-term stability of the DSSCs is limited. Thus, solid state electrolytes were investigated despite the corresponding efficiency loss. A further disadvantage are ruthenium complexes that are expensive and toxic resulting in the research on organic metal-free dyes.^[2,69] In 1998, the group of M. Grätzel fabricated the first efficient solid state DSSC with a PCE of under 1%.^[71] Today, Grätzel cells reach efficiencies of 13% by means of a porphyrin sensitizer and a cobalt(II/III) redox system.^[72] With solid state electrolytes, efficiencies up to 11% are achieved.^[73] The inorganic and organic sensitising dyes can also be exchanged by perovskites. These are materials with the chemical composition AMX_3 where A marks an organic cation like $CH_3NH_3^+$, M denotes a divalent metal cation such as Pb^{2+} and X stands for the halogen anions Cl^- , Br^- or I^- . These components crystallize in a cubic unit known as perovskite structure. Semiconducting polymers and low molecular weight materials are used as HTMs with spirobifluorene derivatives being the most effective ones.^[2,68,74] The first perovskite solar cell was presented in 2009 and exhibited an efficiency of 3.8%.^[75] Since then, the PCE increased incredibly fast to 22%, making perovskite solar cells the most promising candidate among the alternatives to silicon solar cells.^[76]

The unique properties of organic solar cells like flexibility and semi-transparency allows their application in various areas. In Figure 1, examples for innovative organic solar cells are shown. These include decorative sensors in the shape of leaves that monitor presence of persons in a room and regulates lighting^[77] or unique installations like an artificial tree which leaves harvest solar energy allowing the charging of mobile phones via a USB port.^[78] Furthermore, organic solar cells can be integrated in building and cars. OSC modules were combined to form a shade sail in the shape of the African continent which simultaneously harvests energy for the indoor lighting.^[79] Tinted windows made from solar foils that are laminated between glass plates produce energy and give shade.^[80] In addition, roofs for cars can be equipped with solar foil contributing to a clean energy production.^[81] Photovoltaic modules that exhibit semi-transparency in combination with a grey colour are suitable solutions for building integrations.^[82]

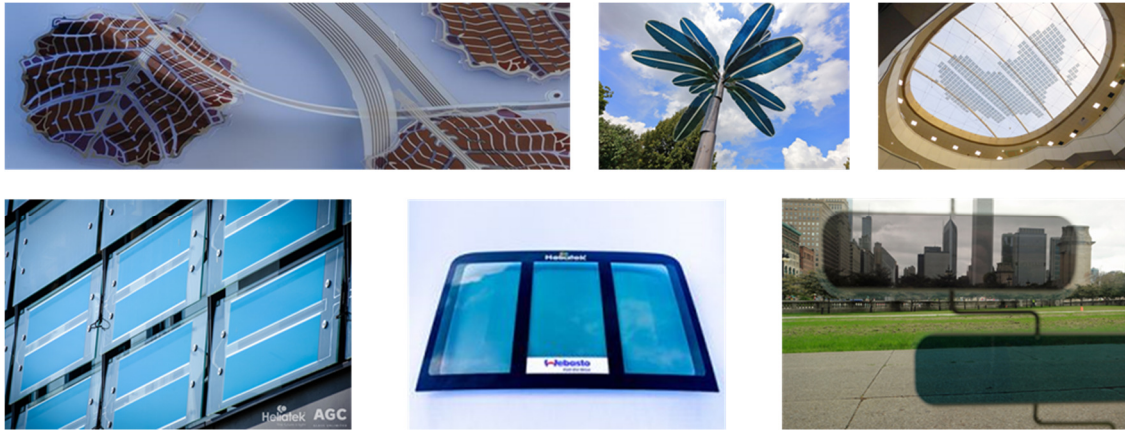


Figure 1: Examples for innovative organic solar cell applications. Presence detector from printed OSC modules in the shape of a leaf by VTT Technical Research Centre of Finland (top left).^[77] Tree with leaves made from flexible OSCs by Opvius GmbH (top middle).^[78] Shade sail in the shape of the African continent for the African Union Peace and Security Building in Addis Ababa by Opvius GmbH. The integrated OSC modules provide the power for the lighting inside the building (top right).^[79] Tinted glass with organic solar foil for the integration into buildings (bottom left).^[80] Roof of a car with integrated organic solar foil by Heliatek GmbH (bottom middle).^[81] Semi-transparent grey photovoltaic modules for the integration in buildings developed by Merck KGaA and Opvius GmbH.^[82]

2.2 Operating mode of organic solar cells

Organic solar cells are built from an active organic layer between two electrodes that generate an internal electrical field facilitating the charge carrier separation and collection. When light is absorbed by the organic material in the active layer, an electron is excited from the ground state to the first excited state.^[24,83] Because organic semiconductors exhibit a low dielectric constant in contrast to inorganic semiconductors, an electron-hole pair, a so-called exciton, is formed which is bound by Coulomb forces.^[23,83,84] This process is followed by an exciton dissociation. In simple solar cells with only one organic semiconductor between two electrodes, the dissociation is located at the junction from the semiconductor to the electrode.^[24] However, the binding energy of excitons in organic semiconductors is quite high with about 0.5 eV. Thus, the thermal energy at room temperature with approximately 0.025 eV is not sufficient to generate free charge carriers from the excitons requiring an additional contribution for efficient dissociation.^[60,85–87]

To facilitate the exciton dissociation in organic semiconductors, C. W. Tang introduced the concept of the heterojunction between a donor and an acceptor in 1986.^[45] At this interface, excitons are separated into free charge carriers within 10^{-15} s. In Figure 2, the operating mode of such a solar cell comprising a donor-acceptor heterojunction is shown. Via exposure to photons, an excited state is generated in the donor material and an electron-hole pair is formed (1). This exciton diffuses towards the donor-acceptor interface D-A (2). The exciton dissociation into electrons and holes is enabled by an electron transfer process to the acceptor material (3). The resulting free charge carriers migrate towards the corresponding electrodes by the means of the internal electric field. The holes move to the anode, the electrons are

2. Introduction

transported in the opposite direction towards the cathode (4). This results in a photocurrent and a corresponding photovoltage.^[4,23,88]

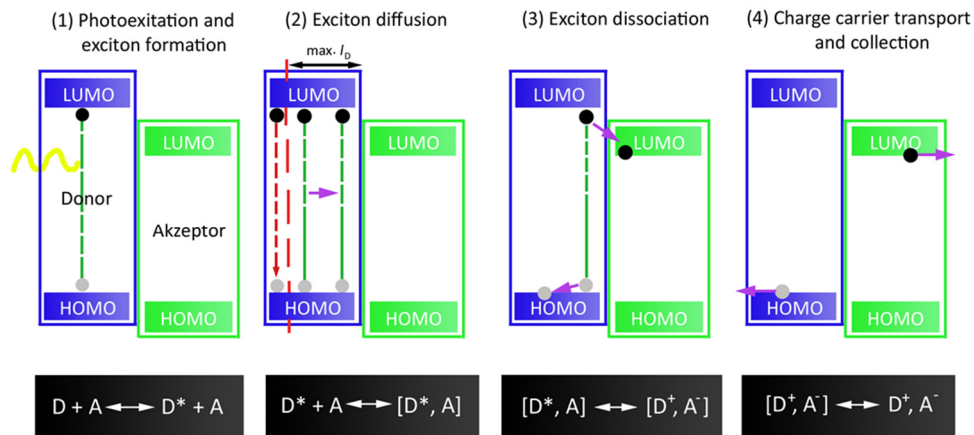


Figure 2: Operating mode of a solar cell with donor-acceptor heterojunction. D denotes the donor material, A represents the acceptor material and l_D illustrates the diffusion length of the excitons.^[23,88]

The energy that is necessary for the dissociation process arises from the difference of the electron affinities and ionisation potentials of the two materials, respectively. If the binding energy of the excitons can be overcome by the energy gain of transferring the electron to the acceptor, the exciton dissociates and the electron is passed to the lowest unoccupied molecular orbital (LUMO) of the acceptor material exhibiting the higher electron affinity. The hole is left on the highest occupied molecular orbital (HOMO) of the donor material with the lower ionisation potential.^[24,60,89]

The diffusion length l_D of the exciton is very small due to its short lifetime of 100 ps to 1 ns and lies between 5 and 14 nm. In consequence, only excitons generated close to the donor-acceptor interface can contribute to the photocurrent. Excitons formed further away of the heterojunction recombine and relax to the ground state before reaching the donor-acceptor interface. This loss of absorbed photons leads to a lower quantum efficiency with the interface area between donor and acceptor being the limiting factor.^[4,23,90]

2.3 Solar cell characteristics

For the characterization of new materials in a solar cell, the photocurrent spectrum is an important starting point because the incident photon to current efficiency (*IPCE*) can be determined from the spectrum. The *IPCE* describes the ratio of the number of generated electrons $n_{\text{electrons}}$ and the number of the incident photons n_{photons} in dependence of the wavelength of the excitation light λ :

$$IPCE(\lambda) = \frac{n_{\text{electrons}}}{n_{\text{photons}}} = \frac{I \cdot h\nu}{P \cdot e} = \frac{I \cdot hc}{P \cdot e\lambda} = \frac{1240 \cdot I}{P \cdot \lambda} \quad (\text{Equation 1})$$

The current density in Am^{-2} is denoted by I , the incident light power in Wm^{-2} by P , the Planck's constant by h , the frequency of the incident light beam by ν , the elementary charge by e , and the velocity of light by c . The measured photocurrent is the current that is outcoupled of the solar cell. For this reason, the $IPCE$ is also called external quantum efficiency (EQE). The photocurrent spectrum is achieved by monitoring the photocurrent in dependence of the wavelength of the incident light. An example for a photocurrent spectrum is presented in Figure 3.^[4,60]

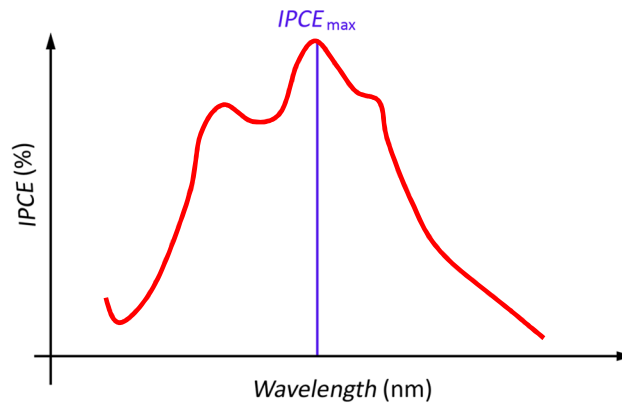


Figure 3: Exemplary $IPCE$ curve of a solar cell with $IPCE_{max}$ as maximal incident photon to current efficiency.^[4]

The value of the $IPCE$ is dependent on three parameters:

$$IPCE(\lambda) = LHE(\lambda) \cdot \Phi_{inj} \cdot \Phi_{col} \quad (\text{Equation 2})$$

In Equation 2, $LHE(\lambda)$ is the light harvesting efficiency of the active materials, Φ_{inj} is the quantum efficiency for the charge injection from the donor to the acceptor for FHJ and BHJ solar cells and Φ_{col} is the collection efficiency of the charge carriers at the external electrodes. The maximal value of the incident photon to current efficiency $IPCE_{max}$ is an important parameter for the description of the solar cell and the assignment of the performance to the absorption and molecular structure of the active materials. Thus, a high photocurrent correlates with a high $IPCE$ value and a broad photocurrent spectrum.^[4,91]

Whereas the photocurrent spectrum characterizes the ability of a solar cell to convert photons into electrons at different wavelengths or intensities of the incident light, for technical application usually the current density I in Am^{-2} and the photovoltage V under simulated AM1.5 sunlight are measured.^[4] This air mass 1.5 spectrum represents an incident solar radiation at sea level onto a surface tilted by 37° and weakened by the earth atmosphere.^[42] Figure 4 shows an exemplary I - V curve.

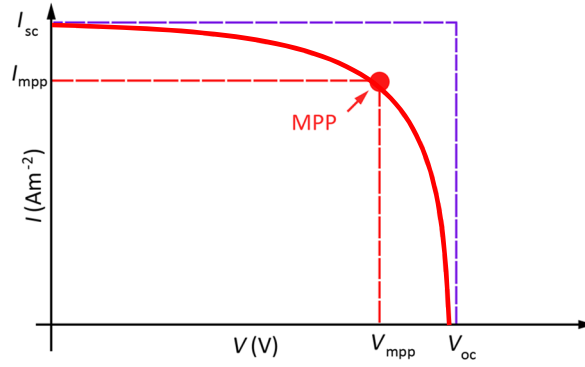


Figure 4: Example for a typical I - V curve of a solar cell. MPP illustrates the maximum power point of the I - V curve with the corresponding current value I_{mpp} and V_{mpp} . The short circuit current is denoted by I_{sc} and the open circuit voltage is depicted by V_{oc} .^[4]

In the I - V curve, I_{mpp} and V_{mpp} represents the current and the voltage at the maximum power point (MPP). The MPP is characterized by the maximum rectangle under the I - V curve given by $I_{mpp} \cdot V_{mpp}$. Further characteristics of the I - V curve are the highest values measured for the photocurrent and the photovoltage, the short circuit current I_{sc} and the open circuit voltage V_{oc} , respectively. By means of these parameters, the fill factor (FF) of the solar cell can be determined:

$$FF = \frac{V_{mpp} \cdot I_{mpp}}{V_{oc} \cdot I_{sc}} \quad \text{(Equation 3)}$$

Ideally, a solar cell exhibits a rectangular I - V curve and thus a FF of about 100%. The power conversion efficiency η can be calculated by:

$$\eta = \frac{P_{out}}{P_{in}} = \frac{FF \cdot V_{oc} \cdot I_{sc}}{P_{in}} \quad \text{(Equation 4)}$$

Here, the maximum electrical output power P_{out} in Wm^{-2} of the photovoltaic device under illumination and the incident light power P_{in} in Wm^{-2} are considered.^[4,91]

The value of V_{oc} can be calculated based on the redox potentials of the active materials. In heterojunction solar cells, the open circuit voltage is mostly estimated as the difference of the HOMO of the donor and the LUMO level of the acceptor. For a solar cell made from polymer as donor material and fullerene as acceptor material, the open circuit voltage V_{oc} is evaluated by:

$$V_{oc} \approx E_{LUMO,acceptor} - E_{HOMO,donor} - 0,3 \text{ V} \quad \text{(Equation 5)}$$

The 0.3 V subtracted in Equation 5 depicts the energy that is lost during the photoinduced charge carrier generation.^[4] In 2006, M. C. Scharber established a relationship between the LUMO level of the donor and the acceptor, the bandgap of the donor and the power conversion efficiency of the solar cell. Accordingly, BHJ solar cells can reach PCEs of 10% and higher.^[92] The maximal open circuit voltage can be predicted according to R. A. J. Janssen:

$$V_{oc,max} \approx E_g - 0,6 \text{ V} \quad \text{(Equation 6)}$$

Corresponding to Equation 6, the maximum of V_{oc} in an organic BHJ solar cell is dependent on the lowest optical bandgap E_g , either of the donor or of the acceptor.^[93] The short circuit current I_{sc} can be estimated via:

$$I_{sc} = ne\mu E \quad \text{(Equation 7)}$$

The charge carrier density is depicted by n , the elementary charge by e , the charge carrier mobility by μ , and the electrical field by E .^[42] In conclusion, the power conversion efficiency and stability of a solar cell depends on the choice of materials with suitable redox potentials, absorption, and self-organization of molecules being of vital importance.^[4,52,87]

2.4 Geometries of organic solar cells

In organic solar cells, the active layer made from organic semiconducting materials is arranged between two electrodes. One of the electrodes has to be optically transparent. Indium tin oxide (ITO) is suited due to its high optical transparency and electrical conductivity as anode material whereas materials with a low work function like aluminium, calcium, and silver as well as their alloys are used as cathodes.^[60,61] For collecting the generated electrons and holes at the corresponding electrodes, an electrical field is necessary. This is accomplished by the different ionisation energies and work functions of the electrodes, respectively.^[24,61] Glass is usually applied as a substrate, but organic solar cells can also be realized by printing on flexible plastic substrates.^[4,49,61,94]

In the regular solar cell device structure, holes are transported from the donor to the ITO anode and electrons from the acceptor to the metal cathode. In addition, an inverted geometry is enabled by the ability of ITO to collect both electrons and holes due to a work function of about 4.5 – 4.7eV that is between the HOMO and LUMO levels of established organic semiconducting materials.^[4,95] In Figure 5, the regular and inverted OSC structures are shown.

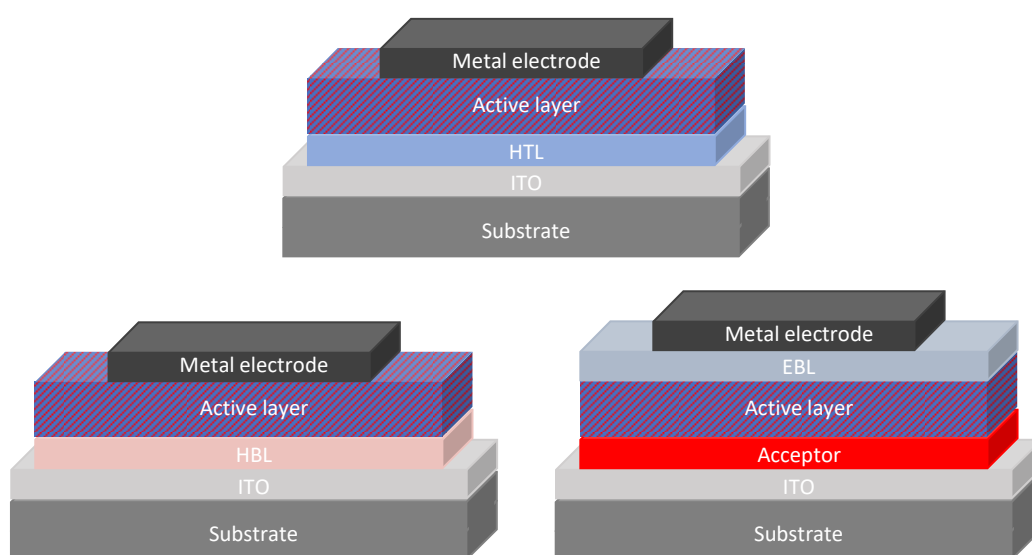


Figure 5: Geometries of regular organic solar cells (top) and inverted organic solar cells (bottom).^[4,96]

The polarity of the ITO electrode is influenced by the modification of the surface. Hole outcoupling in regular devices is achieved by direct deposition of the donor or an additional hole transporting layer (HTL) of a material with high work function like poly(3,4-ethylenedioxythiophene):poly(styrenesulfonate) (PEDOT:PSS). However, the application of hole blocking layers (HBL) made from substances like zinc oxide, titanium dioxide or caesium carbonate leads to an electron collecting ITO electrode for the use in an inverted device. Another possibility is the deposition of an acceptor material onto the ITO layer and the insertion of a p-type electron blocking layer (EBL) of semiconductors like PEDOT:PSS, vanadium oxide or molybdenum oxide between the active layer and the metal electrode. Organic semiconductors used for the active layers are the same for regular and inverted devices. The advantages of inverted structures include an increased device stability due to the elimination of the PEDOT:PSS layer that etches the ITO layer and causes diffusion of indium into the active layer. Furthermore, the low work-function metal cathode that also limits the device stability because of oxidation can be exchanged by more stable metals like silver. In contrast to regular devices, the inverted geometry exhibits slightly lower efficiencies and short-circuit currents.^[4,95–97]

The setup of organic solar cells is usually described according to the geometry of the active layer. Two basic architectures exist, the flat heterojunction (FHJ) and the bulk heterojunction (BHJ). Both approaches are applied in the fabrication of single junction solar cells, that is cells comprising only one heterojunction between a donor and an acceptor material.^[94,98,99] However, some intrinsic problems regarding organic solar cells like limited absorption of the solar light and energy losses due to exciton dissociation and recombination restrict their efficiencies.^[100–102] The enhancement of organic solar cell performance can be achieved by several methods with respect to the solar cell setup. The extension of the spectral absorption is mostly based on the implementation of an additional absorber. This can be realized by the application of a mixture of several active materials like a ternary blend^[103–105]. Furthermore, multijunction solar cells that comprise two or even more heterojunctions can be fabricated. In the different subcells, often absorbers with complementary absorption are used.^[99–102,106] Finally, additional donor or acceptor layers as well as other functional layers like hole or electron transporting materials can be inserted in the device stack resulting in multilayer structures. Advantageously, the different layers can be optimized separately using this multilayer concept.^[53,88,107]

2.4.1 FHJ solar cells

The first organic solar cell with two components was presented by C. W. Tang in 1986. The device comprised basically two active layers on top of each other.^[45] This geometry is called flat heterojunction, planar heterojunction or bilayer heterojunction. As shown in Figure 6, the FHJ configuration consists of a layer of the p-type donor material responsible for the hole transport and a layer of the n-type acceptor material that transports the electrons.^[23,88] This structure can be fabricated by two methods depending on the applied materials.^[108] The single layers are often

realized by subsequent vacuum deposition. Thus, usually small organic molecules like phthalocyanines as donor materials and fullerenes as acceptor materials are applied.^[4,109] Besides vacuum deposition of small molecules that also allows the fabrication of multilayer structures with several functional layers, polymeric materials are solution processed via spin coating. The deposition of a second layer is difficult with polymer solutions as the underlying layer is dissolved upon spin coating of the upper material. Thus, multilayer devices are dependent on the insolubility of the underlying layer either achieved by orthogonal solvents or by crosslinking of the material.^[108]

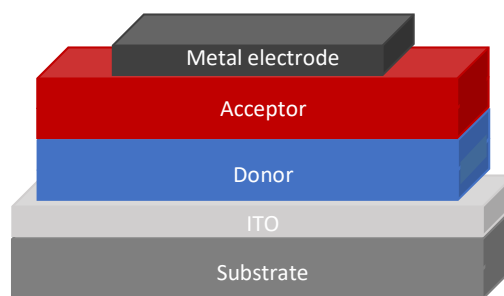


Figure 6: Geometry of a FHJ solar cell.^[4,98,110]

In the first planar heterojunction solar cell by C. W. Tang, the two active layers comprising copper phthalocyanine as donor and 3,4,9,10-perylenetetracarboxylic-bis-benzimidazole as acceptor are sandwiched between an ITO anode and a silver cathode. An efficiency of about 1% was achieved.^[45] In 1989, S. R. Forrest replaced the acceptor by 3,4,9,10-perylenetetracarboxylic dianhydride which he found out to be the better n-type material.^[111] N. S. Sariciftci was the first who applied C₆₀ as acceptor material in 1993.^[50,51]

In FHJ solar cells, the interface between donor and acceptor is relatively small. Thus, the number of electrons that can contribute to the photocurrent is limited. Only excitons that are generated in a very thin layer close to the interface are able to reach the interface due to their small diffusion length. However, the optical absorption length is much higher than the diffusion length. In consequence, most of the generated excitons are lost by recombination processes.^[4] Because of the low charge carrier mobilities in organic semiconductors, the free charge carriers can form space charges after exciton dissociation which influence the solar cell performance.^[60] This can result in recombination of the charge carriers at the interface.^[112] The insertion of a transparent exciton blocking layer between the active layer and the metal electrode ensures that the excitons only migrate within the active layer and thus prevents the quenching of excitons at defect states of the interface between acceptor and cathode. Furthermore, also damage like trap levels due to the evaporation of the cathode is circumvented. In addition, the exciton blocking layer reduces the resistance between the organic material and the cathode and serves as an optical spacer that redistributes the optical density within the active layer enhancing the total absorption and the efficiency of the solar cell.^[4,60,113,114] Applying the same organic semiconductors as C. W. Tang in his first efficient organic solar cell, the group of S. R. Forrest achieved an efficiency increase to 2.4% by integration of an exciton blocking layer

2. Introduction

made from bathocuproine (BCP).^[115] Moreover, by the exchange of the perylene derivative with C₆₀ as a better acceptor, efficiencies of 3.6%^[116] and 4.2% can be reached, respectively.^[117] Insertion of tris(4-(5-phenylthiophen-2-yl)phenyl)amine as an additional exciton blocking layer at the anode, a solar cell with an tetraphenylidibenzoperiflanthene donor, a C₆₀ acceptor, and BCP as the cathode buffer layer achieved 5.3% efficiency.^[118] The highest efficiency for planar heterojunction solar cells with about 6% was reached by K. Cnops with the donor α -sexithiophene and the acceptor boron subnaphthalocyanine chloride in combination with a BCP exciton blocking layer towards the cathode.^[119] The chemical structures of the applied active materials are depicted in Figure 7. Further enhancement of the efficiency of FHJ structures is very difficult to achieve because the interface between the donor and the acceptor is small and the thickness of the two active layers is limited due to the short diffusion length of the excitons.^[110,120] In addition, the application of thick absorber layers would result in optical filter effects decreasing the photocurrent.^[98] However, efficiency increase is enabled by the combination of several active materials in multilayer devices. K. Cnops realized a three-layer planar heterojunction device that comprises the acceptor boron subphthalocyanine chloride in addition to the previously used subnaphthalocyanine chloride acceptor and the α -sexithiophene donor achieving a PCE of 8.4%.^[119] The additional acceptor material is also illustrated in Figure 7.

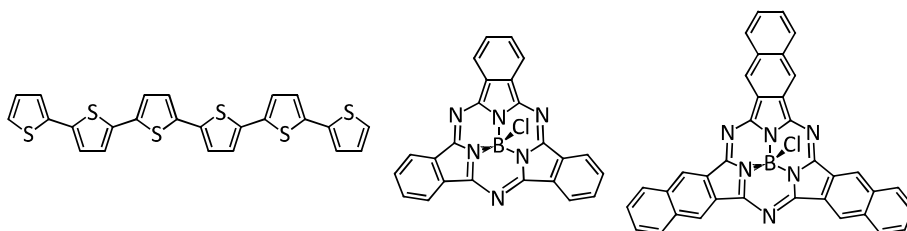


Figure 7: Chemical structures of α -sexithiophene, subphthalocyanine chloride, and subnaphthalocyanine chloride as used in the best FHJ solar cells.^[119]

Although the FHJ geometry is not suited for achieving very high efficiencies with organic semiconducting materials, this setup is frequently used for fundamental research concerning the processes at the donor-acceptor interface. The planar heterojunction is an ideal model system for such basic studies due to the inherent advantages of the structure. For the understanding of interfacial actions, the morphology of the interface is of vital importance and has to be controlled accurately. This is possible due to the planarity of the interface between donor and acceptor that restricts unpredictable and uncontrollable variations which arise from mixing of the materials. Thus, different material systems are comparable when using a planar structure. However, the conditions regarding solar cell fabrication have to be chosen carefully as the interfacial morphology can be significantly influenced by the mixing of donor and acceptor. This is possible if vacuum deposited low molecular weight materials diffuse into the underlying layer that consists either of evaporated small molecules as well or of solution processed polymers. Furthermore, the charge transport pathways are clearly separated in FHJ structures as the hole is transported within the donor and the electron migrates through the

acceptor. Because of the easier requirements, planar heterojunctions are often used for device simulations allowing the comparison of experiment and simulation.^[108]

2.4.2 BHJ solar cells

For enhancement of the efficiency of FHJ solar cells, the concept of bulk heterojunction was introduced. This geometry is based on an enlargement of the donor-acceptor interface at which the excitons dissociate. Using a blend made from donor and acceptor material, an interpenetrating network of donor and acceptor is formed due to the phase separation of the two components. Thus, the excitons generated by light absorption of the active materials are only few nanometres away from an interface allowing their dissociation into electrons and holes. The quantum efficiency is significantly increased.^[4,23,121] Figure 8 presents the schematic setup of a typical BHJ solar cell. Onto the ITO anode, a transparent conducting layer often made from poly(3,4-ethylenedioxythiophene):poly(styrenesulfonate) (PEDOT:PSS) or metal oxides like MoO_3 are deposited. This layer serves both as a hole transporting and electron blocking layer and enhances the performance of the solar cell.^[107]

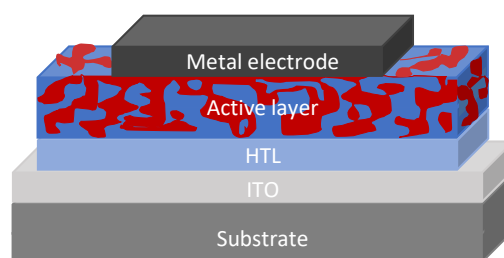


Figure 8: Geometry of a BHJ solar cell.^[4,98,110]

A solar cell including a BHJ geometry was presented by M. Hiramoto for the first time. The BHJ layer made from a perylene derivative and phthalocyanine was applied between layers of the pure dyes. The blend was realized by cosublimation of the two materials.^[46,47] In 2005, the group of S. R. Forrest optimized this device by exchanging the perylene derivative by C_{60} and using copper phthalocyanine. A PCE of 5% was achieved.^[122,123]

Both active components should show phase separation to form separated donor and acceptor phases and thus ensure continuous transport pathways for the electrons and holes towards the corresponding electrodes.^[4,49] The better the length scale of the phase separation conforms to the diffusion length of the excitons, the more excitons can dissociate.^[60,124] The bicontinuous network provides two channels for the charge carrier transport, one for the holes in the donor phase and one for the electrons in the acceptor phase. For this reason, high efficiencies concerning charge carrier collection can be achieved.^[23,49] A schematic illustration of the morphology of the active layer of a BHJ solar cell is illustrated in Figure 9.

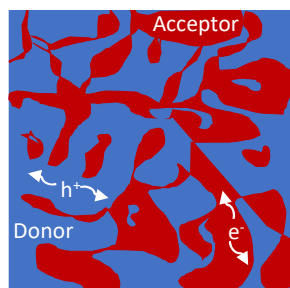


Figure 9: Scheme of the morphology of the active layer of a BHJ solar cell.^[61,96,110]

BHJ solar cells from small molecules are mostly fabricated via cosublimation of the donor and the acceptor material. As this is relatively expensive, the production costs are reduced by the application of solution processed materials like conjugated polymers. Today, the most frequently used combination is using a conjugated polymer as a donor and a fullerene derivative as an acceptor. Application of a plastic substrate covered with a transparent conducting electrode allows the fabrication of flexible solar cells via printing processes.^[4,49,110] In comparison to FHJ solar cells, solution processing of a BHJ layer circumvents the problems of surface damage due to spin coating.^[23] The discovery of a very fast reversible, metastable and photoinduced electron transfer in a blend film of conjugated polymers and C₆₀ was observed independently by K. Yoshino^[125] as well as G. Yu and A. J. Heeger.^[54,55] In 1995, the latter reported a first BHJ solar cell with a polymer as donor material. They used poly(2-methoxy-5-(2'-ethyl-hexyloxy)-1,4-phenylene vinylene) (MeH-PPV) in combination with phenyl-C₆₁-butyric acid methyl ester (PC₆₁BM) derivatives.^[55] In the same year, G. Yu and A. J. Heeger^[56] as well as J. J. M. Halls^[57] realized a polymer-polymer BHJ solar cell for the first time. Both cells achieved an efficiency of 1%.

The performance of a BHJ solar cell depends on the charge carrier mobilities, the light absorption, and the morphology of the active layer. Different materials with good optical and electronical properties and good nanostructured morphologies were investigated. The solvent showed a significant influence on the originating morphology of the blend. Furthermore, annealing steps are conducted to improve the nanostructure and the charge transport resulting in an increased efficiency. In addition, application of an external electric field can further enhance the PCE. Other parameters are the thickness of the active layer, the ratio of the donor and the acceptor material, and the method for the deposition of the materials. For example, the evaporation rate of the solvent can influence the morphology. One disadvantage of the BHJ geometry is that continuous transport pathways have to exist for electrons and holes leading to the corresponding electrode and ensuring an efficient charge carrier collection.^[60,126] In 2005, the group of A. J. Heeger achieved an efficiency of 5% with a simple BHJ solar cell made from poly(3-hexylthiophene) (P3HT) and PC₆₁BM that was annealed at 150 °C.^[127] Up to now, the combination of the P3HT donor and the PC₆₁ acceptor is one of the most studied material combinations for organic solar cells.^[3,60,107] Figure 10 shows the chemical structures of P3HT and PC₆₁BM.

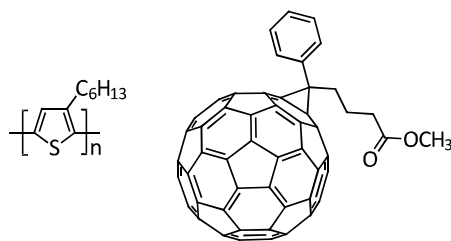


Figure 10: Chemical structures of P3HT and PC₆₁BM.^[3,107]

For further improving the efficiency, electron transporting layers can be inserted between the active layer and the metal cathode. Materials like zinc oxide or titanium oxide are often used. The latter simultaneously works as an optical spacer. By this means, the light intensity within the solar cell is redistributed. A big part of the light can reach the active layer and thus more excitons can be generated. The optical spacer requires a conduction band lying above the Fermi level of the cathode and below the LUMO level of the acceptor facilitating the acceptance of electrons, good electron transporting properties and transparency with respect to the incident light. The distribution of the light intensity is dependent on the thickness of the active layer so that an optical spacer is not always necessary.^[60,107,128] In the case of a solar cell from P3HT and PC₆₁BM, J. Y. Kim and A. J. Heeger reached an efficiency enhancement from 2.3% to 5.0% by the insertion of titanium oxide as an optical spacer layer.^[129]

The development of low bandgap donor polymers that contain electron-rich donor units and electron-deficient acceptor units resulting in a reduced bandgap significantly increases the efficiency towards the 10% value.^[63,130] The chemical structures of the materials applied in the BHJ solar cells with the highest efficiencies are depicted in Figure 11. A PCE of 7.7% for a BHJ solar cell fabricated via spin coating was attained by a cooperation between L. Yu and the Solarmer Energy Inc. in 2009. As a donor, a low bandgap polymer from thienothiophene and benzodithiophene units (PBDTTT-CF) was applied together with phenyl-C₇₁-butyric acid methyl ester (PC₇₁BM) as acceptor material with a ratio of 1:1.5. The copolymer exhibited a low lying HOMO level of -5.2 eV and thus a high open circuit voltage of 0.8 V.^[110,131] Using a low bandgap polymer with naphthothiadiazole and dithienyl thienothiophene units NT812 in combination with PC₇₁BM, high efficiencies of 10.3% and 10.2% were achieved for regular and inverted devices, respectively. Solution processing was carried out with an environmentally friendly solvent and thick active layers with a notably uniform dispersion were fabricated.^[132] In an inverted device, a record efficiency of almost 11% can be reached by combining benzodithiophene and thienothiophene in PTB7-Th and applying PC₇₁BM as acceptor. A novel spin coating method was used that results in a desired vertical donor-acceptor phase separation and thus in a high device performance.^[133] An even higher efficiency of 11.5% was reported by the Toshiba Corporation, but without further details concerning the applied donor polymer.^[134] The combination of a fluorinated benzothiadiazole and quarterthiophene containing copolymer PffBT4T-C₉C₁₃ and PC₇₁BM processed from hydrocarbon solvents achieved an efficiency of 11.7% in an inverted device due to an enhanced nanophase morphology.^[135] A copolymer from

2. Introduction

bithienyl-benzodithiophene and fluorinated benzotriazole units and the non-fullerene acceptor ITIC enabled the fabrication of a solar cell reaching a PCE of 11.4%. This is basically ascribed to the high values for I_{SC} and V_{OC} .^[136] Finally, the highest reported value for a BHJ solar cell is 12.1% and was obtained by a blend of a low bandgap polymer comprising dithienyl benzodithiophene and dithienyl benzodithiophenedione PBDB-T and the small molecule acceptor IT-M. A highly ordered morphology and thus a high short-circuit current and a high open-circuit voltage led to this remarkable result.^[137]

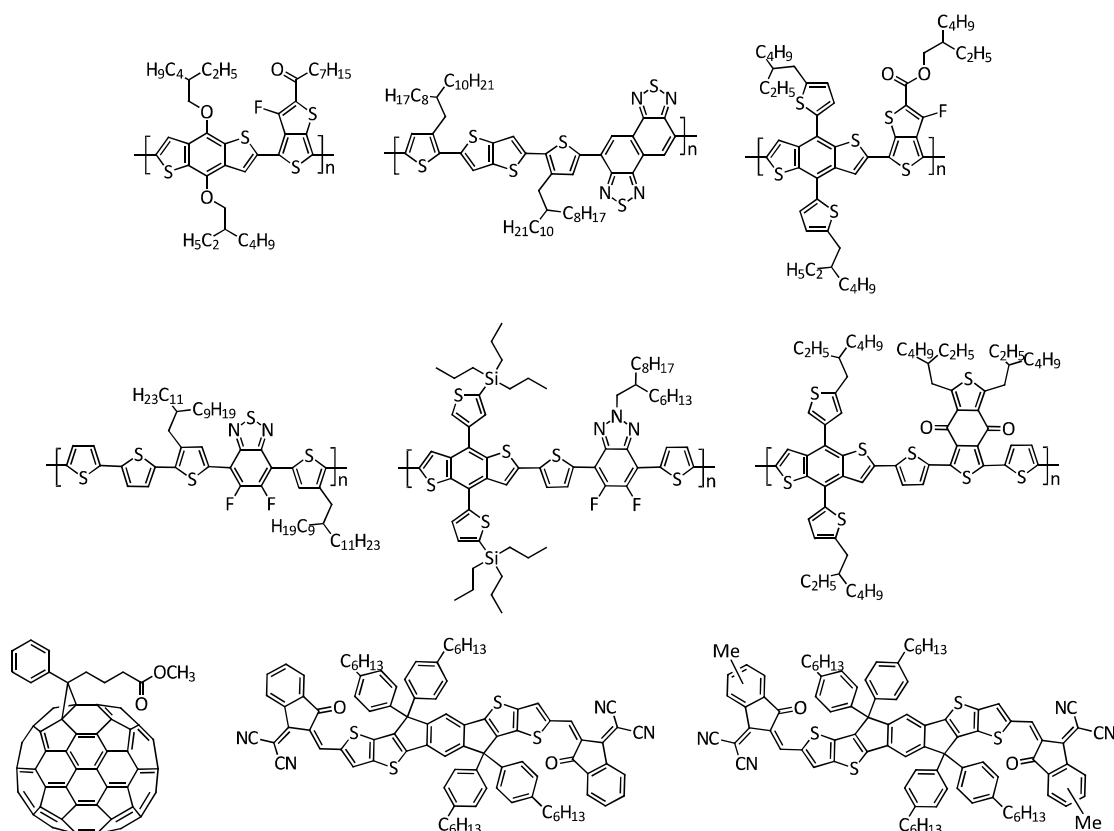


Figure 11: Chemical structures of PBDTTT-CF,^[131] NT812,^[132] PTB7-Th,^[133] PffBT4T-C9-C13,^[135] the copolymer from bithienyl-benzodithiophene and fluorinated benzotriazole,^[136] PBDB-T,^[137] PC₇₁BM,^[3,107] ITIC,^[136,137] and IT-M^[137], as used in the best BHJ solar cells.

2.4.3 Mixed FHJ-BHJ solar cells

Both FHJ and BHJ solar cell geometries exhibit several disadvantages. As the interfacial area in FHJ solar cells is relatively small, only a limited number of excitons are able to dissociate and generate free charge carriers whereas most of the excitons will recombine.^[4] In BHJ solar cells, charge carrier collection could be limited when no continuous pathways exist for the electrons and holes towards their corresponding electrodes leading to charge carrier recombination. Furthermore, a large number of excitons will recombine if the scale of nanophase separation of the active materials lies above the exciton diffusion length. The mixed FHJ-BHJ concept unites both FHJ and BHJ geometries by the embedding of a BHJ layer between layers made from pure

donor and pure acceptor material. Thus, the advantages of BHJ solar cells like the efficient exciton dissociation due to a high interfacial area and a good absorption as well as the advantages of FHJ solar cells such as good charge transport properties towards the corresponding electrodes are assured.^[60,138,139] In Figure 9, the setup of a mixed FHJ-BHJ solar cell is presented.

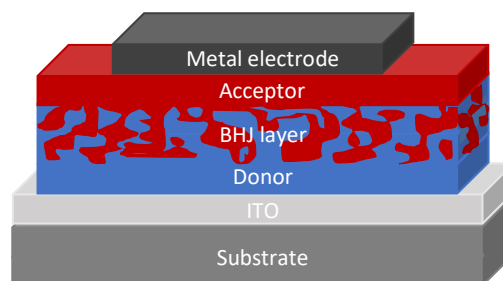


Figure 12: Geometry of a mixed FHJ-BHJ solar cell^[60,139]

The thickness of the homogenous layers correlate approximately to the diffusion length of the excitons. By this means, exciton dissociation is possible both within the blend layer and at the interfaces of the mixed and the pure layers resulting in an enhanced dissociation.^[60] The mobility of the charge carriers within the blend is lower than in the homogenous layers.^[60,138] Thus, it is important to adjust the thickness of the BHJ layer to the diffusion length of the charge carriers for the complete outcoupling of the charge carriers.^[60] In principle, the first BHJ solar cell presented by M. Hiramoto contained simultaneously a mixed FHJ-BHJ structure. A perylene derivative was applied as an acceptor and phthalocyanine as a donor. The mixed layer was realized via cosublimation.^[46,47] However, the thickness of the blend layer was higher than the diffusion length of the charge carriers. This resulted in a low efficiency and thus the advantage of such a solar cell geometry was not recognized.^[60] In 2005, the efficiency of mixed FHJ-BHJ solar cells was increased to 5% by the group of S. R. Forrest by the application of a copper phthalocyanine donor and a C₆₀ acceptor. The mixed layer consisted of the same amounts of the two materials and exhibited a thickness of 10 nm whereas the donor layer thickness was 15 nm and the acceptor layer thickness was 35 nm.^[122,123] In contrast to pure FHJ or BHJ solar cells of these materials, a higher efficiency could be reached. Increasing the thickness of the blend layer resulted in a less efficient device. This is ascribed to the ineffective charge carrier outcoupling.^[60]

For achieving a device structure similar to the mixed FHJ-BHJ geometry, vertical stratification is used in the fabrication of BHJ solar cells. This is of vital importance for the solar cell performance as the fabrication of donor-rich and acceptor-rich phases, respectively, affects charge carrier transport and outcoupling at the electrodes. For example, an acceptor-deficient phases near to the cathode will result in an inefficient collection of charge carriers and thus charge carrier recombination is increased. Vertical stratification can be realized by using appropriate solvents, suitable hole transporting layers and thermal annealing.^[140,141] A further approach is a novel spin coating technique that allows the fabrication of a favourable vertical donor-acceptor stratification. Using this method, a high PCE of almost 11% can be reached with PTB7-Th, a

benzodithiophene and thienothiophene containing low bandgap polymer, in combination with PC₇₁BM as acceptor.^[133] Figure 13 illustrates the chemical structures of the two active materials.

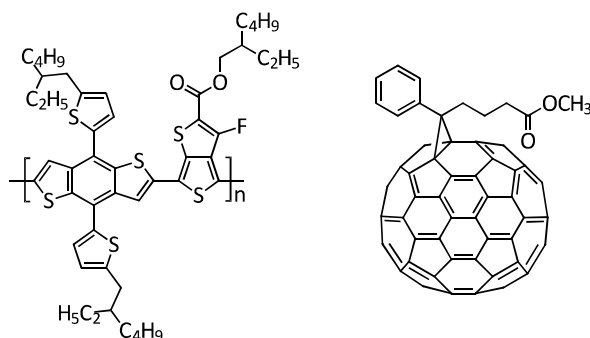


Figure 13: Chemical structures of PTB7-Th and PC₇₁BM as used in the best mixed FHJ-BHJ solar cell.^[133]

In addition, intermixing at the interface between donor and acceptor in bilayer solar cells can also lead to a geometry resembling the mixed FHJ-BHJ structure. This intermixing in planar heterojunctions is either due to diffusion of low molecular weight acceptors like C₆₀ into the donor upon vacuum evaporation or is realized via annealing steps.^[139,142,143]

2.4.4 Tandem solar cells

One of the major reasons for limiting the efficiency in organic solar cells is that the solar spectrum is not covered completely by the absorption range of organic materials.^[60,102] In consequence, M. Hiramoto suggested a tandem configuration comprising a series of two or more cells in 2006. Thus, a higher efficiency can be reached in comparison to a single cell. M. Hiramoto used two FHJ solar cells made from phthalocyanine and a perylene derivative containing a thin gold interlayer.^[144] The tandem structure exhibits a higher optical density over a broader spectral range as a single solar cell without an increase of the resistance. Both small organic molecules and polymers are applied for tandem solar cells. Often, a wide bandgap and a low bandgap material with complementary absorption are combined for exploiting the complete solar spectrum. For preventing a damage of the underlying layers by the deposition of a further layer, suitable interlayers are inserted. Furthermore, orthogonal solvents can be used that circumvents the dissolution of the underlying layers. The interlayer that combines the two solar cells serves as cathode of the bottom cell and as anode of the top cell. Thus, electrons from the top cell can recombine with holes from the bottom cell within the interlayer.^[60,99–101,106] The schematic setup of a tandem solar cell is shown in Figure 14.

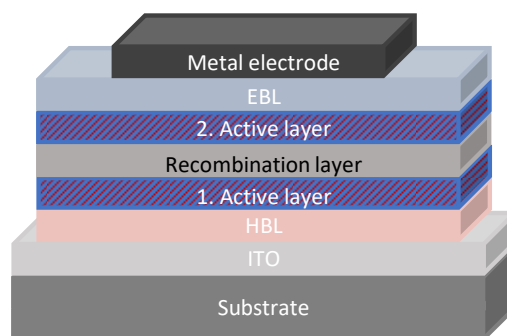


Figure 14: Geometry of a tandem solar cell.^[60,99,106]

S. R. Forrest achieved an efficiency enhancement from 5.0% to 5.7% in comparison to a single cell by connecting two mixed FHJ-BHJ solar cells containing copper phthalocyanine and C_{60} . The interlayer consisted of a doped polymer matrix with imbedded silver nanoparticles. A perylene derivative and BCP were used as exciton blocking layers.^[145] In this tandem device, long wavelengths were absorbed in the first cell close to the transparent anode and short wavelengths were absorbed in the vicinity of the reflecting metal cathode of the second cell.^[60,99] In 2005, J. Drechsel and K. Leo presented a tandem solar cell that reached 3.8% efficiency. This is twice the efficiency for a single cell. The active layers made from zinc phthalocyanine and C_{60} were incorporated into doped p-type and n-type layers, respectively. A very thin gold interlayer connected both subcells.^[146] For further improving the efficiency, materials that absorb in different spectral ranges can be used in the single cells. G. Dennler and N. S. Sariciftci built a tandem solar cell from two mixed FHJ-BHJ subcells. The first one contained zinc phthalocyanine and C_{60} and the second one comprised P3HT and $PC_{61}BM$. However, the PCE was not significantly increased in comparison to both single cells.^[147] This can be attributed to the fact that the total photocurrent is limited by the cell with the lowest generated photocurrent and thus exhibits a value that is equal or even smaller than this limiting current. Because the thickness of the active layers is adjusted to the charge carrier diffusion, the charge carriers accumulate in the cell that generates more excitons. From these accumulated charges, no contribution to the photocurrent is possible. Furthermore, the open-circuit voltage is decreased. Exploiting the advantage of the tandem structure requires the configuration of both subcells in a way that they deliver the same photocurrent.^[60,99]

An inverted tandem solar cell based on small molecules presented by the Heliatek GmbH reached an efficiency of 5.6%. A red-absorbing heterojunction was realized from a fluorinated zinc phthalocyanine as a donor and C_{60} as an acceptor. In contrast, a combination of a sexithiophene derivative with dicyanovinyl endgroups and C_{60} absorbed in the green range. The connection of the two heterojunctions to a tandem solar cell resulted in an absorption covering the complete visible range of the solar spectrum. Several doped hole transport and electron transport materials and a doped recombination layer completed the device stack. The fabrication was realized via vacuum deposition of the single layers. However, two disadvantages can be ascribed to this tandem device. On the one hand, the thickness of the absorbing layers is

still too thin. On the other hand, the C₆₀ contact layer towards the aluminium cathode absorbs light as well. An optimized cell finally attained a certified efficiency of 6.1%.^[148] The group of U. Lemmer realized a tandem solar cell by inserting a solution processed zinc oxide interlayer between the two subcells. The recombination zone was completed by a MoO₃ layer on top of the ZnO. In addition, the ZnO/MoO₃ interface enabled the spincoating of the top cell due to the resistance against the solvent dichlorobenzene. PCDTBT and PC₇₀BM were used for both active layers. The increase of the thickness of the active layer by using the tandem geometry enhanced the quantum yield of the solar cell. However, the efficiency of 4.5% of the tandem cell was not higher than that of the single cells because the fill factor decreased.^[149] Another possibility for the processing of tandem solar cells was also presented by the group of U. Lemmer. A lamination technique was applied to transfer the organic top cell consisting of P3HT and an idene-C₆₀ bisadduct (ICBA) onto the inorganic CIGS bottom cell and the recombination layer. A relatively thick organic absorber layer has to be used to prevent short circuits due to the roughness of the CIGS surface. By this approach, an efficiency of 3.8% could be achieved.^[150] In 2013, the group of R. A. J. Janssen realized a tandem solar cell from polymeric materials with complementary absorption. A copolymer from diketopyrrolopyrrole and terthiophene (PMDPP3T) exhibiting a small bandgap was applied in combination with PC₆₁BM in the top cell and PCDTBT with a wider bandgap was used together with PC₇₁BM in the bottom cell. Orthogonal solvents allowed the deposition of the recombination layers and the top cell onto the underlying layers. An efficiency of 8.9% is reached due to the high quantum efficiencies of the subcells. The incorporation of an additional photoactive layer containing PCDTBT and PC₇₀BM in a triple junction solar cell further increases the efficiency to 9.6%. In this case, the quantum efficiencies of the three subcells were lower because the photons were absorbed in three layers instead of two layers as for the tandem device. The resulting lower short-circuit current is balanced by a high open-circuit voltage of 2.09 V.^[151] A high V_{oc} of about 1.75 V is necessary to use the solar cell for photocatalytic water splitting. A tandem cell comprising a copolymer of thienopyrido isoquinolinedione and benzodithiophene in combination with PC₇₀BM achieved an efficiency of 5.3% and an open-circuit voltage of 1.74 V.^[152] The group of R. A. J. Janssen also presented a tandem device comprising a bottom cell with a donor exhibiting a wider bandgap and a top cell with a small bandgap donor. For the bottom cell, a copolymer of fluorene and dithienyl benzothiadiazole in a blend with PC₆₁BM was applied. The top cell contained a copolymer from diketopyrrolopyrrole and phenylene bithiophene together with PC₆₁BM. An efficiency of 4.6% and an open-circuit voltage of 1.72 V were yielded. For further enhancement of the solar cell performance, a second small bandgap cell was stacked on top. This triple junction solar cell showed an efficiency of also 5.3% and a remarkably high V_{oc} of 2.33 V.^[153]

Further improvements of tandem and triple junction solar cells led to efficiencies exceeding 10%. The chemical structures of the materials used for these highly efficient devices are illustrated in Figure 15. In 2014, the group of S. R. Forrest presented multijunction solar cells with a mixed FHJ-BHJ geometry made by vacuum evaporation of small molecules with

complementary absorption. The bottom cell was built from a DTDCTB donor absorbing in the orange to near infrared and a C₆₀ acceptor whereas the top cell consisted of the UV to yellow absorbing DBP and C₇₀. The tandem cell was able to absorb light from 350 nm to 900 nm and exhibited an efficiency of around 10%. When a second cell from DBP and C₇₀ is added to form a triple junction cell, the PCE is further increased to over 11%.^[154] An efficiency of 11.3% were realized with a tandem cell with active layers of PTB7-Th and PC₇₁BM. As a recombination layer, a hole transporting material was applied ensuring the efficient charge recombination. The high PCE is ascribed to the almost complete light harvesting.^[155] The combination of three donor materials with different bandgaps and fullerenes in inverted tandem and triple junction solar cells was studied by the group of Y. Yang. A bottom cell made from PTB7-Th and PC₇₁BM and a top cell containing a copolymer of dithienopyran and difluorobenzothiadiazole (PDTP-DFBT) together with the acceptor PC₇₁BM were applied for a tandem device reaching an efficiency of 10.7%. When an additional active layer of P3HT and ICBA was inserted as the bottom cell in a triple junction solar cell, the efficiency could be enhanced to over 11%. A simulation approach enabled the adjustment of the layer thicknesses as well as the equalisation of the photocurrent in each subcell. As a consequence of the balanced charge carrier generation and an effective recombination at the recombination layers, a high V_{oc} of 2.28 V could be reached that is almost the total amount of all three subcells.^[156] Furthermore, an inverted tandem solar cell comprising a wide bandgap donor polymer from dithienosilole and dithenophenyl thiazolothiazole (PSEHTT) together with ICBA and the medium bandgap absorber PTB7 in a blend with PC₇₁BM yielded an efficiency of 10.4%. The addition of a bottom cell containing a blend of PMDPP3T and PC₇₁BM led to an increased efficiency of 11.8% for the inverted triple junction device. As the light intensity decreased in the active layers, the open-circuit voltage of 2.24 V could not attain the theoretical value. Besides the choice of materials with suitable energy levels, optimization of the multijunction cells was also supported by optical simulation leading to improved thicknesses of the single layers and thus adjusted photocurrents.^[157] In 2016, the Heliatek GmbH announced a record efficiency of 13.2% for a multijunction device. Three different materials that absorb in the green, red, and near infrared range were combined and allow the conversion of light between 450 nm and 950 nm, but are not further described.^[158]

contacts depends linearly on the value of the so called built-in potential. This parameter describes the difference between the HOMO of the p-type polymer and the LUMO of the n-type fullerene.^[23] The corresponding energy diagram is presented in Figure 16.

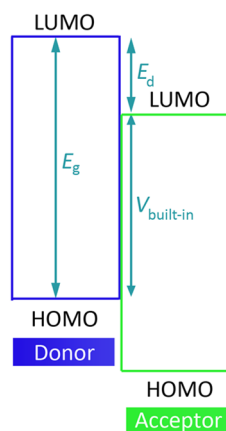


Figure 16: Energy diagram of the HOMO and LUMO levels of the donor and the acceptor. The bandgap of the donor polymer is depicted by E_g , the driving force for the exciton dissociation is denoted by E_d and the built-in potential is described by the difference between the HOMO level of the donor and the LUMO level of the acceptor $V_{built-in}$.^[23]

A donor material with a lower lying HOMO level exhibits a higher value of $V_{built-in}$ and thus reaches a higher open-circuit voltage. However, the bandgap has to be reduced for realizing a broadening of the absorption. This is carried out via the raising of the HOMO level of the donor material that result in a lower value for the bandgap. Furthermore, the LUMO level of the p-type material has to be 0.3 eV higher than that of the fullerene to achieve a driving force for the electron transfer which can overcome the binding energy of the exciton. Thus, a compromise between a low bandgap of the donor and a high built-in potential has to be found.^[23]

The bandgap of conjugated polymers is influenced by several parameters like bond length alternation, planarity, aromatic resonance energy, substituents, intermolecular interactions, and molecular weight.^[42] The simplest way to reach a lower bandgap is to raise the HOMO level and to lower the LUMO level, respectively, or to conduct both options simultaneously.^[23] Several approaches are feasible for the modification of the bandgap. The skeleton of a polyaromatic conjugated polymer can be described as a sequence of successive carbon-carbon single and double bonds. Several approaches are feasible for the modification of the bandgap. The skeleton of a polyaromatic conjugated polymer can be described as a sequence of successive carbon-carbon single and double bonds. Two possible resonance structures with different energies can be derived for the ground state as shown in Figure 17, that is a fully aromatic and a fully quinoid structure. In the aromatic form each benzene or thiophene unit retains the aromaticity. Delocalization of the π -electrons along the conjugated polymer chain, that is a stronger conjugation along the chain, however converts single bonds into double bonds and vice versa resulting in a more quinoid-like character of the structure. In principle, the quinoid form is not as energetically stable as the aromatic structure because the aromaticity of the benzene or thiophene units is

no longer present and thus the stabilization energy is lost. Nevertheless, for a polymer chain the quinoid resonance structure possesses the lower bandgap as it features a stronger conjugation along the backbone of the chain. The contribution of the aromatic and quinoid character of a structure in a polyaromatic conjugated system can be described by the mean bond length alternation. This parameter is defined as the average difference of the length between neighbouring carbon-carbon bonds in a polyene chain, though for aromatic rings the difference between the carbon-carbon bond in the ring and between the rings is considered.^[23,160]

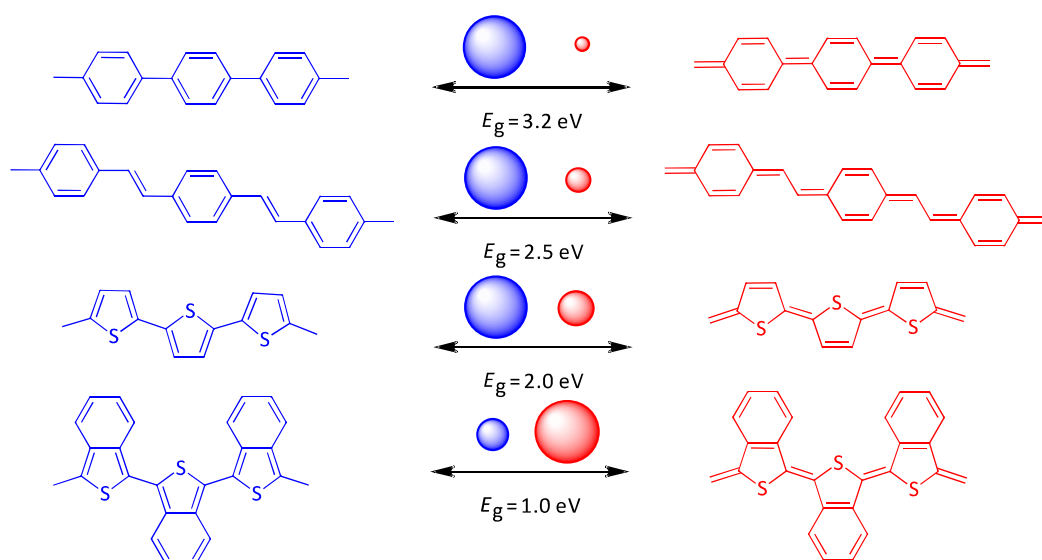


Figure 17: Aromatic and quinoid resonance structures of polyphenylene, polyphenylenevinylene, polythiophene, and polyisothianaphthene. The size of the circles reflects the contribution of the mesomeric structures to the actually prevailing ground state geometry. The bandgap of the polymers is depicted by E_g .^[23]

The more the aromatic structure predominates in the ground state, the bigger is the value of the bond length alternation in this definition. This is because the single benzene or thiophene units retain their aromaticity and are connected via single bonds. When the contribution of the quinoid structure increases due to delocalization of π -electrons along the polymer chain, the value of the bond length alternation is decreased as the single bonds between the neighbouring benzene or thiophene rings adopt a double bond character. In consequence, the bandgap drops linearly with increasing quinoid character and decreasing bond length alternation, respectively. The critical factor in this respect is the aromatic resonance stabilization. If the stabilization energy is low, the quinoid form can be adopted more easily. Thus, the bandgap is reduced from 3.2 eV for polyphenylene via 2.4 eV for polyphenylenevinylene and 2.0 eV for polythiophene to 1.0 eV for polyisothianaphthene due to a decreasing aromaticity of the units.^[23,160]

Furthermore, also the implementation of steric and electronical effects on the conjugated polymer backbone can reduce the bandgap. The planarization between adjacent aromatic units allows interaction between p-orbitals and thus an extended conjugation and delocalization. This again results in a lower bond length alteration value and a lower bandgap. The higher the conjugation length is, the lower the bandgap is in consequence. However, an infinite increase of the conjugation only leads to a finite lowering of the bandgap. The easiest way to planarization

is the rigidification of aromatic units via covalent bonds.^[23] By using this method, J. Roncali and R. Viruela showed a lowered bandgap of 1.2 eV when bridging a bithiophene unit with a ketal group.^[161,162] The application of carbon-bridged terthiophene reduces the bandgap to 1.1 eV as presented in Figure 18.^[163]

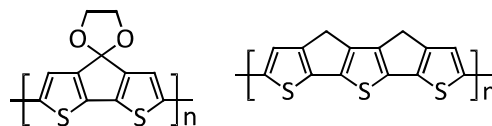


Figure 18: Bridged thiophenes.^[161–163]

The integration of electron-donating or electron-withdrawing substituents at the aromatic units of the polymer backbone depicts a further method for the modification of the molecular orbitals by inductive and mesomeric effects. In general, electron-donating groups raise the HOMO level and electron-withdrawing groups lower the LUMO level resulting in a decreased bandgap.^[23] Thus, a bandgap of 1.1 eV can be reached by electron-withdrawing nitro groups and electron-donating amino groups, respectively. As can be seen in Figure 19, this is due to the generated high zwitterionic and quinoid character.^[164]

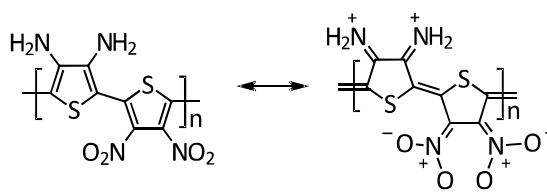


Figure 19: Influence of electron-donating and electron-withdrawing groups.^[23,164]

The most successful approach to materials with a reduced bandgap is the design of low bandgap polymers. These polymers consist of an alternating arrangement of electron-rich donor units D and electron-deficient acceptor unit A in the polymer backbone. The introduced push and pull forces facilitate the electron delocalisation and the formation of quinoid mesomeric structures $D-A \rightarrow D^+=A^-$ that lowers the bond length alteration and the bandgap. The alternating donor and acceptor group cause a photoinduced intramolecular charge transfer from the high lying HOMO of the donor unit to the low lying LUMO of the acceptor unit. This is ascribed to the hybridisation of the molecular orbitals of the donor and the acceptor in the D-A polymer and is illustrated in Figure 20.^[23,42]

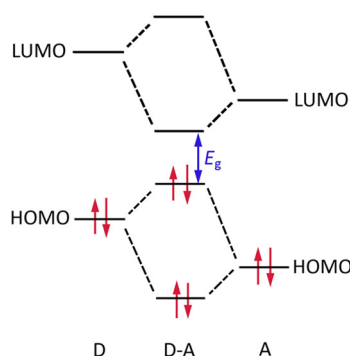


Figure 20: Hybridisation of the molecular orbitals of donor D and acceptor A in an alternating D-A polymer. The bandgap of the polymer is depicted by E_g .^[23]

2. Introduction

The HOMO of the donor group interacts with the HOMO of the acceptor unit and two new HOMO levels for the D-A polymer are formed. The same applies to the LUMO levels. As the electrons are redistributed to the hybridised orbitals, a higher lying HOMO and a lower lying LUMO are generated. In consequence, the alternating D-A polymer exhibits a lower bandgap. The value of the bandgap can be influenced by the choice of donor and acceptor in the favoured way. Thus, applying a strong donor like pyrrole and a strong acceptor such as benzothiadiazole leads to a bandgap of 1.1 eV. This can also be attributed to additional intramolecular hydrogen bonds that results in planarization and supramolecular interactions. Thus, a densely packed and ordered crystalline structure is built in the solid state.^[23] All strategies for the modification of the bandgap are summarized in Figure 21.

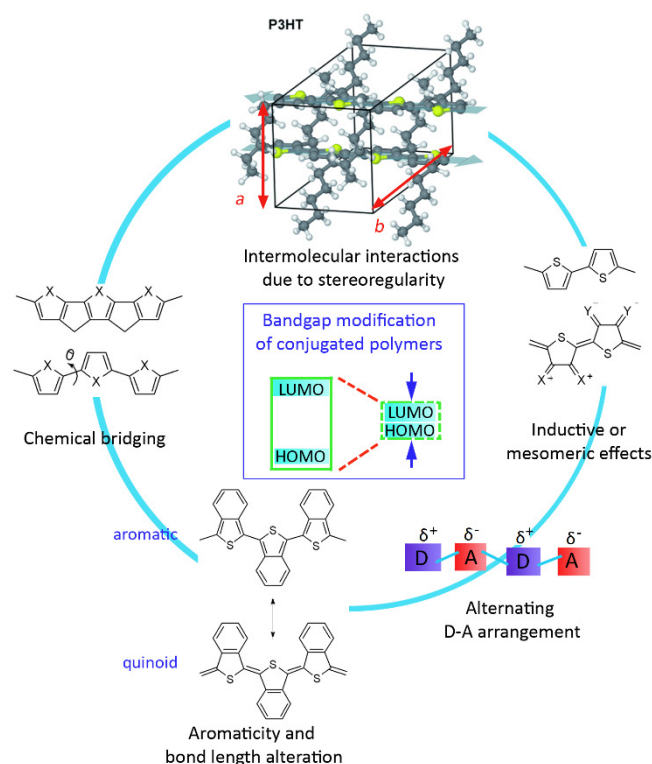


Figure 21: Strategies for the bandgap modification of conjugated polymers. The lattice parameters are denoted by a and b and the angle of torsion is illustrated by θ .^[23,165]

Another important parameter for the classification of conjugated polymers as materials for solar cells is the charge carrier mobility.^[23,42] The properties of the material regarding the charge transport are strongly associated with the methods for the design of conjugated polymers. A facile electron delocalisation and the planarity of the molecules are of vital importance for a high hole transport mobility.^[23] Low charge carrier mobilities are the reason for bimolecular charge carrier recombination that is in competition with charge carrier collection. Due to recombination, the photocurrent is reduced. In addition, the value of the fill factor decreases and the charge separation becomes more inefficient because of the bad charge carrier mobility. In 2010, W. Zhang presented a conjugated polymer with a hole transport mobility of $1 \text{ cm}^2 \text{ V}^{-1} \text{ s}^{-1}$.^[166] On the other hand, the balanced charge transport of holes and electrons within

the blend is an important factor for the performance of BHJ solar cells. An imbalanced transport leads to the accumulation of space charges and a high recombination rate that limits the fill factor.^[42]

For the fabrication of solar cells, conjugated polymers have to be solved in organic solvents. The solubility of the polymer depends on several structural parameters like the degree of polymerisation, the chain length of aliphatic spacers, the polarity of substituents, the rigidity of the polymer backbone, the regioregularity, and the intermolecular interactions. The solubility in turn influences the crystallinity, the phase behaviour, the morphology, and the contact between the different active materials and thus affects the solar cell performance. The major reason for the insolubility of polyaromatic conjugated polymers is the strong π - π interaction between the polymer chains. The incorporation of aliphatic side chains that are attached covalently to the main chain of the polymer improves the solubility. Branched alkyl chains are more effective than unbranched spacers. However, it has to be taken into account that the increasing amount of isolating alkyl chains compared to the hole transporting fraction in the polymer can reduce the charge carrier mobility.^[23] Thus, the choice of the solubilizing groups and their positioning has to be carried out carefully.^[23,42] The aliphatic spacers also influence the self-assembling ability of the molecules and the angle of torsion. To prevent steric effects, the substituents are attached regioregular.^[42]

Further important properties of conjugated polymers for the application in organic solar cells besides the already mentioned parameters are facile processability, a simple synthesis, high attainable purities, and photochemical stability.^[42]

2.6 General synthetic strategies for conjugated polymers

Commonly, conjugated polymers are synthesized by the efficient formation of a carbon-carbon single bond between two unsaturated carbons of the aromatic monomers. Besides electrochemical or chemical oxidative polymerizations, especially transition metal catalysed crosscoupling reactions are suited for the development of C_{sp^2} - C_{sp^2} and C_{sp} - C_{sp^2} bonds. These reactions comprise an oxidative addition between a carbon-halogen bond of an electrophile catalysed by a transition metal, a subsequent transmetallation with an organometallic main group nucleophile and a concluding reductive elimination that leads to the formation of the carbon-carbon-bond while retaining the catalyst.^[23] The schematic illustration of such a catalytic cycle is shown in Figure 22.

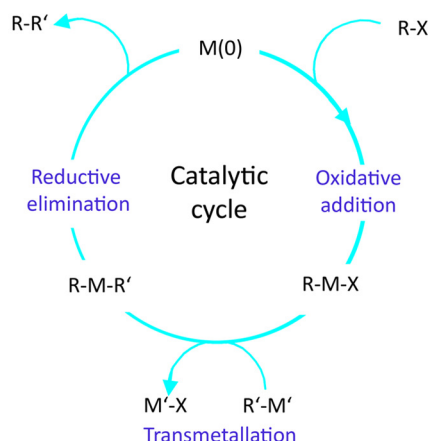


Figure 22: Catalytic cycle of a transition metal catalyzed crosscoupling reaction. The catalyst is represented by $M(0)$, the organohalide by $R-X$, the organometallic compound by $R'-M'$ and the resulting product by $R-R'$.^[23]

The most frequently used catalysts are nickel and palladium complexes.^[23] As organometallic nucleophiles, Grignard reagents (Kumada-Corriu coupling),^[167] tin organyls (Stille coupling),^[168] boron compounds (Suzuki-Miyaura coupling)^[169] or copper compounds (Sonogashira coupling)^[170] are applied. The conjugation length of the product is increased with each passage of the catalytic cycle. Another advantage are the mild reaction conditions that tolerate a lot of functional groups. Stille and Suzuki couplings are the most efficient methods for the synthesis of alternating copolymers. It has to be pointed out that stannyl functionalities exhibit a poor reactivity with aryl halides under Stille conditions. Thus, Stille couplings are used for polymers on the basis of thiophene with the stannyl groups attached to the thiophene ring. However, the Suzuki coupling is suitable for benzene-based polymers. Here, the benzene ring of the monomer carries the boron group. The homopolymerization of a single monomer is conducted via a nickel-catalyzed Yamamoto coupling that comprises a dehalogenation. For the formation of a carbon-carbon double bond for a polymer containing vinylene, Wittig-Horner reactions or Knoevenagel condensations are utilized.^[23] Furthermore, PPVs can also be synthesized from organohalides and vinylbenzene units via Heck coupling reactions under palladium catalysis.^[23,171]

2.7 Polycarbazoles as materials for organic solar cells

Carbazole presents an interesting unit for conjugated polymers for several reasons. On the one hand, *9H*-carbazole is an inexpensive starting material. The completely aromatic configuration implicates a good stability. On the other hand, the nitrogen atom can be easily substituted with a multitude of functional groups. By this means, the solubility as well as the optical and electronical properties of the polymer can be influenced without causing steric interactions close to the polymer backbone. The bandgap of polycarbazole derivatives is lower than for polyphenylenes because of the bridged biphenyl unit. The carbazoles can be linked either at the positions 3 and 6 leading to poly(3,6-carbazole) or at the positions 2 and 7 resulting in poly(2,7-carbazole). The two polymers exhibit different properties and thus different fields of application.

Figure 23 shows the chemical structures of both polycarbazoles as well as the 9*H*-carbazole unit.^[59,172]

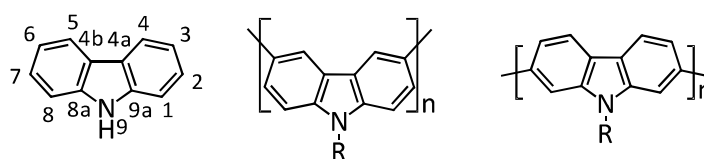


Figure 23: Chemical structures of 9*H*-carbazole (left), poly(3,6-carbazole) (middle), and poly(2,7-carbazole) (right).^[172]

Poly(3,6-carbazole)s possess a meta-linkage of the monomers units. In consequence, the conjugation length of dimeric units that can be considered as 4,4'-biphenyl building blocks is short.^[23,172] The materials are suited for the application in OFETs and OLEDs due to their high charge carrier mobilities as well as a blue luminescence arising from the short conjugation length.^[172,173] The para-linkage and thus the higher conjugation length enables the better migration of charge carriers along the polymer chain. For this reason, poly(2,7-carbazole) can be used as an efficient donor material for organic solar cells.^[23,172] Further factors are the low-lying HOMO level of the poly(2,7-carbazole)s that is important for the stability of the material in air and a high open-circuit voltage. With suitable structures and a good self-organization of the polymer chains, high hole transport mobilities can be achieved. Finally, the absorption spectrum can be adjusted to the solar spectrum by the copolymerisation with appropriate comonomers.^[23,59]

The synthetic route towards the 2,7-dibromocarbazole starting material requires several steps.^[174–176] The group of K. Müllen reported an efficient synthesis with only two steps in 2003 as depicted in Figure 24.^[177]

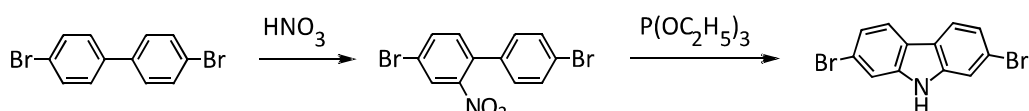


Figure 24: Synthetic strategy for the 2,7-dibromocarbazole unit.^[177]

The first step is the nitration of 4,4'-dibromobiphenyl using concentrated nitric acid yielding 4,4'-dibromo-2-nitrobiphenyl. Subsequently, 2,7-dibromocarbazole was received by a reductive Cadogan ring closure in presence of triethyl phosphate.^[177–179]

K. Müllen et al. applied a soluble and thus well processable poly(2,7-carbazole) as a donor material in a BHJ solar cell for the first time. The polymer was equipped with a branched 2-decyltetradecyl substituent and was synthesized via Yamamoto coupling. Perylene tetracarboxydiimide was used as an acceptor. The donor polymer exhibited a low HOMO level of -5.6 eV yet a relatively high bandgap of 3.0 eV. The solar cell reached a high V_{oc} value of 0.71 V, but just 0.6% efficiency could be achieved. This is attributed to the absorption spectrum of the

2. Introduction

active layer that only conforms badly to the solar spectrum.^[180] The chemical structures of the applied materials are presented in Figure 25.

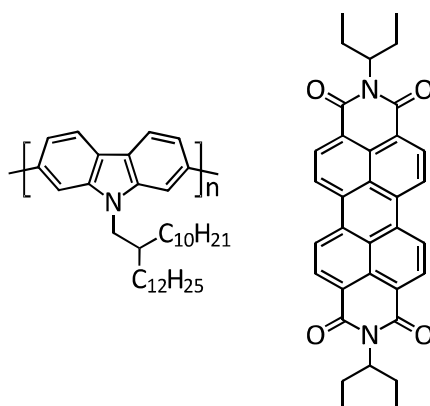


Figure 25: Chemical structures of the materials of the first organic solar cell comprising a poly(2,7-carbazole) derivative.^[180]

For a better correlation of the absorption with the solar spectrum, poly(2,7-carbazolevinylene) derivatives exhibiting a low bandgap were synthesized by using electron-withdrawing comonomers and thus realizing D-A polymers. Mostly Horner-Emmons reactions were conducted as these lead to a very high purity of the materials but a further polymer was also synthesized via Stille coupling.^[23,59] The chemical structures of the polymers can be seen in Figure 26.

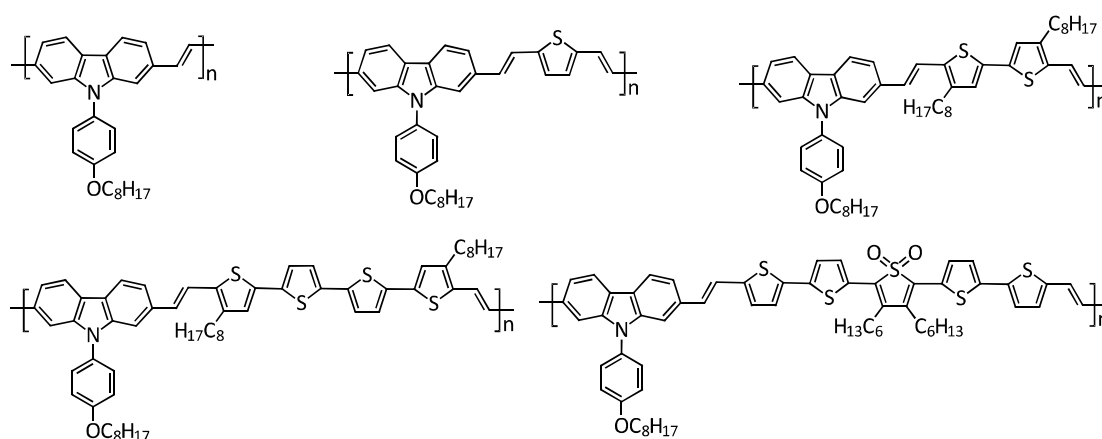


Figure 26: Chemical structures of different poly(2,7-carbazolevinylene)s.^[59]

The polymers show bandgaps between 2.3 eV and 1.7 eV while the HOMO levels lie between -5.6 eV and -5.5 eV.^[23] The bandgap decreases with increasing number of thiophene rings. The HOMO levels are also reduced with rising conjugation length except for the polymer with the non-aromatic thienyl dioxide unit. This building block possesses two localized carbon-carbon double bonds and two sulphur-oxygen bonds resulting in a higher electron affinity and thus a lower LUMO level.^[59] However, the efficiencies of solar cells comprising the presented donor polymers and PCBM as acceptor remain low between 0.2% and 0.4% for the first four materials. The best PCE of 0.8% was achieved with the thienyl dioxide containing polymer. Furthermore, a high open-circuit voltage of 0.8 V was observed.^[23,59] In fact, the polymers exhibit

a low solubility and a low molecular weight that limits the performance of the solar cells. A further reason for the loss of efficiency is that the vinylene unit can also be damaged due to photooxidation.^[59]

Several poly(2,7-carbazole) derivatives including electron-withdrawing units were synthesized in the group of M. Leclerc.^[181,182] Figure 27 shows the chemical structures of these polymers.

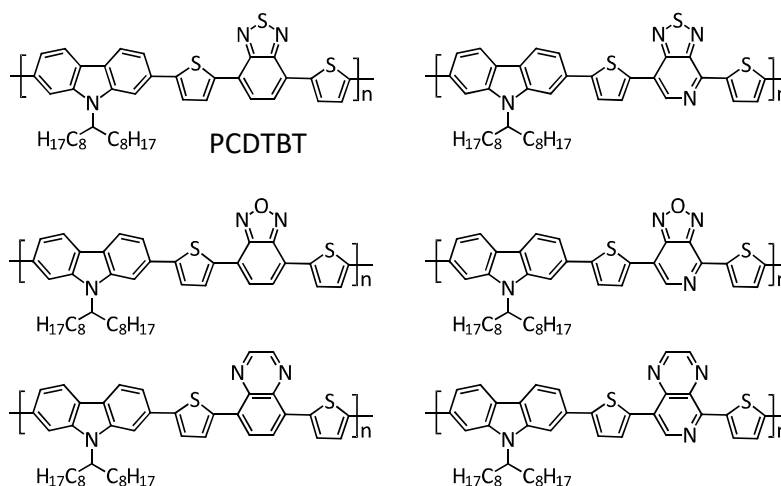


Figure 27: Chemical structures of different alternating poly(2,7-carbazole) copolymers including PCDTBT.^[182]

Three of the electron-deficient units are symmetric and possess a benzene core. The other three building blocks include an asymmetric pyridine core. The HOMO levels of the polymers lie between -5.6 eV and -5.4 eV what is mostly determined by the carbazole part. The LUMO levels differ depending on the electron-withdrawing unit. The polymers containing pyridine are optimized with regard to the LUMO values that lie 0.25 eV lower than that of the benzene-based polymers. However, a better structural organisation of the symmetric polymers in the solid state leads to a higher charge carrier mobility and thus to a better performance of the solar cells in combination with PCBM as acceptor. The polymers with pyridine core show PCE values between 0.7% and 1.1% whereas the polymers with benzene core reach efficiencies between 1.8% and 3.6%. Using the symmetric polymers, also higher open-circuit voltages between 0.8 V and 1.0 V are achieved.^[23] The best results were received with the combination of carbazole and a 2,1,3-benzothiadiazole unit yielding poly-[(*N*-heptadecan-9'-yl)-2,7-carbazole-*alt*-5,5-(4',7'-bis(thien-2-yl)-2',1',3'-benzothiadiazole)] (PCDTBT).^[181] High molecular weights, good film-forming properties and high hole mobilities up to $3 \cdot 10^{-3} \text{ cm}^2\text{V}^{-1}\text{s}^{-1}$ could be realized.^[59] In combination with different acceptor fullerenes, the hole mobilities of the blends lie in the range of $10^{-4} \text{ cm}^2\text{V}^{-1}\text{s}^{-1}$.^[183] The bandgap of PCDTBT is 1.9 eV with a HOMO level of -5.5 eV and a LUMO value of -3.6 eV. An open-circuit voltage of 0.9 V and a PCE of 3.6% were achieved.^[23] This conforms to the findings of the group of W. H. Jo about the evaluation of the effects of different acceptor units identifying benzothiadiazole as an optimal acceptor monomer. The performance of low bandgap polymers containing 2,1,3-benzothiadiazole BT, diketopyrrolopyrrole DPP, isoindigo I, thieno[3,4-*c*]pyrrole-4,6-dione TPD, and 3-fluorothieno[3,4-*b*]thiophene TT regarding the short-circuit current, the open-circuit voltage, the fill factor, and the power

conversion efficiency was compared. Whereas DPP polymers show the highest I_{sc} due to the low bandgaps, TPD-based polymers exhibit the highest V_{oc} ascribed to the deep HOMO levels. Polymers comprising BT and TT achieve intermediate values. Regarding the fill factor, DPP and isoindigo polymers reach lower values than the others. In the case of the PCE, the best results are attained with polymers based on BT and TT. The values of 9.55% and 9.30%, respectively, represent the average values of the top five devices that were reported for the polymer containing the corresponding acceptor unit.^[184]

The performance of PCDTBT were optimized by the group of A. J. Heeger. The use of a titanium dioxide electron transport layer and the incorporation of silver nanoparticles in blends composed of PCDTBT and PC₇₀BM led to an increased open-circuit voltage, short-circuit current, fill factor, and EQE that can be attributed to an improved light absorption and charge transport. In summary, an efficiency of 7.1% is reached.^[185] In addition, BHJ solar cells made from PCDTBT and PC₇₀BM were modified with an electron transport layer of graphene oxide that was deposited via a stamping procedure. By combining the graphene oxide layer with titanium oxide, a high efficiency of 7.5% is achieved.^[186]

2.8 Polycyclopentadithiophenes as materials for organic solar cells

The aromatic unit 4*H*-cyclopenta[2,1-*b*:3,4-*b'*]dithiophene (CPDT) is of particular interest as a donor monomer for the synthesis of low bandgap polymers as it shows some beneficial properties. CPDT exhibits structural analogy to fluorene due to the covalent bridging of a 2,2'-bithiophene unit by a sp^3 hybridized carbon atom at the 3,3'-position resulting in a completely coplanar structure. Thus, the intrinsic properties of the basic bithiophene are modified towards enhanced intermolecular interactions and a widened conjugation leading to a lower bandgap. In addition, the 4-position of the carbon bridging atom of CPDT can be substituted by two side chains that not only improve the solubility but also allow the adjustment of electrical and steric properties. Figure 28 depicts the chemical structures of the 4*H*-CPDT core and the corresponding disubstituted polycyclopentadithiophene homopolymer.^[23,187,188]

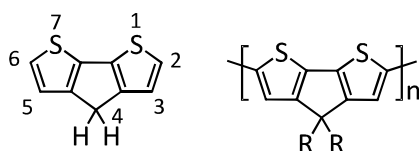


Figure 28: Chemical structures of 4*H*-cyclopentadithiophene (left) and the disubstituted polycyclopentadithiophene homopolymer (right).^[188]

Several steps are needed for the synthesis of the CPDT starting material.^[189–192] For cyclopentadithiophene-4-one that acts as a precursor for CPDT, an efficient synthetic route including only three steps was presented in 2002. Here, a lithiation and subsequent nucleophilic addition is combined with a lithiation and iodination reaction receiving bis(2-iodothiophen-3-

yl)methanol out of 3-bromothiophene in one step.^[193] However, only low yields were achieved due to the limited control of the reaction. Thus, the group of C.-S. Hsu introduced two separate steps as shown in Figure 29.^[187]

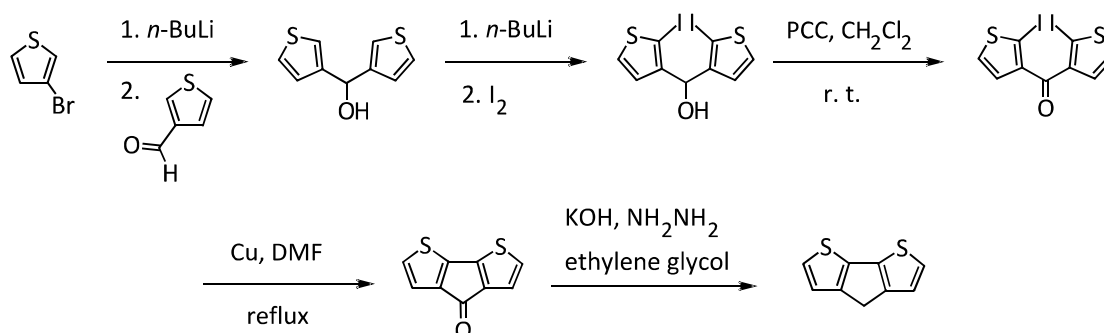


Figure 29: Synthetic strategy for the CPDT unit.^[187]

In this case, 3-bromothiophene is first lithiated with *n*-butyllithium and reacted with 3-formylthiophene giving di(thiophen-3-yl)methanol. Subsequent lithiation of this secondary alcohol and conversion with iodine leads to bis(2-iodothiophen-3-yl)methanol. After oxidation in presence of pyridinium chlorochromate PCC, the ring closure of the received ketone is carried out via an Ullmann coupling. The last step to the CPDT core is a Wolff-Kishner reduction with hydrazine.^[187]

Electropolymerized homopolymers of cyclopentadithiophene-4-one and 4-(dicyanomethylene)-cyclopentadithiophene are illustrated in Figure 30. The ketone and cyano functionalities at the bridging atom act as electron withdrawing units leading to a lower aromaticity and thus increasing the quinoid character. In consequence, narrow bandgaps of 1.2 eV and 0.8 eV can be achieved, respectively.^[23,194,195]

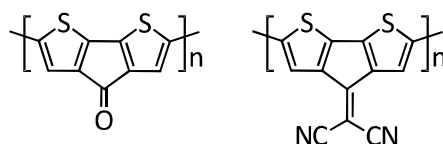


Figure 30: Chemical structures of polycyclopentadithiophen-4-one (left) and poly(4-(dicyanomethylene)cyclopentadithiophene) (right).^[23]

P. Coppo et al. presented the first polycyclopentadithiophene that can be processed from solution due to the substitution with two aliphatic spacers. Hexyl, octyl, and hexadecyl side chains were applied. The polymers were realized by oxidative polymerization in presence of iron(III) chloride as well as Kumada coupling reactions catalysed by nickel. In comparison to poly(3-alkylthiophene) and polyfluorene that bear the analogous spacers, the bandgap could be decreased to about 1.7 eV to 1.8 eV. No self-assembling ability of the polymer chains could be observed as there is no change in position of the absorption maximum of solution and thin film spectra.^[23,196]

Donor-acceptor polymers containing CPDT cores as donor units and different acceptor units were realized to achieve a broader exploitation of the solar spectrum. The well-known PCPDTBT comprises benzothiadiazole groups besides the CPDT units and was first synthesized by the group of C. J. Brabec. In addition, the absorption properties of this alternating copolymer were finetuned by the variation of the ratio of donor and acceptor to cover the complete solar spectrum. This was realized by reducing the amount of benzothiadiazole acceptor monomer and including both CPDT and bithiophene donor monomers, leading to a series of copolymers with a random arrangement of the donor-acceptor segments. For comparison, the copolymer from the two donor units CPDT and bithiophene was also realized. The polymerizations were carried out under Stille conditions.^[23,197] Figure 31 depicts the corresponding chemical structures of the polymers.

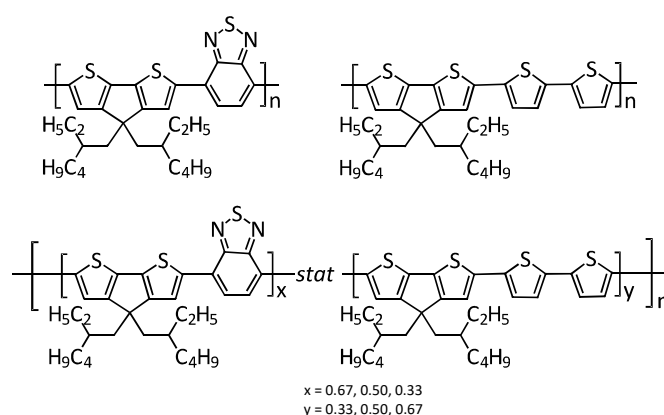


Figure 31: Chemical structures of PCPDTBT (top left), an alternating copolymer comprising CPDT and bithiophene units (top right) and a statistical copolymer of CPDT, bithiophene and benzothiadiazole (bottom).^[197]

By comparing the absorption of PCPDTBT and the copolymer made from the two donor monomers, the importance of acceptor units to cover longer wavelength regions is pointed out. The absorption shifts to the blue when unbridged bithiophene donor units are combined with cyclopentadithiophene. When applying a ratio of the two donor monomers between 2:1 and 1:2 in the statistical copolymers, the complete visible range is covered. The absorption of the polymer films exhibit a significant shift to the red in comparison to the solution spectra, correlating with an increasing amount of benzothiadiazole units. Thus, intramolecular interactions are introduced by the addition of benzothiadiazole acceptor monomers. In contrast, no self-assembling ability could be observed for the CPDT homopolymer. The most promising polymer out of this series is PCPDTBT, showing a high solubility in organic solvents because of the substitution with two ethylhexyl chains. The fabrication of BHJ solar cells is facilitated as PCPDTBT is well miscible with PCBM. A HOMO level of -5.3 eV and a LUMO level of -3.6 eV were determined. Solid-state absorption measurements revealed an optical bandgap of 1.4 eV that is in the ideal range for BHJ solar cells comprising donor polymers and acceptor fullerenes. A short-circuit current of 11.8 mA/cm² and an open-circuit voltage of 0.65 V resulting in an efficiency of 3.5% could be reached with a BHJ solar cell made from PCPDTBT and PC₇₁BM. In contrast, the copolymers with additional bithiophene donor units gave PCEs up to 3%. The good result

achieved with the PCPDTBT blend can be ascribed to an increased EQE that is higher than 25% in the spectrum between 400 nm and 800 nm with a maximum value of 38% at 700 nm.^[23,197] Furthermore, photocurrent generation also occurs above 900 nm. Besides the broad absorption range, the planar geometry of PCPDTBT is responsible for a good intermolecular charge carrier transport with hole mobilities about $2 \cdot 10^{-2} \text{ cm}^2\text{V}^{-1}\text{s}^{-1}$.^[23,198] The performance of solar cells made from blends of PCPDTBT and PC₇₁BM can be enhanced to 5.5% when using 1,8-octanedithiol as a processing additive in the spin coating solution. This is attributed to an optimization of the active layer morphology resulting in an increased photoconductivity and charge carrier lifetime.^[23,199] As PCPDTBT is a mainly amorphous donor polymer and shows only small crystalline fractions, the morphology can be improved more easily by the application of processing additives than by thermal annealing after spin coating of the active layer.^[23,200,201] In 2007, A. J. Heeger and coworkers presented a tandem solar cell comprising PCPDTBT as a small bandgap donor in one subcell and P3HT that exhibits a larger bandgap in the other subcell. The combination of the two complementary absorbers results in an efficient exploitation of the sunlight. Thus, an efficiency of over 6% was reached.^[23,202] Because PCPDTBT was one of the first low bandgap polymers that achieved high efficiencies in organic solar cells, the photophysical properties of blends with PCBM were comprehensively studied. These investigations included photoconductivity,^[203] charge separation,^[204] as well as charge transport.^[205]

A PCPDTBT derivative with hexyldecyl spacers instead of ethylhexyl chains were realized by the group of K. Müllen.^[206] The chemical structure of this polymer is shown in Figure 32.

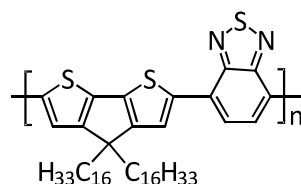


Figure 32: Chemical structure of a PCPDTBT derivative with hexyldecyl spacers.^[206]

The unbranched hexyldecyl substituents support a better alignment of the polymer chains leading to a high hole mobility of $0.17 \text{ cm}^2\text{V}^{-1}\text{s}^{-1}$ in OFET devices.^[206]

Besides benzothiadiazole, also other acceptor monomers were combined with the CPDT donor core. A. J. Moulé et al. compared PCPDTBT with two novel low bandgap polymers comprising quinoxaline and dithienylbenzothiadiazole units as presented in Figure 33.^[207]

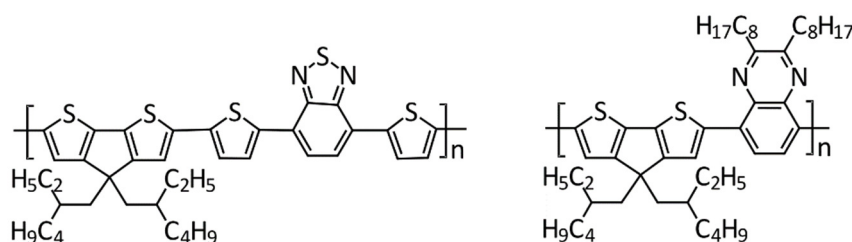


Figure 33: Chemical structures of different poly(cyclopentadithiophene)s.^[207]

Several solvent mixtures for device preparation were examined. The best results were achieved with a volume ratio of 19:1 of chlorobenzene and anisole for a blend from the polymer comprising CPDT and dithienylbenzothiadiazole and PC₆₁BM. By this means, an efficiency of 2.1% was achieved due to an improved active layer morphology.^[207] In addition, benzothiadiazole was also substituted by the structurally analogous 2,1,3-benzoselenadiazole and coupled with CPDT in a Stille reaction.^[208] Figure 34 illustrates the resulting polymer.

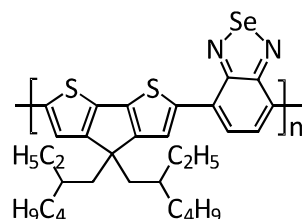


Figure 34: Chemical structure of a PCPDTBT derivative with benzoselenathiazole.^[208]

However, a PCE of only 0.89% with a short-circuit current of 5 mA/cm² and an open-circuit voltage of 0.52 V was reached in a blend with PC₇₀BM. This could be attributed to the lower absorption in comparison to PCPDTBT and an unbalanced transport of holes and electrons in the blend layer.^[208] Further studies applying different acceptor units like benzoxadiazole or thienopyrazine were carried out by the groups of C.-S. Hsu and M. L. Turner.^[187,209] Furthermore, the optimal ratio of CPDT and benzothiadiazole in a low bandgap polymer was investigated. The best results were achieved with a 2:1 ratio.^[210]

The best solar cell performance of 3.5% of PCPDTBT can be further increased by the fluorination of the benzothiadiazole acceptor monomer at the 5-position. In combination with PC₇₀BM, the best device reached a PCE of 6.2%. This can be attributed to a higher V_{oc} due to a larger ionization energy of the fluorinated derivative. Furthermore, the recombination of electrons and holes is reduced leading to a higher fill factor and I_{sc}.^[211]

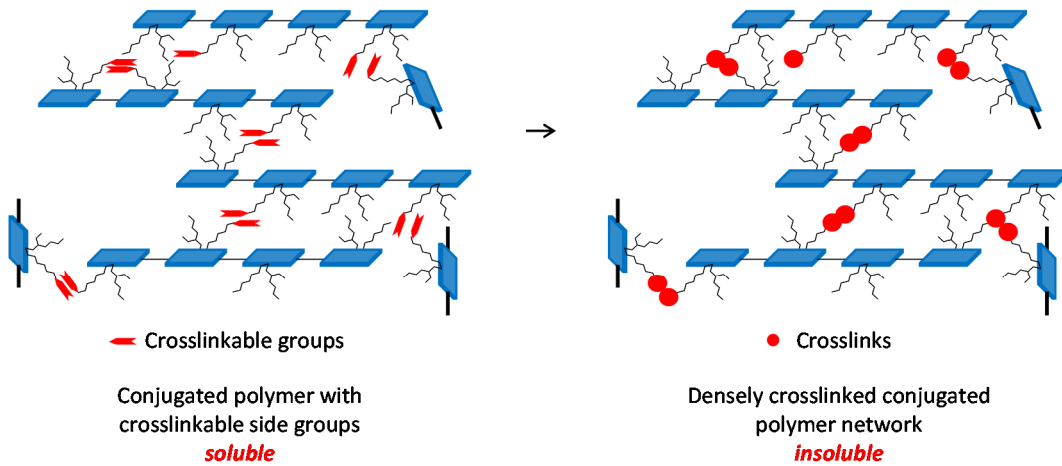
2.9 Stabilization of organic solar cells via crosslinking

The active layer of organic solar cells that consist of an electron donor and an electron acceptor is fabricated by different methods with respect to the solar cell geometry. The blend layer of BHJ solar cells is solution processed. Conjugated polymers are often used as donor materials and low molecular weight fullerenes are applied as acceptors.^[63,184,212,213] In opposite to the solution processing approach, vacuum evaporation enables the subsequent deposition of several layers made from different small molecules. By this means, each layer can be optimized separately from the others. Both FHJ and BHJ morphologies as well as multilayer and tandem solar cells can be realized by vacuum evaporation. Nanostructured active layers combine the advantage of a high interfacial area that allow the excitons to reach the interface within their diffusion length of about 10 nm and act as direct charge transport pathways towards the electrodes.^[214] However, the long-term stability of organic solar cells is a major issue as the devices suffer from

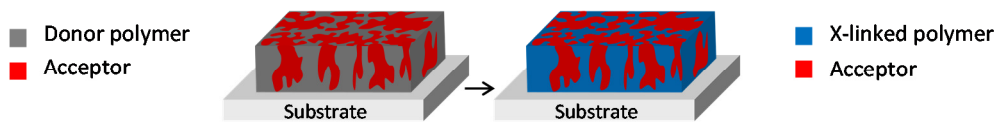
the exposure to heat or light as well as chemical and mechanical demands.^[96] If the device is encapsulated, the damage of the solar cell regarding oxygen and water can be inhibited.^[215] Thermal stress enhances the diffusion of small molecule acceptors like fullerenes within the donor polymer matrix. This leads to the formation of large fullerene aggregates diminishing the device performance.^[216–218] The realization of multilayer solar cells made from solution processed polymers is difficult compared to evaporable low molecular weight materials as the underlying layer is dissolved and damaged by the spin coating of a second polymer solution. Thus, for the prevention of the dissolution of the first polymer layer orthogonal solvents can be used for the different deposition steps.^[219] Furthermore, inorganic interlayers are often used for the fabrication of tandem solar cells.^[149,151,155] In addition, nanoimprinted patterns can also be protected from damage by the use of orthogonal solvents.^[214,220]

Crosslinking presents one possibility to solve the stability issues concerning organic solar cells.^[221,222] The basic principle of crosslinking is shown in Figure 35a. As an example, a conjugated polymer bearing crosslinkable units is chosen. This polymer can be solution processed due to its solubility before crosslinking. A (photo)initiator, UV light or heat can be used to start the crosslinking reaction. During the crosslinking procedure, the single polymer chains get connected by the formation of covalent bonds formed by the crosslinkable groups. Thus, the soluble conjugated polymer is transferred into a densely crosslinked network that is insoluble. That means, that the initial morphology of the material is advantageously “frozen” upon crosslinking. By means of crosslinking of materials, different concepts concerning the morphology of organic solar cells become realizable. First, the BHJ geometry can be stabilized as presented in Figure 35b. A crosslinkable donor polymer is exemplarily used. The crosslinking process renders the polymer insoluble and thus the morphology of the initial donor-acceptor blend is saved. Additionally, the small molecular weight acceptors like C₆₀ or PCBM are hindered to diffuse through the polymer matrix. As a consequence, the BHJ morphology of organic solar cells can be stabilized. Second, the realization of multilayer solar cells by solution processing of polymers is facilitated. Figure 35c illustrates the multilayer formation made from a donor and an acceptor material that can be crosslinked. The first step is the spin coating of the donor onto a substrate followed by crosslinking via an initiator. The acceptor solution can be deposited on top due to the achieved insolubility of the donor layer that prevents the underlying layer from damage or dissolution. Even complex multilayer devices where each layer exhibits a specific function can be designed when the functional materials are available in a crosslinkable form. The last issue is the stabilization of nanostructures at the donor-acceptor interface as depicted in Figure 35d. Here, a crosslinkable donor polymer is deposited on a substrate and imprinted by a stamp. The subsequent crosslinking renders the donor material insoluble and thus the pattern is stabilized. Acceptor deposition either from solution or vacuum evaporation is possible without damage of the underlying layer.

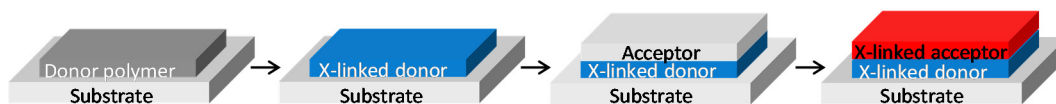
a) Crosslinking principle



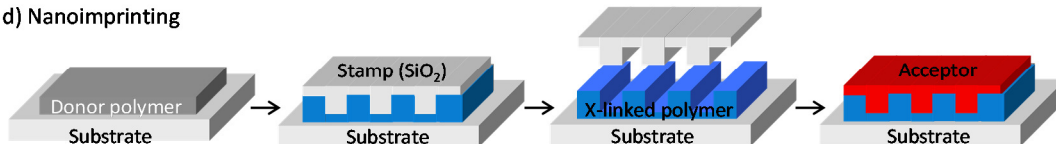
b) BHJ stabilization



c) Multilayer formation



d) Nanoimprinting



e) Popular crosslinkable units and requirements for crosslinking

Crosslinkable unit	Structure	Requirements
Bromine		UV exposure or thermal activation
Vinyl		Additional annealing step
Acrylate		photoinitiator, UV exposure or thermal activation Additional annealing step
Azide		UV exposure or thermal activation Additional annealing step
Oxetane		Photoacid generator or acid Annealing step

Figure 35: a) Basic crosslinking procedure applying a crosslinkable donor polymer. b) BHJ morphology stabilization via crosslinking of the donor polymer. c) Realization of a multilayer setup with crosslinkable donor and acceptor materials. d) Nanoimprinting with a stamp using a crosslinkable donor polymer. e) Crosslinkable units and corresponding requirements for the crosslinking process. Reprinted from Appendix D.

Active layers of organic solar cells can be crosslinked by either crosslinking the donor or the acceptor as well as crosslinking both materials. The most popular approach is the application of crosslinkable donor materials. Conjugated polymers with aliphatic sidechains required for solubilisation are often used as donor materials. Thus, the crosslinkable groups are usually attached to these sidechains. Frequently used crosslinkable units include bromine, vinyl, acrylate, azide, and oxetane functionalities. Figure 35e illustrates the chemical structures as well as the crosslinking requirements for the different units.^[222] The initiation of the crosslinking process is conducted by exposure to UV light or thermal activation in the case of bromine, vinyl, acrylate, and azide crosslinking groups. Regarding acrylates, photoinitiators can also be applied to start the crosslinking reaction. Oxetane functionalities are crosslinked via cationic ring opening polymerisation that is activated with a photoacid generator, acid or prolonged heat exposure.^[223] As for all cyclic ethers, this polymerisation mechanism proceeds with high reaction rate.^[224] An annealing step is required for oxetane units to ensure complete crosslinking of the polymer, whereas this treatment is optional in the crosslinking protocol of bromide, vinyl, acrylate, and azide groups. Besides the advantages discussed above, crosslinking can yet induce some issues depending on the different functionalities. The charge carrier mobility and other device properties can deteriorate if unreacted bromine units remain in the material. When photoinitiators are applied for the crosslinking of acrylates the decomposition products of the photoinitiator stay in the polymer and can negatively influence the device performance. The crosslinking of azide groups proceeds via the elimination of nitrogen and the formation of nitrene species. These nitrenes exhibit a very high reactivity and thus the crosslinking reaction may not only be limited to the aliphatic sidechains of the polymer but also the conjugated polymer backbone can be attacked. Regarding oxetane crosslinking, remaining acid or the photoinitiator residues like counterions can decrease the device properties. Compared to the free radical reaction mechanism in the case of bromine, vinyl, and acrylate, a big advantage of the cationic ring opening polymerization of oxetane groups is that the crosslinking process can be also executed in the presence of fullerenes that are known as radical scavengers.^[225–228] Further advantages of oxetane crosslinking include no inhibition by oxygen, insignificant impact on electronical and optical characteristics as well as tolerance of the oxetane unit towards the highly basic conditions of coupling reactions catalysed by transition metals.^[229] In contrast, Suzuki coupling does not tolerate acrylate units. Thus, protective group chemistry has to be used. Afterwards, the acrylate functionalities have to be recovered by polymer analogous reactions.^[230,231]

A variety of polymers have already been modified with the presented crosslinkable units. Figure 36 depicts the chemical structures of these crosslinkable polymers.

2. Introduction

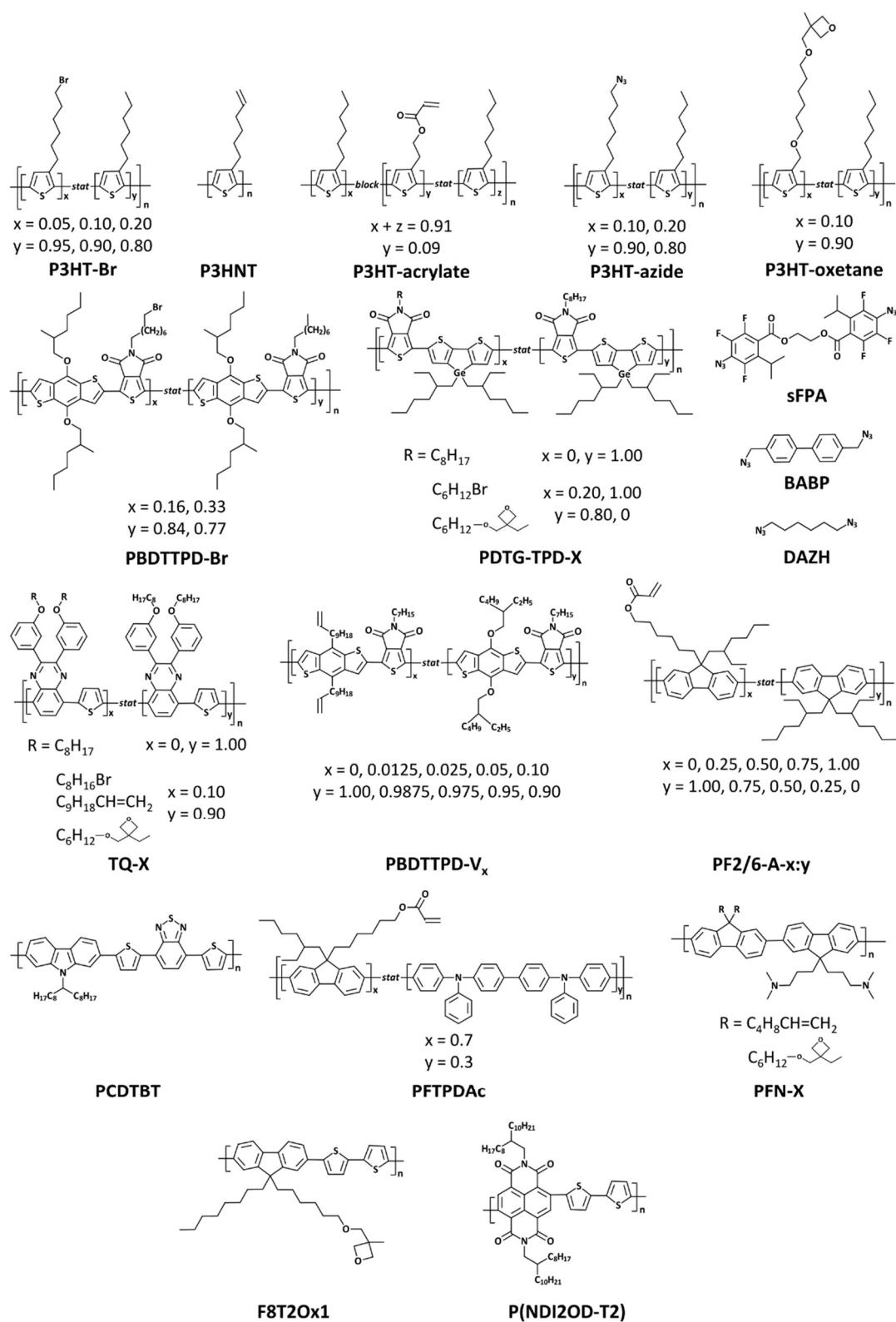


Figure 36: Chemical structures of different crosslinkable conjugated polymers and small molecule crosslinkers. The IUPAC nomenclature was applied with *-stat-* for statistical and *-block-* for block copolymers. Reprinted from Appendix D.

The frequently applied donor polymer P3HT has been described bearing different crosslinking functionalities. The bromine containing derivative P3HT-Br has been synthesized by Kim et al. with a bromine content up to 20%. Via photocrosslinking by exposure to UV light, planar as well as bulk heterojunction geometries were realized. While the best FHJ solar cell exhibited an efficiency of 2.2% by applying a polymer with 10% bromine, an efficiency of 3.4% could be achieved with a BHJ architecture comprising a P3HT-Br with 5% bromine content. The efficiency stabilization of the two setups upon crosslinking was tested at 150 °C. The FHJ device revealed stability up to three days whereas the BHJ device was stable up to two days.^[232] Miyanishi et al. presented P3HNT that was modified with vinyl functionalities. BHJ solar cells were prepared by thermal crosslinking. Stability tests were performed at 150 °C for 10 h and verified by optical microscopy. The stability of the non-crosslinked P3HT reference cells was lower than the crosslinked cells containing P3HNT. However, the aggregation of PCBM could not be completely prevented.^[233] Acrylate units were attached to one block of a P3HT diblock copolymer. Thermal crosslinking of BHJ solar cells containing this derivative resulted in the retention of 85% of the initial efficiency after annealing the devices at 110 °C for 165 h. The reference cells containing non-crosslinkable P3HT revealed a drop of their initial efficiency to 65%.^[234] Furthermore, a P3HT derivative with up to 20% of azide was synthesized. BHJ solar cells were prepared from P3HT mixed with 15% of the derivative containing 10% azide units and PCBM. The stability of the photocrosslinked cells was confirmed after annealing at 150 °C for 40 h. The devices retained their initial efficiency of 3.3%.^[235] Finally, Brotas et al. realized a P3HT derivative that can be crosslinked by a cationic mechanism by introducing 10% of oxetane groups. Crosslinking was initiated by the exposure to UV light in presence of a photoacid generator and completed with an annealing step. However, the efficiency of the BHJ solar cells made from the modified polymer decreased to 1.1% in contrast to 1.9% for the P3HT reference device. The efficiency is further reduced to 0.2% when the active layer is crosslinked but the devices remains stable after illumination for 40 min.^[236]

For a better exploitation of the solar spectrum, the concept of low bandgap polymers was developed in the last years. The first crosslinkable low bandgap polymer that was used in BHJ devices was a PBDTTPD derivative modified with 16% and 33% bromine functionalities, respectively. The crosslinking was carried out via UV exposure. A notably high efficiency of 4.6% was achieved for a solar cell made from the derivative with 16% bromine after annealing at 150 °C for 72 h. In contrast, the efficiency of the non-crosslinkable reference cell degrades from 5.2% to 3.9% efficiency upon annealing.^[237] Other examples for crosslinkable donor materials are low bandgap polymers modified with bromine,^[238,239] copolymers containing azide,^[240] copolymers with attached bromine, azide, and vinyl functionalities,^[241] as well as a low bandgap polymer based on fluorene and dithienylbenzothiadiazole functionalized with oxetane units that was used for photodynamic cancer therapy.^[242]

The low bandgap polymer TQ1 was used to examine different crosslinkable units by Krebs and co-workers in 2012. The attached alkyl chain was either modified with bromide, vinyl, azide or

oxetane groups. Illumination with UV light initiated the crosslinking reaction, an additional photoacid generator was used in the case of the oxetane functionality. No damage of the conjugated polymer backbone was observed by the formation of insoluble polymer layers as confirmed by absorption spectroscopy. Aging of the solar cells was performed in the dark or under AM1.5 illumination in either ambient or inert atmosphere for the investigation of the photochemical and thermal stability of the devices. By optical microscopy, a reduced phase separation and thus aggregation of PCBM molecules was observed for thermally aged cells. This could be ascribed to the crosslinking of the active layers. However, the device performance showed no stabilization upon crosslinking when aged under illumination in ambient atmosphere as photodegradation seems to be predominant. In contrast, crosslinked cells showed a stabilized efficiency depending on the crosslinkable group when illuminated in an inert atmosphere.^[243] The difference between bromine and oxetane units was further investigated by the group of Heeney using the low bandgap polymer PDTG-TPD. Both the bromine and oxetane containing polymers could be crosslinked whereas crosslinking of a blend with fullerene was only possible for the polymer containing oxetanes because fullerene acts as a radical scavenger. A high efficiency of 5.02% was reached with a PDTG-TPD derivative with 20% oxetane units. Additionally, the device exhibits an increased stability after annealing at 120 °C for 30 min.^[244] In the case of PBDTPD-V_x, reducing the amount of crosslinkable vinyl units to only 2.5% also resulted in a high efficiency of 6.06% in a BHJ solar cell with PC₇₁BM. This is one of the best results achieved with crosslinked active layers. After annealing at 150 °C for 40 h, still 91% of the PCE is retained.^[245]

The crosslinking process of oxetane units that proceeds via a cationic ring-opening polymerization is typically initiated by an acid.^[221,222,244,246,247] One possibility is to use a photoacid generator that is spin coated together with the oxetane material and expose the film to UV light. The generated protons start the crosslinking process, but the counterions remain in the crosslinked material and may decrease the device performance.^[222,244] In contrast, the crosslinking via the exposure to acid vapour exhibits several advantages. The neat material can be deposited as a film without the addition of a photoacid generator. Trifluoroacetic acid (TFA) is often used due to the low boiling point of 78 °C and the high vapour pressure which enables the permeation of the protons through the film at elevated temperature. Furthermore, the excess of TFA can be removed from the material by a heating or a vacuum step.^[223,244] However, Knauer et al. found that oxetane crosslinking is also possible by prolonged exposure to heat. By this means, a BHJ solar cell with an extended long-term stability was realized.^[223] Additionally, the absence of decomposition products of initiators is a big advantage regarding the device performance like charge carrier mobility. Using PF2/6-A-x:y, a polyfluorene containing different amounts of acrylate, Kahle et al. examined the influence of different photoinitiators and crosslinking on the charge carrier mobility determined by metal-insulator-semiconductor charge extraction by linearly increasing voltage (MIS-CELIV) measurements. An initiator based on titanium or high amounts of ca. 1 wt% of an organic initiator led to decreased charge transport

properties. However, the charge carrier mobility was not decreased by small amounts of about 0.1 wt% of organic photoinitiators or thermal crosslinking in comparison to the non-crosslinked reference.^[248] Furthermore, exposure to acid can not only induce crosslinking but also p-doping of the treated polymer as shown for neat PCDTBT without crosslinkable groups. Films of PCDTBT were placed in a solution of phosphomolybdic acid giving highly insoluble layers with an increased conductivity of 5.5 Scm^{-1} that allows the application of the p-doped PCDTBT as a hole transport layer. Increased p-doping with longer exposure times was observed via absorption spectroscopy that depicts an enhanced absorption in the red region up to near infrared.^[249] In the case of PEDOT:PSS, partial dedoping was possible with ethylene glycol and led to a higher conductivity.^[250] Complete dedoping of PEDOT:PSS was achieved with diethylenediamine as the amine molecules show a strong reducing property. After exposure to diethylenetriamine vapour for 1 h, the PEDOT:PSS films turned dark blue indicating the dedoping and the conductivity decreased by 5 orders of magnitude.^[251]

In addition to the attachment of crosslinkable units at the side chains of the polymer, it is also possible to modify the polymer backbone itself. A series of copolymers including triple bonds in the backbone was presented by Bui et al. in 2016. UV light was used to start the crosslinking process. Two of the polymers were applied in inverted organic solar cells to realize interface modification of the hole blocking zinc oxide layer. The crosslinked polymeric buffer layer raised the hydrophobicity of the zinc oxide that results in an enhanced efficiency of 3.1% whereas the reference cell achieved only 2.7% efficiency.^[252]

Besides of crosslinking only the donor material, the donor can also be crosslinked directly with the acceptor. As fullerenes acts a radical scavengers, the best method to realize a crosslinking reaction between the two substances is the use of azide units.^[235,253,254] However, the donor polymer PCDTBT can be crosslinked with PC₇₁BM without any additional crosslinkable group as presented by the group of Leclerc in 2014. The chemical structure of PCDTBT is included in Figure 36. In this case, the crosslinking is based on photochemical reactions that comprise the scission of the N-C bond between the carbazole core of PCDTBT and the aliphatic spacer and the subsequent reaction of the polycarbazolyl radicals and the radical scavenging fullerene molecules. The crosslinking was investigated by accelerated photoaging experiments as well as thermal annealing in combination with (light-induced) electron paramagnetic resonance measurements. The latter confirmed that the crosslinking can mainly be ascribed to polymer crosslinking besides the oligomerization of PCBM.^[255] BHJ solar cells made from PCDTBT and PCBM exhibit an initial drop of the device performance of approximately 25%. This so called "burn-in loss" can be explained by the development of a covalent network that finally leads to a remarkable long-term stability and estimated average lifetimes up to 7 years that present the best results for organic solar cells containing a polymeric donor and a fullerene acceptor up to now.^[256,257]

The third option for the stabilization of organic solar cells is the crosslinking of the acceptor material. As fullerenes are often used as the electron accepting component, several crosslinkable derivatives were realized.^[221,222,258–263] As already mentioned, fullerenes act as electron scavengers and prevent radical reactions. Thus, only few functional units can be applied and fullerene crosslinking is rarely used for the stabilization of active layers.^[221] However, self-assembled insoluble interlayers are often realized by the application of crosslinkable fullerenes. By this means, multilayer solar cells as well as tandem or triple junction devices that are usually made from evaporable small molecules can be processed from solution without the necessity of orthogonal solvents for the different materials.^[264] These stable interlayers are often deployed as exciton blocking layers or electron transport layers at the interface towards an electrode resulting in passivated trap states and a reduced contact resistance.^[265,266] Further layers can be spin coated without damage to the underlying layer and without interdiffusion of the two layers.^[267–274] However, multilayer solar cells consisting of several crosslinked functional layers are not realized so far. Multijunction solar cells as presented by the groups of Janssen^[151] and Leo^[275] are still based on the insertion of inorganic interlayers or evaporable small molecules. Yet, crosslinked polymeric interlayers are successfully applied in multilayer solar cells as shown for PFN-X. The vinyl containing derivative PFN-V was included as a cathode interlayer in inverted solar cells comprising PTB7-Th and PC₇₁BM achieving an efficiency of 9.18%. In comparison to the reference, this depicts an increase of 195% that can be assigned to a favourable surface energy and thus an improved vertical phase separation.^[276] Exchanging the vinyl group by oxetane in PFN-Ox, an enhancement of even 204% to a PCE of 9.28% was reached.^[274] The effect of limiting the fullerene diffusion by the means of a crosslinked matrix is difficult to investigate.^[216–218,277] Fischer et al. presented an optical measurement on three-layer devices based on the quenching of the photoluminescence of a sensor layer made from MeH-PPV. The quenching occurs due to electron transfer from the excited sensor to the fullerene molecules when they have diffused through a polymer transport layer deposited on top of the sensor layer. Furthermore, it could be shown that a densely crosslinked layer can reduce the diffusion coefficient of C₆₀ at 140 °C by three orders of magnitude compared to the non-crosslinked reference. The crosslinkable derivative PF2/6-x:y with different contents of acrylate units was applied.^[278] In the case of non-fullerene acceptors, crosslinkable derivatives have not yet been realized but are of particular research interest.^[279]

Crosslinkable materials can also be used to stabilize nanostructured interfaces that lead to a favoured nanomorphology comprising direct charge percolation paths.^[30,214,280] The structuring of the active layer can be achieved by different methods such as photopatterning of the crosslinkable material acting as a negative photoresist,^[230,231,281] nanotemplating of a blend^[246,282,283] or nanoimprinting allowing resolutions under 10 nm that is in the range of the exciton diffusion length.^[284–289] Farinhas et al. applied nanotemplating to a blend of the crosslinkable polymer F8T2Ox1 and polystyrene. Columnar structures of F8T2Ox1 were realized by the spontaneous demixing of the polymers, crosslinking of F8T2Ox1 and subsequent removal

of polystyrene. Afterwards, PCBM was refilled into the pattern. However, only very low efficiencies below 1% were achieved.^[283]

In addition to the functionalization of materials with respect to crosslinking, the application of small molecule crosslinkers presents a versatile method. The chemical structures of different bisazide crosslinkers are shown in Figure 36. The group of Friend realized the successful crosslinking of different non-functionalized conjugated polymers by the addition of the reactive bisazide sFPA.^[290] By this means, a device with three planar polymer layers could be fabricated from solution. The polymers exhibited an energy level cascade leading to an efficiency of 0.45%.^[291] Tao et al. showed bilayer device made from P3HT crosslinked with sFPA and PCBM as acceptor. A PCE of 3.0% was measured for the crosslinked cell in comparison with the non-crosslinked reference that achieved 3.3% efficiency.^[292] The bisazide BABP was applied for fullerene crosslinking via mild thermal activation in BHJ solar cells with several donor polymers. A P3HT based cell resulted in an efficiency of 3.3% that could retain 90% of this initial PCE after annealing at 85 °C for 120 days. The efficiency of cells comprising PTB7 dropped from 5.8% to 4.6% when annealed at 150 °C for 16 h. Furthermore, annealing at 150 °C for 15 h resulted in a decrease from 4.5% to 3.0% for PDPPTBT.^[293] An efficiency improvement for BHJ devices from 6.0% to 7.0% was observed by the group of McCulloch when SiIDT-BT was crosslinked with the bisazide DAZH. After annealing at 85 °C for 130 h, the crosslinked cell still reached an efficiency of 4.1% whereas the efficiency of the reference cell decreased to 3.5%.^[294] Small molecule crosslinkers were also applied for the fabrication of nanostructured interfaces. In 2014, the group of Schmidt-Mende introduced nanoimprinting lithography (NIL)^[295] of the active layer that enables the investigation of the interface morphology on the device performance due to the variation of spatial dimensions. Comb-like bilayer morphologies from the polymeric acceptor P(NDI2OD-T2) that is depicted in Figure 36 and P3HT were fabricated with complete control of the interface. Crosslinking of P(NDI2OD-T2) was carried out via exposure to deep UV light in presence of the crosslinker sFPA. Thus, the pattern was stabilized and P3HT can be subsequently solution processed. Although exciton harvesting could be increased because of a larger donor-acceptor interface, polaron recombination was also facilitated. This led to efficiencies lower than 1% showing the necessity for both spatial and energetical optimization.^[285]

In conclusion, a crosslinking method with only minimal influences of the conjugated material should be chosen. This is often achieved when the modification with the crosslinkable unit is located on the polymer side chains or by using small molecule crosslinkers. The crosslinking reaction should not attack the polymer backbone, but should be selective to the side chains. Residues due to the initiator should not negatively influence the device performance like the charge carrier mobility. This can be circumvented by the application of suitable initiators as well as the use of functional groups that allow thermal initiation or photoinitiation such as acrylates.

2.10 Triarylamine as hole conducting comonomers

Substitution of ammonia with three aryl units results in triarylamine TAA.^[296] The most common TAA, triphenylamine TPA, was first synthesized in 1873 using aniline or diphenylamine, potassium and bromobenzene.^[297] Some years later, TPA was synthesized via an Ullmann coupling between diphenylamine and iodobenzene.^[298] Since then, numerous TAA derivatives were realized by modified Ullmann and Buchwald-Hartwig reactions. The nitrogen atom in the centre of TPA is sp^2 hybridized and exhibits a planar configuration together with the bonded carbon atoms of the phenyl rings.^[296] Furthermore, the nitrogen is surrounded by the phenyl groups in a propeller formation.^[296,299] Besides their high thermal stability and amorphous morphology, TAAs are excellent electron donors as they can be easily oxidized at the nitrogen. The radical cations that are generated electrically or via photochemical reactions are stable and allow the transport of positive charges.^[299,300] Furthermore, hole injection and transport is facilitated by low ionization potentials.^[296] Upon oxidation, unsubstituted TPA forms the dimer triphenyldiamine TPD which exhibits a better oxidizability than TPA.^[300] TPD substituted with methyl groups is also synthesized from *N,N'*-diphenylbenzidine and bromotoluene.^[281] The chemical structures of unsubstituted TPA and TPD are shown in Figure 37.

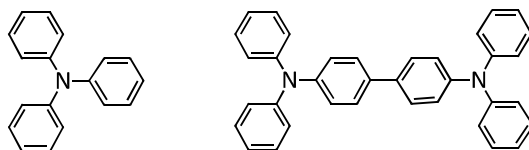


Figure 37: Chemical structures of TPA and TPD.^[300]

High hole transport mobilities of about $10^{-2} \text{ cm}^2\text{V}^{-1}\text{s}^{-1}$ were reached for vacuum evaporated films of a TPD derivative.^[301] Another possibility for achieving good transport properties is the doping of polymers with TPD molecules. By that means, hole mobilities up to $10^{-3} \text{ cm}^2\text{V}^{-1}\text{s}^{-1}$ were determined.^[302] Small molecule derivatives, oligomeric TAA materials as well as main chain and side chain TAA-based polymers were applied as hole transport materials in OLEDs, OFETs and OSCs.^[296,299,300,303,304] In addition, crosslinkable TPA materials have been reported. M. Bender et al. synthesized a copolymer combining fluorene and TPA moieties that was modified with cinnamate. An insoluble hole transport layer was prepared from this copolymer which allows the realization of a multilayer OLED.^[305] Nanorods made from a TPA with pendant vinyl groups were obtained by an imprinting step and the pattern was rendered insoluble via crosslinking. By this method, a first step towards nanostructured organic solar cells was realized.^[288] Furthermore, an azide functionalized TPA derivative was used to stabilize blends of a donor polymer and PCBM by an intramolecular crosslinking reaction between the TPA material and intermolecular crosslinking to the acceptor molecules. This results in OSC devices with increased thermal stability.^[306]

References

- [1] S. B. Darling, F. You, *RSC Adv.* **2013**, *3*, 17633.
- [2] K. G. Reddy, T. G. Deepak, G. S. Anjusree, S. Thomas, S. Vadukumpully, K. R. V. Subramanian, S. V. Nair, A. S. Nair, *Phys. Chem. Chem. Phys.* **2014**, *16*, 6838.
- [3] P.-L. T. Boudreault, A. Najari, M. Leclerc, *Chem. Mater.* **2011**, *23*, 456.
- [4] C. Li, M. Liu, N. G. Pschirer, M. Baumgarten, K. Müllen, *Chem. Rev.* **2010**, *110*, 6817.
- [5] G. Beaucarne, *Adv. Optoelectron.* **2007**, *2007*, 36970.
- [6] X. Zhan, D. Zhu, *Polym. Chem.* **2010**, *1*, 409.
- [7] M. Alnifro, S. T. Taqvi, M. S. Ahmad, K. Bensaida, A. Elkamel, *IOP Conf. Ser. Earth Environ. Sci.* **2017**, *83*, 12018.
- [8] S.-H. Bae, H. Zhao, Y.-T. Hsieh, L. Zuo, N. De Marco, Y. S. Rim, G. Li, Y. Yang, *Chem.* **2016**, *1*, 197.
- [9] A. E. Becquerel, *Comptes Rendus Acad. Sci.* **1839**, *9*, 561.
- [10] C. E. Fritts, *Am. J. Sci.* **1883**, *26*, 465.
- [11] R. S. Ohl, *US Patent 2402662, Light-Sensitive Electric Device* **1946**.
- [12] D. M. Chapin, C. S. Fuller, G. L. Pearson, *J. Appl. Phys.* **1954**, *25*, 676.
- [13] T. Saga, *NPG Asia Mater.* **2010**, *2*, 96.
- [14] Kaneka Corporation, *New World Record Established for Conversion Efficiency in a Crystalline Silicon Solar Cell: —Conversion Efficiency of 26.63% Achieved in a Practical Cell Size—*, Osaka **2017**.
- [15] K. Yoshikawa, H. Kawasaki, W. Yoshida, T. Irie, K. Konishi, K. Nakano, T. Uto, D. Adachi, M. Kanematsu, H. Uzu, K. Yamamoto, *Nat. Energy* **2017**, *2*, 17032.
- [16] J. Benick, A. Richter, R. Müller, H. Hauser, F. Feldmann, P. Krenckel, S. Riepe, F. Schindler, M. C. Schubert, M. Hermle, A. W. Bett, S. W. Glunz, *IEEE J. Photovoltaics* **2017**, *7*, 1171.
- [17] S. E. Shaheen, D. S. Ginley, G. E. Jabbour, *MRS Bull.* **2005**, *30*, 10.
- [18] Shah, A., Torres, P., Tschanner, R., Wyrsh, N., Keppner, H., *Science* **1999**, *285*, 692.
- [19] T. Matsui, H. Sai, T. Suezaki, M. Matsumoto, K. Saito, I. Yoshida, M. Kondo, *Proc. 28th EU PVSEC* **2013**.
- [20] Centre for Solar Energy and Hydrogen Research Baden-Württemberg, *ZSW Sets New World Record for Thin-film Solar Cells: CIGS PV's efficiency ratings rising fast*, Stuttgart **2016**.
- [21] D. Knipp, V. Jovanov, A. Tamang, V. Wagner, A. Salleo, *Nano Energy* **2017**, *31*, 582.
- [22] Georgia Institute of Technology, *Nano-Manhattan: 3D Solar Cells Boost Efficiency While Reducing Size, Weight and Complexity of Photovoltaic Arrays*, Atlanta **2007**.
- [23] Y.-J. Cheng, S.-H. Yang, C.-S. Hsu, *Chem. Rev.* **2009**, *109*, 5868.
- [24] H. Spanggaard, F. C. Krebs, *Sol. Energy Mater. Sol. Cells* **2004**, *83*, 125.
- [25] D. Kearns, M. Calvin, *J. Chem. Phys.* **1958**, *29*, 950.
- [26] G. M. Delacote, J. P. Fillard, F. J. Marco, *Solid State Commun.* **1964**, *2*, 373.
- [27] G. A. Chamberlain, *Solar Cells* **1983**, *8*, 47.
- [28] A. Facchetti, *Chem. Mater.* **2011**, *23*, 733.
- [29] C. J. Brabec, N. S. Sariciftci, J. C. Hummelen, *Adv. Funct. Mater.* **2001**, *11*, 15.
- [30] K. M. Coakley, M. D. McGehee, *Chem. Mater.* **2004**, *16*, 4533.
- [31] B. J. Schwartz, *Annu. Rev. Phys. Chem.* **2003**, *54*, 141.
- [32] M. Leclerc, K. Faid, *Adv. Mater.* **1997**, *9*, 1087.

- [33] M. Leclerc, *Adv. Mater.* **1999**, *11*, 1491.
- [34] A. Pochettino, *Rend. Mat. Acc. Lincei* **1906**, *15*, 355.
- [35] M. Volmer, *Ann. Phys.* **1913**, *345*, 775.
- [36] H. Shirakawa, E. J. Louis, A. G. MacDiarmid, C. K. Chiang, A. J. Heeger, *J. Chem. Soc. Chem. Commun.* **1977**, *0*, 578.
- [37] B. R. Weinberger, M. Akhtar, S. C. Gau, *Synth. Met.* **1982**, *4*, 187.
- [38] T. Masuda, B. Z. Tang, T. Higashimura, H. Yamaoka, *Macromolecules* **1985**, *18*, 2369.
- [39] Lam, Jacky W. Y., B. Z. Tang, *Acc. Chem. Res.* **2005**, *38*, 745.
- [40] T. Masuda, *J. Polym. Sci. A Polym. Chem.* **2007**, *45*, 165.
- [41] E. Bundgaard, F. C. Krebs, *Sol. Energy Mater. Sol. Cells* **2007**, *91*, 954.
- [42] C. L. Chochos, S. A. Choulis, *Prog. Polym. Sci.* **2011**, *36*, 1326.
- [43] S. Glenis, G. Tourillon, F. Garnier, *Thin Solid Films* **1986**, *139*, 221.
- [44] S. Karg, W. Riess, V. Dyakonov, M. Schwoerer, *Synth. Met.* **1993**, *54*, 427.
- [45] C. W. Tang, *Appl. Phys. Lett.* **1986**, *48*, 183.
- [46] M. Hiramoto, H. Fujiwara, M. Yokoyama, *Appl. Phys. Lett.* **1991**, *58*, 1062.
- [47] M. Hiramoto, H. Fukusumi, M. Yokoyama, *Appl. Phys. Lett.* **1992**, *61*, 2580.
- [48] A. J. Heeger, *Adv. Mater.* **2014**, *26*, 10.
- [49] H. Kang, G. Kim, J. Kim, S. Kwon, H. Kim, K. Lee, *Adv. Mater.* **2016**, *28*, 7821.
- [50] N. S. Sariciftci, D. Braun, C. Zhang, V. I. Srdanov, A. J. Heeger, G. Stucky, F. Wudl, *Appl. Phys. Lett.* **1993**, *62*, 585.
- [51] N. S. Sariciftci, L. Smilowitz, A. J. Heeger, F. Wudl, *Synth. Met.* **1993**, *59*, 333.
- [52] S. M. Ryno, M. K. Ravva, X. Chen, H. Li, J.-L. Brédas, *Adv. Energy Mater.* **2017**, *7*, 1601370.
- [53] C. Cui, Y. Li, Y. Li, *Adv. Energy Mater.* **2017**, *7*, 1601251.
- [54] G. Yu, K. Pakbaz, A. J. Heeger, *Appl. Phys. Lett.* **1994**, *64*, 3422.
- [55] G. Yu, J. Gao, J. C. Hummelen, F. Wudl, A. J. Heeger, *Science* **1995**, *270*, 1789.
- [56] G. Yu, A. J. Heeger, *J. Appl. Phys.* **1995**, *78*, 4510.
- [57] Halls, J. J. M., C. A. Walsh, Greenham, N. C., E. A. Marseglia, Friend, R. H., S. C. Moratti, Holmes, A. B., *Nature* **1995**, *376*, 498.
- [58] List, Emil. J. W., Scherf, U., *Adv. Mater.* **2002**, *14*, 477.
- [59] N. Blouin, M. Leclerc, *Acc. Chem. Res.* **2008**, *41*, 1110.
- [60] P. Kumar, S. Chand, *Prog. Photovolt. Res. Appl.* **2012**, *20*, 377.
- [61] R. C. Chiechi, R. W.A. Havenith, J. C. Hummelen, Koster, L. Jan Anton, M. A. Loi, *Mater. Today* **2013**, *16*, 281.
- [62] H. Kang, W. Lee, J. Oh, T. Kim, C. Lee, B. J. Kim, *Acc. Chem. Res.* **2016**, *49*, 2424.
- [63] H. Benten, D. Mori, H. Ohkita, S. Ito, *J. Mater. Chem. A* **2016**, *4*, 5340.
- [64] M. C. Gather, A. Köhnen, K. Meerholz, *Adv. Mater.* **2011**, *23*, 233.
- [65] W. Brütting, J. Frischeisen, T. D. Schmidt, B. J. Scholz, C. Mayr, *Phys. Status Solidi A* **2013**, *210*, 44.
- [66] Y. Yamashita, *Sci. Technol. Adv. Mater.* **2009**, *10*, 24313.
- [67] B. Lüssem, C.-M. Keum, D. Kasemann, B. Naab, Z. Bao, K. Leo, *Chem. Rev.* **2016**, *116*, 13714.
- [68] D. Li, P. Liao, X. Shai, W. Huang, S. Liu, H. Li, Y. Shen, M. Wang, *RSC Adv* **2016**, *6*, 89356.
- [69] J. Gong, K. Sumathy, Q. Qiao, Z. Zhou, *Renew. Sustain. Energy Rev.* **2017**, *68*, 234.
- [70] B. O'Regan, M. Grätzel, *Nature* **1991**, *353*, 737.

- [71] M. Grätzel, U. Bach, D. Lupo, P. Comte, J. E. Moser, F. Weissörtel, J. Salbeck, H. Spreitzer, *Nature* **1998**, *395*, 583.
- [72] S. Mathew, A. Yella, P. Gao, R. Humphry-Baker, B. F. E. Curchod, N. Ashari-Astani, I. Tavernelli, U. Rothlisberger, M. K. Nazeeruddin, M. Grätzel, *Nat. Chem.* **2014**, *6*, 242.
- [73] Y. Cao, Y. Saygili, A. Ummadisingu, J. Teuscher, J. Luo, N. Pellet, F. Giordano, S. M. Zakeeruddin, J.-E. Moser, M. Freitag, A. Hagfeldt, M. Grätzel, *Nat. Commun.* **2017**, *8*, 15390.
- [74] Z. Song, S. C. Wathage, A. B. Phillips, M. J. Heben, *J. Photon. Energy* **2016**, *6*, 22001.
- [75] A. Kojima, K. Teshima, Y. Shirai, T. Miyasaka, *J. Am. Chem. Soc.* **2009**, *131*, 6050.
- [76] W. S. Yang, B.-W. Park, E. H. Jung, N. J. Jeon, Y. C. Kim, D. U. Lee, S. S. Shin, J. Seo, E. K. Kim, J. H. Noh, S. I. Seok, *Science* **2017**, *356*, 1376.
- [77] VTT Technical Research Centre of Finland LTD,
http://www.vttresearch.com/img/Services/Health%20and%20Wellbeing/Wearable%20technology/04_Solar-electricity_harvesting_to_enable_self-powered_devices.jpg?RenditionID=4.
- [78] Opvius GmbH,
http://www.opvius.com/files/OPVIUS/casestudies/photos/Solartree/097A5128_klein.jpg.
- [79] Opvius GmbH,
http://www.opvius.com/files/OPVIUS/casestudies/photos/Addis/OPVIUS_casestudy_1130x754_AddisAbeba_01.jpg.
- [80] Heliatek GmbH,
[http://www.heliatek.com/files/content/downloads/fotos/preview/HeliaFilm%20in%20glass%20\(1\)_Heliatek_Dresden.jpg](http://www.heliatek.com/files/content/downloads/fotos/preview/HeliaFilm%20in%20glass%20(1)_Heliatek_Dresden.jpg).
- [81] Heliatek GmbH, http://www.heliatek.com/assets/images/a/Pilot_Glass%20car%20roof-3c3594aa.jpg.
- [82] Merck KGaA, Opvius GmbH,
https://www.merckgroup.com/content/dam/web/corporate/images/pr/2015/nov/global/Merck_GrayOPV_Chicago2.jpg.
- [83] G. Lakhwani, A. Rao, R. H. Friend, *Annu. Rev. Phys. Chem.* **2014**, *65*, 557.
- [84] M. Stephen, K. Genevičius, G. Juška, K. Arlauskas, R. C. Hiorns, *Polym. Int.* **2016**, *66*, 13.
- [85] D. M. Stoltzfus, J. E. Donaghey, A. Armin, P. E. Shaw, P. L. Burn, P. Meredith, *Chem. Rev.* **2016**, *116*, 12920.
- [86] K. M. Pelzer, S. B. Darling, *Mol. Syst. Des. Eng.* **2016**, *1*, 10.
- [87] S. Few, J. M. Frost, J. Nelson, *Phys. Chem. Chem. Phys.* **2015**, *17*, 2311.
- [88] G. J. Hedley, A. Ruseckas, I. D. W. Samuel, *Chem. Rev.* **2017**, *117*, 796.
- [89] P. Peumans, A. Yakimov, S. R. Forrest, *J. Appl. Phys.* **2003**, *93*, 3693.
- [90] T. M. Clarke, J. R. Durrant, *Chem. Rev.* **2010**, *110*, 6736.
- [91] I. Fraga Domínguez, A. Distler, L. Lüer, *Adv. Energy Mater.* **2017**, *7*, 1601320.
- [92] M. C. Scharber, D. Mühlbacher, M. Koppe, P. Denk, C. Waldauf, A. J. Heeger, C. J. Brabec, *Adv. Mater.* **2006**, *18*, 789.
- [93] D. Veldman, Meskers, Stefan C. J., Janssen, René A. J., *Adv. Funct. Mater.* **2009**, *19*, 1939.
- [94] B. P. Rand, J. Genoe, P. Heremans, J. Poortmans, *Prog. Photovolt. Res. Appl.* **2007**, *15*, 659.
- [95] L.-M. Chen, Z. Hong, G. Li, Y. Yang, *Adv. Mater.* **2009**, *21*, 1434.

- [96] P. Cheng, X. Zhan, *Chem. Soc. Rev.* **2016**, *45*, 2544.
- [97] M. Jørgensen, J. E. Carlé, R. R. Søndergaard, M. Lauritzen, N. A. Dagnæs-Hansen, S. L. Byskov, T. R. Andersen, T. T. Larsen-Olsen, A. P.L. Böttiger, B. Andreasen, L. Fu, L. Zuo, Y. Liu, E. Bundgaard, X. Zhan, H. Chen, F. C. Krebs, *Sol. Energy Mater. Sol. Cells* **2013**, *119*, 84.
- [98] S. Günes, H. Neugebauer, N. S. Sariciftci, *Chem. Rev.* **2007**, *107*, 1324.
- [99] A. Hadipour, B. de Boer, Blom, P. W. M., *Adv. Funct. Mater.* **2008**, *18*, 169.
- [100] C. Duan, A. Furlan, van Franeker, Jacobus J., R. E. M. Willems, M. M. Wienk, Janssen, René A. J., *Adv. Mater.* **2015**, *27*, 4461.
- [101] K. H. Hendriks, W. Li, M. M. Wienk, Janssen, René A J, *J. Am. Chem. Soc.* **2014**, *136*, 12130.
- [102] R. Meerheim, C. Körner, K. Leo, *Appl. Phys. Lett.* **2014**, *105*, 63306.
- [103] E. Klump, I. Constantinou, T.-H. Lai, F. So, *Org. Electron.* **2017**, *42*, 87.
- [104] H. Huang, L. Yang, B. Sharma, *J. Mater. Chem. A* **2017**, *5*, 11501.
- [105] H. Li, K. Lu, Z. Wei, *Adv. Energy Mater.* **2017**, *7*, 1602540.
- [106] H. Tan, A. Furlan, W. Li, K. Arapov, R. Santbergen, M. M. Wienk, M. Zeman, A. H. M. Smets, Janssen, René A. J., *Adv. Mater.* **2016**, *28*, 2170.
- [107] S. O. Oseni, G. T. Mola, *Sol. Energy Mater. Sol. Cells* **2017**, *160*, 241.
- [108] K. Nakano, K. Tajima, *Adv. Mater.* **2017**, *29*, 1603269.
- [109] R. Fitzner, E. Reinold, A. Mishra, E. Mena-Osteritz, H. Ziehlke, C. Körner, K. Leo, M. Riede, M. Weil, O. Tsaryova, A. Weiß, C. Uhrich, M. Pfeiffer, P. Bäuerle, *Adv. Funct. Mater.* **2011**, *21*, 897.
- [110] Y. Liang, L. Yu, *Acc. Chem. Res.* **2010**, *43*, 1227.
- [111] S. R. Forrest, L. Y. Leu, F. F. So, W. Y. Yoon, *J. Appl. Phys.* **1989**, *66*, 5908.
- [112] H. Yu, R. Yi, J. Zhang, A. Yu, H. Peng, J. Qin, X. Hou, *J. Phys. D Appl. Phys.* **2016**, *49*, 205105.
- [113] S. Grob, M. Gruber, A. N. Bartynski, U. Hörmann, T. Linderl, M. E. Thompson, W. Brütting, *Appl. Phys. Lett.* **2014**, *104*, 213304.
- [114] S. R. Forrest, *MRS Bull.* **2005**, *30*, 28.
- [115] P. Peumans, V. Bulović, S. R. Forrest, *Appl. Phys. Lett.* **2000**, *76*, 2650.
- [116] P. Peumans, S. R. Forrest, *Appl. Phys. Lett.* **2001**, *79*, 126.
- [117] J. Xue, S. Uchida, B. P. Rand, S. R. Forrest, *Appl. Phys. Lett.* **2004**, *84*, 3013.
- [118] M. Hirade, C. Adachi, *Appl. Phys. Lett.* **2011**, *99*, 153302.
- [119] K. Cnops, B. P. Rand, D. Cheyns, B. Verreert, M. A. Empl, P. Heremans, *Nat. Commun.* **2014**, *5*, 3406.
- [120] X. Zhao, Z. Li, T. Zhu, B. Mi, Z. Gao, W. Huang, *J. Phys. D Appl. Phys.* **2013**, *46*, 195105.
- [121] S. Steinberger, A. Mishra, E. Reinold, J. Levichkov, C. Uhrich, M. Pfeiffer, P. Bäuerle, *Chem. Commun.* **2011**, *47*, 1982.
- [122] J. Xue, B. P. Rand, S. Uchida, S. R. Forrest, *J. Appl. Phys.* **2005**, *98*, 124903.
- [123] J. Xue, B. P. Rand, S. Uchida, S. R. Forrest, *Adv. Mater.* **2005**, *17*, 66.
- [124] R. Fitzner, C. Elschner, M. Weil, C. Uhrich, C. Körner, M. Riede, K. Leo, M. Pfeiffer, E. Reinold, E. Mena-Osteritz, P. Bäuerle, *Adv. Mater.* **2012**, *24*, 675.
- [125] K. Yoshino, X. H. Yin, S. Morita, T. Kawai, A. A. Zakhidov, *Solid State Commun.* **1993**, *85*, 85.

- [126] S. Kwon, H. Kang, J.-H. Lee, J. Lee, S. Hong, H. Kim, K. Lee, *Adv. Energy Mater.* **2017**, *7*, 1601496.
- [127] W. Ma, C. Yang, X. Gong, K. Lee, A. J. Heeger, *Adv. Funct. Mater.* **2005**, *15*, 1617.
- [128] C. Liu, D. Zhang, Z. Li, X. Zhang, W. Guo, L. Zhang, L. Shen, S. Ruan, Y. Long, *ACS Appl. Mater. Interfaces* **2017**, *9*, 8830.
- [129] J. Y. Kim, S. H. Kim, H.-H. Lee, K. Lee, W. Ma, X. Gong, A. J. Heeger, *Adv. Mater.* **2006**, *18*, 572.
- [130] A. Nitti, R. Po, G. Bianchi, D. Pasini, *Molecules* **2016**, *22*, 21.
- [131] H.-Y. Chen, J. Hou, S. Zhang, Y. Liang, G. Yang, Y. Yang, L. Yu, Y. Wu, G. Li, *Nat. Photonics* **2009**, *3*, 649.
- [132] Y. Jin, Z. Chen, S. Dong, N. Zheng, L. Ying, X.-F. Jiang, F. Liu, F. Huang, Y. Cao, *Adv. Mater.* **2016**, *28*, 9811.
- [133] J. Huang, J. H. Carpenter, C.-Z. Li, J.-S. Yu, H. Ade, A. K.-Y. Jen, *Adv. Mater.* **2016**, *28*, 967.
- [134] S. Mori, H. Oh-oka, H. Nakao, T. Gotanda, Y. Nakano, H. Jung, A. Iida, R. Hayase, N. Shida, M. Saito, K. Todor, T. Asakura, A. Matsui, M. Hosoya, *MRS Proc.* **2015**, *1737*, 2236.
- [135] J. Zhao, Y. Li, G. Yang, K. Jiang, H. Lin, H. Ade, W. Ma, H. Yan, *Nat. Energy* **2016**, *1*, 15027.
- [136] H. Bin, L. Gao, Z.-g. Zhang, Y. Yang, Y. Zhang, C. Zhang, S. Chen, L. Xue, C. Yang, M. Xiao, Y. Li, *Nat. Commun.* **2016**, *7*, 13651.
- [137] S. Li, L. Ye, W. Zhao, S. Zhang, S. Mukherjee, H. Ade, J. Hou, *Adv. Mater.* **2016**, *28*, 9423.
- [138] B. P. Rand, J. Xue, S. Uchida, S. R. Forrest, *J. Appl. Phys.* **2005**, *98*, 124902.
- [139] G. D'Avino, L. Muccioli, F. Castet, C. Poelking, D. Andrienko, Z. G. Soos, J. Cornil, D. Beljonne, *J. Phys. Condens. Matter* **2016**, *28*, 433002.
- [140] Y. Yan, X. Liu, T. Wang, *Adv. Mater.* **2017**, *29*, 1601674.
- [141] T. Wang, N. W. Scarratt, H. Yi, I. F. Coleman, Y. Zhang, R. T. Grant, J. Yao, Skoda, Maximilian W. A., Dunbar, Alan D. F., Jones, Richard A. L., A. Iraqi, D. G. Lidzey, *J. Mater. Chem. C* **2015**, *3*, 4007.
- [142] J.-H. Huang, K.-C. Li, D. Kekuda, H. H. Padhy, H.-C. Lin, K.-C. Ho, C.-W. Chu, *J. Mater. Chem.* **2010**, *20*, 3295.
- [143] D. E. Markov, E. Amsterdam, Blom, Paul W. M., A. B. Sieval, J. C. Hummelen, *J. Phys. Chem. A* **2005**, *109*, 5266.
- [144] M. Hiramoto, M. Suezaki, M. Yokoyama, *Chem. Lett.* **1990**, *19*, 327.
- [145] J. Xue, S. Uchida, B. P. Rand, S. R. Forrest, *Appl. Phys. Lett.* **2004**, *85*, 5757.
- [146] J. Drechsel, B. Männig, F. Kozlowski, M. Pfeiffer, K. Leo, H. Hoppe, *Appl. Phys. Lett.* **2005**, *86*, 244102.
- [147] G. Dennler, H.-J. Prall, R. Koeppel, M. Egginger, R. Autengruber, N. S. Sariciftci, *Appl. Phys. Lett.* **2006**, *89*, 73502.
- [148] M. Riede, C. Urich, J. Widmer, R. Timmreck, D. Wynands, G. Schwartz, W.-M. Gnehr, D. Hildebrandt, A. Weiss, J. Hwang, S. Sundarraj, P. Erk, M. Pfeiffer, K. Leo, *Adv. Funct. Mater.* **2011**, *21*, 3019.
- [149] A. Puetz, F. Steiner, J. Mescher, M. Reinhard, N. Christ, D. Kutsarov, H. Kalt, U. Lemmer, A. Colmann, *Org. Electron.* **2012**, *13*, 2696.
- [150] M. Reinhard, P. Sonntag, R. Eckstein, L. Bürkert, A. Bauer, B. Dimmler, U. Lemmer, A. Colmann, *Appl. Phys. Lett.* **2013**, *103*, 143904.

- [151] W. Li, A. Furlan, K. H. Hendriks, M. M. Wienk, Janssen, René A. J., *J. Am. Chem. Soc.* **2013**, *135*, 5529.
- [152] S. Esiner, van Pruissen, Gijs W. P., M. M. Wienk, Janssen, René A. J., *J. Mater. Chem. A* **2016**, *4*, 5107.
- [153] S. Esiner, H. van Eersel, M. M. Wienk, Janssen, René A. J., *Adv. Mater.* **2013**, *25*, 2932.
- [154] X. Che, X. Xiao, J. D. Zimmerman, D. Fan, S. R. Forrest, *Adv. Energy Mater.* **2014**, *4*, 1400568.
- [155] H. Zhou, Y. Zhang, C.-K. Mai, S. D. Collins, G. C. Bazan, T.-Q. Nguyen, A. J. Heeger, *Adv. Mater.* **2015**, *27*, 1767.
- [156] C.-C. Chen, W.-H. Chang, K. Yoshimura, K. Ohya, J. You, J. Gao, Z. Hong, Y. Yang, *Adv. Mater.* **2014**, *26*, 5670.
- [157] A. R. b. M. Yusoff, D. Kim, H. P. Kim, F. K. Shneider, W. J. da Silva, J. Jang, *Energy Environ. Sci.* **2015**, *8*, 303.
- [158] Heliatek GmbH, *Heliatek erreicht neuen Organischen Photovoltaik Weltrekord mit einer Effizienz von 13,2%*, Dresden **2016**.
- [159] X. Xiao, J. D. Zimmerman, B. E. Lassiter, K. J. Bergemann, S. R. Forrest, *Appl. Phys. Lett.* **2013**, *102*, 73302.
- [160] J. L. Brédas, *J. Chem. Phys.* **1985**, *82*, 3808.
- [161] H. Brisset, C. Thobie-Gautier, A. Gorgues, M. Jubault, J. Roncali, *J. Chem. Soc. Chem. Commun.* **1994**, *92*, 1305.
- [162] E. Ortí, M. J. Sanchís, P. M. Viruela, R. Viruela, *Synth. Met.* **1999**, *101*, 602.
- [163] J. Roncali, C. Thobie-Gautier, *Adv. Mater.* **1994**, *6*, 846.
- [164] Q. T. Zhang, J. M. Tour, *J. Am. Chem. Soc.* **1998**, *120*, 5355.
- [165] Packing of P3HT,
http://onlinelibrary.wiley.com/store/10.1002/anie.201205075/asset/image_m/mcontent.gif?v=1&s=d9876abe0376f5b884f1682110e7b18cf8af877a.
- [166] W. Zhang, J. Smith, S. E. Watkins, R. Gysel, M. McGehee, A. Salleo, J. Kirkpatrick, S. Ashraf, T. Anthopoulos, M. Heeney, I. McCulloch, *J. Am. Chem. Soc.* **2010**, *132*, 11437.
- [167] K. Tamao, K. Sumitani, M. Kumada, *J. Am. Chem. Soc.* **1972**, *94*, 4374.
- [168] J. K. Stille, *Angew. Chem. Int. Ed. Engl.* **1986**, *25*, 508.
- [169] N. Miyaura, A. Suzuki, *Chem. Rev.* **1995**, *95*, 2457.
- [170] K. Sonogashira, *J. Organomet. Chem.* **2002**, *653*, 46.
- [171] Z. Bao, Y. Chen, R. Cai, L. Yu, *Macromolecules* **1993**, *26*, 5281.
- [172] J.-F. Morin, M. Leclerc, D. Adès, A. Siove, *Macromol. Rapid Commun.* **2005**, *26*, 761.
- [173] A. Siove, D. Adès, *Polymer* **2004**, *45*, 4045.
- [174] J.-F. Morin, M. Leclerc, *Macromolecules* **2001**, *34*, 4680.
- [175] G. Zotti, G. Schiavon, S. Zecchin, J.-F. Morin, M. Leclerc, *Macromolecules* **2002**, *35*, 2122.
- [176] M. Sonntag, P. Stroehriegl, *Chem. Mater.* **2004**, *16*, 4736.
- [177] F. Dierschke, A. C. Grimsdale, K. Müllen, *Synthesis* **2003**, *2003*, 2470.
- [178] Cadogan, J. I. G., M. Cameron-Wood, R. K. Mackie, Searle, R. J. G., *J. Chem. Soc.* **1965**, *0*, 4831.
- [179] Cadogan, J. I. G., *Q. Rev. Chem. Soc.* **1968**, *22*, 222.
- [180] J. Li, F. Dierschke, J. Wu, A. C. Grimsdale, K. Müllen, *J. Mater. Chem.* **2006**, *16*, 96.
- [181] N. Blouin, A. Michaud, M. Leclerc, *Adv. Mater.* **2007**, *19*, 2295.

- [182] N. Blouin, A. Michaud, D. Gendron, S. Wakim, E. Blair, R. Neagu-Plesu, M. Belletête, G. Durocher, Y. Tao, M. Leclerc, *J. Am. Chem. Soc.* **2008**, *130*, 732.
- [183] M. A. Faist, S. Shoaee, S. Tuladhar, Dibb, George F. A., S. Foster, W. Gong, T. Kirchartz, Bradley, Donal D. C., J. R. Durrant, J. Nelson, *Adv. Energy Mater.* **2013**, *3*, 744.
- [184] J. W. Jung, J. W. Jo, E. H. Jung, W. H. Jo, *Org. Electron.* **2016**, *31*, 149.
- [185] D. H. Wang, K. H. Park, J. H. Seo, J. Seifter, J. H. Jeon, J. K. Kim, J. H. Park, O. O. Park, A. J. Heeger, *Adv. Energy Mater.* **2011**, *1*, 766.
- [186] D. H. Wang, J. K. Kim, J. H. Seo, I. Park, B. H. Hong, J. H. Park, A. J. Heeger, *Angew. Chem. Int. Ed.* **2013**, *52*, 2874.
- [187] C.-H. Chen, C.-H. Hsieh, M. Duboscq, Y.-J. Cheng, C.-S. Hsu, *Macromolecules* **2010**, *43*, 697.
- [188] T. B. Raju, P. Gopikrishna, P. K. Iyer, *RSC Adv.* **2014**, *4*, 37738.
- [189] A. Kraak, A. K. Wiersema, P. Jordens, H. Wynberg, *Tetrahedron* **1968**, *24*, 3381.
- [190] A. T. Jeffries, K. C. Moore, D. M. Ondeyka, A. W. Springsteen, D. W. H. MacDowell, *J. Org. Chem.* **1981**, *46*, 2885.
- [191] R. Beyer, M. Kalaji, G. Kingscote-Burton, P. J. Murphy, Pereira, V. M. S. C., D. M. Taylor, G. O. Williams, *Synth. Met.* **1998**, *92*, 25.
- [192] P. Lucas, N. E. Mehdi, H. A. Ho, D. Bélanger, L. Breau, *Synthesis* **2000**, *2000*, 1253.
- [193] J. Z. Brzeziński, J. R. Reynolds, *Synthesis* **2002**, *2002*, 1053.
- [194] J. P. Ferraris, T. L. Lambert, *J. Chem. Soc. Chem. Commun.* **1991**, *85*, 1268.
- [195] T. L. Lambert, J. P. Ferraris, *J. Chem. Soc. Chem. Commun.* **1991**, *85*, 752.
- [196] P. Coppo, D. C. Cupertino, S. G. Yeates, M. L. Turner, *Macromolecules* **2003**, *36*, 2705.
- [197] Z. Zhu, D. Waller, R. Gaudiana, M. Morana, D. Mühlbacher, M. Scharber, C. Brabec, *Macromolecules* **2007**, *40*, 1981.
- [198] D. Mühlbacher, M. Scharber, M. Morana, Z. Zhu, D. Waller, R. Gaudiana, C. Brabec, *Adv. Mater.* **2006**, *18*, 2884.
- [199] J. Peet, J. Y. Kim, N. E. Coates, W. L. Ma, D. Moses, A. J. Heeger, G. C. Bazan, *Nat. Mater.* **2007**, *6*, 497.
- [200] J. Peet, C. Soci, R. C. Coffin, T. Q. Nguyen, A. Mikhailovsky, D. Moses, G. C. Bazan, *Appl. Phys. Lett.* **2006**, *89*, 252105.
- [201] M. Dante, A. Garcia, T.-Q. Nguyen, *J. Phys. Chem. C* **2009**, *113*, 1596.
- [202] J. Y. Kim, K. Lee, N. E. Coates, D. Moses, T.-Q. Nguyen, M. Dante, A. J. Heeger, *Science* **2007**, *317*, 222.
- [203] C. Soci, I.-W. Hwang, D. Moses, Z. Zhu, D. Waller, R. Gaudiana, C. J. Brabec, A. J. Heeger, *Adv. Funct. Mater.* **2007**, *17*, 632.
- [204] I.-W. Hwang, C. Soci, D. Moses, Z. Zhu, D. Waller, R. Gaudiana, C. J. Brabec, A. J. Heeger, *Adv. Mater.* **2007**, *19*, 2307.
- [205] M. Morana, M. Wegscheider, A. Bonanni, N. Kopidakis, S. Shaheen, M. Scharber, Z. Zhu, D. Waller, R. Gaudiana, C. Brabec, *Adv. Funct. Mater.* **2008**, *18*, 1757.
- [206] M. Zhang, H. N. Tsao, W. Pisula, C. Yang, A. K. Mishra, K. Müllen, *J. Am. Chem. Soc.* **2007**, *129*, 3472.
- [207] A. J. Moulé, A. Tsami, T. W. Bünnagel, M. Forster, N. M. Kronenberg, M. Scharber, M. Koppe, M. Morana, C. J. Brabec, K. Meerholz, U. Scherf, *Chem. Mater.* **2008**, *20*, 4045.
- [208] J. Hou, T. L. Chen, S. Zhang, Y. Yang, *J. Phys. Chem. C* **2009**, *113*, 1601.

- [209] M. Horie, L. A. Majewski, M. J. Fearn, C.-Y. Yu, Y. Luo, A. Song, B. R. Saunders, M. L. Turner, *J. Mater. Chem.* **2010**, *20*, 4347.
- [210] M. Horie, J. Kettle, C.-Y. Yu, L. A. Majewski, S.-W. Chang, J. Kirkpatrick, S. M. Tuladhar, J. Nelson, B. R. Saunders, M. L. Turner, *J. Mater. Chem.* **2012**, *22*, 381.
- [211] S. Albrecht, S. Janietz, W. Schindler, J. Frisch, J. Kurpiers, J. Kniepert, S. Inal, P. Pingel, K. Fostiropoulos, N. Koch, D. Neher, *J. Am. Chem. Soc.* **2012**, *134*, 14932.
- [212] L. Bian, E. Zhu, J. Tang, W. Tang, F. Zhang, *Prog. Polym. Sci.* **2012**, *37*, 1292.
- [213] H. Zhou, L. Yang, W. You, *Macromolecules* **2012**, *45*, 607.
- [214] J. Weickert, R. B. Dunbar, H. C. Hesse, W. Wiedemann, L. Schmidt-Mende, *Adv. Mater.* **2011**, *23*, 1810.
- [215] D. Yu, Y.-Q. Yang, Z. Chen, Y. Tao, Y.-F. Liu, *Opt. Commun.* **2016**, *362*, 43.
- [216] N. D. Treat, T. E. Mates, C. J. Hawker, E. J. Kramer, M. L. Chabinyc, *Macromolecules* **2013**, *46*, 1002.
- [217] N. D. Treat, M. A. Brady, G. Smith, M. F. Toney, E. J. Kramer, C. J. Hawker, M. L. Chabinyc, *Adv. Energy Mater.* **2011**, *1*, 82.
- [218] B. A. Collins, E. Gann, L. Guignard, X. He, C. R. McNeill, H. Ade, *J. Phys. Chem. Lett.* **2010**, *1*, 3160.
- [219] H. Kong, J. Sinha, D. Hoeft, S. B. Kirschner, D. H. Reich, H. E. Katz, *Org. Electron.* **2013**, *14*, 703.
- [220] Y. Yang, K. Mielczarek, A. Zakhidov, W. Hu, *ACS Appl. Mater. Interfaces* **2016**, *8*, 7300.
- [221] G. Wantz, L. Derue, O. Dautel, A. Rivaton, P. Hudhomme, C. Dagron-Lartigau, *Polym. Int.* **2014**, *63*, 1346.
- [222] J. W. Rumer, I. McCulloch, *Mater. Today* **2015**, *18*, 425.
- [223] P. Knauer, T. Hahn, A. Köhler, P. Strohhriegl, *J. Mater. Chem. C* **2016**, *4*, 10347.
- [224] S. Jungermann, N. Riegel, D. Müller, K. Meerholz, O. Nuyken, *Macromolecules* **2006**, *39*, 8911.
- [225] Y. Chen, K.-C. Lin, *J. Polym. Sci. A Polym. Chem.* **1999**, *37*, 2969.
- [226] S. Chambon, A. Rivaton, J.-L. Gardette, M. Firon, *Sol. Energy Mater. Sol. Cells* **2007**, *91*, 394.
- [227] S. Chambon, A. Rivaton, J.-L. Gardette, M. Firon, *Sol. Energy Mater. Sol. Cells* **2008**, *92*, 785.
- [228] M. Manceau, S. Chambon, A. Rivaton, J.-L. Gardette, S. Guillerez, N. Lemaître, *Sol. Energy Mater. Sol. Cells* **2010**, *94*, 1572.
- [229] M. C. Gather, A. Köhnen, A. Falcou, H. Becker, K. Meerholz, *Adv. Funct. Mater.* **2007**, *17*, 191.
- [230] E. Scheler, E. Betthausen, P. Strohhriegl, *Macromol. Chem. Phys.* **2010**, *211*, 2081.
- [231] E. Scheler, P. Strohhriegl, *J. Mater. Chem.* **2009**, *19*, 3207.
- [232] B. J. Kim, Y. Miyamoto, B. Ma, Fréchet, Jean M. J., *Adv. Funct. Mater.* **2009**, *19*, 2273.
- [233] S. Miyanishi, K. Tajima, K. Hashimoto, *Macromolecules* **2009**, *42*, 1610.
- [234] F. Ouhib, M. Tomassetti, J. Manca, F. Piersimoni, D. Spoltore, S. Bertho, H. Moons, R. Lazzaroni, S. Desbief, C. Jerome, C. Detrembleur, *Macromolecules* **2013**, *46*, 785.
- [235] H. J. Kim, A.-R. Han, C.-H. Cho, H. Kang, H.-H. Cho, M. Y. Lee, Fréchet, Jean M. J., J. H. Oh, B. J. Kim, *Chem. Mater.* **2012**, *24*, 215.
- [236] G. Brotas, J. Farinhas, Q. Ferreira, J. Morgado, A. Charas, *Synth. Met.* **2012**, *162*, 2052.

- [237] G. Griffini, J. D. Douglas, C. Piliago, T. W. Holcombe, S. Turri, Fréchet, Jean M. J., J. L. Mynar, *Adv. Mater.* **2011**, *23*, 1660.
- [238] D. Qian, Q. Xu, X. Hou, F. Wang, J. Hou, Z. 'a. Tan, *J. Polym. Sci. A Polym. Chem.* **2013**, *51*, 3123.
- [239] K. Yao, L. Chen, T. Hu, Y. Chen, *Org. Electron.* **2012**, *13*, 1443.
- [240] C. J. Mueller, T. Klein, E. Gann, C. R. McNeill, M. Thelakkat, *Macromolecules* **2016**, *49*, 3749.
- [241] X. Chen, L. Chen, Y. Chen, *J. Polym. Sci. A Polym. Chem.* **2013**, *51*, 4156.
- [242] Y. Tang, H. Chen, K. Chang, Z. Liu, Y. Wang, S. Qu, H. Xu, C. Wu, *ACS Appl. Mater. Interfaces* **2017**, *9*, 3419.
- [243] J. E. Carlé, B. Andreasen, T. Tromholt, M. V. Madsen, K. Norrman, M. Jørgensen, F. C. Krebs, *J. Mater. Chem.* **2012**, *22*, 24417.
- [244] C. P. Yau, S. Wang, N. D. Treat, Z. Fei, Tremolet de Villers, Bertrand J., M. L. Chabinyk, M. Heeney, *Adv. Energy Mater.* **2015**, *5*, 1401228.
- [245] X.-Q. Chen, X. Yao, X. Xiang, L. Liang, W. Shao, F.-G. Zhao, Z. Lu, W. Wang, J. Li, W.-S. Li, *J. Mater. Chem. A* **2016**, *4*, 9286.
- [246] A. Charas, Q. Ferreira, J. Farinhas, M. Matos, L. Alcácer, J. Morgado, *Macromolecules* **2009**, *42*, 7903.
- [247] S. Feser, K. Meerholz, *Chem. Mater.* **2011**, *23*, 5001.
- [248] F.-J. Kahle, I. Bauer, P. Stroehriegl, A. Köhler, *J. Polym. Sci. B Polym. Phys.* **2017**, *55*, 112.
- [249] N. Aizawa, C. Fuentes-Hernandez, V. A. Kolesov, T. M. Khan, J. Kido, B. Kippelen, *Chem. Commun.* **2016**, *52*, 3825.
- [250] H. L. Kwok, *J. Mater. Sci. Mater. Electron.* **2014**, *25*, 1571.
- [251] S. Fabiano, S. Braun, X. Liu, E. Weverberghs, P. Gerbaux, M. Fahlman, M. Berggren, X. Crispin, *Advanced materials (Deerfield Beach, Fla.)* **2014**, *26*, 6000.
- [252] T. T. T. Bui, S. Park, M. Jahandar, C. E. Song, S. K. Lee, J.-C. Lee, S.-J. Moon, W. S. Shin, *RSC Adv.* **2016**, *6*, 61284.
- [253] B. Gholamkhash, S. Holdcroft, *Chem. Mater.* **2010**, *22*, 5371.
- [254] C.-Y. Nam, Y. Qin, Y. S. Park, H. Hlaing, X. Lu, B. M. Ocko, C. T. Black, R. B. Grubbs, *Macromolecules* **2012**, *45*, 2338.
- [255] A. Tournebize, A. Rivaton, J.-L. Gardette, C. Lombard, B. Pépin-Donat, S. Beaupré, M. Leclerc, *Adv. Energy Mater.* **2014**, *4*, 1301530.
- [256] C. H. Peters, I. T. Sachs-Quintana, J. P. Kastrop, S. Beaupré, M. Leclerc, M. D. McGehee, *Adv. Energy Mater.* **2011**, *1*, 491.
- [257] C. H. Peters, I. T. Sachs-Quintana, W. R. Mateker, T. Heumueller, J. Rivnay, R. Noriega, Z. M. Beiley, E. T. Hoke, A. Salleo, M. D. McGehee, *Adv. Mater.* **2012**, *24*, 663.
- [258] C.-Z. Li, H.-L. Yip, A. K.-Y. Jen, *J. Mater. Chem.* **2012**, *22*, 4161.
- [259] C.-P. Chen, C.-Y. Huang, S.-C. Chuang, *Adv. Funct. Mater.* **2015**, *25*, 207.
- [260] N. Deb, R. R. Dasari, K. Moudgil, J. L. Hernandez, S. R. Marder, Y. Sun, A. Karim, D. G. Bucknall, *J. Mater. Chem. A* **2015**, *3*, 21856.
- [261] J.-F. Nierengarten, S. Setayesh, *New J. Chem.* **2006**, *30*, 313.
- [262] Y.-J. Cheng, C.-H. Hsieh, P.-J. Li, C.-S. Hsu, *Adv. Funct. Mater.* **2011**, *21*, 1723.
- [263] M. Drees, H. Hoppe, C. Winder, H. Neugebauer, N. S. Sariciftci, W. Schwinger, F. Schäffler, C. Topf, M. C. Scharber, Z. Zhu, R. Gaudiana, *J. Mater. Chem.* **2005**, *15*, 5158.

- [264] K. Meerholz, *Nature* **2005**, *437*, 327.
- [265] Y.-J. Cheng, F.-Y. Cao, W.-C. Lin, C.-H. Chen, C.-H. Hsieh, *Chem. Mater.* **2011**, *23*, 1512.
- [266] W.-W. Liang, C.-Y. Chang, Y.-Y. Lai, S.-W. Cheng, H.-H. Chang, Y.-Y. Lai, Y.-J. Cheng, C.-L. Wang, C.-S. Hsu, *Macromolecules* **2013**, *46*, 4781.
- [267] N. Cho, H.-L. Yip, J. A. Davies, P. D. Kazarinoff, D. F. Zeigler, M. M. Durban, Y. Segawa, K. M. O'Malley, C. K. Luscombe, A. K.-Y. Jen, *Adv. Energy Mater.* **2011**, *1*, 1148.
- [268] C.-E. Tsai, M.-H. Liao, Y.-L. Chen, S.-W. Cheng, Y.-Y. Lai, Y.-J. Cheng, C.-S. Hsu, *J. Mater. Chem. C* **2015**, *3*, 6158.
- [269] B. Meng, Z. Xie, J. Liu, L. Wang, *Chem. Asian J.* **2016**, *11*, 1218.
- [270] Y.-J. Cheng, C.-H. Hsieh, Y. He, C.-S. Hsu, Y. Li, *J. Am. Chem. Soc.* **2010**, *132*, 17381.
- [271] C.-H. Hsieh, Y.-J. Cheng, P.-J. Li, C.-H. Chen, M. Dubosc, R.-M. Liang, C.-S. Hsu, *J. Am. Chem. Soc.* **2010**, *132*, 4887.
- [272] Y. Sun, S.-C. Chien, H.-L. Yip, Y. Zhang, K.-S. Chen, D. F. Zeigler, F.-C. Chen, B. Lin, A. K.-Y. Jen, *Chem. Mater.* **2011**, *23*, 5006.
- [273] Q. Xu, F. Wang, D. Qian, Z. Tan, L. Li, S. Li, X. Tu, G. Sun, X. Hou, J. Hou, Y. Li, *ACS Appl. Mater. Interfaces* **2013**, *5*, 6591.
- [274] K. Zhang, C. Zhong, S. Liu, C. Mu, Z. Li, H. Yan, F. Huang, Y. Cao, *ACS Appl. Mater. Interfaces* **2014**, *6*, 10429.
- [275] R. Meerheim, C. Körner, B. Oesen, K. Leo, *Appl. Phys. Lett.* **2016**, *108*, 103302.
- [276] J. Wang, K. Lin, K. Zhang, X.-F. Jiang, K. Mahmood, L. Ying, F. Huang, Y. Cao, *Adv. Energy Mater.* **2016**, *6*, 1502563.
- [277] D. Chen, F. Liu, C. Wang, A. Nakahara, T. P. Russell, *Nano Lett.* **2011**, *11*, 2071.
- [278] F. Fischer, T. Hahn, H. Bässler, I. Bauer, P. Strohrriegl, A. Köhler, *Adv. Funct. Mater.* **2014**, *24*, 6172.
- [279] C. B. Nielsen, S. Holliday, H.-Y. Chen, S. J. Cryer, I. McCulloch, *Acc. Chem. Res.* **2015**, *48*, 2803.
- [280] P. K. Watkins, A. B. Walker, G. L. B. Verschoor, *Nano Lett.* **2005**, *5*, 1814.
- [281] E. Scheler, P. Strohrriegl, *Chem. Mater.* **2010**, *22*, 1410.
- [282] B. Liu, R.-Q. Png, L.-H. Zhao, L.-L. Chua, R. H. Friend, P. K. H. Ho, *Nat. Commun.* **2012**, *3*, 1321.
- [283] J. Farinhas, Q. Ferreira, Di Paolo, Roberto E., L. Alcácer, J. Morgado, A. Charas, *J. Mater. Chem.* **2011**, *21*, 12511.
- [284] H. C. Hesse, D. Lembke, L. Dössel, X. Feng, K. Müllen, L. Schmidt-Mende, *Nanotechnology* **2011**, *22*, 55303.
- [285] T. Pfadler, M. Coric, C. M. Palumbiny, A. C. Jakowetz, K.-P. Strunk, J. A. Dorman, P. Ehrenreich, C. Wang, A. Hexemer, R.-Q. Png, P. K. H. Ho, P. Müller-Buschbaum, J. Weickert, L. Schmidt-Mende, *ACS Nano* **2014**, *8*, 12397.
- [286] C.-Y. Chang, C.-E. Wu, S.-Y. Chen, C. Cui, Y.-J. Cheng, C.-S. Hsu, Y.-L. Wang, Y. Li, *Angew. Chem. Int. Ed. Engl.* **2011**, *50*, 9386.
- [287] X. He, F. Gao, G. Tu, D. Hasko, S. Huttner, U. Steiner, N. C. Greenham, R. H. Friend, Huck, Wilhelm T. S., *Nano Lett.* **2010**, *10*, 1302.
- [288] N. Haberkorn, J. S. Gutmann, P. Theato, *ACS Nano* **2009**, *3*, 1415.
- [289] R. Bai, M. Ouyang, R.-J. Zhou, M.-M. Shi, M. Wang, H.-Z. Chen, *Nanotechnology* **2008**, *19*, 55604.

-
- [290] R.-Q. Png, P.-J. Chia, J.-C. Tang, B. Liu, S. Sivaramakrishnan, M. Zhou, S.-H. Khong, Chan, Hardy S. O., J. H. Burroughes, L.-L. Chua, R. H. Friend, P. K. H. Ho, *Nat. Mater.* **2009**, *9*, 152.
- [291] Z.-K. Tan, K. Johnson, Y. Vaynzof, A. A. Bakulin, L.-L. Chua, P. K. H. Ho, R. H. Friend, *Adv. Mater.* **2013**, *25*, 4131.
- [292] C. Tao, M. Aljada, P. E. Shaw, K. H. Lee, H. Cavaye, M. N. Balfour, R. J. Borthwick, M. James, P. L. Burn, I. R. Gentle, P. Meredith, *Adv. Energy Mater.* **2013**, *3*, 105.
- [293] L. Derue, O. Dautel, A. Tournebize, M. Drees, H. Pan, S. Berthumeyrie, B. Pavageau, E. Cloutet, S. Chambon, L. Hirsch, A. Rivaton, P. Hudhomme, A. Facchetti, G. Wantz, *Adv. Mater.* **2014**, *26*, 5831.
- [294] J. W. Rumer, R. S. Ashraf, N. D. Eisenmenger, Z. Huang, I. Meager, C. B. Nielsen, B. C. Schroeder, M. L. Chabiny, I. McCulloch, *Adv. Energy Mater.* **2015**, *5*, 1401426.
- [295] L. J. Guo, *Adv. Mater.* **2007**, *19*, 495.
- [296] J. Wang, K. Liu, L. Ma, X. Zhan, *Chem. Rev.* **2016**, *116*, 14675.
- [297] V. Merz, W. Weith, *Ber. Dtsch. Chem. Ges.* **1873**, *6*, 1511.
- [298] I. Goldberg, M. Nimerovsky, *Ber. Dtsch. Chem. Ges.* **1907**, *40*, 2448.
- [299] P. Agarwala, D. Kabra, *J. Mater. Chem. A* **2017**, *5*, 1348.
- [300] M. Thelakkat, *Macromol. Mater. Eng.* **2002**, *287*, 442.
- [301] P. M. Borsenberger, L. Pautmeier, R. Richert, H. Bässler, *J. Chem. Phys.* **1991**, *94*, 8276.
- [302] P. M. Borsenberger, W. T. Gruenbaum, L. J. Sorriero, N. Zumbulyadis, *Jpn. J. Appl. Phys.* **1995**, *34*, L1597-L1598.
- [303] M. Redecker, D. D.C. Bradley, M. Inbasekaran, W. W. Wu, E. P. Woo, *Adv. Mater.* **1999**, *11*, 241.
- [304] D. Vak, J. Jo, J. Ghim, C. Chun, B. Lim, A. J. Heeger, D.-Y. Kim, *Macromolecules* **2006**, *39*, 6433.
- [305] M. Bender, K. M. Schelkle, N. Jürgensen, S. Schmid, G. Hernandez-Sosa, U. H. F. Bunz, *Macromolecules* **2016**, *49*, 2957.
- [306] Y.-C. Chao, C.-H. Chuang, H.-L. Hsu, H.-J. Wang, Y.-C. Hsu, C.-P. Chen, R.-J. Jeng, *Sol. Energy Mater. Sol. Cells* **2016**, *157*, 666.

3. Objective of the thesis

Organic solar cells have gained a large research interest over the last years as a potential alternative to silicon cells. However, organic solar cells still do not provide efficiencies and long-term stabilities high enough for commercialization. Some of the major unsolved problems in organic solar cells arise from their instability regarding different stress factors like heat or light exposure. Bulk heterojunction solar cells contain a mixture of donor and acceptor material. They often suffer from diffusion and subsequent aggregation of the low molecular weight acceptor upon device operation over a long time or at elevated temperatures. Hence, the device performance is decreased. The formation of multilayer solar cells is mainly restricted to the evaporation of low molar mass materials. Polymers are difficult to use in multilayer cells as they are solution processed. By spin coating a second polymer solution on top of the first polymer, the underlying layer is often dissolved or damaged. This is also the reason for the collapse of nanoimprinted patterns when applying the second active material.

Regarding these challenges, research on degradation mechanisms and device fabrication concerning a prolonged stability is of major importance. The dissolution problem can be avoided using orthogonal solvents for the different active materials. Furthermore, inorganic interlayers can be inserted which are not soluble in organic solvents. Tandem solar cells are a prominent example for that method. A versatile possibility to solve the problems associated with device stability is the application of crosslinkable materials. Such conjugated polymers bearing crosslinkable groups can be processed from solution. Upon crosslinking started by an initiator, exposure to UV light or heat, covalent bonds are formed between the polymer chains and the initial morphology is frozen. This results in a densely crosslinked polymer network which is insoluble. Using crosslinkable materials, three concepts for the stabilization of organic solar cells can be realized. First, a blend containing a crosslinkable donor polymer can be used for bulk heterojunction solar cells. Thus, the crosslinking of the donor prevents the diffusion and aggregation of the low molecular weight acceptor and the solar cell performance is retained. The formation of multilayer devices from solution is a second aspect. Processing and subsequent crosslinking of a polymer results in an insoluble layer which allows the spin coating of a second polymer solution on top without dissolving the underlying layer. Nanoimprinted structures can also be stabilized. Therefore, a donor polymer is deposited and patterned by means of a stamp. Crosslinking turns the structure totally insoluble and an acceptor can be spin coated or vacuum evaporated without damaging the pattern.

Furthermore, investigations of intrinsic mechanisms like charge carrier generation and recombination are essential for the basic understanding of the behaviour of different donor and acceptor materials in organic solar cells. For this purpose, polymers with properties that allow these specific studies are needed.

In this work, the synthesis of novel low bandgap polymers is described. These polymers are used in both device fabrication and fundamental studies. Chemical modifications of the low bandgap

polymers PCDTBT and PCPDTBT are realized. The chemical structures of the two polymers are shown in Figure 38.

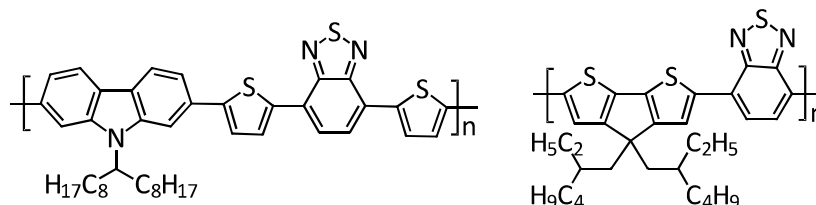


Figure 38: Chemical structures of PCDTBT (left) and PCPDTBT (right).

The idea behind was not to invent totally new donor materials for organic solar cells, but to use well-known low bandgap polymers and modify them with respect to different properties taking advantage of the existing knowledge about PCDTBT and PCPDTBT.

The chemical modifications done on the polymers can be divided into two parts. On the one hand, crosslinkable derivatives of PCDTBT and PCPDTBT are synthesized. Oxetane is chosen as the crosslinking unit and is attached to the side chains of the donor units of the low bandgap polymers. This includes the synthesis of linear and branched aliphatic spacers bearing an oxetane unit as well as attaching the crosslinkable spacers to the donor cores carbazole and cyclopentadithiophene. The alternating copolymers are synthesized via palladium-catalysed Suzuki polycondensations. Additionally, the corresponding non-crosslinkable reference materials are also synthesized. On the other hand, comonomers are incorporated into the basic polymer structure of PCDTBT. Triphenyldiamine is selected as a comonomer due to its good hole transport characteristics. Therefore, a triphenyldiamine donor unit is prepared and polymerized in combination with the PCDTBT monomers via palladium-catalysed Suzuki couplings. In this work, these polymers are referred to as “low bandgap copolymers” to distinguish them from the polymers with only one donor and acceptor unit, which are known as low bandgap polymers but are actually also copolymers. Furthermore, the acceptor monomer is applied with and without aliphatic spacer. By means of this approach, a series of copolymers with varying properties is obtained. The corresponding reference polymers without the additional comonomer are synthesized as well.

The polymers are characterized regarding their chemical, thermal, optical, and electronic properties. Detailed analyses are performed with respect to the different polymer modifications. For the crosslinkable low bandgap polymers, the main focus lies on the crosslinking procedure. The mechanism behind the crosslinking of oxetane, as for other cyclic ethers, is a cationic ring-opening polymerization with high reaction rate. The influence of the crosslinking process and conditions on the polymer properties is examined. In the case of the low bandgap copolymers, the influence of the additional triphenyldiamine units as well as the spacers located at the acceptor monomers should be investigated in comparison to the reference polymers. This includes primarily the variation of the thermal properties due to the incorporation of the bulky comonomer as well as the solubilizing aliphatic spacers. Furthermore,

3. Objective of the thesis

the effect of the additional comonomer on the electronic properties of the polymers is examined by mobility measurements.

A possibility for the fabrication of multilayer devices from solution is the application of crosslinkable polymers. Thus, one aim of the thesis was to prepare a three-layer organic solar cell by making use of the insolubility obtained by crosslinking. This enables spin-coating of a second material on top.

Planar heterojunction solar cells are used as model systems for fundamental research, aiming at the detailed understanding of the processes at the donor acceptor interface. The low bandgap copolymers prepared in this work are used in basic studies concerning photogeneration and charge carrier recombination. Concerning prolonged device stability, the investigation of the diffusion of small acceptor molecules within the donor polymer is an important subject. A further aim of this work is the examination of the diffusion behaviour of fullerene in combination with different low bandgap polymers and a novel copolymer.

4. Overview of the thesis

This thesis covers the synthesis and characterization of low bandgap polymers and copolymers as well as their application in both device fabrication and fundamental studies. A deeper understanding of degradation mechanisms and enhancing device stability is very important for the fabrication of solar cells with prolonged lifetime. One way to achieve this goal is the use of crosslinkable polymers that allow the stabilization of the solar cell morphology. In addition, basic research on the behavior of donor and acceptor materials in organic solar cells is dependent on the availability of materials that allow such specific studies because of their intrinsic properties.

The synthetic part of this work includes strategies towards new monomers with functional groups and their corresponding polymers. The thermal, optical, and electronic properties of the synthesized materials are examined with respect to their chemical structure. According to their properties, the polymers can be used on the one hand for the formation of multilayer solar cells or on the other hand for investigations concerning photogeneration, charge carrier recombination and diffusion of small acceptor molecules.

The main aspect of this thesis is to obtain chemically modified derivatives of the well-known low-bandgap polymers PCDTBT and PCPDTBT (Figure 38) with specific properties that are used as donor materials for organic solar cells. The chemical modifications can be divided into two parts and are illustrated in Figure 39. The first part deals with the attachment of crosslinkable groups to the polymer resulting in crosslinkable low bandgap polymers. Oxetane is chosen as crosslinkable unit and both PCDTBT and PCPDTBT derivatives are synthesized. Therefore, linear and branched aliphatic spacers containing oxetane groups are developed. Carbazole and cyclopentadithiophene cores are equipped with these spacers and converted into the crosslinkable polymers. The crosslinking procedure is examined in detail for the crosslinkable PCDTBT and PCPDTBT polymers. By using a crosslinked polymer layer, the formation of a three-layer solar cell is described.

The second part of the thesis focuses on the incorporation of comonomers in the chemical structure of PCDTBT. Triphenyldiamine exhibits good hole transport properties and is applied as a comonomer. The synthetic strategy comprises the development of a triphenyldiamine unit and the subsequent polymerization with the PCDTBT monomers. The synthesized polymers containing an additional comonomer are referred to as “low bandgap copolymers” in this work. This allows the differentiation of these polymers from the “low bandgap polymers” with only one donor and acceptor unit which are actually also copolymers. By the use of aliphatic spacers attached to the acceptor monomer, a series of low bandgap copolymers is obtained. The characterization elucidates the influences of the triphenyldiamine units and the aliphatic spacers, especially on the thermal properties and the charge carrier mobility. As the synthesized low bandgap copolymers show properties allowing fundamental studies, investigations of the photogeneration and charge carrier recombination in organic bilayer solar cells are conducted.

4. Overview of the thesis

Furthermore, the low bandgap polymers and a novel copolymer are used in a detailed study on the diffusion behaviour of the low molecular weight acceptor fullerene.

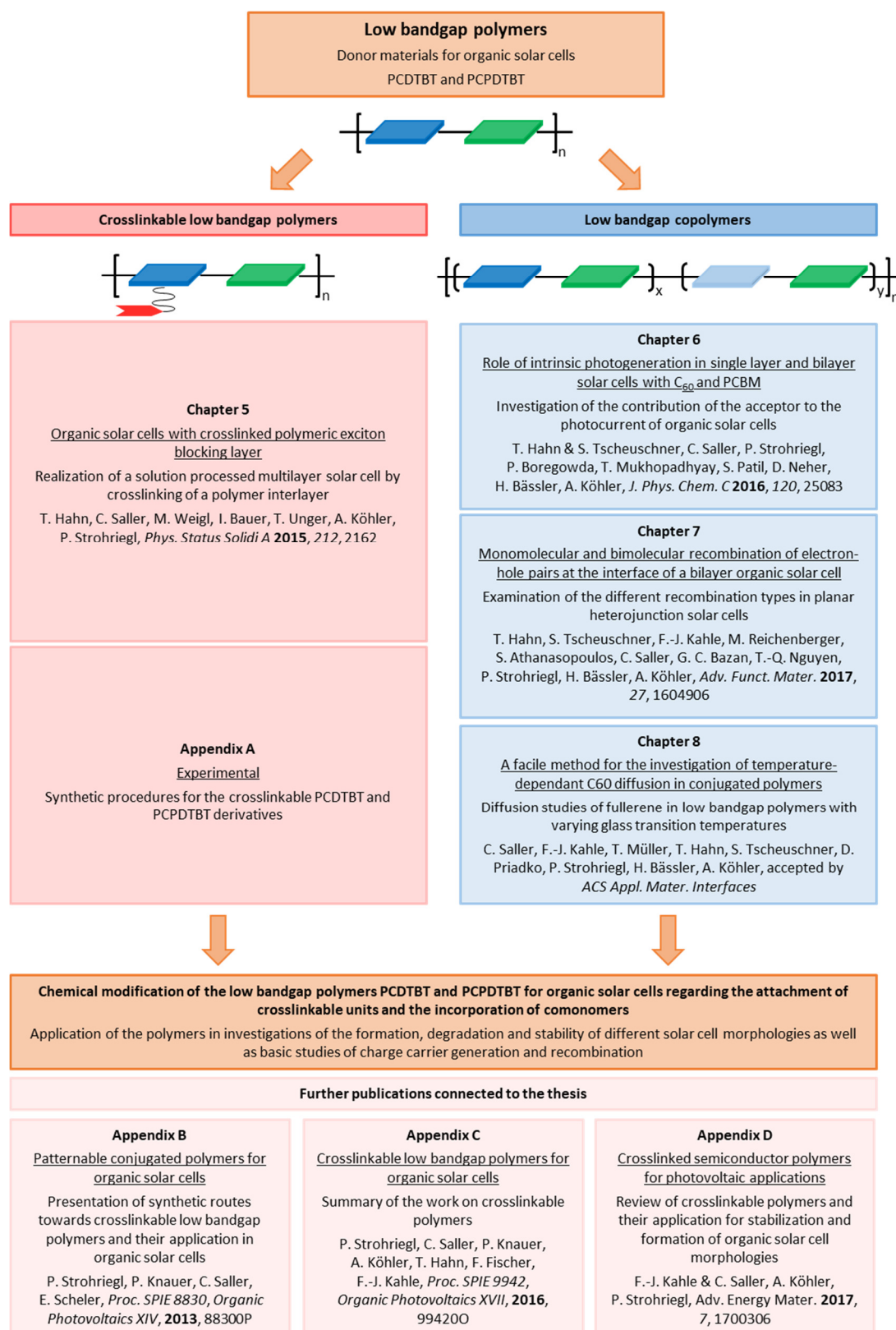


Figure 39: Schematic overview of the thesis including the two main synthetic routes and the corresponding publications as well as further publications connected to the thesis.

The first section concerning the crosslinkable polymers describes the realization of a first solution processed three-layer solar cell (Chapter 5). Usually, multilayer solar cells are made from vacuum evaporated small molecules. This work extends the concept of multilayer formation to solution processed low bandgap polymers. This was enabled by a crosslinked and thus insoluble polymer interlayer which allows spin coating of a second polymer layer on top without damaging the underlying layer. For examination of the influence of the additional crosslinked layer, the three-layer cell was compared to a bilayer reference cell without this crosslinked layer. This approach is the first step to multilayer devices when further crosslinkable materials, for example crosslinkable donor polymers, are applied.

The optimized synthetic strategies for the crosslinkable PCDTBT and PCPDTBT derivatives can be found in Appendix A. One approach for the PCDTBT derivative with attached oxetane units is also presented in Appendix B. However, the synthesis of the branched aliphatic spacer via the proposed reaction pathway was difficult to reproduce. In addition, the complete purification of the desired monomer was tedious. To overcome these problems, the synthesis of the PCDTBT with crosslinkable oxetane units was adapted at two main points. This includes an adjusted synthesis of the branched aliphatic spacer as well as a new sequence of the donor and the acceptor monomer. This allows the successful synthesis of the desired crosslinkable PCDTBT derivative. In the case of the crosslinkable PCPDTBT, the synthesis of a short aliphatic spacer, a crosslinkable donor monomer and a subsequent polymerization has been developed.

Chapter 6 introduces the second part of the thesis dealing with the incorporation of comonomers in the polymer structure of PCDTBT. From this polymer series, a material for a basic study on photogeneration is selected. In many cases, only the dissociation of excitons on the donor acceptor interface is considered. But there is an additional intrinsic contribution from the donor material as well as from the acceptor. This work examines the intrinsic contribution of the acceptor materials C₆₀ and PCBM to the photocurrent of organic solar cells. Bilayer solar cells were used as model systems as they are suitable for fundamental research issues. The applied donor material should exhibit a negligible intrinsic dissociation so that the contribution from the acceptor could be evaluated properly. This is the case for a synthesized PCDTBT derivative modified with triphenyldiamine units. The dependence of the photogeneration of fullerenes on the excitation energy and the effect on the overall device efficiency is examined.

A further basic investigation addresses the different recombination types of excitons at the donor-acceptor interface (Chapter 7). Here, as in Chapter 6, planar heterojunction solar cells are used because they allow the evaluation of the different contributions from monomolecular and bimolecular recombination. For recombination studies, the solar cell should exhibit a good device performance without extraction problems as well as morphological stability. This means that the efficiency is independent from possible annealing steps or extraction layers. These requirements are fulfilled using a PCDTBT derivative with incorporated triphenyldiamine units and aliphatic spacers attached to the acceptor monomer. The recombination behaviour is

studied by investigating the influence of the donor layer thickness and the excitation light intensity on the fill factor of the bilayer solar cells.

Chapter 8 closes the circle between the studies concerning device fabrication, degradation and stabilization as well as the fundamental research. The diffusion of small acceptor molecules and subsequent aggregation often leads to phase separation and decreased device performance. This part of the thesis deals with the question how the diffusion of low molecular weight acceptor like C₆₀ in donor polymers for organic solar cells can be evaluated. We developed a bilayer setup for the investigation of the diffusion of fullerene via photoluminescence measurements. The effect of small changes in the chemical structure of the polymers on the diffusion behaviour is examined by the application of three different low bandgap (co)polymers with and without the incorporation of triphenyldiamine and short aliphatic spacers on the acceptor monomers, respectively. The results allow the selective adjustment of annealing times and temperatures during device fabrication towards an optimized morphology.

Furthermore, three additional publications are connected to this thesis. Appendix B contains the first synthetic strategy for the crosslinkable PCDTBT derivative with attached oxetane units in the side chains. This work transfers crosslinking, which is well-known for the fabrication of patterned organic light-emitting diodes, to organic solar cells. Three concepts for the application of crosslinkable materials with different solar cell morphologies are presented concerning the formation, degradation and stability of different solar cell morphologies like bulk heterojunction solar cells, multilayer devices and nanoimprinted cells. The multilayer concept is further discussed in Chapter 5, where a first three-layer solar cell made from solution-processed low-bandgap polymers and fullerene is presented. The synthesized new crosslinkable donor polymer PCDTBTOx depicts the next step towards multilayer setups that are dependent on the availability of crosslinkable active materials. Appendix A shows the optimized synthesis for PCDTBTOx as well as for PCPDTBTOx. A summary of the work on crosslinkable polymers and their application in both device fabrication and fundamental studies can be found in Appendix C. The last attachment is a review of crosslinkable polymers and their application for stabilizing organic solar cell morphologies (Appendix D). Here, the problems and possible solutions concerning device formation, degradation and stability of organic solar cells are discussed.

4.1 Crosslinkable low bandgap polymers

The first part of this thesis deals with the synthesis of crosslinkable conjugated polymers. Therefore, crosslinkable units are attached to the side chains of the polymers. This allows the crosslinking of the polymer after solution processing via an initiator, UV light or heat. During the crosslinking process, covalent bonds between the single polymer chains are formed which result in a densely crosslinked and thus insoluble polymer network. Furthermore, the initial morphology that was prepared via the solution processing is frozen. The application of crosslinkable materials presents one possibility for the fabrication and stabilization of organic solar cell morphologies. This morphology stabilization is necessary because organic solar cells often suffer from degradation upon prolonged operation and thus exhibit unsatisfactory device lifetimes. Problems with device stability can arise from different reasons thermal or optoelectronic stress. Crosslinking can prevent or limit some of this degradation mechanisms with respect to the different solar cell morphologies. In particular, three different concepts can be realized by the application of crosslinkable polymers in organic solar cells. The frequently used bulk heterojunction cells comprise a blend of a donor and an acceptor material. Besides low bandgap polymers as donor, fullerene and its derivatives are the most prominent acceptors. However, the small molecule acceptor can diffuse within the donor polymer when the device is operated over a long time or at elevated temperatures. Finally, this leads to an aggregation of acceptor molecules which degrades the device performance and efficiency. If a crosslinked donor polymer is applied, the diffusion and aggregation of the fullerene can be slowed down and the device performance is not decreased. Multilayer solar cells are usually made from vacuum evaporable small molecules. The fabrication of multilayer setups from polymer solutions is difficult as spin coating of a second material on top of a first layer dissolves and damages the underlying layer. Applying a crosslinked polymer in the first layer allows spin coating of a second polymer solution without damaging the underlying layer.

In the next section, a first three-layer solar cell is shown that presents the first step towards solution processed multilayer setups. This is the proof of concept for the development of multilayer solar cells that contain more functional layers. The next step towards such multilayer cells is the availability of crosslinkable donor polymers. During this thesis, crosslinkable derivatives of the low bandgap polymers PCDTBT and PCPDTBT (Figure 38) were designed. Therefore, oxetane was chosen as the crosslinkable unit and attached to the side chains of the polymers. The optimized synthesis of PCDTBT_{ox} and PCPDTBT_{ox} is presented in detail.

4.1.1 Organic solar cells with crosslinked polymeric exciton blocking layer

This chapter presents the realization of a first three-layer solar cell made from solution processed polymers. In contrast to the mostly solution processed bulk heterojunction solar cells, multilayer solar cells are often fabricated via vacuum evaporation of small molecules. The advantage of such multilayer setups is that the properties of each layer can be optimized

separately. This method is widely used for commercial organic light-emitting diodes and is transferred to organic solar cells, especially in the field of tandem solar cells. Polymers are difficult to use because they are solution processed. Spin coating a second material on top causes damage and dissolution of the underlying layer. However, solution processing is more efficient for the fabrication of large modules as roll to roll processes are not as expensive as vacuum evaporation. Orthogonal solvents suitable for the active materials avoid the dissolution of the underlying layer. In tandem solar cells, inorganic interlayers are often introduced because of their insolubility in organic solvents. One alternative possibility to overcome this problem is the application of crosslinkable materials. When a crosslinkable polymer is used, the dissolution of the polymer is prevented due to the formation of an insoluble, covalently bound polymer network upon crosslinking. Thus, spin-coating of a second material is possible because the crosslinked layer cannot be dissolved anymore. When additional crosslinkable materials are applied, multilayer devices can be realized.

This work contributes to the multilayer formation studies by realizing a first three-layer solar cell made from solution processed low bandgap polymers and fullerene. Each of the three active layers exhibit a specific function. The two consecutive polymer layers were enabled by the crosslinking of the underlying layer. Therefore, we used PFTPDAC, a copolymer consisting of fluorene and triphenyldiamine moieties (Figure 40). The crosslinkable acrylate units are attached to the side chains of the fluorene units. The idea behind the incorporation of the triphenyldiamine monomer into the polyfluorene structure was to expand the spectral absorption from the UV range to the red and to improve the hole transport ability. In Figure 40, the setup of the three-layer cell is shown. The solar cell was built on an ITO covered glass substrate with MoO₃ as hole-transporting layer. On top of the MoO₃ layer, we spin coated a thin PFTPDAC interlayer. The acrylate groups were crosslinked via a free radical mechanism by exposure to UV light in presence of a photoinitiator. Heating ensures the complete crosslinking of the polymer film. Due to its insolubility, the donor polymer PCDTBT could be spin-coated on top without damaging the PFTPDAC layer. Finally, the C₆₀ acceptor layer and an aluminium electrode were vacuum evaporated. Besides the three-layer solar cell, two reference cells were fabricated. The thickness of the MoO₃ layer is the same for the three cells. The three-layer cell comprises a PFTPDAC interlayer with 8 nm thickness, a 20 nm thick PCDTBT donor layer and a 30 nm thick C₆₀ acceptor layer. The reference cells consist only of PCDTBT and C₆₀ without the PFTPDAC interlayer. Once, 20 nm of PCDTBT and 30 nm of C₆₀ were chosen (reference 20), correspondingly to the three-layer cell. Furthermore, reference 30 contains a PCDTBT layer and a C₆₀ layer of both 30 nm thickness to maintain the overall active layer thickness of about 60 nm for the three-layer cell.

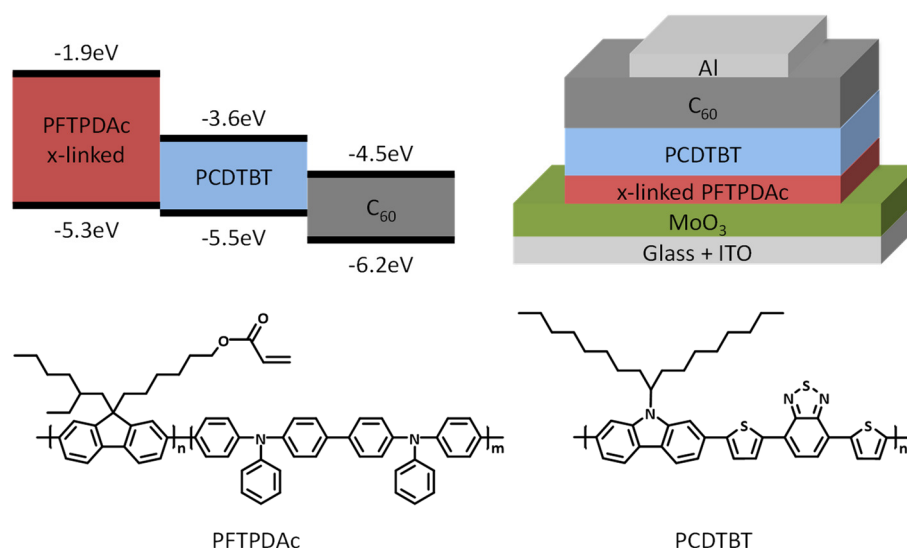


Figure 40: Cascading energy levels of the three active layer materials (left), device setup of the three-layer cell (right) and chemical structures of the crosslinkable polymer PFTPDAc and the donor polymer PCDTBT. Reprinted from Chapter 5.

We found an increased device performance for the three-layer solar cell. The EQE spectra as well as the current-voltage characteristics for the three-layer cell and the reference cells are presented in Figure 41. In the EQE spectra, a significant increase of the efficiency in the red part of the spectrum between 400 and 650 nm can be seen in comparison to the two reference cells. This enhancement correlates with the absorption of PCDTBT, especially at the absorption maximum at 580 nm, but not with the absorption of the crosslinked PFTPDAc interlayer. The current-voltage characteristics measured under sunlight conditions show that the open-circuit voltages of the three-layer cell and the reference cells are similar. However, the short-circuit current increases by 35% for the three-layer cell. This results in an efficiency enhancement from 1.4% for reference 30 and 1.6% for reference 20, respectively, to 1.8% for the three-layer cell.

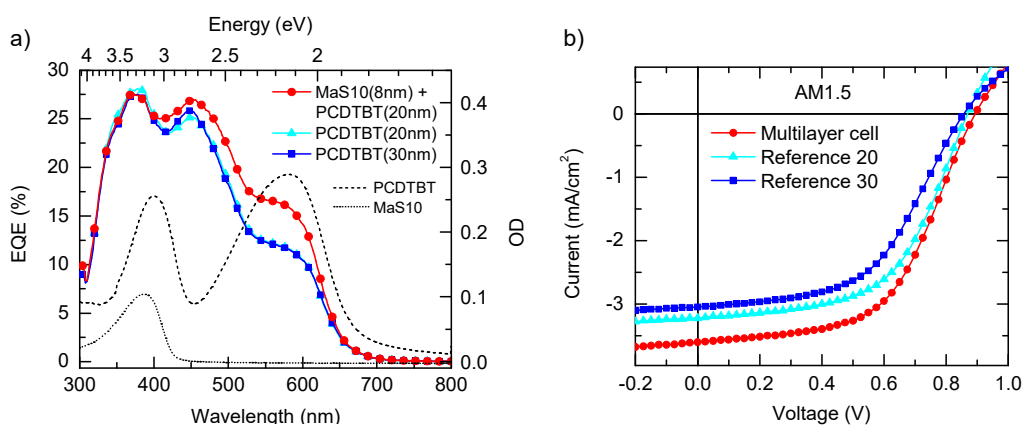


Figure 41: a) EQE spectra for the three-layer cell and the reference cells as well as absorption spectra of a PFTPDAc layer (8 nm) and a PCDTBT layer (30 nm). b) Current-voltage characteristics under sunlight AM1.5 conditions for the three-layer cell and the reference cells. Reprinted from Chapter 5.

As the absorption of the PFTPDAc is very low in the range of the EQE increase, an intrinsic contribution from this polymer to the total photogeneration can be excluded. Furthermore, the interface between the crosslinked PFTPDAc interlayer and the PCDTBT donor could attribute to

the photocurrent. For the evaluation of this aspect, bilayer cells from PFTPDAc as donor and PCDTBT as acceptor without C_{60} were fabricated. These solar cells showed a negligible efficiency smaller than 0.1% at 580 nm and thus no contribution to the efficiency increase. To evaluate the correlation between the absorption of PCDTBT and the efficiency enhancement, the absorption and photoluminescence of PCDTBT films were measured on different substrates. The optical density at the absorption maximum at 580 nm were identical for PCDTBT directly on MoO_3 and PCDTBT on a crosslinked PFTPDAc interlayer covering the MoO_3 layer. In both samples, the same amount of excitons is generated in the PCDTBT donor. In contrast, the photoluminescence intensity of the sample without the crosslinked PFTPDAc interlayer is reduced compared to the sample including the crosslinked interlayer. In addition to the steady state measurements, lifetime measurements of excitons formed in a PCDTBT layer on different substrates were conducted. The sample with the crosslinked PFTPDAc interlayer exhibits an exciton lifetime of 970 ps which is comparable to the 940 ps exciton lifetime of PCDTBT on glass. However, the PCDTBT sample directly on MoO_3 shows a reduced exciton lifetime of only 800 ps. The reduced photoluminescence intensity as well as the shorter exciton lifetimes of the samples without the crosslinked interlayer can be attributed to the diffusion of excitons generated in the PCDTBT layer towards the MoO_3 layer resulting in exciton quenching at the MoO_3 interface. As the exciton diffusion length is about 10 nm, quenching is an important loss mechanism in solar cells with thin active layer thicknesses and vanishes for increasing active layer thicknesses. Hence, we attribute the efficiency enhancement of the three-layer cell to the exciton-blocking effect of the crosslinked PFTPDAc layer. Considering the initial idea of improving the hole transport with the crosslinkable polymer, the photocurrent should increase over the total spectral range because it is irrelevant for the hole extraction if the charge generation was located in the donor or in the acceptor. However, the efficiency enhancement is not observed in the C_{60} dominated region between 350 nm and 400 nm but in the range of the PCDTBT absorption. The generated exciton density is high at the absorption maximum of PCDTBT and consequently the probability for exciton quenching at the MoO_3 interface is also high. The insertion of the crosslinked PFTPDAc interlayer prevents exciton quenching resulting in an increased device performance. It is known from tandem solar cells that additional layers can reduce the absorption of the active layers affecting the efficiency negatively. The thickness of the exciton blocking layer was therefore optimized to 8 nm. Thicker PFTPDAc layers also showed exciton blocking but the internal filter effect decreased the overall efficiency.

Exciton quenching is of general importance for multilayer solar cells as usually thin layers with thicknesses in the range of the exciton diffusion length are applied. Furthermore, the quenching is not restricted to MoO_3 hole-transporting layers but is a problem for all anode interlayers. In this work, the exciton quenching could also be observed for PEDOT:PSS. Exciton blocking layers are standard in an OLED setup and can also be found in multilayer solar cells based on vacuum evaporated small molecules. Thus, the realized three-layer solar cell comprising a crosslinked exciton blocking layer presents the first step towards multilayer setups from solution processed

polymers exhibiting a specific function for each layer. Based on this proof of concept, the fabrication method is dependent on the availability of crosslinkable functional materials like donor polymers or fullerene acceptors. Appendix D shows the synthetic strategy towards two crosslinkable low bandgap polymers which can be applied as a donor material in organic solar cells.

4.1.2 Optimized synthetic procedures for PCDTBT and PCPDTBT

In Chapter 5, the successful fabrication of a three-layer solar cell could be shown. The insertion of a crosslinked exciton blocking layer allowed the spin coating of a second polymer layer on top. Extending the concept to multilayer solar cells with a large number of layers relates to the availability of crosslinkable materials. This section deals with the design and synthesis of two novel crosslinkable low bandgap polymers suitable as donor materials for organic solar cells. As the idea was not to create totally new donor materials, we chose to modify the well-known low bandgap polymers PCDTBT and PCPDTBT by inserting the crosslinking ability.

Crosslinking of the polymers were enabled by the attachment of crosslinkable units to the side chains of the polymers. Oxetane was chosen as crosslinkable group due to several advantages. The crosslinking mechanism of the oxetane unit is a cationic ring opening polymerization. A photoinitiator, which releases a proton upon UV exposure, acid vapour or thermal initiation can be used to start the crosslinking process. By this means, an undesirable premature crosslinking, as it is often the case for acrylates, is prevented. Furthermore, the tolerance of the oxetane unit towards the Suzuki polycondensation necessary for the alternating arrangement of the monomer moieties is an important aspect. The crosslinkable oxetane units were attached to linear and branched aliphatic spacers. The donor monomers carbazole and cyclopentadithiophene were alkylated with the crosslinkable spacers. By subsequent Suzuki polycondensation, the crosslinkable low bandgap polymers were obtained.

The first synthetic strategy for the PCDTBT derivative with crosslinkable oxetane units at the side chains is presented in Appendix B. There, the crosslinkable oxetane units were added to dibromohexane. The branching was introduced via a Grignard reaction between the oxetane containing spacer and 1,2-epoxydecane. After tosylation, the branched spacer was attached to the carbazole core. Borylation of the carbazole yielded the donor monomer with crosslinkable oxetane units. However, the reproduction of the Grignard reaction in the presence of the oxetane group was complicated. Furthermore, the diborolane monomer could not be purified without major difficulties.

These problems required the adaption of the synthesis of the crosslinkable PCDTBT derivative with respect to both synthesis of the spacer and monomer purification. At first, the synthesis of the branched aliphatic spacer was realized by first building the branched structure via a Grignard reaction between bromooctane and 9-bromononanal and not till then adding the oxetane

group. Secondly, the sequence of the two monomers was changed. A carbazole donor monomer and a dithienylbenzothiadiazole acceptor monomer were applied so far. Now the two thiophene rings flanking the benzothiadiazole were attached to the carbazole donor unit. This new donor monomer was then combined with benzothiadiazole as acceptor monomer obtaining the desired PCDTBT derivative with crosslinkable oxetane units at the carbazole sidechains. In Figure 42, the optimized synthetic strategy for PCDTBTOx, a crosslinkable PCDTBT derivative with oxetane units attached to the side chains of the carbazole moieties, is presented.

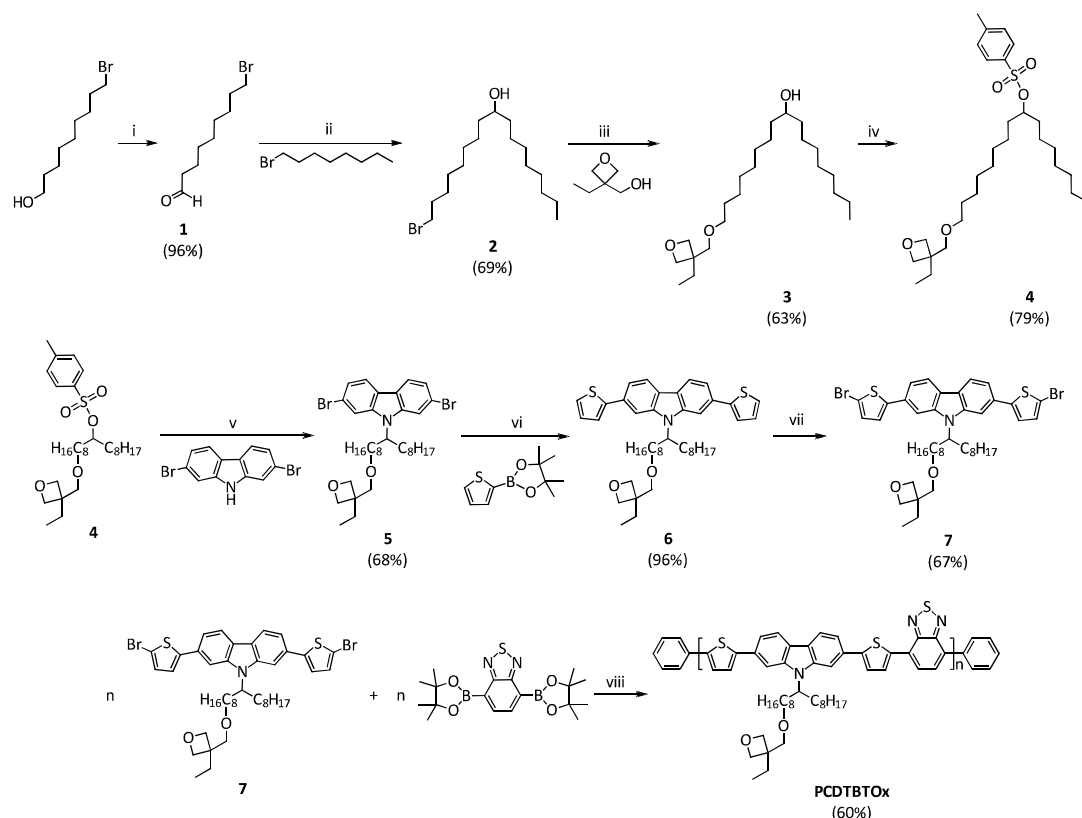


Figure 42: Synthetic strategy for the crosslinkable low bandgap polymer PCDTBTOx. Reaction conditions: i) 1. DMSO, oxalyl chloride, CH_2Cl_2 , -78°C , 5 min, 2. bromononanol, -78°C , 30 min, 3. $\text{N}(\text{Et})_3$, -78°C , 15 min, 4. r. t., H_2O ; ii) 1. bromooctane, THF abs., Mg, reflux, 30 min, 2. bromononanal, r. t., 3 h, 3. H_2O ; iii) (3-ethyloxetan-3-yl)-methanol, hexanes, aq. NaOH solution (45 wt%), $(\text{Bu})_4\text{NBr}$, reflux, 6 h; iv) 1. tosyl chloride, CH_2Cl_2 , Et_3N , $\text{Me}_3\text{N} \cdot \text{HCl}$, 0°C , 90 min, 2. r. t., overnight; v) 1. 2,7-dibromo-9H-carbazole, DMSO, KOH, 2. addition of 4 over 1 h, 3. r. t., overnight; vi) 2-(4',4',5',5'-tetramethyl-1',3',2'-dioxaborolan-2'-yl)-thiophene, toluene, aq. Na_2CO_3 solution (2 M), Aliquat 336, $\text{Pd}(\text{PPh}_3)_4$, reflux, 90 h; vii) 1. CHCl_3 , N-bromosuccinimide, 0°C , 1 h, in the dark, 2. r. t., overnight, in the dark; viii) 1. toluene, aq. Na_2CO_3 solution (2 M), Aliquat 336, $\text{Pd}(\text{PPh}_3)_4$, reflux, 90 h, 2. bromobenzene, reflux, 1 h, 3. phenylboronic acid, reflux, overnight.

The first step towards the branched crosslinkable spacer is a Swern oxidation of commercially available 9-bromononanol to the corresponding aldehyde. Therefore, dimethyl sulfoxide is activated with oxalyl chloride obtaining a sulfonium ion which reacts with an alcohol to an alkoxy-sulfonium ion. The base triethylamine deprotonates this ion to a sulfonium ylide. After rearrangement of the ylide an aldehyde and dimethyl sulfide are obtained. 9-bromononanal 1 is yielded with 96% and further reacted without purification. Afterwards, bromooctane is transferred to a Grignard reagent and reacted with 9-bromononanal 1. After column chromatography, the branched aliphatic spacer with a hydroxide group at the branching point

and bromine at one chain end is obtained. The yield of 1-bromoheptadecan-9-ol **2** is 69%. By a Williamson etherification, the bromine functionality is replaced by the crosslinkable oxetane unit. This reaction is conducted in a two-phase system of hexanes and aqueous 45wt% sodium hydroxide solution. As the oxetane shows good solubility in the aqueous phase and the branched spacer is dissolved by the organic phase, tetrabutylammonium bromide is added as phase transfer catalyst to accelerate the etherification. The product **3** is obtained with 63% yield after column chromatography. The hydroxide functionality is transferred to a better leaving group by tosylation. The reagent tosyl chloride is activated with the combined bases triethylamine and trimethylammonium hydrochloride resulting in a sulfammonium salt. This salt reacts with the secondary alcohol **3** in a nucleophilic attack on the novel crosslinkable branched spacer **4** with 79% yield after column chromatography. In the following step, 2,7-dibromocarbazole is alkylated with the spacer molecule **4**. In the presence of potassium hydroxide, a nucleophilic attack on the carbon atom of the tosylate **4** takes place. After elimination of the tosylate group, the alkylated carbazole **5** is obtained. Purification via column chromatography yielded 68% of **5**. Subsequently, the thiophene rings were attached to the carbazole by a palladium catalysed Suzuki coupling. A two-phase system of toluene and 2 M aqueous sodium carbonate solution under inert gas was applied and Aliquat 336 was used as phase transfer catalyst. Because the palladium catalyst tetrakis(triphenylphosphine)palladium(0) is very sensitive against oxygen, several freeze-thaw cycles were conducted to remove oxygen from the reaction system. The coupling product **6** was obtained with a very high yield of 96% after column chromatography. The bromination step was conducted under cooling of the reaction system and in the dark with *N*-bromosuccinimide as bromine source. Reaction control was achieved via NMR spectroscopy to ensure that the thiophene flanked carbazole was brominated twice. Column chromatography yielded the novel crosslinkable donor monomer **7** with 67%. Together with benzothiadiazole as acceptor monomer, the monomer **7** was polymerized by Suzuki polycondensation using the same conditions as for the Suzuki coupling of the thiophene and the carbazole. Endcapping was achieved by adding bromobenzene and phenylboronic acid subsequently. The novel crosslinkable polymer PCDTBTOx was obtained with 60% yield after Soxhlet extraction.

For the crosslinkable PCPDTBT, short aliphatic spacers bearing oxetane units were synthesized and subsequently attached to a cyclopentadithiophene core. Afterwards, this new donor monomer was polymerized with benzothiadiazole as acceptor monomer. The synthetic strategy towards PCPDTBTOx is shown in Figure 43.

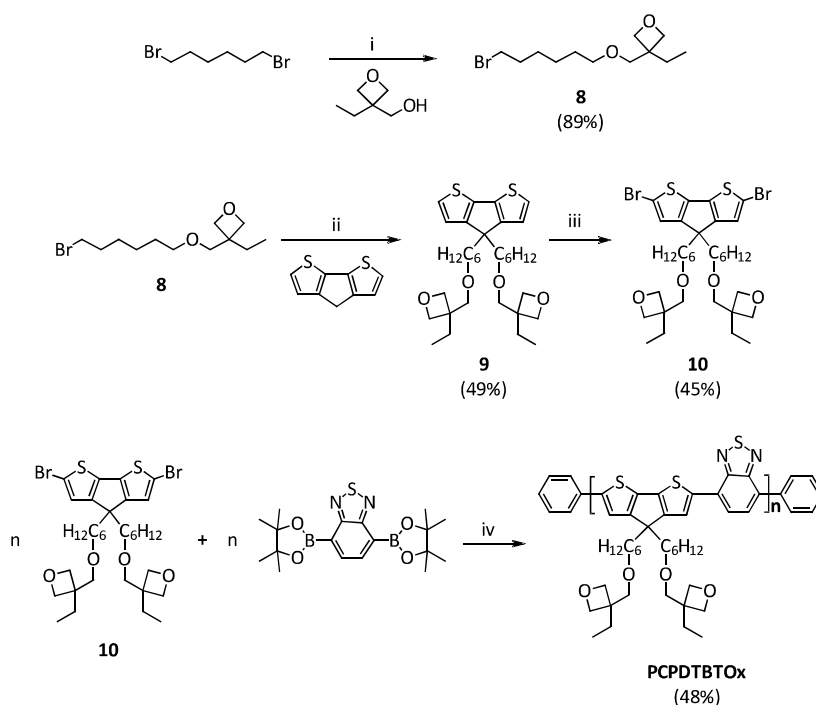


Figure 43: Synthetic strategy for the crosslinkable low bandgap polymer PCPDTBTx. Reaction conditions: i) (3-ethyloxetan-3-yl)-methanol, hexanes, aq. NaOH solution (45 wt%), $(\text{Bu})_4\text{NBr}$, reflux, 6 h; ii) 1. 4*H*-cyclopenta[2,1-*b*;3,4-*b'*]dithiophene, DMSO, KI, 2. addition of KOH in portions, 0 °C, 3. r. t., overnight; iii) 1. DMF, *N*-bromosuccinimide, 0 °C, 1 h, in the dark, 2. r. t., overnight, in the dark; iv) 1. toluene, aq. Na_2CO_3 solution (2 M), Aliquat 336, $\text{Pd}(\text{PPh}_3)_4$, reflux, 90 h, 2. bromobenzene, reflux, 1 h, 3. phenylboronic acid, reflux, overnight.

In this case, only a short aliphatic spacer is needed, because the cyclopentadithiophene core is alkylated twice. The crosslinkable spacer is synthesized via a Williamson etherification which is performed in a two-phase system of hexanes and aqueous 45 wt% sodium hydroxide solution. The oxetane unit is well soluble in the aqueous phase, whereas 1,6-dibromohexane is dissolved in the organic phase. For acceleration of the reaction, tetrabutylammonium bromide is used as phase transfer catalyst. After column chromatography, the crosslinkable spacer **8** is obtained with 89% yield. Subsequently, the core cyclopentadithiophene is alkylated with the short spacer **8**. Addition of potassium iodide leads to halogen exchange via a Finkelstein reaction. The presence of potassium hydroxide allows the nucleophilic attack on the carbon atom of the iodide. The alkylated product **9** is yielded with 49% after column chromatography. As bromination agent, *N*-bromosuccinimide is used. For ensuring bromination at the positions 2 and 6, the reaction was conducted under cooling and in the dark. A yield of 45% was achieved for the novel crosslinkable donor monomer **10** after column chromatography. The monomer **10** is reacted with benzothiadiazole as acceptor monomer via a Suzuki polycondensation. As a two-phase system of toluene and 2 M aqueous sodium carbonate solution is used, Aliquat 336 was added as phase transfer catalyst. Due to the oxygen sensitivity of the palladium catalyst tetrakis(triphenylphosphine)palladium(0), the polycondensation was carried out under inert atmosphere and several freeze-thaw cycles were applied. Bromobenzene and phenylboronic acid were used for endcapping of the polymer. The crosslinkable polymer PCPDTBTx was obtained with 48% yield after Soxhlet extraction.

Molecular weight distributions of polymers are normally obtained by size exclusion chromatography (SEC). Due to the low solubility of the synthesized conjugated polymers, the measurement has to be performed at high temperatures and in halogenated aromatic solvents. Trichlorobenzene is often used as an eluent above 150 °C. However, a little ratio of hydrogen chloride is present in chlorinated benzenes at these high temperatures. The determination of the number-averaged and weight-averaged molecular weight M_n and M_w of the crosslinkable derivatives PCDTBTOx and PCPDTBTOx was thus not possible via SEC measurements as the hydrogen chloride initiated the crosslinking of the oxetane units to the silica gel. Alternatively, the molecular weight distribution of the two polymers was obtained by matrix-assisted laser desorption/ionization time of flight (MALDI-ToF) mass spectroscopy. However, low bandgap polymers often show low signal intensities due to insufficient desorption and ionization. In addition, fragmentation leads to a falsified statement about the molecular weight. Thus, the MALDI-ToF measurements of PCDTBTOx and PCPDTBTOx were only evaluated as a hint towards the real molecular weight distributions.

Figure 44 presents the MALDI-ToF spectra of PCDTBTOx and PCPDTBTOx. The main series marked in blue represent the oligomers $[M_n]$ with a molecular weight of 816.2 gmol^{-1} for the repeating unit of PCDTBTOx and 707.0 gmol^{-1} for the repeating unit of PCPDTBTOx. Aside, the green series can be attributed to $[M_n - \text{benzothiadiazole}]$. Furthermore, $[M_n + \text{benzothiadiazole}]$ is indicated by the yellow peaks. An exception is the orange peak in the spectrum of PCPDTBTOx that corresponds to $[M_6 + 2 \text{ benzothiadiazole}]$. In comparison, the molecular weight of PCDTBTOx seems to be lower than that of PCPDTBTOx whereas the latter shows lower signal intensities. The reason for the detection of only short chains and the low signal intensity could originate from a weak desorption and ionisation rate for the longer chains as well as fragmentation into smaller pieces. In the case of PCPDTBTOx, also a SEC measurement at room temperature with THF as an eluent was performed. Here, the longer polymer chains could not be dissolved in THF leading to an underestimated molecular weight distribution. The data basically complies with the results from the MALDI-ToF spectroscopy indicating a slightly higher molecular weight of the polymer.

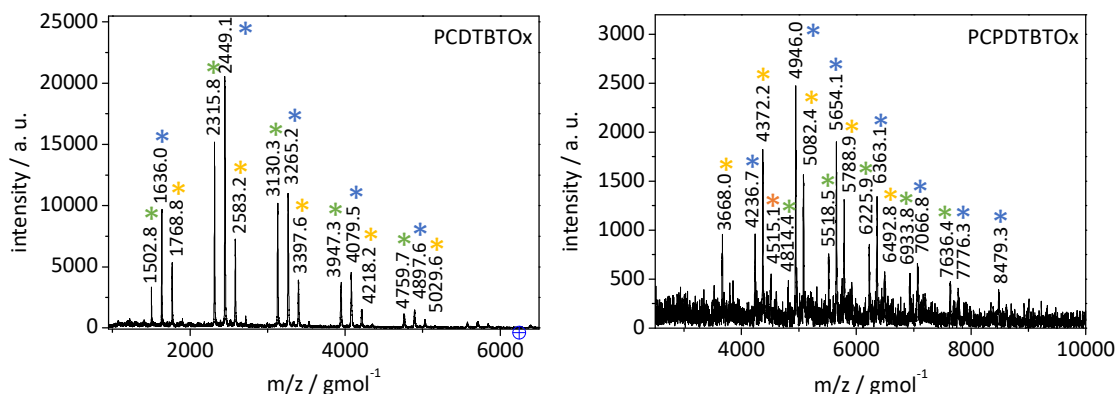


Figure 44: MALDI-ToF spectra of PCDTBTOx (left) and PCPDTBTOx (right). As a matrix, *trans*-2-[3-(4-*tert*-butylphenyl)-2-methyl-2-propenylidene]malononitrile (DCTB) was used.

Solubility tests were conducted with the two crosslinkable polymers PCDTBTOx and PCPDTBTOx to evaluate the crosslinking ability. For this purpose, absorption measurements were performed at different stages of the crosslinking procedure. The optical density reflects the film thickness and allows the evaluation of the effectivity of the polymer network formation. After spin coating of the polymers, drying in vacuum at 60 °C for 1 h and measuring the absorption, the films were exposed to TFA vapour that starts the cationic ring-opening polymerization. This step was carried out at 80 °C in an inert atmosphere as the boiling point of TFA is 78 °C and the permeation of the protons is facilitated by the movement of the polymer chains. Excess TFA was removed by a vacuum step for 1 h and the absorption spectra were recorded. Afterwards, the crosslinked films were rinsed in THF for 30 s to remove material that was not crosslinked. The absorption was measured and the film retention was determined by comparing the absorption spectra of the film as cast and the film after rinsing. The absorption spectra of the crosslinking tests of PCDTBTOx and PCPDTBTOx are depicted in Figure 45.

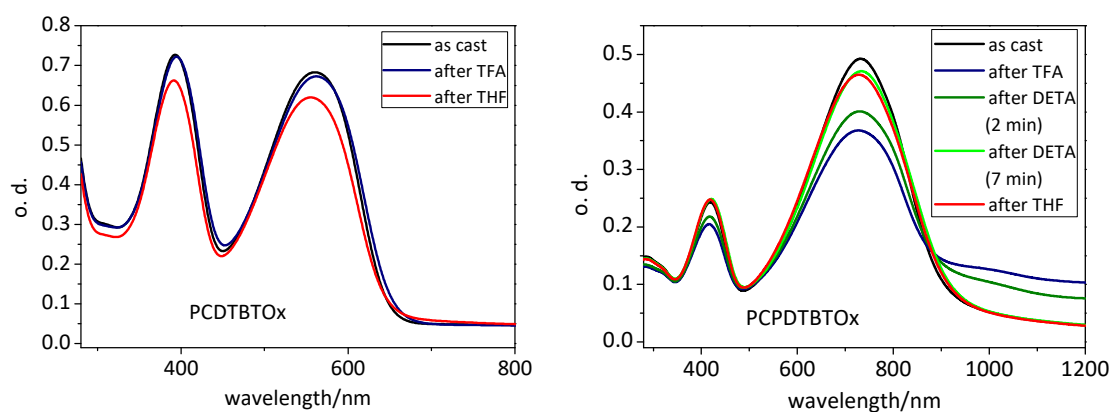


Figure 45: Absorption spectra of films of PCDTBTOx (left) and PCPDTBTOx (right). In the case of PCDTBTOx, the absorption of the film as cast (black), after the exposure to TFA vapour for 10 min (blue), and after rinsing with THF for 30 s (red) is shown. For PCPDTBTOx, the absorption of the film as cast (black), after exposure to TFA vapour for 2 min (blue), after exposure to DETA vapour for 2 min (dark green) and 7 min (light green) after crosslinking, and after rinsing with THF for 30 s (red) is depicted.

In the case of PCDTBTOx, the optical density is mainly unchanged after the exposure of the polymer film to TFA vapour at 80 °C for 10 min. After rinsing with THF for 30 s, the optical density is slightly reduced indicating that the film thickness is decreased. The remaining polymer film is densely crosslinked and thus insoluble. From the absorption maxima, a film retention of 90% is determined. PCPDTBTOx was exposed to TFA vapour at 80 °C for 2 min. The absorption spectrum after the crosslinking step exhibits an increased optical density in the range above 900 nm. This increase denotes a doping of the polymer upon the acid treatment. For dedoping the polymer film, the sample was subsequently exposed to DETA vapour for 2 min and 7 min. The absorption spectra show that 2 min were not sufficient to dedope the polymer completely as the optical density is not decreased to the value of the film as cast. However, DETA treatment for 7 min achieved efficient dedoping of the polymer film. Rinsing with THF for 30 s resulted in a slightly reduced optical density in comparison with the film as cast giving a film retention of 94%. Thus, both PCDTBTOx and PCPDTBTOx can be crosslinked efficiently.

4.2 Low bandgap copolymers

The second part of the thesis presents the modification of PCDTBT via the incorporation of comonomers. PCDTBT is applied as donor polymer in organic solar cells and exhibits moderate efficiencies and good device stabilities due to photoinduced crosslinking that leads to the stabilization of the blend morphology. The hole mobility of PCDTBT is already quite high and lies in the range of 10^{-3} to 10^{-4} $\text{cm}^2\text{V}^{-1}\text{s}^{-1}$. For a further improvement of the hole mobility, triphenyldiamine was chosen as a comonomer in this work as it shows good hole transport abilities. Consequently, the novel polymers comprise *two* donor monomers, a carbazole unit and triphenyldiamine, as well as one acceptor unit including benzothiadiazole. In contrast, the polymer structure of low bandgap polymers like PCDTBT consists of one donor and one acceptor monomer. Therefore, the polymers with the additional donor monomer are referred to “low bandgap copolymers” in this work to distinguish them from the common low bandgap polymers with one donor and one acceptor which are of course also copolymers.

The synthesis of the low bandgap copolymers consists of the preparation of a triphenyldiamine donor monomer as well as the subsequent polymerization combined with the donor and acceptor monomer of PCDTBT. In the case of the acceptor unit, a variation is included via short aliphatic spacers that are attached to the thiophene rings. Figure 46 presents the synthetic strategy towards the low bandgap copolymers PCDTBT_{0.7}/TPDDTBT_{0.3} and PCDHTBT_{0.7}/TPDDHTBT_{0.3}.

The first step of the synthesis of the triphenyldiamine comonomer is the palladium-catalysed *N*-arylation of the commercially available starting material *N,N'*-diphenylbenzidine with 4-bromotoluene. The reaction system comprises tri-*tert*-butylphosphine as a ligand and sodium-*tert*-butylate as a base ensuring the efficient abstraction of a proton during the transmetallation reaction. After precipitation, *N,N'*-bis(4-methylphenyl)-*N,N'*-diphenyl-benzidine **11** is obtained with 93% yield. For the insertion of functional groups, the monomer core **11** is brominated via *N*-bromosuccinimide. The amine group directs the substitution both in ortho and para position. Due to steric hindrance of the adjacent phenyl rings, mainly the para product is formed. Column chromatography yielded the product **12** with 52%. As the triphenyldiamine unit is applied as donor monomer in the polymerization and replaces a part of the actual carbazole donor monomer, the bromine groups have to be transferred into borolane units. Therefore, substance **12** is first lithiated and then reacted with 2-isopropoxy-4,4,5,5-tetramethyl-1,3,2-dioxaborolane. The triphenyldiamine monomer **13** was recrystallized with a yield of 68%. The two polymers PCDTBT_{0.7}/TPDDTBT_{0.3} and PCDHTBT_{0.7}/TPDDHTBT_{0.3} were both synthesized via a palladium-catalysed Suzuki polycondensation. Normally, the donor and the acceptor monomer are applied in a ratio of 1:1. In the case of the low bandgap copolymers, 30% of the actual carbazole donor monomer is replaced by the triphenyldiamine unit. Thus, an alternating arrangement of either carbazole and dithiophene benzothiadiazole or triphenyldiamine and dithiophene benzothiadiazole is formed. The arrangement of the respective donor-acceptor

4. Overview of the thesis

groups is not predictable and thus statistical copolymers are obtained. Dithiophene benzothiadiazole is applied with and without hexyl spacers attached to the thiophene rings. The three monomers are reacted in a two-phase system of toluene and 2 M aqueous sodium carbonate solution in presence of the phase transfer catalyst Aliquat 336 under inert gas. Several freeze-thaw cycles were performed to protect the catalyst tetrakis(triphenylphosphine)-palladium(0) from oxygen. The addition of bromobenzene and phenylboronic acid saturates the reactive chain ends. After Soxhlet extraction, PCDTBT_{0.7}/TPDDTBT_{0.3} is obtained with a yield of 28% and PCDHTBT_{0.7}/TPDDHTBT_{0.3} with a yield of 93%.

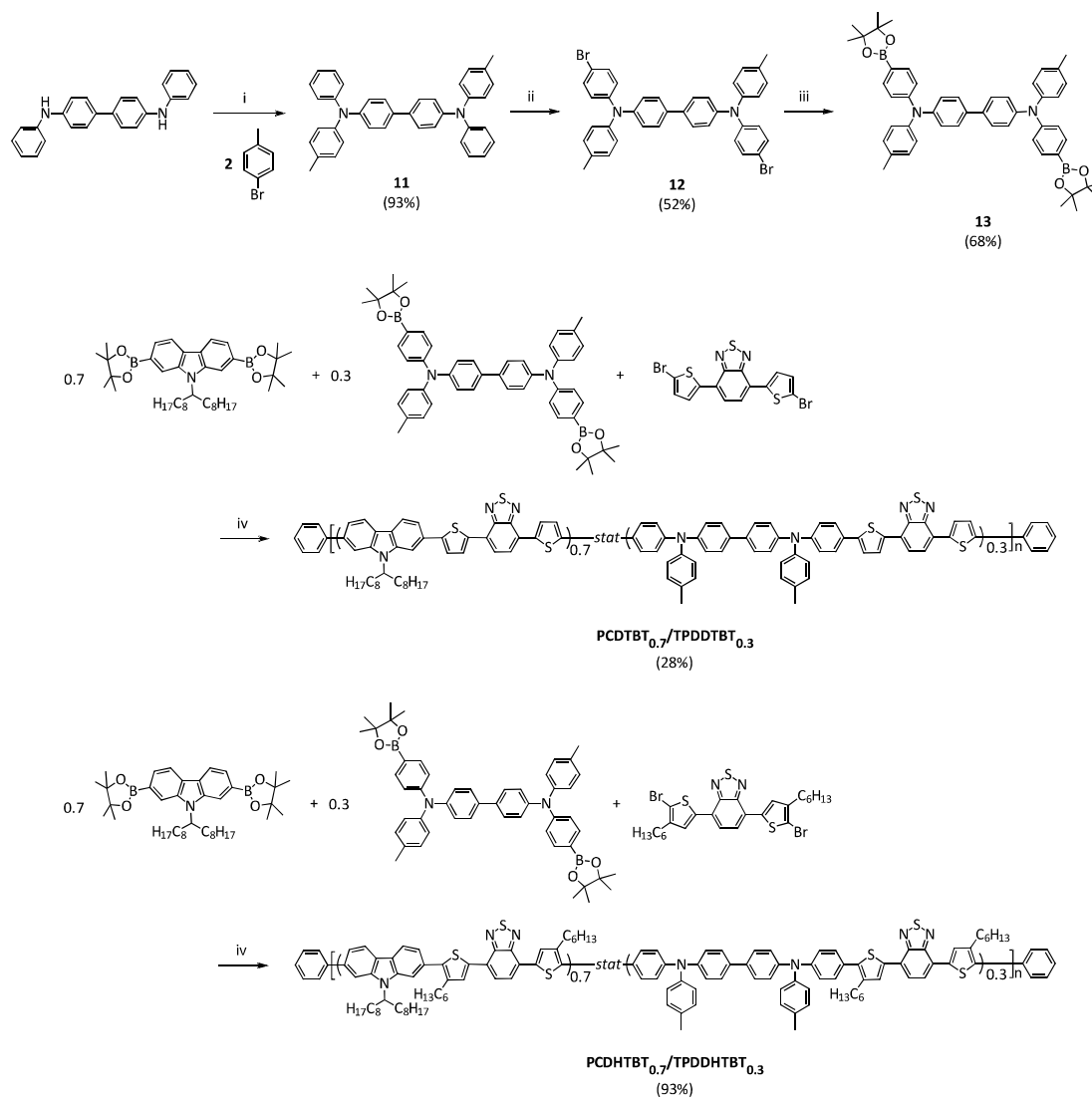


Figure 46: Synthetic strategy for the low bandgap copolymers PCDTBT_{0.7}/TPDDTBT_{0.3} and PCDHTBT_{0.7}/TPDDHTBT_{0.3}. Reaction conditions: i) 4-bromotoluene, THF abs., Pd(OAc)₂, Na-*tert*-butylate, tri-*tert*-butylphosphine, 80 °C, 3h; ii) 1. CHCl₃, *N*-bromosuccinimide, r. t., 1 h, 2. AcOH, r. t., 6,5 h; iii) 1. THF abs., *n*-BuLi, -78 °C, 1 h, 2. 2-isopropoxy-4,4,5,5-tetramethyl-1,3,2-dioxaborolane, -78 °C, 1 h, 3. r. t., overnight; iv) 1. toluene, aq. Na₂CO₃ solution (2 M), Aliquat 336, Pd(PPh₃)₄, reflux, 72 h, 2. bromobenzene, reflux, 1 h, 3. phenylboronic acid, reflux, overnight.

By the combination of the additional triphenyldiamine comonomer and the optional aliphatic spacers in the acceptor monomers, a series of low bandgap copolymers is obtained. The properties of the polymers vary according to the modifications of the basic PCDTBT structure.

From this library, materials for different fundamental studies were chosen due to their specific properties allowing the investigation of a particular question.

Basic research comprising charge carrier generation and recombination aims at the detailed understanding of the behaviour of donor and acceptor at the interface of the active layer. Besides the availability of materials that enable basic investigations due to their intrinsic properties, the choice of the solar cell geometry is important. Only low efficiencies can be achieved with planar heterojunction devices. Due to the short exciton diffusion length, only a part of the generated excitons can reach the donor-acceptor interface and contribute to the photocurrent. In contrast, high efficiencies can be attained with bulk heterojunction solar cells as almost all generated excitons can diffuse to the donor-acceptor interface. However, this complex device geometry is difficult to use for fundamental studies. Planar heterojunction solar cells are the ideal model systems for studying fundamental issues because of their planar setup, clearly separated charge transport pathways as well as easier conditions for device simulations.

In the following chapters, the application of the novel low bandgap copolymers with the additional triphenyldiamine comonomer in bilayer devices for fundamental studies is presented. On the one hand, an investigation about the photogeneration in organic solar cells was conducted. The contribution of the frequently used acceptor C_{60} to the charge carrier generation was evaluated. On the other hand, recombination plays an important role as a loss mechanism in organic solar cells. The fractions of monomolecular and bimolecular recombination were elucidated using bilayer solar cells that allow the differentiation of the two recombination types. In addition, the diffusion of low molecular weight acceptor within the donor polymer determines the stability of organic solar cells. Thus, an examination of the diffusion behaviour of fullerene in different low bandgap polymers and a novel copolymer is presented.

4.2.1 Role of intrinsic photogeneration in single layer and bilayer solar cells with C_{60} and PCBM

This chapter focuses on the examination of photogeneration in organic solar cells. The dissociation of excitons into free charges is usually considered to be located at the donor-acceptor interface and no other contributions are included. However, exciton dissociation can occur in the donor layer and in the acceptor layer as well. In normal low bandgap polymers, this intrinsic contribution to the external quantum efficiency is low, that means that an acceptor is needed anyway for an effective dissociation. In contrast, fullerenes show a high intrinsic dissociation. Thus, the intrinsic contribution of the acceptor materials C_{60} and PCBM to the photocurrent of organic solar cells is investigated in this work. We used single and bilayer geometries as they allow the basic study about the evaluation of the acceptor contribution. For the investigation of the dissociation behaviour in the acceptor materials, the intrinsic contribution from the applied donor materials should be insignificant. The novel PCDTBT derivative with and additional triphenyldiamine comonomer $PCDTBT_{0.7}/TPDDTBT_{0.3}$ exhibits such a negligible intrinsic dissociation. This polymer is referred to as $PCDTBT_{co}$ in this chapter. In

addition, the small donor molecule Ph-TDPP-Ph was compared to the donor polymer. We investigated the correlation between the photogeneration in the fullerene acceptors and the excitation energy as well as the consequences for the efficiency of the solar cells.

In Figure 47, the dependence of the external quantum efficiency of single layer cells from C₆₀ and PCBM on the excitation energy is shown. The intrinsic photogeneration in both acceptor materials is initiated at a photon energy of about 2.25 eV. In the low-energy range below 2.25 eV, the generated exciton is located on only one fullerene molecule and is tightly bound. Thus, no contribution to the external quantum efficiency can be observed in this region. In contrast, excitation energies higher than 2.25 eV result in charge-transfer states that are delocalized over two fullerene molecules. This threshold value lies 0.4 eV higher than the first singlet excited state S₁. The generated charge-transfer states in the acceptor material are short-lived and can either autoionize or relax to the S₁ state consistent with the original Onsager theory. Therefore, the intrinsic dissociation yield increases with increasing excitation energy.

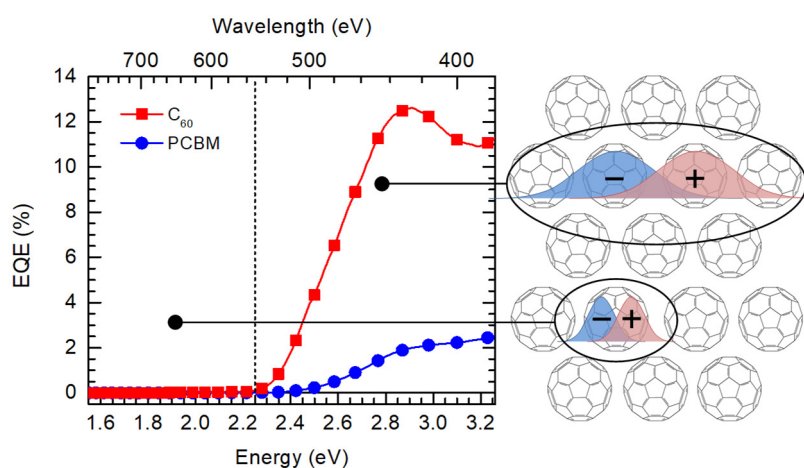


Figure 47: EQE spectra of single layer devices from C₆₀ and PCBM in dependence on the excitation energy and schematic illustration of the generated states. The dotted line indicates the threshold value at about 2.25 eV for the intrinsic dissociation in the fullerene acceptors. Reprinted from Chapter 6.

The effect of the intrinsic contribution to the photocurrent of the C₆₀ acceptor on organic bilayer solar cells is presented in Figure 48. The external quantum efficiency is depicted in dependence of the internal electric field of the solar cell. By this method, the dissociation behaviour of C₆₀ can be evaluated. As donor materials, the small molecule Ph-TDPP-Ph and the low bandgap copolymer PCDTBT_{co} were used. The bilayer solar cells were excited at two photon energies. As the threshold for the intrinsic contribution of C₆₀ lies at 2.25 eV, the first excitation is conducted at 2.14 eV which is below this threshold. Both donor materials show a high absorption at this wavelength. In consequence, the photocurrent at this excitation energy arises from the donor-acceptor interface. The second excitation is fixed at 2.94 eV for the small molecule donor and at 3.35 eV for the donor polymer. These energies exceed the threshold energy for the intrinsic dissociation of charge-transfer states within the bulk of C₆₀ and both donor and the C₆₀ acceptor absorb at these wavelengths.

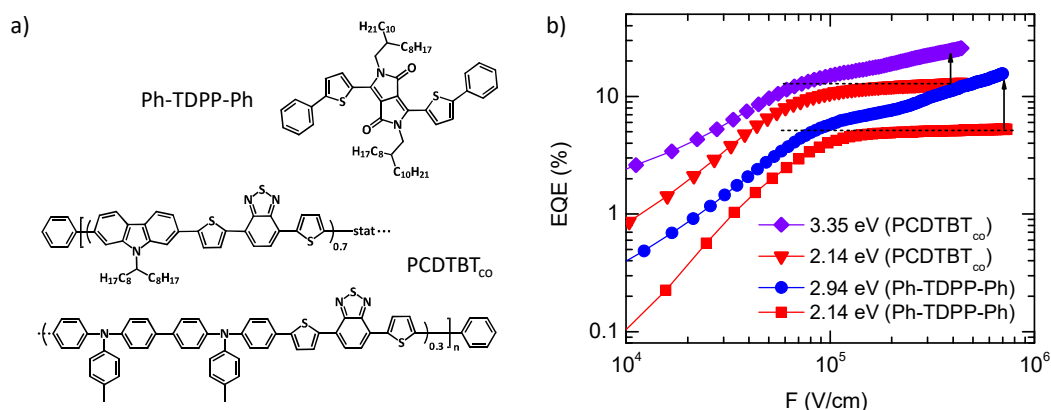


Figure 48: a) Chemical structures of the small molecule Ph-TDPP-Ph and the low bandgap copolymer PCDTBT_{co}. b) EQE in dependence of the field for bilayer devices made from either PCDTBT_{co} and C₆₀ or Ph-TDPP-Ph and C₆₀. The bilayer solar cells are excited at 3.35 eV and 2.14 eV in the case of the PCDTBT_{co} donor and at 2.94 eV and 2.14 eV in the case of the Ph-TDPP-Ph donor. The intrinsic contribution of the C₆₀ acceptor for excitation at 3.35 eV and 2.94 eV are indicated with black arrows. Reprinted from Chapter 6.

A saturation can be observed for both bilayer solar cells at a photon energy of 2.14 eV which mainly excites the donor materials, because the donors exhibit no significant intrinsic contribution. When exciting both donor and C₆₀ at photon energies of 3.35 eV and 2.94 eV, an additional slope at high electric field strengths can be observed. This increase can be attributed to the intrinsic dissociation of C₆₀ because the excitation energy is higher than the threshold value of 2.25 eV and charge-transfer states are generated in the C₆₀ layer. Thus, both the donor-acceptor interface as well as the intrinsic dissociation in the C₆₀ contribute to the solar cell performance in this energy range.

For the complete dissociation of photogenerated excitons into free charges, the charge-transfer states have to couple with the charge-transporting states. This coupling is by a factor of 3 lower in PCBM than in C₆₀. By applying an Onsager fit to the data, the Coulomb binding energies, separation of the electron-hole pairs as well as the electrical gap can be estimated. We found that the binding energies of the charge-transfer states generated by optical excitation decreases with increasing photon energy from 220 meV to 100 meV for excitation energies between 2.25 eV and the electrical gap at 2.45 eV. This results in an increase of the electron-hole separation of the charge-transfer states from 2.0 nm to 2.5 nm which supports the delocalisation of the charge-transfer states over two fullerene molecules. The coupling of these states to charge-transporting states is achieved by ionisation upon thermal excitation. Charge-transfer states generated by excitation exceeding 2.45 eV undergo thermalization. In this case, the dependence of the electron-hole distance and the binding energy on the photon energy is weaker. By thermal excitation, the thermalized charge-transfer states also couple to charge-transporting states.

In conclusion, the dependence of the intrinsic dissociation on the excitation energy was examined in this work. By this means, we were able to evaluate the intrinsic contribution from the acceptors C₆₀ and PCBM to the overall device efficiency of organic bilayer solar cells.

4.2.2 Monomolecular and bimolecular recombination of electron–hole pairs at the interface of a bilayer organic solar cell

A further project aimed at the investigation of the recombination processes in organic bilayer solar cells. Recombination is an important loss mechanism at the donor-acceptor interface and can be divided into two main types. Geminate recombination describes the recombination of an electron and a hole that were generated from the same exciton. In contrast, non-geminate recombination means that an electron and a hole originating from different excitons recombine. In this work, we evaluate the contributions from both geminate and non-geminate recombination in organic bilayer systems. The bilayer geometry is chosen because it enables the differentiation between the different recombination types. The devices have to meet several requirements for the recombination studies. Besides a general good solar cell performance, the extraction of the charge carriers should exhibit no difficulties and the solar cell morphology should be stable. Thus, annealing or the insertion of extraction layers should not affect the device efficiency. These demands are fulfilled when applying the novel low bandgap copolymer PCDHTBT_{0.7}/TPDDHTBT_{0.3} with triphenyldiamine units and additional hexyl spacers at the thiophene units as the donor material. For convenience, this copolymer is named PCDTBT_{stat} in this work. In comparison to the donor polymer, also the small molecule donor p-DTS(FBTTh₂)₂ known for its high efficiency was used. As acceptor material, C₆₀ was applied. For the investigation of the contributions of geminate and non-geminate recombination, the fill factor of the bilayer solar cells is observed in dependence on the donor layer thickness and excitation light intensity. The fill factor depicts the ratio of the generated charge carriers that can be extracted by the electrodes. Thus, it is a measure of the fraction of recombining charge carriers. For the intensity dependent recombination study, bilayer solar cells are fabricated from PCDTBT_{stat} and C₆₀. The polymer donor was applied with layer thicknesses of 14 nm, 36 nm, and 66 nm. The acceptor layer was kept constant at 30 nm. The excitation light intensity was varied between 0.02 mWcm⁻² and 100 mWcm⁻² using optical density filters. From the measured current-voltage characteristics, the fill factor can be calculated. Figure 49 illustrates the fill factor for bilayer solar cells in dependence of the excitation light intensity for different polymer layer thicknesses.

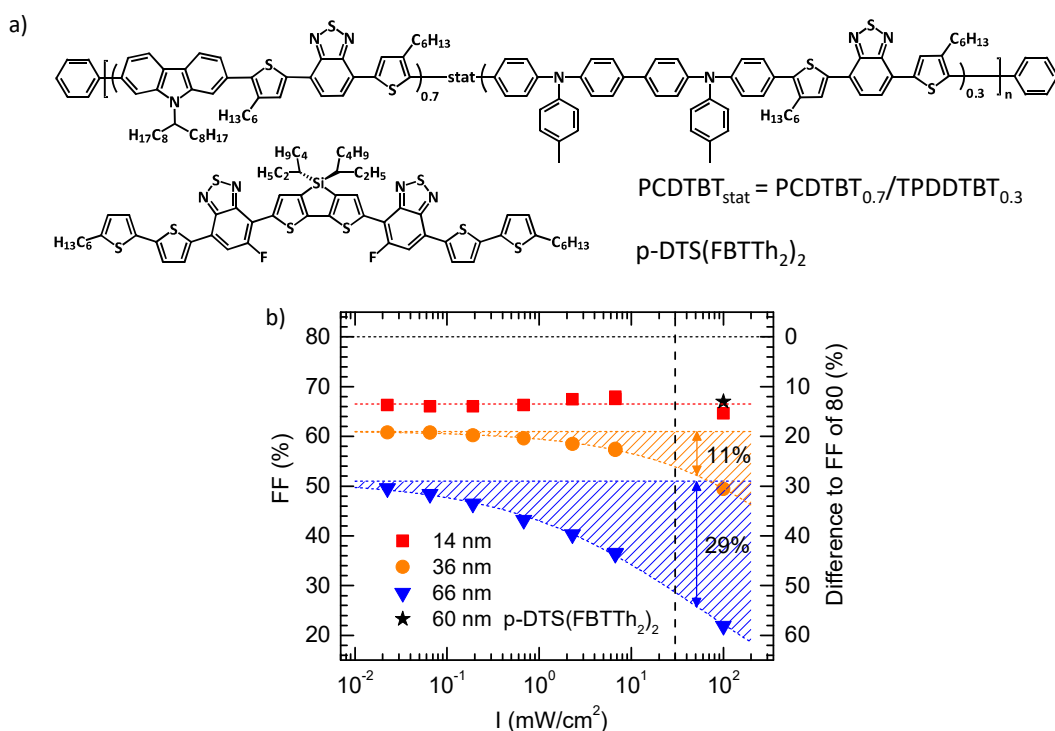


Figure 49: Chemical structures of the small molecule p-DTS(FBTTh₂)₂ and the low bandgap copolymer PCDTBT_{stat}. b) Fill factor in dependence of the excitation light intensity for bilayer devices made from either PCDTBT_{stat} and C₆₀ or p-DTS(FBTTh₂)₂ and C₆₀. Excitation was conducted at a wavelength of 580 nm. Polymer layer thicknesses of 14 nm, 36 nm, and 66 nm were applied. Right of the dashed vertical line, the fill factors for AM1.5 illumination is shown. The right axis displays the difference to an estimated ideal fill factor limit of 80%. The horizontal lines illustrate the asymptotic value for the fill factor at infinitely low illumination as calculated by a fit and extrapolation of the data. Geminate recombination is expected to cause the deviation between the horizontal lines and the assumed fill factor of 80%. The shaded area between the horizontal lines and the data points depicts the deficit due to non-geminate recombination. The losses due to non-geminate recombination at AM1.5 excitation are illustrated by arrows. Reprinted from Chapter 7.

The fill factor of the solar cell with 14 nm donor thickness remains constant at 67% over the whole range of the light intensity. However, the fill factor drops from 61% to 50% at AM1.5 excitation for the cell with the 36 nm thick polymer layer and from 51% to 22% for the device with 66 nm thickness, respectively. In addition, the fill factor for a bilayer cell made from the low molecular weight donor p-DTS(FBTTh₂)₂ with a thickness of 60 nm in combination with C₆₀ is shown. At AM1.5 excitation, the same fill factor of 67% as for the device with the 14 nm thick donor layer is achieved.

At low light intensities, only few excitons are formed. The charges diffuse within their Coulomb potential and can recombine before dissociating into free charge carriers. This process is called primary geminate recombination. When the charges diffuse out of the Coulomb radius, they either can be extracted by the electrodes or they diffuse back and recombine which is referred to as secondary geminate recombination. Both primary and secondary geminate recombination are monomolecular mechanisms. The increase of the donor layer thickness results in a longer diffusion path and thus the probability for recombination is enhanced, leading to a decrease of the initial fill factor from 67% to 50% with increasing polymer thickness from 14 nm to 66 nm. For an ideal solar cell, a fill factor of 80% is assumed. The difference between this value and the

highest fill factors of the cells can be attributed to geminate recombination and is indicated by the horizontal lines. At high light intensities, more excitons are generated. Now the probability for non-geminate bimolecular recombination gets higher. This means that the charge carriers can recombine with charge carriers originating from other excitons. For the 14 nm thick polymer layer, no non-geminate recombination can be observed because the free charge carriers are extracted faster than they can recombine. The contribution from non-geminate recombination that reduces the initial fill factor are illustrated by the shaded areas. The findings were supported by Monte Carlo simulations that confirms the increase of the photocurrent when using thin donor layers.

The competing process to recombination in organic solar cells is charge extraction. With increasing hole mobility, more holes should be collected at the electrode. In consequence, high fill factors should be achievable even with high layer thicknesses. This is confirmed by measurements of a bilayer solar cell consisting of 60 nm p-DTS(FBTTh₂)₂ and C₆₀. As can be seen in Figure 49, this solar cell exhibits a much higher fill factor than the solar cell from PCDTBT_{stat} with a similar thickness at low light intensity. The hole mobility of the small molecular donor detected by the metal-insulator-semiconductor charge-extraction-by-linearly-increasing-voltage (MIS-CELIV) method is two orders of magnitude higher than that of PCDTBT_{stat}.

Figure 50 summarizes the competition between geminate and non-geminate recombination at the donor-acceptor interface and charge carrier extraction at the electrodes. At low excitation light intensities, diffusion within the Coulomb radius of the exciton can cause recombination of the hole with the corresponding electron according to the primary geminate recombination process (1). When exceeding the Coulomb radius, the hole can be either extracted at the electrode or it diffuses back and recombines with the electron originating from the same exciton by secondary geminate recombination (2). Both mechanisms are monomolecular as the hole and the electron arise from the same exciton. Non-geminate recombination becomes important at high light intensities. Here, holes and electrons from different excitons recombine in a bimolecular procedure.

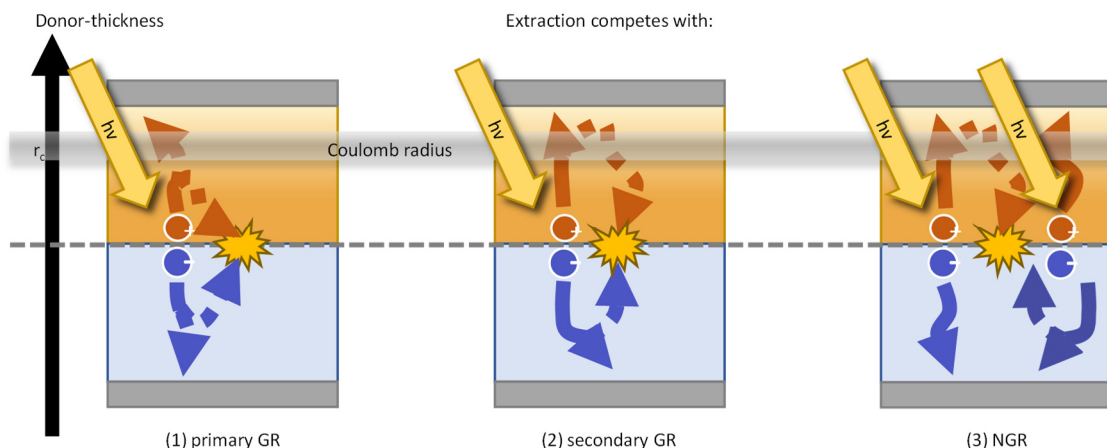


Figure 50: Schematic overview of the competition between monomolecular geminate and bimolecular non-geminate recombination at the donor-acceptor interface as well as charge carrier extraction at the electrodes. The Coulomb radius is abbreviated by r_c . Reprinted from Chapter 7.

In this work, we investigated the dependence of the fill factor on the excitation light intensity and the donor layer thickness. Thus, we were able to evaluate the contribution of both geminate and non-geminate recombination in bilayer solar cells.

4.2.3 A facile method for the investigation of temperature-dependant C60 diffusion in conjugated polymers

This section depicts the connection between the fundamental studies on photogeneration and recombination and the research on device fabrication, degradation and stabilization. The morphology of the active layer is of vital importance for the performance of organic solar cells. Frequently, a polymeric donor material is combined with low molecular weight acceptors like fullerene and its derivatives. Thermal annealing is often performed to enhance the interface morphology, especially for bilayer systems. In this case, a certain intrusion of the fullerene molecules into the donor layer is favoured. By this method, the interfacial area is increased but the percolation paths which ensure the extraction of the charge carriers are retained. The obtained morphology thus combines the advantages of both bulk heterojunction and planar heterojunction. Finding suitable annealing times and temperatures is yet often based on trial and error. A series of different conditions is often probed by solar cell measurements and the success is evaluated in terms of device efficiency. In consequence, the wrong annealing steps as well as device operation at elevated temperatures, especially for bulk heterojunction solar cells, often leads to a deterioration of the efficiency. The decrease can be attributed to the diffusion of small acceptor molecules and the formation of large aggregates due to phase separation. This work contributes to this issue by investigating the diffusion behaviour of fullerenes within donor polymers. The presented approach provides a guide for the choice of adjusted annealing times and temperatures for the fabrication of efficient devices.

The method described in this work constitutes the extension of the diffusion experiments already performed with C_{60} in polyfluorenes. For this study, a three-layer setup was used. A glass substrate is covered with a fluorescent sensor layer of MeHPPV. In a subsequent step, the polymer to be investigated is applied as a transport layer. Finally, a thin layer of C_{60} is deposited on one half of the sample. The other half without C_{60} serves as a reference for the measurement. The sensor layer is excited by a laser and the photoluminescence is recorded by CCD cameras. If this experiment is conducted at room temperature, no change in the sensor emission can be observed over the experiment time in comparison to the device part without C_{60} layer. But at increased temperature C_{60} molecules are injected into the transport layer. They diffuse towards the sensor layer and will eventually quench the photoluminescence, as C_{60} acts as an exciton trap. Therefore, the decrease of the photoluminescence of the sensor layer can be connected to the diffusion time of the C_{60} molecules through the polymer transport layer. The more molecules arrive at the sensor layer over the time, the more the photoluminescence will decrease. From the arrival time and the thickness of the transport layer, the diffusion coefficient can be calculated in dependence of the temperature. By using a polyfluorene crosslinked via acrylate groups, a decrease of the diffusion coefficient is observed. The drop can be ascribed to the lowered mobility of the polymer chains when a densely crosslinked polymer network is formed. This means that the C_{60} molecules need longer time to diffuse through the polymer layer. The decrease of the diffusion is linked to the content of acrylate groups in the polymer. The higher the acrylate content, the higher the density of the polymer network is and therefore the diffusion is lower. In fact, the diffusion of C_{60} in polyfluorene can be reduced by three orders of magnitude by crosslinking. Thus, crosslinking depicts an efficient method to stabilize the morphology in organic solar cells.

However, extending this concept to other transport materials is difficult. For mere excitation of the sensor layer, the photoluminescence of the sensor has to be red-shifted in comparison to the transport layer. The investigation of the diffusion of fullerene in frequently used low bandgap polymers is not possible due to their photoluminescence in the red region. Thus, sensor materials with a photoluminescence in the infrared would be necessary. In addition, the fabrication of the three-layer setup is only possible in this case because of the insolubility of MeHPPV upon the application of an annealing step at elevated temperature. Otherwise, deposition of the transport layer would lead to dissolution of the sensor layer. To overcome these problems, we developed a novel setup for the diffusion measurements. Instead of a three-layer system, we used a bilayer setup without additional sensor layer. This means that the photoluminescence is measured directly in the material to be investigated. By this means, the diffusion of C_{60} in low bandgap polymers can be studied. In addition, suitable annealing conditions for bilayer solar cells can be derived from these measurements.

Figure 51 presents the bilayer setup for the diffusion measurements. The polymer to be investigated is spin coated onto a quartz glass substrate. Subsequently, a C_{60} layer is vacuum evaporated on half of the sample by means of a shadow mask. The photoluminescence of the

polymer layer is measured using laser excitation. By increasing the temperature, C_{60} molecules are injected into the polymer layer and diffuse through it. This quenches the photoluminescence of the polymer layer in reference to the sample side without C_{60} . The more fullerene molecules diffuse into the polymer layer, the more the photoluminescence is quenched.

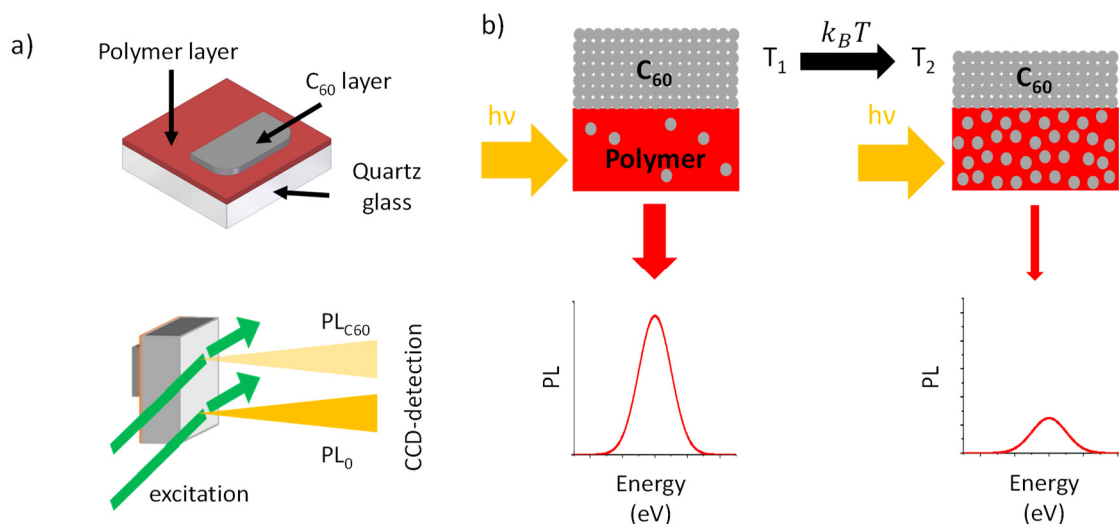


Figure 51: a) Sample setup for the photoluminescence measurements. The samples were fabricated via spin coating of the polymer layer (red) onto quartz glass and subsequent vacuum evaporation of C_{60} (grey) on one half of the sample using a shadow mask. b) Schematic overview of the diffusion measurements applying a bilayer setup. Upon temperature activation, C_{60} molecules start to diffuse into the polymer layer. The photoluminescence of the polymer layer is quenched in dependence of the fullerene concentration. Reprinted from Chapter 8.

For comparison of the novel bilayer setup with the previously used three-layer geometry, bilayer samples of the crosslinked polyfluorene PF2/6-A-75:25 with 75% acrylate content in the sidechains were measured. The chemical structure of the crosslinkable polymer is illustrated in Figure 52. PF2/6-A-75:25 was already applied in the three-layer setup and allows the deposition of acceptors from solution for further investigations. Photoluminescence measurements were carried out by heating the bilayer samples made from 200-270 nm of PF2/6-A-75:25 and 30 nm of C_{60} to different temperatures between 115 °C and 140 °C and fitted afterwards. As an example, the decay of the photoluminescence of the crosslinked PF2/6-A-75:25 when heating the sample from 22 °C to 120 °C is depicted in Figure 52. Furthermore, Figure 52 illustrates the Arrhenius plots of the diffusion coefficients obtained from both the previously presented three-layer samples and the novel bilayer geometry. The results showed that both setups are comparable as the activation energies derived from the slope of the plots for the bilayer samples are in accordance with the values for the three-layer setup while the absolute values for the bilayer geometry were 2-3 times higher. As the equilibrium concentration at elevated temperature is very low and crosslinking prevents the aggregation of C_{60} , clustering of the C_{60} molecules can be excluded.

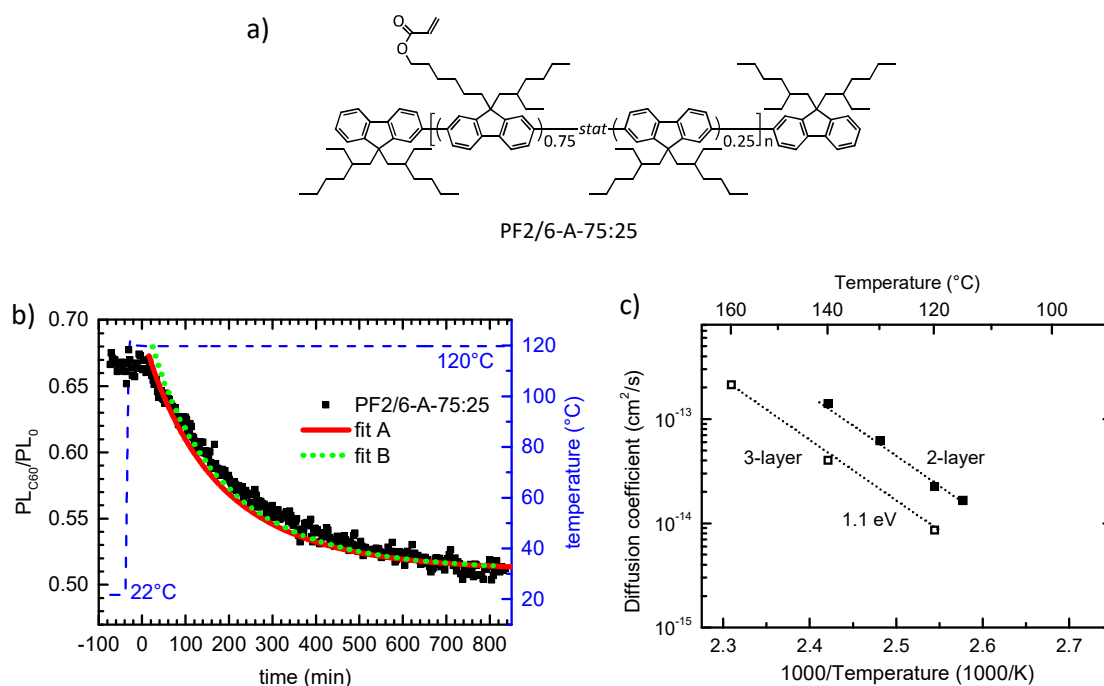


Figure 52: a) Chemical structure of PF2/6-A-75:25 with 75% acrylate content. b) Decrease of the photoluminescence upon temperature increase from 22 °C to 120 °C for a sample of the crosslinked polyfluorene PF2/6-A-75:25. Fits using different initial conditions are shown in red and green. c) Arrhenius plots of the diffusion coefficient in dependence of the temperature for crosslinked PF2/6-A-75:25. The open squares present the results for the three-layer setup, the filled squares depict the results of the bilayer geometry. The activation energy of the diffusion can be derived from the slope as shown by the dotted lines. Reprinted from Chapter 8.

For the investigation of the diffusion process of C_{60} through a polymer matrix, a series of three low bandgap polymers and copolymers was applied. This allows to determine the impact of small changes in the chemical structure of the basic PCDTBT polymer on the diffusion behaviour. The polymers are shown in Figure 53. Within this series, the glass transition temperatures T_g of the polymers is varied systematically. As a reference, PCDTBT was used exhibiting a T_g of 112 °C. Addition of hexyl spacers to the thiophene groups in the acceptor unit yielded PCDHTBT. Its chains are much more flexible and therefore the T_g decreases to about 60 °C. Furthermore, this polymer exhibits the lowest molecular weight in the series. In contrast, incorporation of bulky triphenyldiamine units would lead to a lower flexibility. However, this is balanced by the hexyl spacers in the acceptor units in the copolymer PCDHTBT_{0.7}/TPDDHTBT_{0.3}, denoted as PCDTBT_{stat}. Thus, the glass transition temperature at 110 °C for the copolymer is almost the same as for PCDTBT. The glass transition temperatures were obtained via differential scanning calorimetry (DSC) as presented in Figure 53.

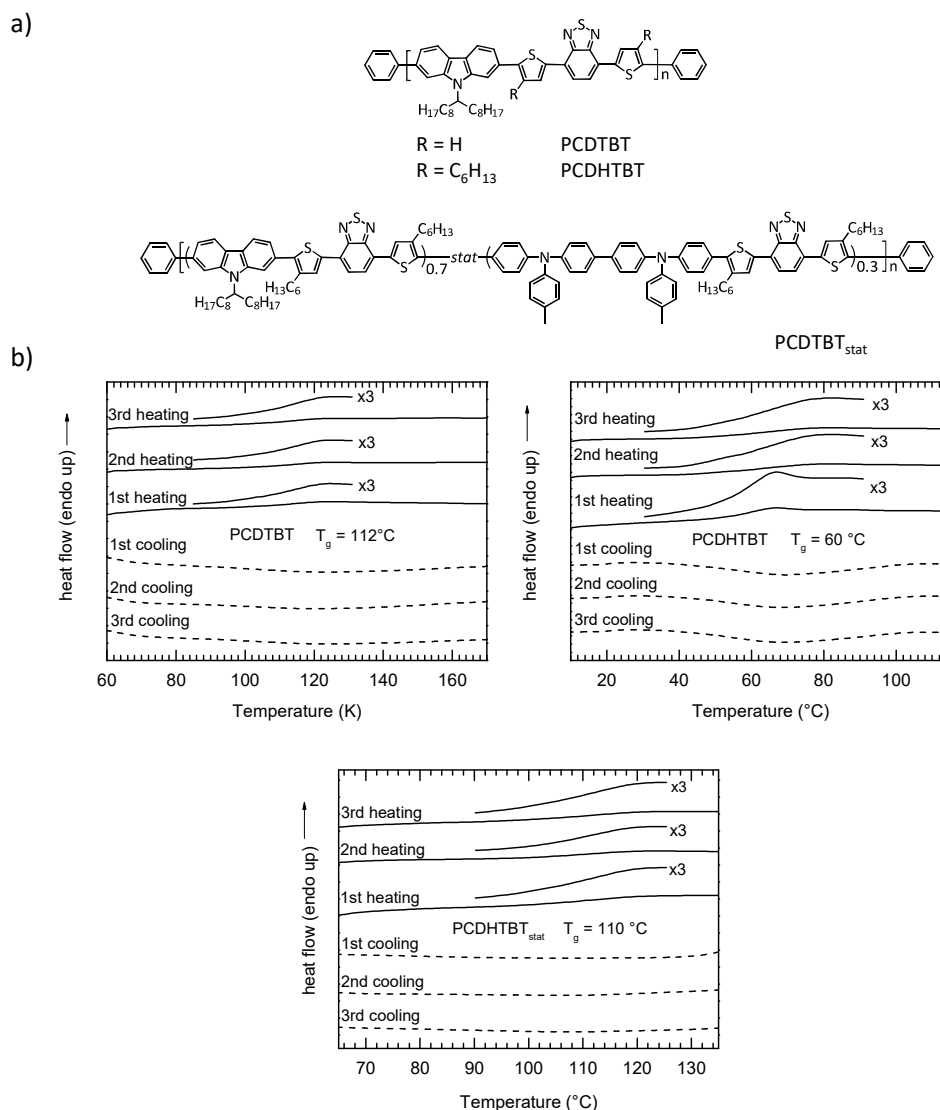


Figure 53: a) Chemical structures of PCDTBT, PCDHTBT, and PCDTBT_{stat}. b) DSC measurements of PCDTBT (left), PCDHTBT (middle), and PCDTBT_{stat} (right) with a heating and cooling rate of 40 Kmin⁻¹ under nitrogen atmosphere. Reprinted from Chapter 8.

Furthermore, dynamic-mechanical analysis (DMA) was applied to confirm the T_g values. Figure 54 shows the DMA measurements of PCDTBT, PCDHTBT and PCDTBT_{stat}. As the loss modulus E'' showed only a small transition, the storage modulus E' and $\tan\delta$ were used for the determination of the glass transition temperatures. Thus, $T_g(\text{onset})$ is 109 °C and $T_g(\text{peak})$ is 118 °C for PCDTBT. The lower glass transition temperature for PCDHTBT could be approved by DMA with a $T_g(\text{onset})$ of 65 °C and a $T_g(\text{peak})$ of 73 °C. Furthermore, a $T_g(\text{onset})$ of 103 °C and a $T_g(\text{peak})$ of 112 °C were determined for PCDTBT_{stat}. Typically, the values from the peak of $\tan\delta$ lie above the T_g measured by DSC which would also apply for the value from the onset of E'' . In contrast, the values estimated from the onset of E' lie below the T_g identified by DSC except for $T_g(\text{onset})$ of PCDHTBT that is also higher than the value derived from DSC analysis. This could suggest that the glass transition temperature is slightly higher than 60 °C measured by DSC.

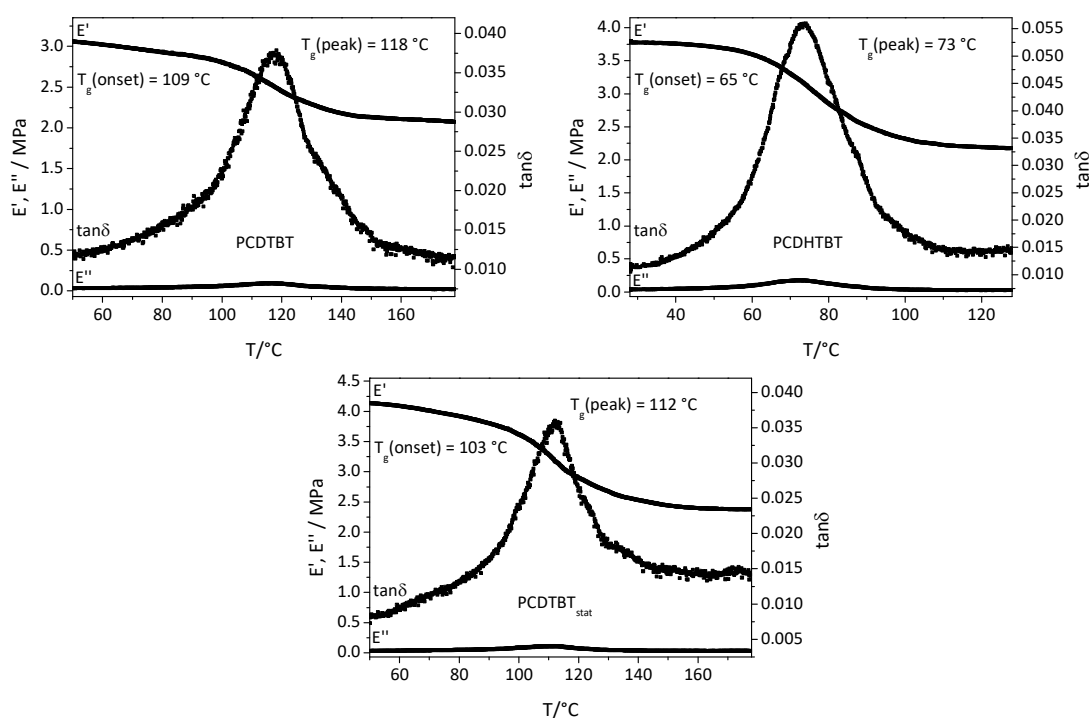


Figure 54: DMA measurements of PCDTBT (top left), PCDHTBT (top right), and PCDTBT_{stat} (bottom). The analyses were performed with a temperature rate of 2 Kmin⁻¹ and a frequency of 2 Hz.

Bilayer samples with a 30-70 nm thick polymer layer and a 30 nm thick C₆₀ layer were fabricated. The development of the photoluminescence for all three polymers was measured during different temperature increases between 60 °C and 140 °C. All applied temperatures were above the glass transition temperature of PCDHTBT whereas the measurements of PCDTBT and PCDTBT_{stat} were conducted below and above T_g. In Figure 55, the decay of the normalized photoluminescence of PCDTBT for different temperatures is shown as an example. The higher the final temperature was, the faster the C₆₀ diffusion and thus the quenching of the photoluminescence occurred. This observation was also valid for PCDHTBT and PCDTBT_{stat}. Furthermore, the diffusion coefficients of the C₆₀ diffusion within the different polymers could be evaluated in dependence of the temperature. This was possible by fitting the experimental data and calculating the respective C₆₀ concentrations within the polymer using a theoretical model. When the final temperature was increased, both the equilibrium concentration of C₆₀ within the polymers and the diffusion coefficients became higher. Yet, the exclusion of clustering of the fullerene molecules was possible due to the overall low equilibrium concentrations of C₆₀.

The diffusion coefficients determined for different temperatures for PCDTBT, PCDHTBT, and PCDTBT_{stat} as well as for the crosslinked PF2/6-A-75:25 are illustrated in Figure 55. For PCDHTBT, thermally induced diffusion can be assumed from the linear slope of the Arrhenius plot above the T_g of 60 °C with an activation energy of 0.70 eV. Despite the small differences in the polymer structure, the results for PCDTBT and PCDTBT_{stat} are comparable due to the similar molecular weight and glass transition temperatures of about 110 °C. The diffusion is also activated by temperature leading to an activation energy of 0.40 eV below T_g and 1.00 eV above T_g. In

comparison, all three polymers exhibit a similar diffusion coefficient of $3 \cdot 10^{-15} \text{ cm}^2\text{s}^{-1}$ above T_g that is lower than that of PF2/6-A-75:25. In the case of PCDHTBT, also the activation energy is lower. Remarkably, no significant drop of the diffusion coefficients below T_g for PCDTBT and PCDTBT_{stat} was observed that would be expected due to an increased viscosity of the polymer below the glass transition. This was attributed to the local movement of the sidechains that enabled the diffusion of the fullerene molecules through the polymer matrix. When reaching the glass transition temperature, the diffusion is enhanced because of the beginning motion of the polymer backbone.

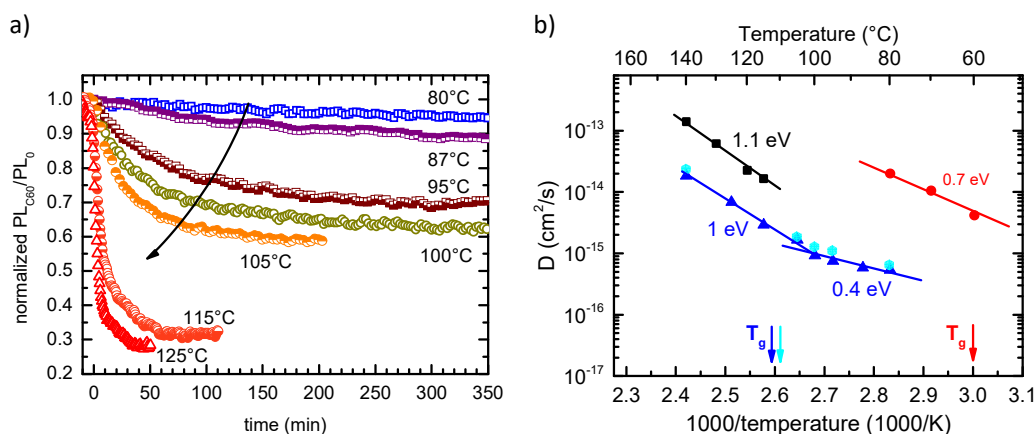


Figure 55: a) Normalized photoluminescence of a PCDTBT sample in dependence of the time for different final temperatures. b) Arrhenius plots of the diffusion coefficient in dependence of the temperature for crosslinked PF2/6-A-75:25 (black squares), PCDTBT (blue triangles), PCDHTBT (red circles), and PCDTBT_{stat} (light blue hexagons). The activation energy of the diffusion can be derived from the slope as shown by the solid lines. Corresponding glass transition temperatures are shown by arrows. Reprinted from Chapter 8.

The presented results illustrate that the C₆₀ diffusion within donor polymers exhibiting a photoluminescence in the red can be evaluated by time-dependent photoluminescence measurements at elevated temperatures by the use of a bilayer setup. Via time-dependent photoluminescence measurements at elevated temperatures, the diffusion coefficients as well as the equilibrium concentrations of fullerene in the polymer matrix could be determined. We examined a series of three low bandgap polymers with small changes in the polymer structure. The findings state that the diffusion of C₆₀ molecules already occurs below the glass transition temperature due to the local motion of the sidechains. As the novel setup allows the evaluation of different diffusion conditions, this information can be used in a further step for the prediction of suitable annealing times and temperatures for the adjustment of the donor-acceptor interface leading to efficient organic solar cells.

4.3 Individual contributions to joint publications

In the following, the individual contributions of the authors to the publications are specified.

Chapter 5

This work is published in *Physica Status Solidi A*, **2015**, *212*, 2162-2168, doi: 10.1002/pssa.201532040, with the title:

Organic solar cells with crosslinked exciton blocking layer

by Tobias Hahn, Christina Saller, Marlene Weigl, Irene Bauer, Thomas Unger, Anna Köhler, and Peter Strohriegl.

This publication is reprinted in Chapter 5 and deals with the realization of a first three-layer solar cell. I synthesized and characterized the applied donor polymer, interpreted the data together with the co-authors and wrote parts of the manuscript. Furthermore, I corrected the whole manuscript. Marlene Weigl synthesized the crosslinkable polymer. Irene Bauer assisted in the synthetic work. Tobias Hahn fabricated and measured the solar cells, did the data evaluation and interpreted the data together with the co-authors. He wrote large parts of the manuscript and corrected the manuscript. Thomas Unger performed the exciton lifetime measurements. Anna Köhler and Peter Strohriegl supervised the project, were involved in the scientific discussion and finalized the manuscript.

Chapter 6

This work is published in *The Journal of Physical Chemistry C* **2016**, *120*, 25083-25091, doi: 10.1021/acs.jpcc.6b08471, with the title:

Role of intrinsic photogeneration in single layer and bilayer solar cells with C₆₀ and PCBM

by Tobias Hahn, Steffen Tscheuschner, Christina Saller, Peter Strohriegl, Puttaraju Boregowda, Tushita Mukhopadhyay, Satish Patil, Dieter Neher, Heinz Bässler, and Anna Köhler.

This publication is reprinted in Chapter 6 and evaluates the contribution of the acceptor to the photogeneration in organic solar cells. I designed and synthesized the applied donor polymer, did the characterization concerning the polymer properties and wrote the corresponding part of the manuscript. Furthermore, I corrected the whole manuscript. Tobias Hahn fabricated and measured the solar cells, did the data evaluation and interpreted the data together with the co-authors. He wrote parts of the manuscript and corrected the manuscript. Steffen Tscheuschner conducted the Onsager fit of the data and did the data interpretation together with the co-authors. He wrote parts of the manuscript and corrected the manuscript. Tobias Hahn and Steffen Tscheuschner contributed equally to this work. Puttaraju Boregowda and Tushita Mukhopadhyay synthesized and characterized the small donor molecule and were supervised

by Satish Patil. Peter Strohrriegl, Dieter Neher, and Heinz Bässler were involved in the scientific discussion. Anna Köhler supervised the project, was involved in the scientific discussion and corrected the manuscript.

Chapter 7

This work is published in *Advanced Functional Materials* **2017**, *12*, 1604906, doi: 10.1002/adfm.201604906, with the title

Monomolecular and bimolecular recombination of electron–hole pairs at the interface of a bilayer organic solar cell

by Tobias Hahn, Steffen Tscheuschner, Frank-Julian Kahle, Markus Reichenberger, Stavros Athanasopoulos, Christina Saller, Guillermo C. Bazan, Thuc-Quyen Nguyen, Peter Strohrriegl, Heinz Bässler, and Anna Köhler.

This publication is reprinted in Chapter 7 and focuses on the examination of the different recombination types in organic solar cells. I designed and synthesized the applied donor polymer, did the characterization concerning the polymer properties and wrote the corresponding part of the manuscript. Furthermore, I corrected the whole manuscript. Tobias Hahn fabricated and measured the solar cells, did the data evaluation and interpreted the data together with the co-authors. He wrote parts of the manuscript and corrected the manuscript. Steffen Tscheuschner conducted the fit to the data. Frank-Julian Kahle performed the MIS-CELIV measurements of the materials and wrote the corresponding part of the paper. Markus Reichenberger provided data about the small donor molecule, was involved in the scientific discussion and corrected the manuscript. Stavros Athanasopoulos conducted the Monte Carlo simulations and wrote the corresponding parts of the manuscript. Guillermo C. Bazan and Thuc-Quyen Nguyen provided the small donor molecule and were involved in the scientific discussion together with Peter Strohrriegl and Heinz Bässler. Anna Köhler supervised the project, was involved in the scientific discussion and corrected the manuscript.

Chapter 8

This work is accepted to be published in *ACS Applied Materials & Interfaces* **2018**, doi: 10.1021/acsami.8b05520, with the title

Facile method for the investigation of temperature-dependant C₆₀ diffusion in conjugated polymers

by Christina Saller, Frank-Julian Kahle, Thomas Müller, Tobias Hahn, Steffen Tscheuschner, Denys Priadko, Peter Strohrriegl, Heinz Bässler, and Anna Köhler.

This publication is reprinted in Chapter 8 and depicts diffusion studies of fullerene in low bandgap polymers and copolymers. I synthesized the low bandgap polymers, designed and synthesized the low bandgap copolymer and did the characterization concerning the polymer properties. I prepared and measured three-layer and bilayer samples for the comparison with a previously published method together with Steffen Tscheuschner and Frank-Julian Kahle. Furthermore, I wrote parts of the manuscript. Frank-Julian Kahle prepared and measured three-layer and bilayer samples for the method comparison as well as bilayer samples of the low bandgap polymers. He did the data evaluation and interpreted the data together with the co-authors. Furthermore, he verified the theoretical model and wrote parts of the manuscript. Frank-Julian Kahle and I contributed equally to this work. Thomas Müller prepared and measured the bilayer samples of the low bandgap polymers, did the data evaluation and interpreted the data together with the co-authors. The manuscript is based on his master thesis on this topic. Tobias Hahn was involved in the scientific discussion. Furthermore, he wrote parts of the manuscript. Steffen Tscheuschner prepared and measured three-layer and bilayer samples for the method comparison together with me. He did the data evaluation and interpreted the data together with the co-authors. Furthermore, he verified the theoretical model. Denys Priadko contributed experimental advice and was involved in the scientific discussion together with Heinz Bässler. Peter Strohrriegl and Anna Köhler supervised the project and were involved in the scientific discussion.

Appendix A

The chapter presented in Appendix A comprises the experimental section for the optimized synthesis of the crosslinkable donor polymers PCDTBTOx and PCPDTBTOx. I synthesized and characterized both polymers and wrote the manuscript.

Appendix B

This work is published in *Proceedings of SPIE 8830, Organic Photovoltaics XIV*, **2013**, 88300P, doi: 10.1117/12.2023899, with the title

Patternable conjugated polymers for organic solar cells

by Peter Strohrriegl, Philipp Knauer, Christina Saller, and Esther Scheler.

This publication is reprinted in Appendix B and describes the synthesis and application of crosslinkable donor polymers. I designed and synthesized the crosslinkable carbazole-based low bandgap polymer, did the characterization concerning the polymer properties and wrote parts of the manuscript. Furthermore, I corrected the whole manuscript. Philipp Knauer synthesized and characterized the crosslinkable fluorene-based low bandgap polymer. He wrote parts of the manuscript and corrected the manuscript. Esther Scheler synthesized and characterized the

crosslinkable polyfluorenes. Peter Stroehriegl supervised the project and finalized the manuscript.

Appendix C

This work is published in *Proceedings of SPIE 9942, Organic Photovoltaics XVII*, **2016**, 994200, doi: 10.1117/12.2239400, with the title

Crosslinkable low bandgap polymers for organic solar cells

by Peter Stroehriegl, Christina Saller, Philipp Knauer, Anna Köhler, Tobias Hahn, Florian Fischer, and Frank-Julian Kahle.

This publication is reprinted in Appendix C and summarizes the work on crosslinkable fluorene-based low bandgap polymers. I contributed to the section about the realization of a three-layer solar cell as described for Chapter 5. Furthermore, I wrote large parts of the manuscript and corrected the manuscript. Philipp Knauer was involved in the parts about synthesis, crosslinking procedure and stabilization of bulk heterojunction solar cells. He wrote parts of the manuscript. Tobias Hahn worked on the sections about the three-layer solar cells, C₆₀ diffusion in polyfluorenes, and stabilization of bulk heterojunction solar cells. Florian Fischer contributed to the part about C₆₀ diffusion in polyfluorenes. Frank-Julian Kahle did the charge carrier mobility studies. Anna Köhler was involved in the scientific discussion. Peter Stroehriegl supervised the project, was involved in the scientific discussion and finalized the manuscript.

Appendix D

This work is published in *Advanced Energy Materials* **2017** 7, 1700306, doi: 10.1002/aenm.201700306, with the title

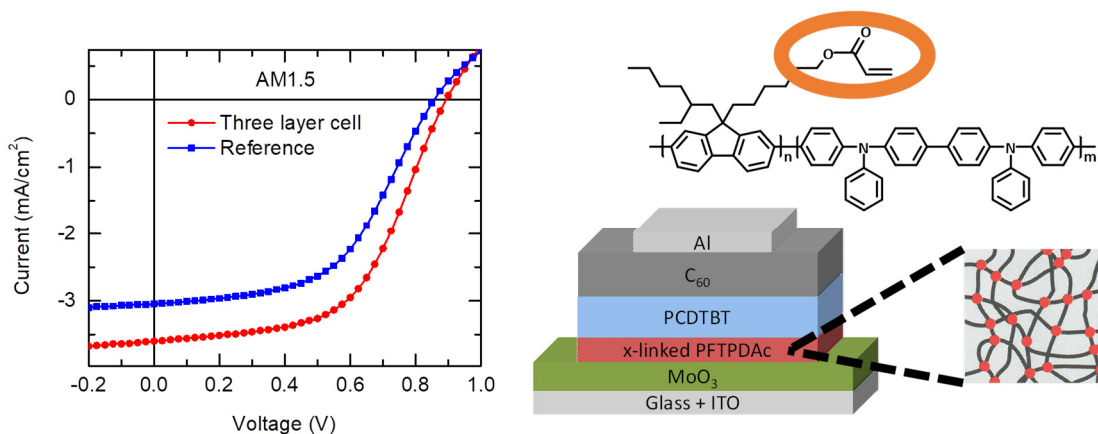
Crosslinked semiconductor polymers for photovoltaic applications

by Frank-Julian Kahle, Christina Saller, Anna Köhler, and Peter Stroehriegl.

This publication is reprinted in Appendix D and reviews crosslinkable polymers for morphology stabilization in organic solar cells. I wrote parts of the manuscript and corrected the manuscript. Frank-Julian Kahle wrote parts of the manuscript and corrected the manuscript. Frank-Julian Kahle and I contributed equally to this work. Anna Köhler and Peter Stroehriegl supervised the project, were involved in the scientific discussion and corrected the manuscript.

5. Organic solar cells with crosslinked polymeric exciton blocking layer

Tobias Hahn, Christina Saller, Marlene Weigl, Irene Bauer, Thomas Unger,
Anna Köhler, and Peter Strohriegel



Published in *Physica Status Solidi A*

doi: 10.1002/pssa.201532040

Reprinted with permission from *Physica Status Solidi A*, **2015**, 212, 2162-2168

Copyright © 2015 WILEY-VCH Verlag GmbH & Co. KGaA, Weinheim

Organic solar cells with crosslinked polymeric exciton blocking layer

T. Hahn¹, C. Saller², M. Weigl², I. Bauer¹, T. Unger¹, A. Köhler^{1,3}, and P. Strohriegl^{*,2,3}

¹ Experimental Physics II, University of Bayreuth, 95440 Bayreuth, Germany

² Macromolecular Chemistry I, University of Bayreuth, 95440 Bayreuth, Germany

³ Bayreuth Institute of Macromolecular Science (BIMF), University of Bayreuth, 95440 Bayreuth, Germany

Received 18 December 2014, revised 30 April 2015, accepted 15 May 2015

Published online 12 June 2015

Keywords excitons, MoO₃, organic solar cells, PCDTBT, photocrosslinking

* Corresponding author: e-mail peter.strohriegl@uni-bayreuth.de, Phone: +49 921 553296, Fax: +49 921 553206

We show that the performance of an organic solar cell can be increased by the introduction of an additional polymeric exciton blocking layer. In order to realize this, the novel polymer PFTPDAc with pendant acrylate groups is developed. Thin films are coated from a PFTPDAc solution and subsequently cross-linked by irradiation. Thereby, the film becomes completely insoluble and allows spincoating of a second polymer layer on top. We realize a three layer solar cell which contains a

crosslinked PFTPDAc interlayer on top of the molybdenum oxide anode and layers of the low-bandgap polymer PCDTBT and C₆₀. In comparison with a reference cell without the interlayer, the EQE is significantly increased in the spectral region between 400 and 650 nm. From current–voltage measurements a power conversion efficiency of 1.8% is determined. PL measurements show that the increase of solar cell performance is attributed to exciton blocking by the PFTPDAc interlayer.

© 2015 WILEY-VCH Verlag GmbH & Co. KGaA, Weinheim

1 Introduction Organic solar cells (OSCs) have achieved increasing interest during the last decade. Two different strategies exist for the processing of organic solar cells. The first is the subsequent vacuum evaporation of small molecules. Such cells often consist of a large number of layers and in many cases have more than one absorber layer. In a triple junction solar cell, a power conversion efficiency of 11.1% has been reported in scientific literature [1], while companies have announced efficiencies up to 12.0% [2]. The most popular organic solar cell architecture are bulk heterojunction (BHJ) cells made from a polymer donor and a small molecule acceptor by solution processing. The best investigated BHJ organic solar cell consists of poly-3-hexylthiophene (P3HT) as donor and the C₆₀ derivative PCBM as electron acceptor. With this combination, efficiencies of about 5% are reached [3]. If more efficient low-bandgap polymers are used instead of P3HT the power conversion efficiency of organic solar cells can be increased up to 10.8% [4].

One major difference between vacuum evaporated and solution processed organic solar cells is that the evaporation technique allows the fabrication of solar cells with a large number of layers by subsequent evaporation of organic molecules. One advantage of this concept is that the

different layers can be optimized separately. Extending this concept to solution processing with polymers is a challenge since the underlying polymer layer is often dissolved when a second polymer solution is spincoated on top. This problem can be circumvented using polymers that dissolve in orthogonal solvents [5] or by the introduction of insoluble interlayers of inorganic oxides like ZnO. The concept of inorganic interlayers is often used to realize tandem cells with two different absorbers [6–8].

An alternative way to deposit two polymer layers on top of each other is the use of polymers that can be chemically crosslinked. The use of chemical crosslinking for organic devices has first been explored in organic light-emitting diodes (OLEDs), where light-emitting polymers with oxetane sidegroups were crosslinked by cationic photopolymerization [9]. OLEDs with red, green, and blue pixels have been realized by spincoating and subsequent crosslinking of red, green, and blue emitting polymers. Upon crosslinking, the polymers become completely insoluble and a second polymer layer can be spincoated on top without problems. Later on this concept has been extended to organic solar cells. Fréchet et al. described a P3HT derivative with photocrosslinkable bromine units and prepared both BHJ and flat heterojunction (FHJ) organic solar cells with efficiencies

© 2015 WILEY-VCH Verlag GmbH & Co. KGaA, Weinheim

of about 3 and 2%, respectively [10]. In addition to bromine, various other functional groups, for example, acrylate [11] and oxetane [12] have been used for crosslinking. Studies of low-bandgap polymers with crosslinkable units have been presented by Krebs [13], Xu [14], and Heeney [15]. All polymers described above contain photocrosslinkable groups covalently attached to the polymer. In 2010, Friend and coworkers presented a different concept in which a reactive bis-nitrene crosslinker is added to non-functionalized conjugated polymers [16]. With this concept, a planar heterojunction organic solar cell with three polymer layers on top of each other was realized [17]. The organic solar cell which uses cascaded energy levels reaches a power conversion efficiency of 0.45%. In the papers mentioned above, the absorbing polymer layers of the OSCs have been crosslinked. In addition, crosslinked anode [14, 18, 19] and cathode interlayers [20] which facilitate hole or electron extraction have been described in the literature.

Interlayers can also be used to prevent exciton quenching at the cathode or anode. The introduction of exciton blocking layers was one important step in advancing the efficiencies of OLEDs [21, 22]. In organic solar cells, light is incident through the transparent anode, typically

ITO + MoO₃ or ITO + PEDOT:PSS. Thus, a critical interface where photogenerated excitons can be quenched is the interface from donor to anode. From small molecule organic solar cells, it is known that the insertion of an exciton blocking layer between donor and anode prevents quenching at this interface, thus enhancing the solar cell power conversion efficiency [23, 24].

In this paper, a solution processable, photocrosslinkable exciton blocking layer and its application in organic solar cells is presented for the first time using the novel photocrosslinkable conjugated polymer PFTPDAc. The chemical structure of PFTPDAc is shown in Fig. 1. The copolymer contains fluorene and hole transporting aromatic amino units. Acrylate groups which can be polymerized by a free radical mechanism are attached to the fluorene moieties. Photocrosslinking makes the PFTPDAc layer insoluble and allows the fabrication of the three layer organic solar cell shown in Fig. 1. In the paper, an organic solar cell with a crosslinked PFTPDAc interlayer is compared to reference cells in which PFTPDAc is omitted. It is shown that the use of a thin PFTPDAc interlayer leads to an increase of the solar cell power conversion efficiency to 1.8%.

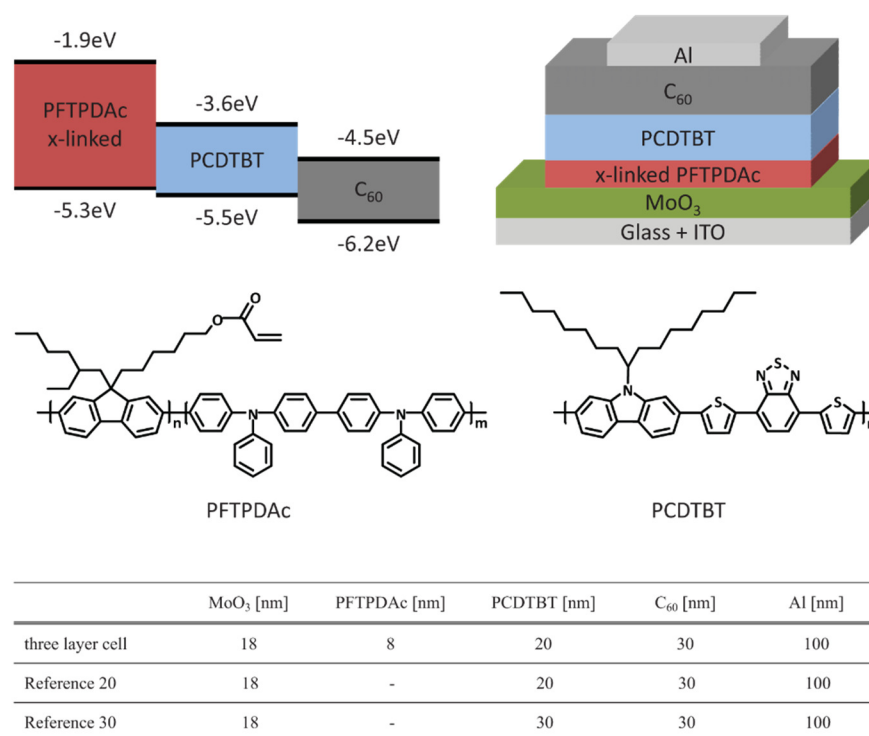


Figure 1 Cascading energy levels of the different materials in the three layer solar cell (left), device structure of the cell (right), chemical structure of the polymers PFTPDAc and PCDTBT, and layer thicknesses of the solar cells investigated. For detailed information on the energy levels of MoO₃ and hole extraction at a MoO₃ organic interface see Meyer et al. [30].



2 Experimental Poly-9-(2-ethylhexyl)-9-(6-acryloyloxy-hexyl)-fluorene-*stat*-N,N'-bis-(4-methylphenyl)-N,N'-diphenyl-benzidine (PFTPDAC) was synthesized by Yamamoto coupling according to the following procedure. The molar ratio of the fluorene and the benzidine units in PFTPDAC is 7:3.

A Schlenk flask was charged with nickel dicyclooctadiene (Ni(COD), 1.00 g, 3.64 mmol), cyclooctadiene (COD, 0.39 g, 3.64 mmol), 2,2'-bipyridyl (0.57 g, 3.64 mmol), and 18 mL dry DMF under argon. The mixture was degassed by three freeze–thaw cycles before it was heated to 80 °C for 30 min while stirring. The monomers 2,7-dibromo-9-(2-ethylhexyl)-9-((6-acryloyloxy)-hexyl)-fluorene (0.488 g, 0.827 mmol) and N,N'-bis(4-methylphenyl)-N,N'-bis(4-bromophenyl)-benzidine (0.239 g, 0.354 mmol) were weighed into a separate flask under argon. A trace of BHT and 68 mL of dry toluene were added and the mixture was degassed by three freeze–thaw cycles. Subsequently, the monomer mixture was added to the catalyst using a syringe. The reaction mixture was stirred at 80 °C for five days in the dark before 2-bromo-9,9-bis-(2-ethylhexyl)-fluorene (0.05 g, 0.10 mmol) was added as endcapper. After stirring for 24 h at 80 °C, the mixture was poured into methanol/HCl (conc.) 1:1 and stirred at room temperature for 2 h. The organic layer was separated from the HCl layer, which was then washed with ether in order to remove low molecular weight polymer. PFTPDAC was extracted from the aqueous phase by dissolving the solid residue in a 1:1 THF/toluene mixture. The THF/toluene phase was washed with an alkaline EDTA solution (5%) and water and most of the solvent was evaporated. The product was precipitated into methanol and the crude product was further purified by reprecipitation from THF into methanol and dried under vacuum, yielding 0.280 g (52%) of PFTPDAC as a pale yellow powder. From the ether phase, 0.100 g (19%) of PFTPDAC with a lower molecular weight was isolated. The molecular weight of the copolymer was measured by size exclusion chromatography (SEC) in THF solution and is 137,000 gmol⁻¹ (M_w) and 52,000 gmol⁻¹ (M_n) with a polydispersity index of 2.64. ¹H NMR (300 MHz, CDCl₃, 25 °C): δ = 0.50–1.30 (m, CH₂, CH₃), 2.10 (br, CH₂), 2.37 (s, ar-CH₃), 4.03 (br, OCH₂), 5.75 (d, =CH₂), 6.06 (m, =CH), 6.35 (d, =CH₂), 7.04–7.90 (m, ar-CH). From the integration of the three protons of the acrylate unit and the six protons of the methyl groups in the benzidine unit a molar ratio of 7:3 was calculated.

PCDTBT was synthesized according to the procedure described by Leclerc [25]. After precipitation in methanol/water 10:1, the polymer was fractionated via Soxhlet extraction using acetone, hexane, and toluene. The reduced toluene fraction was precipitated in methanol/water 10:1 and dried in vacuum overnight. Yield: 0.468 g (61%) of a violet powder. A molecular weight of 37,000 gmol⁻¹ (M_w) and 16,000 gmol⁻¹ (M_n) was determined by high temperature polymer SEC in trichlorobenzene with a PDI of 2.25.

C₆₀ (American Dye Source, Inc.) was used as the acceptor in the three layer solar cells.

The absorption spectra were measured from films with a Cary 5000 (Varian) UV-VIS spectrometer. The photoluminescence was recorded with a Jasco FP-8600 spectrofluorometer. Both spectra were measured in 1 nm steps. For spectroscopic measurements, polymer films were spun from chlorobenzene or toluene solution (5 mg mL⁻¹) on quartz glass substrates. The polymer layer thickness of the spectroscopic sample was identical to the layer thickness of the donor layer of the corresponding solar cell. Layer thickness was measured with a Dektak (Veeco) profilometer. Fluorescence lifetime of PCDTBT was measured using a time correlated single photon counting (TCSPC) setup from PicoQuant GmbH at excitation wavelength 485 nm with a time resolution of 140 ps. Lifetimes are extracted by deconvolution analysis using a monoexponential fit.

For photocurrent measurements, heterojunction three layer solar cell devices were fabricated on structured ITO-coated glass substrates. To avoid edge effects, a circular active area on the device was defined on top of the ITO anode using photolithography as described by Schwarz et al. [26]. On the active area, an 18 nm thick MoO₃ (Sigma–Aldrich) layer was brought up by vacuum evaporation. The MoO₃ layer ensures a low dark current and a good diode behavior. The crosslinked 8 nm thick PFTPDAC layer, forming the first organic layer of the three layer system, was spun from toluene solution (2 mg mL⁻¹) on top of the device. The crosslinking of the acrylate groups was carried out by photopolymerization using 1 wt% of the commercial photoinitiator Irgacure 784. The PFTPDAC film was irradiated at 40 °C for 10 min with a 50 W xenon lamp with UV filter [27]. Crosslinking was checked by solubility measurements. The absorption spectrum of a thin film of PFTPDAC was measured directly after crosslinking. Then the crosslinked film was immersed into THF for 1 min, rinsed and measured again. Figure S2 in the Supporting Information (online at: www.pss-a.com) proves that the optical density remains constant which means that the film is fully crosslinked and contains no soluble material. Enabled by the insolubility of the crosslinked PFTPDAC layer, in the next step a 20 nm thick PCDTBT layer forming the second organic layer in the three layer system was spincoated from a chlorobenzene solution (5 mg mL⁻¹). The thickness of each layer is precisely controlled by profilometer and optical density measurements. Finally, the acceptor, a 30 nm thick C₆₀ layer and a 100 nm thick aluminium cathode are vacuum evaporated. All solar cells were annealed at 140 °C for 10 min. The complete solar cell fabrication and the irradiation for crosslinking were done in a nitrogen atmosphere using a glovebox with direct access to the evaporation chamber.

Monochromatic current–voltage characteristics were measured using vacuum conditions at room temperature and monochromatic illumination from a 450 W xenon lamp (Osram) with monochromator. The light intensity on the solar cell (after monochromator and lens system) was measured using a Hamamatsu S1337-33BQ photodiode. Current–voltage characteristics under AM1.5 sun light

condition were measured with a Newport sun simulator and an appropriate sample holder. For solar cell measurements a Keithley 236 and 238 source-measure-unit was used.

3 Results and discussion We have prepared an organic solar cell containing three organic layers on top of each other. This device architecture is enabled by the novel photocrosslinkable polymer PFTPDAc. The structure of the devices is shown in Fig. 1. On an ITO glass, a thin molybdenum oxide layer was evaporated which leads to a low dark current and improves the diode behavior. On top, an 8 nm thin layer of the photocrosslinkable polymer PFTPDAc was spincoated and subsequently crosslinked by irradiation with a xenon lamp. Upon crosslinking, the PFTPDAc layer becomes completely insoluble and a second layer consisting of the low-bandgap polymer PCDTBT can be spincoated on top. The device fabrication was finished by evaporating C_{60} and an aluminum top electrode. This results in well-adjusted energy levels as shown in Fig. 1. Two bilayer cells without the PFTPDAc layer were prepared as reference (Fig. 1). In the reference cell Reference 20, the PFTPDAc layer is omitted and all other layers are kept identical. The idea behind the reference cell Reference 30 is to keep the active layer thickness constant. This leads to a similar situation regarding the electric field in the three layer cell with the exciton blocking layer and the Reference 30. The C_{60} thickness of 30 nm was the same for all solar cells.

We now report the results of the solar cell measurements of our three layer cell and the two references. Figure 2a shows the external quantum efficiency (EQE) spectra of the solar cells and the optical densities of the PCDTBT and the PFTPDAc layer. Data prove that within the wavelength interval between 400 and 650 nm the EQE of the three layer solar cell is higher compared to both reference cells. Especially at the PCDTBT low energy absorption band at 580 nm, the EQE of the three layer cell is significantly increased. Further analysis shows that the increase of EQE is correlated with the absorption spectrum of PCDTBT. In the absorption maximum, the exciton density in the PCDTBT layer is high. Thus, there is a high quenching probability for excitons created at that wavelength. A contribution of the PFTPDAc layer to the EQE at 580 nm can be excluded since PFTPDAc shows no absorption above 440 nm. Furthermore, we proved that charge carrier dissociation at the PFTPDAc/PCDTBT interface can be neglected. This was demonstrated by making a solar cell without C_{60} , which only consists of a blend of PFTPDAc and PCDTBT (1:1) as active layer. This cell showed an EQE lower than 0.1% at 580 nm (see Supporting Information, Fig. S1). Consequently, the increased EQE is attributed to the three layer system itself. From tandem solar cells, it is known that the absorption of additional layers can reduce the absorption of the active layer leading to decreased external quantum efficiency [6]. A cell with a 20 nm thick PFTPDAc layer, not shown here, exhibits reduced EQE at 385 nm because of this internal filter effect. In the three layer cell with an 8 nm thick

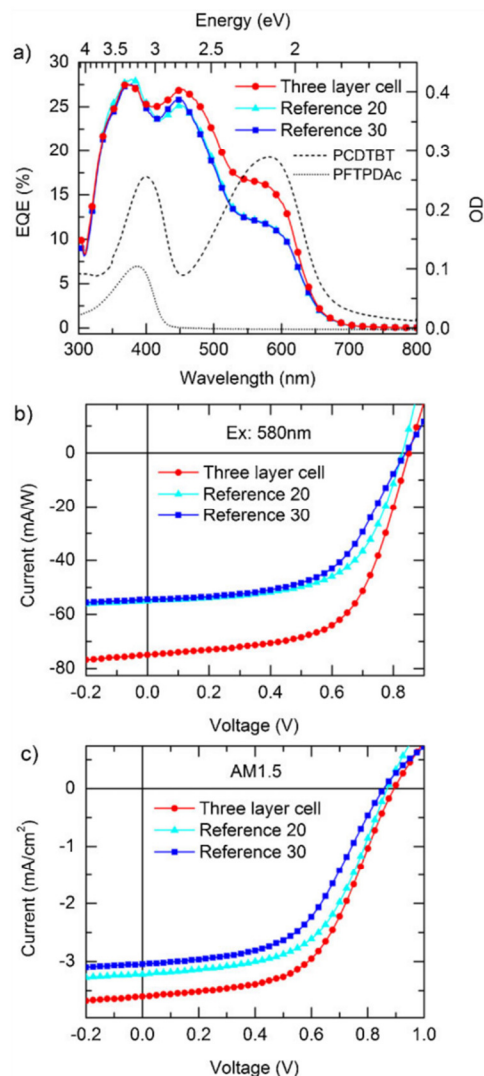


Figure 2 EQE spectrum (a), current–voltage characteristics for monochromatic excitation at 580 nm (b), and current–voltage characteristics under sunlight AM1.5 conditions (c) for the three layer cell (red circles) and for Reference 20 (cyan triangles) and Reference 30 (blue squares). Part (a) also shows the optical density of the 8 nm thick PFTPDAc layer (dotted line) and the 30 nm thick PCDTBT layer (dashed line).

PFTPDAc layer, the PFTPDAc absorption is negligible and the external quantum efficiency is increased over a broad spectral range.

The current–voltage characteristics of the solar cells were measured under monochromatic conditions at the maximum of the optical density of the PCDTBT layer at 580 nm (Fig. 2b) and under AM1.5 sun light conditions

Table 1 Fill factors and power conversion efficiencies of the solar cell measurements shown in Fig. 2 for monochromatic excitation at 580 nm and for AM1.5 sunlight conditions.

	FF(%)	η (%)	FF(%)	η (%)
	580 nm	580 nm	AM1.5	AM1.5
three layer cell	62	4.0	56	1.8
Reference 20	61	2.8	57	1.6
Reference 30	60	2.7	53	1.4

(Fig. 2c). Table 1 shows the fill factors and efficiencies. Whereas the open-circuit voltage (V_{OC}) of the three layer cell and the two references are approximately the same, the short-circuit current (I_{SC}) is about 35% higher if a PFTPDAC interlayer is used. This results in an increase of the power conversion efficiency from 2.7 (Reference 30) or 2.8 (Reference 20) to 4% in the three layer solar cell for monochromatic illumination at 580 nm. Measurements under AM1.5 sun light conditions confirm these observations. Here the power conversion efficiency increases from 1.4 (Reference 30) or 1.6 (Reference 20) to 1.8% in the three layer cell. Furthermore, the additional layer lowers the dark current and improves diode behavior. In the following section, the role of the PFTPDAC interlayer as exciton blocker is discussed.

The generation of excitons in the PCDTBT layer was investigated by photoluminescence and lifetime measurements. PCDTBT was spincoated on glass-MoO₃ substrates and on glass-MoO₃-PFTPDAC substrates. The layer thickness of PCDTBT was always 20 nm and the thickness of the PFTPDAC layer was 8 nm like in the corresponding solar cell. Without the PFTPDAC layer between the MoO₃ and the PCDTBT, we observed a reduced PL intensity of the PCDTBT layer (Fig. 3a). The absorption spectra in Fig. 3b show that the optical densities at the absorption maximum of PCDTBT at 580 nm are identical. This means that the same amount of excitons is created in both samples. We attribute the reduced PL intensity to quenching of the PCDTBT excitons at the interface to MoO₃. Exciton quenching at the MoO₃ or PEDOT:PSS surface is a well-known effect [24, 28]. In addition to the steady state investigations, we have carried out lifetime measurements (Fig. 3c). We observe a reduced lifetime of the PCDTBT excitons in the sample without the PFTPDAC interlayer between MoO₃ and PCDTBT. With the PFTPDAC layer, the PCDTBT lifetimes are comparable to that of PCDTBT directly on a quartz glass substrate. The reduced lifetime further supports that exciton quenching takes place at the PCDTBT-MoO₃ interface. In our solar cells, the PCDTBT has a thickness of only 20 nm, which is in the range of about twice the exciton diffusion length. In such thin layers, which are frequently used in vacuum evaporated solar cells [29], quenching becomes increasingly important. The loss of 30% PL intensity correlates with a distinctly reduced amount of PCDTBT excitons. Assigned to our solar cell measurements, this leads to a reduced EQE in the PCDTBT

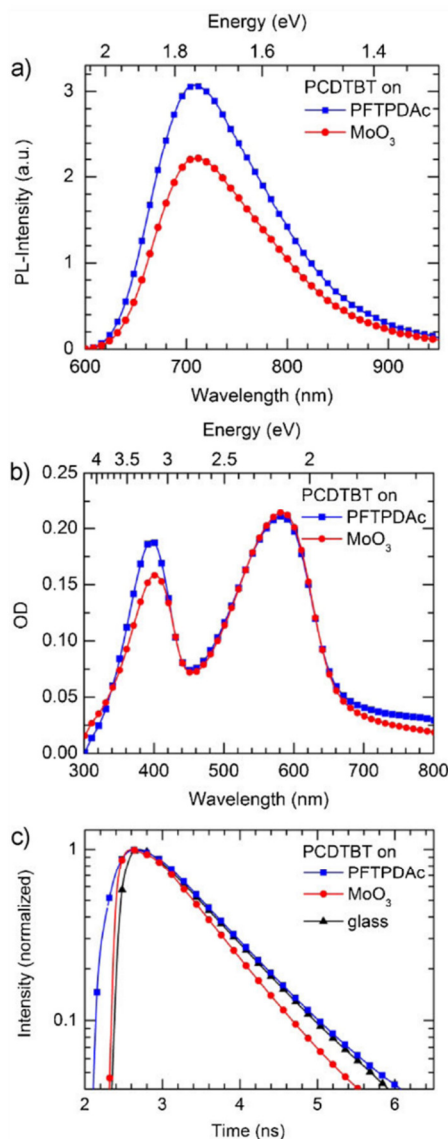


Figure 3 (a) Photoluminescence intensity of a 20 nm thick PCDTBT layer on top of an 18 nm thick MoO₃ layer (red circles) and photoluminescence with an 8 nm thick crosslinked PFTPDAC interlayer between the MoO₃ and the PCDTBT layer (blue squares). PCDTBT was excited at 580 nm. (b) Optical density of both samples corrected for the OD of the MoO₃ layer. (c) Lifetime measurements of PCDTBT on top of PFTPDAC (blue squares, fluorescence lifetime 970 ps), MoO₃ (red circles, fluorescence lifetime 800 ps), and 60 nm of PCDTBT on glass (black triangles, fluorescence lifetime 940 ps).

absorption range. This is consistent with the measurements shown in Fig. 2. This means that the crosslinked polymer PFTPDAC acts as an exciton blocking layer between the MoO₃ and the PCDTBT, like molecular exciton blockers in

three layer organic solar cells made by vacuum evaporation of small molecules [23].

From the steady state and time resolved PL measurements as well as the wavelength dependent increase of the EQE, we conclude that the reduced exciton quenching at the MoO₃ interface by the crosslinked PFTPDAC interlayer is mainly responsible for the increase of the efficiency of the three layer cell. Already very thin layers of PFTPDAC provide efficient exciton blocking. In our experiments, we observe the same reduced exciton quenching for 8 and 20 nm thick PFTPDAC layers, yet in the 8 nm thick exciton blocking layer reabsorption plays only a minor role, so the thinner layer is of advantage. The fact that a very thin layer suffices implies that the main role of the layer is to passivate surface trap states. It is important to mention that exciton quenching is not a sole property of a MoO₃ anode, but a general problem of anode buffer layers [24, 28]. In our solar cell experiments, we observed exciton quenching and a reduced EQE not only in devices with MoO₃ but also with a PEDOT:PSS buffer layer. On PEDOT:PSS, the EQE can also be improved by the use of a PFTPDAC interlayer.

4 Conclusions In conclusion, we have shown that the performance of an organic solar cell can be increased by the introduction of an additional polymeric exciton blocking layer. For this purpose, we have synthesized the novel polymer PFTPDAC with pendant photocrosslinkable acrylate groups. Thin films have been spincoated from a PFTPDAC solution and subsequently crosslinked by irradiation. Thereby, the film becomes insoluble and allows spincoating of a second polymer layer on top. We present a three layer organic solar cell with a crosslinked PFTPDAC interlayer on top of the molybdenum oxide anode and the low-bandgap polymer PCDTBT and C₆₀. The exciton blocking layer has a thickness of only 8 nm to prevent absorption losses. In comparison with the reference cells without the interlayer, the EQE is significantly increased in the spectral region between 400 and 650 nm. From current-voltage measurements, a power conversion efficiency of 1.8% was determined. PL measurements show that the increase of solar cell performance is attributed to exciton blocking by the crosslinked PFTPDAC interlayer. These results encourage to extend the concept of solution processed, crosslinked layers to more efficient solar cells and organic light-emitting diodes in the near future.

Supporting Information

Additional supporting information may be found in the online version of this article at the publisher's website.

Acknowledgements We thank W. Brütting and H. Bässler for helpful discussions. Furthermore, we acknowledge financial support by the Bavarian State Ministry of Science, Research, and the Arts through the Collaborative Research Network "Solar Technologies go Hybrid" and by the German Science Foundation DFG through the doctoral training center "GRK 1640."

References

- [1] X. Z. Che, X. Xiao, J. D. Zimmerman, D. J. Fan, and S. R. Forrest, *Adv. Energy Mater.* **4**, 1400568 (2014).
- [2] Heliatek, heliatek.com, accessed April 2015.
- [3] M. T. Dang, L. Hirsch, and G. Wantz, *Adv. Mater.* **23**, 3597 (2011).
- [4] Y. Liu, J. Zhao, Z. Li, C. Mu, W. Ma, H. Hu, K. Jiang, H. Lin, H. Ade, and H. Yan, *Nature Commun.* **5**, 5293 (2014).
- [5] K. Meerholz, *Nature* **437**, 327 (2005).
- [6] W. W. Li, A. Furlan, K. H. Hendriks, M. M. Wienk, and R. A. J. Janssen, *J. Am. Chem. Soc.* **135**, 5529 (2013).
- [7] A. Puetz, F. Steiner, J. Mescher, M. Reinhard, N. Christ, D. Kutsarov, H. Kalt, U. Lemmer, and A. Colmann, *Org. Electron.* **13**, 2696 (2012).
- [8] H. Q. Zhou, Y. Zhang, C. K. Mai, S. D. Collins, G. C. Bazan, T. Q. Nguyen, and A. J. Heeger, *Adv. Mater.* **27**, 1767 (2015).
- [9] C. D. Müller, A. Falcou, N. Reckefuss, M. Rojahn, V. Wiederhorn, P. Rudati, H. Frohne, O. Nuyken, H. Becker, and K. Meerholz, *Nature* **421**, 829 (2003).
- [10] B. J. Kim, Y. Miyamoto, B. W. Ma, and J. M. J. Frechét, *Adv. Funct. Mater.* **19**, 2273 (2009).
- [11] F. Ouhib, M. Tomassetti, J. Manca, F. Piersimoni, D. Spoltore, S. Bertho, H. Moons, R. Lazzaroni, S. Desbief, C. Jerome, and C. Detrembleur, *Macromolecules* **46**, 785 (2013).
- [12] G. Brotas, J. Farinhas, Q. Ferreira, R. Rodrigues, I. L. Martins, J. Morgado, and A. Charas, *J. Polym. Sci. Pol. Chem.* **52**, 652 (2014).
- [13] J. E. Carlé, B. Andreasen, T. Tromholt, M. V. Madsen, K. Norrman, M. Jorgensen, and F. C. Krebs, *J. Mater. Chem.* **22**, 24417 (2012).
- [14] Q. Xu, F. Z. Wang, D. P. Qian, Z. A. Tan, L. J. Li, S. S. Li, X. H. Tu, G. Sun, X. L. Hou, J. H. Hou, and Y. F. Li, *ACS Appl. Mater. Interf.* **5**, 6591 (2013).
- [15] C. P. Yau, S. Wang, N. D. Treat, Z. Fei, B. J. Tremolet de Villers, M. L. Chabinyc, and M. Heeney, *Adv. Energy Mater.* **5**, 1401228 (2014).
- [16] R. Q. Png, P. J. Chia, J. C. Tang, B. Liu, S. Sivaramakrishnan, M. Zhou, S. H. Khong, H. S. O. Chan, J. H. Burroughes, L. L. Chua, R. H. Friend, and P. K. H. Ho, *Nature Mater.* **9**, 152 (2010).
- [17] Z. K. Tan, K. Johnson, Y. Vaynzof, A. A. Bakulin, L. L. Chua, P. K. H. Ho, and R. H. Friend, *Adv. Mater.* **25**, 4131 (2013).
- [18] Y. Sun, S. C. Chien, H. L. Yip, Y. Zhang, K. S. Chen, D. F. Zeigler, F. C. Chen, B. P. Lin, and A. K. Y. Jen, *Chem. Mater.* **23**, 5006 (2011).
- [19] W. W. Liang, C. Y. Chang, Y. Y. Lai, S. W. Cheng, H. H. Chang, Y. Y. Lai, Y. J. Cheng, C. L. Wang, and C. S. Hsu, *Macromolecules* **46**, 4781 (2013).
- [20] K. Zhang, C. M. Zhong, S. J. Liu, C. Mu, Z. K. Li, H. Yan, F. Huang, and Y. Cao, *ACS Appl. Mater. Interf.* **6**, 10429 (2014).
- [21] H. Becker, S. E. Burns, and R. H. Friend, *Phys. Rev. B* **56**, 1893 (1997).
- [22] D. E. Markov and P. W. M. Blom, *Appl. Phys. Lett.* **87**, 233511 (2005).
- [23] S. Grob, M. Gruber, A. N. Bartynski, U. Hormann, T. Linderl, M. E. Thompson, and W. Brütting, *Appl. Phys. Lett.* **104**, 213304 (2014).



- [24] M. Hirade and C. Adachi, *Appl. Phys. Lett.* **99**, 153302 (2011).
- [25] N. Blouin, A. Michaud, and M. Leclerc, *Adv. Mater.* **19**, 2295 (2007).
- [26] C. Schwarz, H. Bässler, I. Bauer, J. M. Koenen, E. Preis, U. Scherf, and A. Köhler, *Adv. Mater.* **24**, 922 (2012).
- [27] E. Scheler and P. Strohriegel, *Chem. Mater.* **22**, 1410 (2010).
- [28] J. D. Zimmerman, B. Song, O. Griffith, and S. R. Forrest, *Appl. Phys. Lett.* **103**, 243905 (2013).
- [29] M. Riede, C. Urich, J. Widmer, R. Timmreck, D. Wynands, G. Schwartz, W. M. Gnehr, D. Hildebrandt, A. Weiss, J. Hwang, S. Sundarraj, P. Erk, M. Pfeiffer, and K. Leo, *Adv. Funct. Mater.* **21**, 3019 (2011).
- [30] J. Meyer, S. Hamwi, M. Kroger, W. Kowalsky, T. Riedl, and A. Kahn, *Adv. Mater.* **24**, 5408 (2012).

Supporting Information to

Organic solar cells with crosslinked polymeric exciton blocking layer

T. Hahn¹, C. Saller², M. Weigl², I. Bauer¹, T. Unger¹, A. Köhler^{**1,3}, and P. Strohriegl^{*2,3}

¹ Experimental Physics II, University of Bayreuth, 95440 Bayreuth, Germany

² Macromolecular Chemistry I, University of Bayreuth, 95440 Bayreuth, Germany

³ Bayreuth Institute of Macromolecular Science (BIMF), University of Bayreuth, 95440 Bayreuth, Germany

Received 18 December 2014, revised 30 April 2015, accepted 15 May 2015

Published online May 2015

Keywords organic solar cells, photocrosslinking, MoO₃, PCDTBT, excitons

* Corresponding author: e-mail peter.strohriegl@uni-bayreuth.de

** e-mail anna.koehler@uni-bayreuth.de

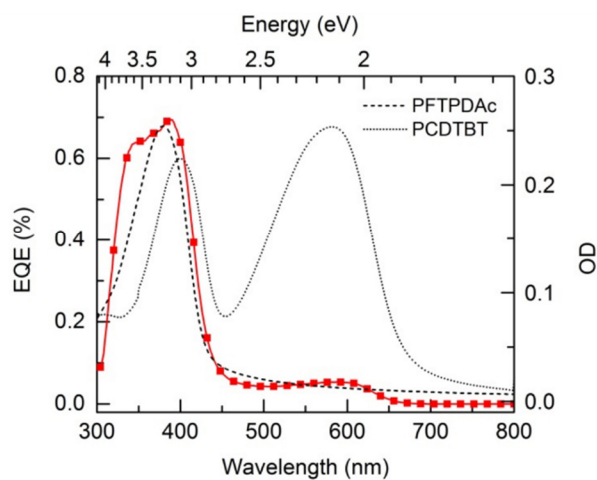


Figure S1 EQE spectrum of 50 nm thick PFTPDAc:PCDTBT (1:1) blend solar cells without the acceptor C₆₀ (average of four cells, red squares). The polymer blend is embedded between the ITO-MoO₃ anode and the aluminum cathode. On the right axis the optical density of a 25 nm thick PFTPDAc layer (dashed line) and a 25 nm thick PCDTBT layer (dotted line) is shown for further analysis.

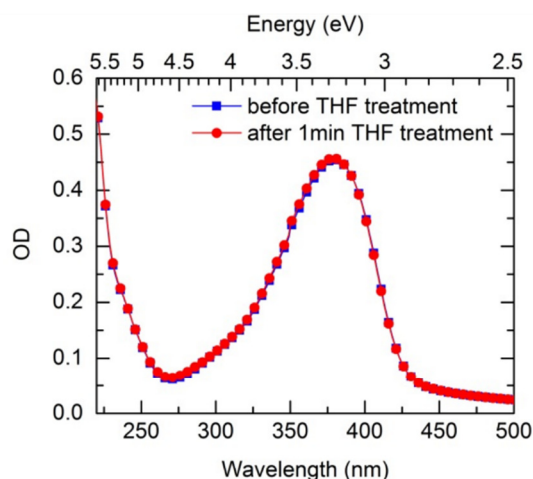


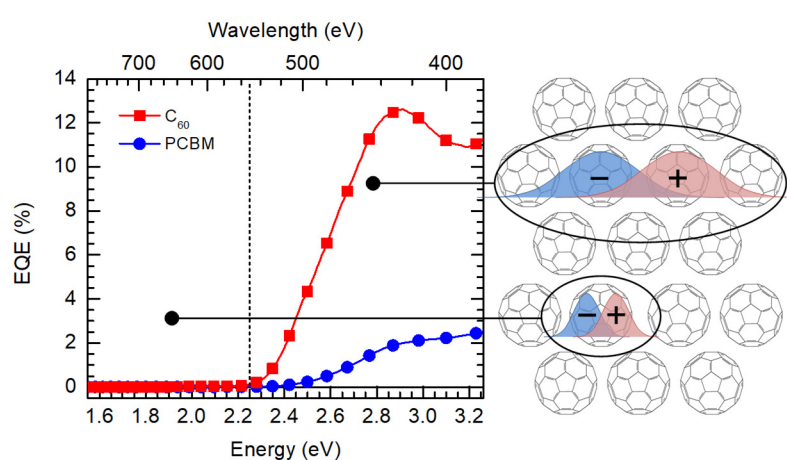
Figure S2 Optical density of a crosslinked PFTPDAc film on a quartz glass substrate before and after a 1 min THF treatment. The exposure time for crosslinking the polymer layer was 10 min.

Is exciton blocking the only reason for the improved performance of our three layer cell?

We cannot rule out that other parameters, e.g. an improved hole transport of the PFTPDAc interlayer, also contribute to the better solar cell performance. The crosslinkable polymer PFTPDAc contains fluorene and TPD repeating units. TPD as an aromatic amine is known to be a good hole transport material often used in organic light emitting diodes. This leads us to the assumption that the PFTPDAc might serve as hole transport layer and facilitates the removal of the positive charges generated at the PCDTBT- C_{60} interface. If this assumption is correct, the photocurrent should increase over the whole spectral range since for the generation of holes it does not matter if the excitation takes place in the PCDTBT or in the C_{60} layer. This is not observed in the experiment. From Fig. 2a we see the increased EQE mainly for the wavelength interval of PCDTBT absorption but not for the C_{60} dominated EQE range between 350 nm and 400 nm. The increase of the EQE in the range of the PCDTBT absorption can be understood if the PFTPDAc acts as exciton blocking layer. In the absorption maximum, the exciton density in the PCDTBT layer is high which results in a high possibility for exciton quenching at the molybdenum oxide interface. Insertion of a PFTPDAc layer reduces exciton quenching and consequently leads to an increase of the efficiency in the absorption maximum of PCDTBT.

6. Role of intrinsic photogeneration in single layer and bilayer solar cells with C₆₀ and PCBM

Tobias Hahn, Steffen Tscheuschner, Christina Saller, Peter Strohriegl,
Puttaraju Boregowda, Tushita Mukhopadhyay, Satish Patil, Dieter Neher,
Heinz Bässler, and Anna Köhler



Published in *The Journal of Physical Chemistry C*

doi: 10.1021/acs.jpcc.6b08471

Reprinted with permission from *The Journal of Physical Chemistry C* **2016**, *120*, 25083-25091

Copyright © 2016 American Chemical Society

Role of Intrinsic Photogeneration in Single Layer and Bilayer Solar Cells with C₆₀ and PCBM

Tobias Hahn,^{†,∇} Steffen Tscheuschner,^{†,∇} Christina Saller,[‡] Peter Strohriegel,^{‡,⊥} Puttaraju Boregowda,[§] Tushita Mukhopadhyay,[§] Satish Patil,[§] Dieter Neher,^{||} Heinz Bässler,[⊥] and Anna Köhler^{*,†,⊥}

[†]Experimental Physics II, University of Bayreuth, 95440 Bayreuth, Germany

[‡]Macromolecular Chemistry I, University of Bayreuth, 95440 Bayreuth, Germany

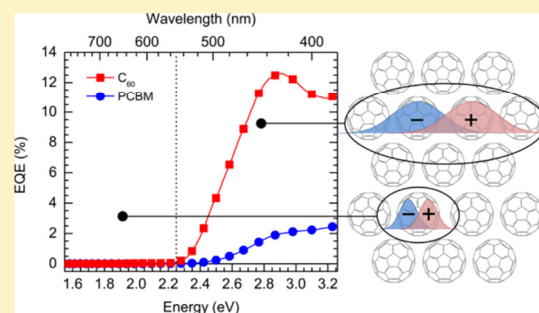
[§]Solid State and Structural Chemistry Unit, Indian Institute of Science, Bangalore, 560012 India

^{||}Institute for Physics and Astronomy, University of Potsdam, 14476 Potsdam-Golm, Germany

[⊥]Bayreuth Institute of Macromolecular Science (BIMF), University of Bayreuth, 95440 Bayreuth, Germany

 Supporting Information

ABSTRACT: In an endeavor to examine how optical excitation of C₆₀ and PCBM contribute to the photogeneration of charge carriers in organic solar cells, we investigated stationary photogeneration in single-layer C₆₀ and PCBM films over a broad spectrum as a function of the electric field. We find that intrinsic photogeneration starts at a photon energy of about 2.25 eV, i.e., about 0.4 eV above the first singlet excited state. It originates from charge transfer type states that can autoionize before relaxing to the lower-energy singlet S₁ state, in the spirit of Onsager's 1938 theory. We analyze the internal quantum efficiency as a function of electric field and photon energy to determine (1) the Coulombic binding and separation of the electron–hole pairs, (2) the value of the electrical gap, and (3) which fraction of photoexcitations can fully separate at a given photon energy. The latter depends on the coupling between the photogenerated charge transfer states and the eventual charge transporting states. It is by a factor of 3 lower in PCBM. Close to the threshold energy for intrinsic photoconduction (2.25 eV), the generating entity is a photo-generated electron–hole pair with roughly 2 nm separation. At higher photon energy, more expanded pairs are produced incoherently via thermalization.



1. INTRODUCTION

It is a generally accepted notion that in single component molecular solids photogeneration of charge carriers is inefficient because the Coulombic binding energy of singlet excitons is large.¹ This process becomes efficient only if an electron donor material is blended with an electron accepting material. If the offset between the highest occupied molecular orbital (HOMO) and the lowest unoccupied molecular orbital (LUMO) levels of the constituents is sufficiently large, the charge transfer (CT) state at the donor–acceptor interface becomes the lowest excited state of the system and can act as a precursor for photogeneration.^{2–9} These CT states are populated by singlet excitons, usually generated in the donor phase, that diffuse toward the donor–acceptor interface. Efficient power conversion in an organic solar cell (OSC) requires that the subsequent dissociation of the CT state or, more generally, the electron–hole pair (eh-pair), is an efficient process. The reason why the escape of the eh-pair from the Coulomb potential can be efficient is subject of current research.^{10–20} There is growing evidence, though, that delocalization of the charges comprising the eh-pair plays a major role.^{21–27}

Optimal power conversion efficiency of an OSC requires an optimal overlap between the absorption spectrum of the solar cell materials and the solar spectrum. This condition is satisfied when using donor materials with high oscillator strength and an absorption edge near 700 nm (1.8 eV) or above. Prototypical donor materials are donor–acceptor type conjugated oligomers or polymers. They are usually combined with C₆₀ or PCBM ((6,6)-phenyl-C₆₁-butyric acid methyl ester) as acceptors. The absorption spectra of these donor materials commonly feature a minimum somewhere around 450 nm (2.7 eV), where a film of C₆₀ absorbs strongly. In bulk heterojunction donor–acceptor blends C₆₀ or PCBM forms aggregates, unless only very small amounts are incorporated that are often not sufficient for efficient OSC operation.²⁸ It is therefore of primary importance to identify the role of optical excitations in these fullerene domains for the operation of such OSCs. There is indeed experimental evidence that optical excitation of C₆₀ or PCBM

Received: August 22, 2016

Revised: October 11, 2016

Published: October 12, 2016

has a significant effect on the performance of donor–acceptor OSCs.^{29–33} However, the underlying mechanism is discussed controversially. From the analysis of the current–voltage ($j(V)$) dependence of a bilayer OSC with a C₆₀ layer as electron acceptor, Jeong et al.³² conclude that excited C₆₀ creates an additional photocurrent while Tress et al.³³ argue that the excited C₆₀ introduces a loss mechanism, caused by an additional hole injection current that leads to a so-called photoshunt. Li et al.³¹ attribute the continuous increase of the photocurrent in CuPc/C₆₀ diodes upon increasing negative bias to an enhancement of hole injection from the cathode due to the interaction of triplet excitons with electrons in C₆₀. On the other hand, Zou and Holmes³⁰ conjecture that in the C₆₀ rich phase a virtually temperature independent bulk ionization process occurs because singlet excitons in C₆₀ are believed to be only very weakly bound. This conclusion is in disagreement with the observation of Mort et al.,³⁴ who have found that photoconduction in a neat C₆₀ film is thermally activated. An in-depth study of photogeneration in a neat C₆₀ and PCBM films should resolve these controversies.

There is a further motivation for studying photogeneration in C₆₀ or PCBM films. There is abundant evidence that charge generation in bulk heterojunction OSCs depends critically on the extent of aggregation of the electron acceptor.^{26,28,35–37} A suggested reason for this charge generation efficiency is associated with an increasing electron delocalization with increasing content of PCBM in bulk-heterojunction cells. This ought to be dependent on the degree of structural order and should therefore be reflected in an analysis of photogeneration of differently prepared films of C₆₀ and PCBM.

Photogeneration in C₆₀ is not a new subject. Early on, Mort et al.^{34,38,39} investigated photogeneration in C₆₀ films employing the xerographic method. In subsequent work, Kazaoui et al. focused on spectrally dependent photoconduction combined with studies of electroabsorption and field assisted photoluminescence using a coplanar interdigitated electrode arrangement and constant electric field.⁴⁰ They observed a weak photocurrent with a threshold energy that is close to the 0–0 feature of the photoluminescence spectrum (1.84 eV) that increases steeply above 2.3 eV. This increase correlates with the onset of electroabsorption that features a maximum at 2.45 eV. The main conclusion of this work is that the source of the intrinsic photocurrent in C₆₀ is a charge transfer state. However, the mechanism of the dissociation of the CT state has not been elucidated and the estimated bandgap of about 3 eV is incompatible with experimental results on the ionization energy and the electron affinity.^{6,41–44}

The aim of the current work is to identify the mechanism of optical photogeneration in bulk films of C₆₀ or PCBM by measuring and analyzing the photocurrent over a broad range of electric fields and photon energies. The experiments were done on a sandwich-type diode with a 30 nm thick C₆₀ or PCBM layer. The advantage of a sandwich arrangement as compared to a gap arrangement, used by Kazaoui et al.,⁴⁰ is that both bimolecular charge recombination is greatly reduced and surface effects are avoided. Moreover, the use of electrodes with different workfunctions allows the operation of the diodes under reverse bias. This prevents exciton induced charge injection from the electrode(s) that might otherwise obscure weak intrinsic photogeneration at low photon energies.⁴⁵

In brief, we find that in C₆₀ and PCBM films intrinsic photogeneration occurs above a photon energy of 2.2–2.3 eV. It originates from charge transfer states that couple efficiently to

charge transporting states and that can escape from their Coulomb potential via an Onsager-like process. Close to the threshold photon energy, eh-pairs with eh-separation of about 2 nm are generated resonantly while at higher $h\nu$ they are produced via an incoherent thermalization process.

2. EXPERIMENTAL METHODS

To fabricate single component C₆₀ or PCBM diodes, ITO-coated substrates were covered with a patterned photoresist as described by Schwarz et al. such as to leave round openings for the active area.⁴⁶ A 15 nm thick MoO₃ (Sigma-Aldrich) layer was evaporated on top of the ITO openings using a shadow mask. C₆₀ (Sigma-Aldrich) films with a thickness of 30 nm were vapor deposited with an evaporation rate of 1 Å/s. Alternatively, 30 nm thick PCBM films (99.5% purity, Sigma-Aldrich) were spin coated from chlorobenzene solution (20 mg/mL). The thickness of the PCBM layer was verified with a Dektak (Veeco) profilometer. Finally, the films were covered by a thermally evaporated 100 nm thick aluminum cathode. The complete diode fabrication was done in a nitrogen atmosphere using a glovebox with direct access to the evaporation chamber. Measurements of the photocurrent were carried out for (i) a single layer C₆₀ (thereafter referred to as C₆₀-only) device measured immediately after fabrication (“C₆₀”), (ii) a C₆₀-only device stored in a nitrogen glovebox for one year (“after 1 year”), (iii) a C₆₀-only device annealed at 140 °C for 26 h under nitrogen (“C₆₀ annealed”), (iv) a PCBM-only device annealed at 140 °C for 30 min and afterward cooled down to 60 °C in a time range of 30 min (“PCBM annealed”), and (v) for a PCBM-only device which was not annealed and measured as cast (“PCBM”). In addition to single layer fullerene diodes, bilayer donor–acceptor type cells were also investigated (shown in Figure 4,) in which a x nm thick donor layer was combined with 30 nm C₆₀ acceptor layer. As a donor, we used once a PCDTBT derivative (PCDTBT_{co}; $x = 14$ nm) and once the small molecule Ph-TDPP-Ph ($x = 25$ nm). Their chemical structures are shown in Figure 4 below. The Ph-TDPP-Ph donor layer was spin coated from a chloroform/chlorobenzene (3:2) solution (7 mg/mL) and the PCDTBT_{co} from a chlorobenzene solution (6 mg/mL) before the C₆₀ layer was vapor deposited. Ph-TDPP-Ph and PCDTBT_{co} were synthesized as described in the Supporting Information (SI). PCDTBT_{co} was synthesized by Strohriegel et al. as described in the SI.

The current–voltage characteristics of the diodes in the dark and upon illumination were measured under vacuum at room temperature. Monochromatic illumination was provided by a 450 W xenon lamp (Osram) using a commercial monochromator. The light intensity impinging on the diode was measured using a Hamamatsu S1337-33BQ photodiode. It was 7.1 mW/cm² for 536 nm irradiation and 6.7 mW/cm² for 580 nm irradiation. The photocurrents were measured with a Keithley 236 source-measure unit.

The electric field in the active layer of the solar cells was taken as $(V_{bi} - V)/d$ where d is the thickness of the active layer, V is the applied voltage, and V_{bi} is the built-in voltage, approximated by the voltage at which the photocurrent is zero. V_{bi} was typically 0.9 ± 0.1 V. The photocurrent was calculated from the difference between the total current under illumination and the dark current.

Calculating the internal quantum efficiency (IQE) of the solar cells requires the absorption spectra of the thin C₆₀ or PCBM films in the diode structures, which is not trivial due to optical effects.⁴⁷ To circumvent this problem, we calculated the effective absorption spectrum of the film embedded in the

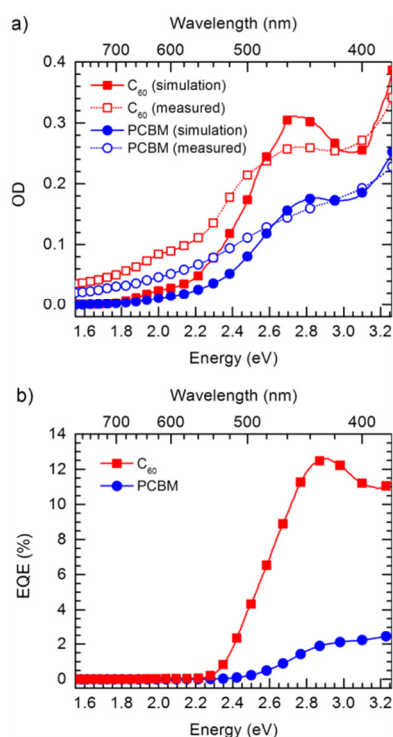


Figure 1. (a) Optical density of C₆₀ (red squares) and PCBM (blue circles) measured from a film on quartz glass (open symbols) and simulated (filled symbols). In the simulation, the absorption of C₆₀ or PCBM was calculated for a layer embedded between ITO/MoO₃ and aluminum, as is the case in a solar cell. (b) EQE measured under short-circuit conditions for a C₆₀-only device (red squares) and a PCBM-only device (blue circles). Both devices were not annealed and measured as cast.

ITO(250 nm)/MoO₃(15 nm)/C₆₀(30 nm)/Al(100 nm) assembly using a transfer matrix approach^{48,49} implemented by Burkhard et al.⁴⁷ For this, we used the literature values for the real and imaginary part of the complex refractive index, n and k , for C₆₀³⁰ or PCBM (provided by Burkhard et al.⁴⁷). A comparison of the calculated spectrum and the measured absorption spectrum of a C₆₀ or PCBM film deposited on a quartz substrate illustrates the importance of eliminating interference effects (Figure 1). We therefore used the calculated absorption for calculating the IQE. Figure 1 also shows that the oscillator strength of the optical transition of PCBM between 2.3 and 3.2 eV is by a factor of 2 lower than that of C₆₀. We estimate that the absolute IQE values have an experimental error of about 20%.

3. EXPERIMENTAL RESULTS

In addition to the calculated and measured absorption spectra for C₆₀ and PCBM, Figure 1 shows the external quantum efficiency (EQE) of single layer solar cells made from C₆₀ or PCBM. By correcting the EQE for the absorption of the C₆₀ or PCBM layer and the transmission of the glass/ITO/MoO₃ substrate, we obtain the internal quantum efficiencies (IQE). In Figure 2a we compare the IQE of differently treated C₆₀ and PCBM films as a function of photon energy, taken under short-

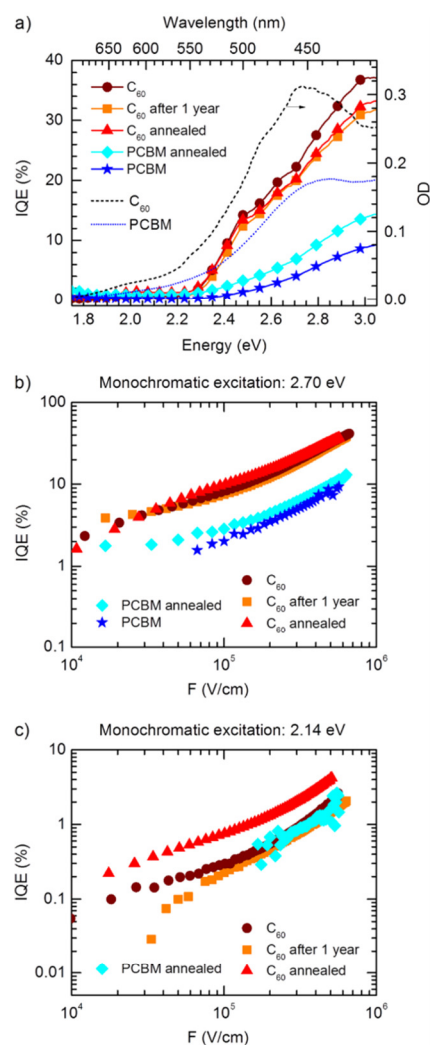


Figure 2. Internal quantum efficiency (IQE) spectra for a C₆₀-only device measured immediately after fabrication (wine circles), a C₆₀-only device after one year (orange squares), a C₆₀-only device annealed at 140 °C (red triangles), a PCBM-only device annealed at 140 °C (cyan diamonds) and for a PCBM-only device measured as cast (blue stars) (a) under short-circuit conditions, (b) as a function of field for a monochromatic excitation energy of 2.70 eV, and (c) as a function of field for a monochromatic excitation energy of 2.14 eV. In (c) the not annealed PCBM sample had an insufficient ratio of photocurrent to dark current at low excitation energies and is therefore not shown. Additionally, on the right axis in (a) the absorption of C₆₀ and PCBM is shown.

circuit conditions. The field dependent photocurrent of the different samples is shown in Figure 2b,c. It turns out that in C₆₀ films neither annealing at 140 °C nor storage during a year have major effects. The IQE of PCBM films is by roughly a factor of 3 lower than that of C₆₀ films when exciting at 2.70 eV. In both materials, the IQE is strongly dependent on the operating voltage at reverse bias ($V \leq V_{bi}$) (Figure 3). Consistent with earlier work,⁴⁰ there is weak photogeneration starting at the

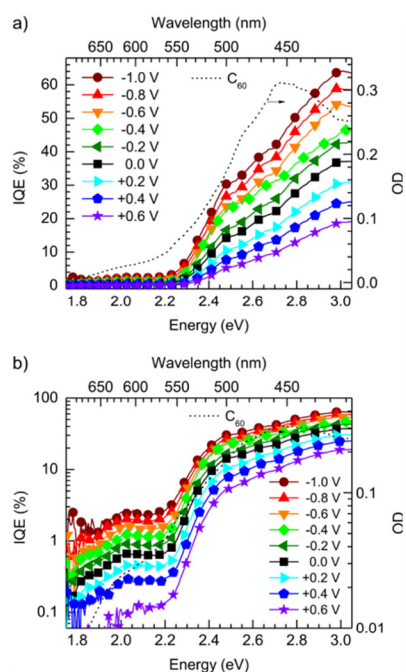


Figure 3. Internal quantum efficiency (IQE) of a C₆₀-only device measured immediately after preparation for different external voltages (symbols) and the associated optical density of the 30 nm thick C₆₀ layer used for calculating the IQE (dashed line) (a) on a linear scale and (b) on a logarithmic scale. Only a quarter of the data points are shown as symbols for clarity of display.

photon energy of about 1.85 eV, i.e., coincident with the onset of the 0–0 feature of the absorption spectrum, and increasing strongly above 2.2–2.3 eV. Below 2.25 eV, the IQE is only about 0.001–0.01 and almost independent of photon energy. At an applied voltage of -1.0 V, corresponding to a field of 6.6×10^5 V/cm, and at a photon energy of 3.0 eV, the IQE is about 60%. Above a photon energy of 2.3 eV, V_{bi} is about $0.9 \text{ V} \pm 0.1 \text{ V}$.

In order to find out in which way optical excitation of C₆₀ contributes to the efficiency of an OSC, we studied also the field dependence of photogeneration in bilayer diodes with a donor material combined with C₆₀ as an acceptor (Figure 4). We chose two donor materials, that is Ph-TDPP-Ph as an example for a molecular donor and PCDTBT_{co} as an example for a low-bandgap polymer. The chemical structures and thin film absorption spectra of the donors are shown in Figure 4a,b, along with the thin film absorption of C₆₀ for ease of comparison. We excited both diodes, once at 2.14 eV where the absorption is dominated by the donor and which is below the threshold energy for significant intrinsic C₆₀ photocurrent generation (cf. Figure 3) and once at 2.94 or 3.35 eV where both donor and C₆₀ absorb and where the intrinsic photocurrent generation of C₆₀ is significant, e.g., with about 30% IQE at 0 V, i.e., for internal fields of about 3×10^5 V/cm. Figure 4c shows how the EQEs evolve as a function of field for the two different excitation ranges, while Figure 4d shows the current–voltage curve, exemplarily for a planar heterojunction made with PCDTBT_{co} and C₆₀.

Upon 2.14 eV excitation, the EQEs nearly (PCDTBT_{co}) or fully (Ph-TDPP-Ph) saturate above 10^5 V/cm. In contrast, for

the high energy excitation, the EQE increases monotonously, with a change of slope at about 10^5 V/cm. This increase in photocurrent for fields above 10^5 V/cm resembles the field dependent intrinsic photocurrent in a single-layer C₆₀ diode as shown in Figure 2. The difference in field-dependent photocurrent that is seen when both, donor and fullerene, are excited compared to donor-only excitation is therefore clear evidence that the extra contribution to the EQE is caused by intrinsic charge carrier generation inside the C₆₀ layer, consistent with the findings by Jeong et al.³² In passing, we comment on the perfect saturation of the EQE at high electric fields upon selective Ph-TDPP-Ph excitation combined with the fact that we could not observe any photocurrent in single layer Ph-TDPP-Ph devices (not shown). This is in contrast to experiments on single layer PCDTBT devices that reveal an intrinsic photogeneration above a threshold photon energy at 2.6 eV.⁵¹ The reason is that in the molecule Ph-TDPP-Ph the singlet exciton is too strongly bound in order to allow the escape from the Coulomb potential while in the donor–acceptor polymer PCDTBT some intrinsic dissociation can occur, albeit only at high electric fields because it proceeds from an on-chain charge transfer state. This explains why in diodes made with C₆₀ and PCDTBT or a PCDTBT derivative there is always a residual increase (see Figure 4) of photogeneration above the electric field at which dissociation of eh-pairs at the donor–acceptor interface already saturates.

For C₆₀-only devices, experimental current–voltage $j(V)$ data taken for different excitation energies are presented in Figure 5, converted into plots of IQE as a function of electric field. Also shown are fits according to the Onsager 1938 model⁵² using eq 17 in reference 53. For reference, representative $j(V)$ curves are available as Supporting Information.

4. DISCUSSION

The kind of field dependence of the intrinsic photogeneration yield, i.e. the IQE, in a neat C₆₀ film shown in Figure 2 is reminiscent of an Onsager-type dissociation process by autoionization.^{1,52} In his 1938 treatise, Onsager considered that a high-energy photon ionizes a molecule and creates a Coulomb-bound pair of a radical cation and anion with an intrapair separation r_0 after thermalization. The medium is considered homogeneous and has a dielectric constant ϵ_r . The cation and the anion undergo a Brownian diffusive motion within the superimposed Coulomb potential and the potential due to the applied electric field. In the course of their motion, the pair has the option to fully dissociate or to recombine geminately upon their encounter. The essential parameters in the Onsager formalism are

- the intrapair separation r_0 and
- the initial yield of eh-pairs with separation of r_0 that are able to fully separate in the high field limit.

In the limit of low fields, the dissociation yield of the eh-pairs is constant. It is simply given by the Boltzmann factor for the thermally activated dissociation of eh-pairs at a distance r_0 with a Coulomb binding energy $E_{\text{coul}} = \frac{e^2}{4\pi\epsilon_r\epsilon_0} \cdot \frac{1}{r_0}$, noting that $\frac{E_{\text{coul}}}{kT} = \frac{r_{\text{coul}}}{r_0}$, where r_{coul} is the Coulomb capture radius, i.e., the radius at which the thermal energy kT equals the Coulomb energy. The textbook example for successful application of Onsager's 1938 theory is the work of Chance and Braun on crystalline anthracene.⁵⁴

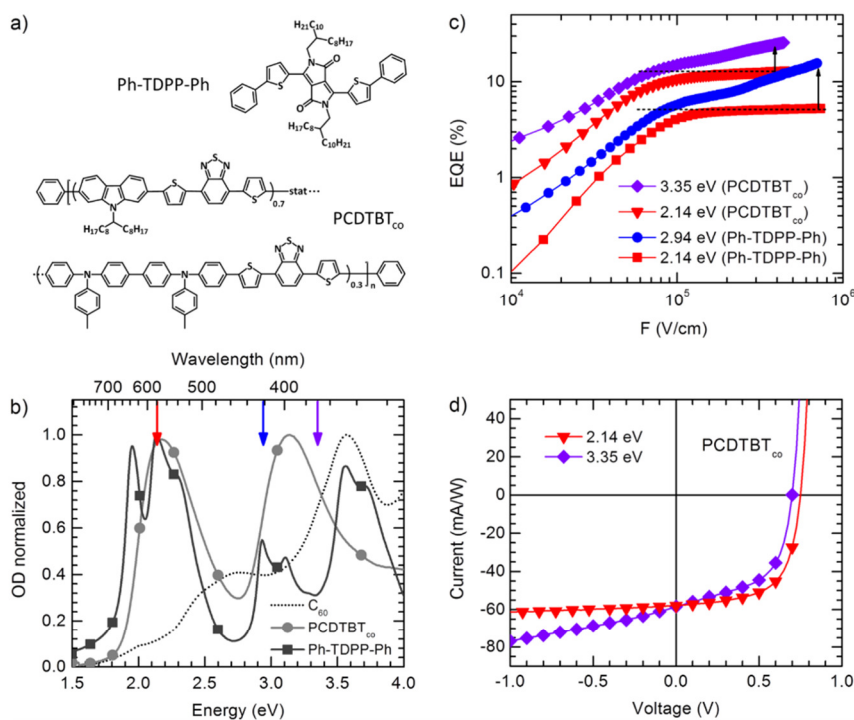


Figure 4. (a) Chemical structure of the copolymer PCDTBT_{co} and the small molecule Ph-TDPP-Ph. (b) Normalized absorption spectra for the photocurrent measurements. (c) External quantum efficiency (EQE) as a function of internal field for the planar heterojunction solar cells (ITO/MoO₃/Ph-TDPP-Ph(25 nm)/C₆₀(30 nm)/Al) excited at 2.94 and 2.14 eV, and for (ITO/MoO₃/PCDTBT_{co}(14 nm)/C₆₀(30 nm)/Al) excited at 3.35 and 2.14 eV. The black arrows indicate the intrinsic contribution of the C₆₀ layer for 2.94 or 3.35 eV excitation. (d) Corresponding current–voltage curves exemplarily for the PCDTBT_{co} corrected by the spectral intensity of the used xenon lamp as described in the experimental section.

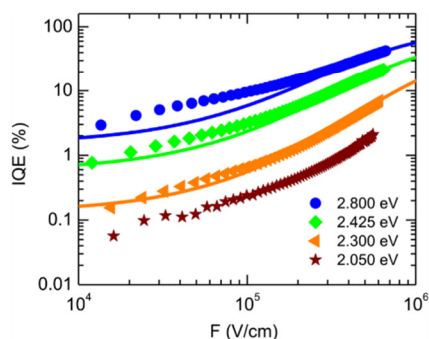


Figure 5. Internal quantum efficiency (IQE) as a function of internal field for a C₆₀-only device (ITO/MoO₃/C₆₀/Al) with a C₆₀ layer thickness of 30 nm for different excitation energies (symbols). The solid lines indicate the Onsager fit to the data points. No Onsager fit is shown for 2.050 eV data points since for this energy the Onsager theory does not apply here.

The facts that (1) the action spectrum of intrinsic photogeneration in C₆₀ features a threshold near 2.2–2.3 eV, i.e., roughly 0.4 eV above the singlet exciton, and (2) the field dependence of the IQE resembles typical Onsager plots of the field dependent yield of photogeneration (e.g., refs 38, 39, and 53), prompted us to analyze the data in terms of Onsager's 1938 theory.

Representative plots of experimental IQE data and fits to the Onsager formalism are shown in Figure 5. The data were fitted according to eq 17 in ref 53. Considering that in the original version of the theory neither the distribution of the r_0 values⁵⁵ nor disorder are considered, the agreement between theory and experiment is satisfactory. In the following, we shall first consider the results for the photon energies above 2.25 eV where IQE rises sharply. We associate this regime with intrinsic photogeneration while below 2.25 eV extrinsic photogeneration prevails (vide infra).

Two essential outcomes of the Onsager 1938 theory are the yield of the quantum efficiency of photogeneration extrapolated to infinite electric field (IQE_{max}), and the Coulomb binding energy (E_{coul}) of the eh-pair that translates into the electron–hole separation of the pair (r_0). E_{coul} is inferred, for different energies of the exciting photon, from the ratio of the photogeneration yields at zero and at infinite field, i.e., $\frac{\text{IQE}(F_0, h\nu)}{\text{IQE}_{\text{max}}} = \exp\left(-\frac{E_{\text{coul}}}{kT}\right)$. We shall first consider the dependence of E_{coul} on photon energy above the intrinsic photogeneration threshold at about 2.25 eV. $\text{IQE}(F_0, h\nu)$ was approximated by the asymptotic value at a field strength of 10⁴ V/cm in Figure 5, and IQE_{max} was taken from the Onsager fits in the limit of infinitely high field. We find that $E_{\text{coul}}(h\nu)$ decreases linearly with photon energy from about 2.25 eV up to about 2.35 eV and levels off at higher $h\nu$ (Figure 6a), with no systematic difference between the data taken from diodes

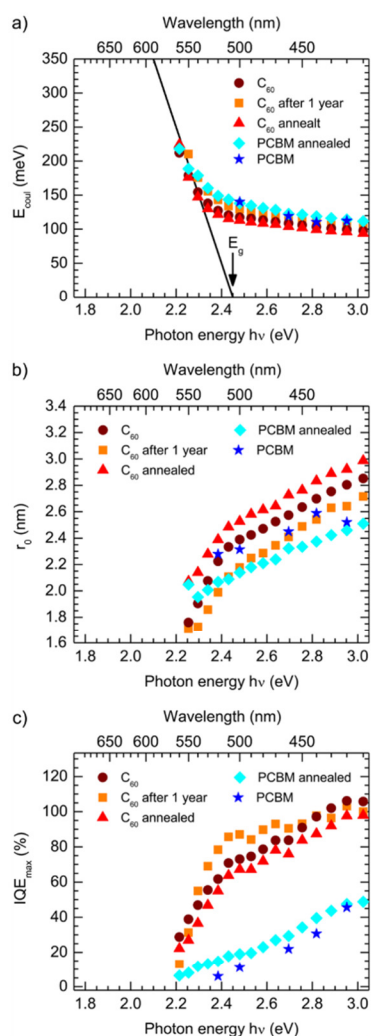


Figure 6. (a) Coulomb binding energy (E_{coul}), (b) eh-distance (r_0), and (c) maximal internal quantum efficiency (IQE_{max}) in the limit of infinite field, all as a function of the excitation energy for differently prepared fullerene single-layer devices. The solid line in (a) indicates the fit according to $E_{\text{coul}} = E_g - h\nu$, with $E_g = 2.45$ eV.

prepared in different ways. The linear decrease of $E_{\text{coul}}(h\nu)$ with increasing $h\nu$ close to the onset of intrinsic photogeneration implies that the dissociating eh-pair is generated resonantly, so that no energy is lost in the course of a thermalization process. Therefore, $E_g = h\nu + E_{\text{coul}}$ should apply where E_g is the electrical gap. This is illustrated in Figure 7. It is gratifying that the range of the $E_{\text{coul}}(h\nu)$ values, 0.10–0.22 eV, is in excellent agreement with the temperature dependence of the photocurrent generated by white light irradiation shown by Mort et al.³⁴ In that work, the curvature of the pertinent Arrhenius graphs are indicative of a distribution of activation energies ranging from 0.15 to 0.25 eV. At photon energies above 2.4 eV, the $E_{\text{coul}}(h\nu)$ dependence acquires a reduced slope. This indicates that above 2.4 eV, the eh-pairs are generated via a thermalization process in which the initially hot eh-pair loses energy by phonon

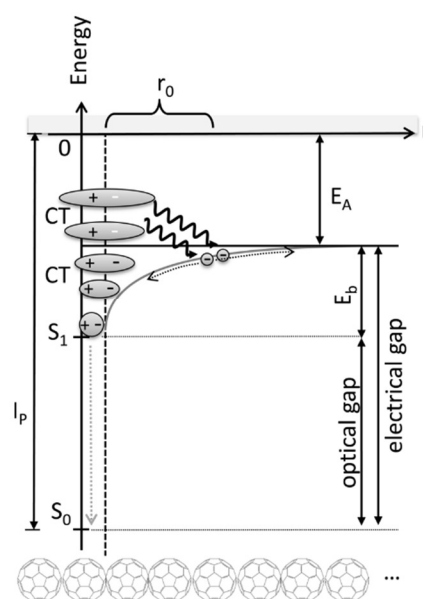


Figure 7. Schematic illustrating the process of eh-separation in a bulk fullerene phase as described in the text. I_p and E_A denote the ionization potential and electron affinity of the fullerene, and r_0 is the separation between the center of mass of the electron and hole wave functions after thermalization. Thermalization only occurs for CT states excited at energies exceeding that of the electrical gap.

emission. This process is well-known from work on molecular crystals.⁵⁴

When fitting the experimental data for $E_{\text{coul}}(h\nu)$ asymptotically to $E_{\text{coul}}(h\nu) = E_g - h\nu$, we obtain an electrical gap of 2.45 ± 0.05 eV (Figure 6a). This is in good agreement with the value of 2.52 eV calculated by Shirley et al.⁵⁶ but in disagreement with the value of 2.98 eV reported by Kazaoui et al.⁴⁰ Since the energy of the singlet exciton in C₆₀ is 1.85 eV, an electrical gap of 2.45 eV implies its binding energy is as large as 0.6 eV, at variance with ref 30. This means the intrinsic dissociation yield at 1.85 eV at room temperature is as low as 10^{-10} . The weak photocurrent we observed below a photon energy of 2.25 eV must therefore be of extrinsic origin, possibly caused by unidentified impurities with higher lying HOMO levels or by exciton dissociation at the electrode(s) under reverse bias.

The above value for E_g for C₆₀ has to be compared to the value that can be derived from photoemission data. The value for ionization energies I_p of C₆₀ in the gas phase is 7.59 eV.⁵⁷ Reported values of I_p for a C₆₀ film are 6.4 ± 0.05 eV.^{41–44} The difference between the gas phase values and the thin-film values is the polarization energy of a hole in solid C₆₀, $P^+ = 1.2 \pm 0.05$ eV. Based upon the gas phase value for the electron affinity $E_A = 2.65$ eV⁵⁸ and assuming that the polarization energies of an electron and a hole in solid C₆₀ are the same, the electron affinity in solid C₆₀ should be about 3.65–3.75 eV. This would be consistent with the value inferred from cyclic voltammetry⁶ and would predict an electrical gap of 2.65–2.75 eV. However, from both photoemission and inverse photoemission, Guan et al.⁴⁴ derived $E_g = 2.37$ eV. Given the uncertainties of the various techniques, we consider this consistent with our value of 2.45 eV.

For PCBM, the E_{coul} values above threshold are identical with those for C₆₀, which indicates that the spectral dependence of the photocurrent in C₆₀ and PCBM is similar. This is plausible because photoemission experiments indicate that in PCBM both the HOMO and LUMO levels only experience an upward shift by 0.4–0.5 eV relative to those of C₆₀.⁴³ Therefore, the value of the band gap is retained.

The activation energies for photogeneration in C₆₀ translates into the values for the intrapair eh-separation r_0 as a function of photon energy by $E_{\text{coul}} = \frac{e^2}{4\pi\epsilon_r\epsilon_0} \cdot \frac{1}{r_0}$. Figure 6b shows the data calculated using the value for the low frequency dielectric permittivity of $\epsilon_r = 5$.⁵⁹ When the photon energy increases from 2.25 to 2.4 eV, r_0 increases approximately linearly. Above 2.4 eV the $r_0(h\nu)$ dependence becomes weaker. This is the spectral range in which thermalization occurs. Taking into account an experimental uncertainty of $\pm 10\%$, there is no significant difference between differently prepared samples and between C₆₀ and PCBM.

We now turn to the IQE at infinite electric field (IQE_{max}) (Figure 6c) that can be inferred from Onsager fits to the experimental IQE($F, h\nu$) plots. The IQE_{max} values of C₆₀ increase with photon energy and reach, within experimental uncertainty, 100% at $h\nu = 3$ eV. This indicates that there is efficient coupling between the charge transfer states and charge transporting states, and that this coupling increases with quantum energy. Evidently, the coupling strength first rises strongly with photon energy for the CT states below the electrical gap, symbiotic with the strong increase in the electron–hole separation. The weaker increase in coupling strength above the electrical gap mirrors the weaker increase in r_0 . For PCBM, the coupling between the photoexcited CT states and the charge transporting states is weaker as evident by the significantly lower IQE_{max} values, even though the binding energy and electron–hole separation in the CT state in PCBM is comparable to C₆₀. We conjecture that this reflects a lesser coupling to the charge transporting states within the PCBM aggregates than within the C₆₀ aggregates.

It is plausible that the coupling between two adjacent fullerenes is also reflected in the oscillator strength of the CT state absorptions. For example, in hexane solution, where charge transfer to an adjacent fullerene is not possible due to lack of neighbor, the CT state absorptions below 3 eV cannot be seen⁶⁰ while in solid C₆₀ these transitions are well visible.^{61,62} Similarly, the observed reduced oscillator strength of PCBM relative to C₆₀ in the spectral range between 2.3 and 3 eV therefore also suggests a weaker coupling for charge transfer events.

The overall interpretation we present goes beyond the concept suggested by Kazaoui et al.⁴⁰ From electroabsorption (EA) spectroscopy, Kazaoui et al. observed that there is an increase of the transition dipole moment above 2.2 eV that is associated with a CT state at 2.43 eV, i.e., resonant with the value we identified for the electrical gap. At first glance, the observation of a discrete CT state appears incompatible with efficient autoionization over a spectral range from above 2.2 eV up to at least 3 eV. However, when modulating a broad absorption spectrum with oscillating electric field, an EA feature can only show up at the lower energy edge of the spectrum. This is reminiscent of a Franz-Keldysh effect on crystalline polydiacetylenes.⁶³ Therefore, there is indeed consistency between EA spectroscopy and photogeneration interpreted in terms of an Onsager process.

In passing, it appears noteworthy to comment on the different dependences of photogeneration on photon energy in a single phase system like C₆₀ compared to a donor–acceptor type heterojunction. While the yield increases with photon energy in the single-phase C₆₀, it is usually observed to be constant in donor–acceptor type heterojunctions.¹⁵ This difference reflects the different generation processes. In the single-phase C₆₀ case, the dissociating entity is a short-lived CT state in the framework of the Onsager 1938 approach,⁵² with energies above the S₁ singlet state. In contrast, in a donor–acceptor type heterojunction, the cold CT state formed between donor and acceptor is the energetically lowest available state that is long-lived and that can make several attempts to fully ionize, as described in the framework of the Onsager-Braun model.²

In this context, it is interesting to consider the implication of our results for a donor–acceptor type system. Gelinis et al.³⁷ explained the observation that in PCDTBT/PCBM bulk heterojunction OCSs the dissociation of geminately bound electron pairs occurs with almost 100% efficiency by ultrafast charge separation through delocalized band-like states in fullerene aggregates. The current results on the spectrally dependent and field assisted photogeneration in C₆₀ or PCBM indicate, however, that mean electron–hole separation in fullerenes is about 2.0–2.5 nm. Thus, the center of mass of the delocalized electron wave function is separated from the center of mass of the delocalized hole wave function by no more than about 2.5 nm.

The present results have an important bearing for the interpretation of bulk or planar heterojunction solar cells since they demonstrate that optical excitation of C₆₀ or, to a lesser degree, PCBM in the form of clusters or solid films contributes to the overall yield of photogeneration above a photon energy of 2.25 eV (550 nm).^{29,32} The photocurrent is therefore a sum of the contribution from dissociation of CT states at the donor–acceptor interface and the intrinsic photocurrent from the fullerene phase. The field dependences of both currents are different. Since the CT state in the bulk fullerene phase is more strongly bound than the CT state at the donor–acceptor interface, the additional current due to the fullerene clusters only saturates at much higher reverse voltages. This yields a higher short circuit current yet a reduced fill factor. These findings provide an alternative explanation to the observation that was recently reported by Tress and co-workers.³³

5. CONCLUSIONS

The overall picture we obtain from our data on the photogeneration of charges in fullerene films is summarized in Figure 7. Between about 2.25 eV and the electrical gap at 2.45 eV, optical excitation creates charge transfer states. Their binding energies reduce with photon energy from 220 to 100 meV while the mean electron–hole separation r_0 within these CT states increases from 2.0 to 2.5 nm. They are ionized by thermal excitation to the electrical gap so that they can couple to charge transporting states, and the relation $E_g = h\nu + E_{\text{coul}}$ applies. For optical excitation exceeding the energy of the electrical gap, photogenerated CT states thermalize to a mean electron–hole distance r_0 that also increases with photon energy, albeit less strongly. Their binding energy, in the range of about 100 meV, also reduces only slightly with photon energy. The thermalized, i.e., cold, CT states, also dissociate by coupling to charge transporting states, again by thermal excitation. The ultimate internal quantum efficiency that can be obtained for infinite field strength depends on the strength of the coupling between

the CT states and the charge transporting states. We find this coupling is stronger for C₆₀ than for PCBM.

■ ASSOCIATED CONTENT

Supporting Information

The Supporting Information is available free of charge on the ACS Publications website at DOI: 10.1021/acs.jpcc.6b08471.

j(V) characteristics for monochromatic excitation at 2.7 eV. Synthesis and ¹H and ¹³C NMR spectra of Ph-TDPP-Ph. Synthesis and ¹H NMR spectrum of PCDTBT_{co}. (PDF)

■ AUTHOR INFORMATION

Corresponding Author

*E-mail: Anna.Koehler@uni-bayreuth.de. Tel: +49 (0)921 55 2600.

Author Contributions

[†]Both authors contributed equally to this work.

Notes

The authors declare no competing financial interest.

■ ACKNOWLEDGMENTS

We acknowledge financial support by the Bavarian State Ministry of Science, Research, and the Arts through the Collaborative Research Network "Solar Technologies go Hybrid" and by the German Science Foundation DFG through the doctoral training center "GRK 1640". Satish Patil thanks the Department of Science and Technology, New Delhi, India for a Swarnajayanti fellowship. We thank Irene Bauer and Frank Schirmer for technical assistance.

■ REFERENCES

- (1) Köhler, A.; Bäessler, H. *Electronic Processes in Organic Semiconductors: An Introduction*; Wiley: New York, 2015.
- (2) Braun, C. L. Electric-Field Assisted Dissociation of Charge-Transfer States as a Mechanism of Photocarrier Production. *J. Chem. Phys.* **1984**, *80*, 4157–4161.
- (3) Vandewal, K.; Tvingstedt, K.; Gadisa, A.; Inganäs, O.; Manca, J. V. Relating the Open-Circuit Voltage to Interface Molecular Properties of Donor:Acceptor Bulk Heterojunction Solar Cells. *Phys. Rev. B: Condens. Matter Mater. Phys.* **2010**, *81*, 125204.
- (4) Veldman, D.; Ipek, Ö.; Meskers, S. C. J.; Sweelssen, J.; Koetse, M. M.; Veenstra, S. C.; Kroon, J. M.; van Bavel, S. S.; Loos, J.; Janssen, R. A. J. Compositional and Electric Field Dependence of the Dissociation of Charge Transfer Excitons in Alternating Polyfluorene Copolymer/Fullerene Blends. *J. Am. Chem. Soc.* **2008**, *130*, 7721–7735.
- (5) Provencher, F.; Sakowicz, M.; Brosseau, C. N.; Latini, G.; Beaupré, S.; Leclerc, M.; Reynolds, L. X.; Haque, S. A.; Leonelli, R.; Silva, C. Slow Geminate-Charge-Pair Recombination Dynamics at Polymer: Fullerene Heterojunctions in Efficient Organic Solar Cells. *J. Polym. Sci., Part B: Polym. Phys.* **2012**, *50*, 1395–1404.
- (6) Faist, M. A.; Kirchartz, T.; Gong, W.; Ashraf, R. S.; McCulloch, I.; de Mello, J. C.; Elkins-Daukes, N. J.; Bradley, D. D. C.; Nelson, J. Competition between the Charge Transfer State and the Singlet States of Donor or Acceptor Limiting the Efficiency in Polymer:Fullerene Solar Cells. *J. Am. Chem. Soc.* **2012**, *134*, 685–692.
- (7) Albrecht, S.; Vandewal, K.; Tumbleston, J. R.; Fischer, F. S. U.; Douglas, J. D.; Fréchet, J. M. J.; Ludwigs, S.; Ade, H.; Salleo, A.; Neher, D. On the Efficiency of Charge Transfer State Splitting in Polymer: Fullerene Solar Cells. *Adv. Mater.* **2014**, *26*, 2533–2539.
- (8) Mendaza, A. D. D.; Melianas, A.; Rossbauer, S.; Bäcke, O.; Nordstierna, L.; Erhart, P.; Olsson, E.; Anthopoulos, T. D.; Inganäs, O.; Müller, C. High-Entropy Mixtures of Pristine Fullerenes for Solution-Processed Transistors and Solar Cells. *Adv. Mater.* **2015**, *27*, 7325–7331.

(9) Halls, J. J. M.; Cornil, J.; dos Santos, D. A.; Silbey, R.; Hwang, D. H.; Holmes, A. B.; Brédas, J. L.; Friend, R. H. Charge- and Energy-Transfer Processes at Polymer/Polymer Interfaces: A Joint Experimental and Theoretical Study. *Phys. Rev. B: Condens. Matter Mater. Phys.* **1999**, *60*, 5721–5727.

(10) Panda, P.; Veldman, D.; Sweelssen, J.; Bastiaansen, J. J. A. M.; Langeveld-Voss, B. M. W.; Meskers, S. C. J. Charge Transfer Absorption for π -Conjugated Polymers and Oligomers Mixed with Electron Acceptors. *J. Phys. Chem. B* **2007**, *111*, 5076–5081.

(11) Clarke, T. M.; Durrant, J. R. Charge Photogeneration in Organic Solar Cells. *Chem. Rev.* **2010**, *110*, 6736–6767.

(12) Servaites, J. D.; Ratner, M. A.; Marks, T. J. Organic Solar Cells: A New Look at Traditional Models. *Energy Environ. Sci.* **2011**, *4*, 4410–4422.

(13) Wiemer, M.; Koch, M.; Lemmer, U.; Pevtsov, A. B.; Baranovskii, S. D. Efficiency of Exciton Dissociation at Internal Organic Interfaces beyond Harmonic Approximation. *Org. Electron.* **2014**, *15*, 2461–2467.

(14) Kaake, L. G.; Zhong, C. M.; Love, J. A.; Nagao, I.; Bazan, G. C.; Nguyen, T. Q.; Huang, F.; Cao, Y.; Moses, D.; Heeger, A. J. Ultrafast Charge Generation in an Organic Bilayer Film. *J. Phys. Chem. Lett.* **2014**, *5*, 2000–2006.

(15) Vandewal, K.; Albrecht, S.; Hoke, E. T.; Graham, K. R.; Widmer, J.; Douglas, J. D.; Schubert, M.; Mateker, W. R.; Bloking, J. T.; Burkhard, G. F.; et al. Efficient Charge Generation by Relaxed Charge-Transfer States at Organic Interfaces. *Nat. Mater.* **2013**, *13*, 63–68.

(16) Few, S.; Frost, J. M.; Nelson, J. Models of Charge Pair Generation in Organic Solar Cells. *Phys. Chem. Chem. Phys.* **2015**, *17*, 2311–2325.

(17) Hendriks, K. H.; Wijpkema, A. S. G.; van Franeker, J. J.; Wienk, M. M.; Janssen, R. A. J. Dichotomous Role of Exciting the Donor or the Acceptor on Charge Generation in Organic Solar Cells. *J. Am. Chem. Soc.* **2016**, *138*, 10026–10031.

(18) Kurpiers, J.; Neher, D. Dispersive Non-Geminate Recombination in an Amorphous Polymer: Fullerene Blend. *Sci. Rep.* **2016**, *6*, 26832.

(19) Ran, N. A.; Love, J. A.; Takacs, C. J.; Sadhanala, A.; Beavers, J. K.; Collins, S. D.; Huang, Y.; Wang, M.; Friend, R. H.; Bazan, G. C.; et al. Harvesting the Full Potential of Photons with Organic Solar Cells. *Adv. Mater.* **2016**, *28*, 1482–1488.

(20) Bartesaghi, D.; Perez, I. D.; Kniepert, J.; Roland, S.; Turbiez, M.; Neher, D.; Koster, L. J. A. Competition between Recombination and Extraction of Free Charges Determines the Fill Factor of Organic Solar Cells. *Nat. Commun.* **2015**, *6*, 7083.

(21) Arkhipov, V. I.; Heremans, P.; Bäessler, H. Why is Exciton Dissociation so Efficient at the Interface between a Conjugated Polymer and an Electron Acceptor? *Appl. Phys. Lett.* **2003**, *82*, 4605–4607.

(22) Deibel, C.; Strobel, T.; Dyakonov, V. Origin of the Efficient Polaron-Pair Dissociation in Polymer-Fullerene Blends. *Phys. Rev. Lett.* **2009**, *103*, 036402.

(23) Bakulin, A. A.; Rao, A.; Pavelyev, V. G.; van Loosdrecht, P. H. M.; Pshenichnikov, M. S.; Niedzialek, D.; Cornil, J.; Beljonne, D.; Friend, R. H. The Role of Driving Energy and Delocalized States for Charge Separation in Organic Semiconductors. *Science* **2012**, *335*, 1340–1344.

(24) Schwarz, C.; Tscheuschner, S.; Frisch, J.; Winkler, S.; Koch, N.; Bäessler, H.; Köhler, A. Role of the Effective Mass and Interfacial Dipoles on Exciton Dissociation in Organic Donor-Acceptor Solar Cells. *Phys. Rev. B: Condens. Matter Mater. Phys.* **2013**, *87*, 155205.

(25) Niklas, J.; Mardis, K. L.; Banks, B. P.; Grooms, G. M.; Sperlich, A.; Dyakonov, V.; Beaupré, S.; Leclerc, M.; Xu, T.; Yu, L. P.; et al. Highly-Efficient Charge Separation and Polaron Delocalization in Polymer-Fullerene Bulk-Heterojunctions: A Comparative Multi-Frequency EPR and DFT Study. *Phys. Chem. Chem. Phys.* **2013**, *15*, 9562–9574.

(26) Bernardo, B.; Cheyns, D.; Verreert, B.; Schaller, R. D.; Rand, B. P.; Giebink, N. C. Delocalization and Dielectric Screening of Charge

- Transfer States in Organic Photovoltaic Cells. *Nat. Commun.* **2014**, *5*, 3245.
- (27) Tscheuschner, S.; Bäessler, H.; Huber, K.; Köhler, A. A Combined Theoretical and Experimental Study of Dissociation of Charge Transfer States at the Donor-Acceptor Interface of Organic Solar Cells. *J. Phys. Chem. B* **2015**, *119*, 10359–10371.
- (28) Im, C.; Tian, W.; Bäessler, H.; Fechtenkötter, A.; Watson, M. D.; Müllen, K. Photoconduction in Organic Donor-Acceptor Systems. *J. Chem. Phys.* **2003**, *119*, 3952–3957.
- (29) Burkhard, G. F.; Hoke, E. T.; Beiley, Z. M.; McGehee, M. D. Free Carrier Generation in Fullerene Acceptors and Its Effect on Polymer Photovoltaics. *J. Phys. Chem. C* **2012**, *116*, 26674–26678.
- (30) Zou, Y. L.; Holmes, R. J. The Role of Exciton Ionization Processes in Bulk Heterojunction Organic Photovoltaic Cells. *Adv. Energy Mater.* **2015**, *5*, 1500019.
- (31) Li, W. B.; Yu, H. M.; Zhang, J. W.; Yao, Y.; Wu, C. Q.; Hou, X. Y. Photoinduced Injection Enhancement in Fullerene-Based Organic Solar Cell Originates from Exciton-Electron Interaction. *J. Phys. Chem. C* **2014**, *118*, 11928–11934.
- (32) Jeong, W. I.; Lee, Y. E.; Shim, H. S.; Kim, T. M.; Kim, S. Y.; Kim, J. J. Photoconductivity of C₆₀ as an Origin of Bias-Dependent Photocurrent in Organic Photovoltaics. *Adv. Funct. Mater.* **2012**, *22*, 3089–3094.
- (33) Tress, W.; Leo, K.; Riede, M. Photoconductivity as Loss Mechanism in Organic Solar Cells. *Phys. Status Solidi RRL* **2013**, *7*, 401–405.
- (34) Mort, J.; Machonkin, M.; Ziolo, R.; Huffman, D. R.; Ferguson, M. I. Temperature-Dependence of Photoconductivity in Buckminsterfullerene Films. *Appl. Phys. Lett.* **1992**, *60*, 1735–1737.
- (35) Jamieson, F. C.; Domingo, E. B.; McCarthy-Ward, T.; Heeney, M.; Stingelin, N.; Durrant, J. R. Fullerene Crystallisation as a Key Driver of Charge Separation in Polymer/Fullerene Bulk Heterojunction Solar Cells. *Chem. Sci.* **2012**, *3*, 485–492.
- (36) Hedley, G. J.; Ward, A. J.; Alekseev, A.; Howells, C. T.; Martins, E. R.; Serrano, L. A.; Cooke, G.; Ruseckas, A.; Samuel, I. D. W. Determining the Optimum Morphology in High-Performance Polymer-Fullerene Organic Photovoltaic Cells. *Nat. Commun.* **2013**, *4*, 2867.
- (37) Gelinias, S.; Rao, A.; Kumar, A.; Smith, S. L.; Chin, A. W.; Clark, J.; van der Poll, T. S.; Bazan, G. C.; Friend, R. H. Ultrafast Long-Range Charge Separation in Organic Semiconductor Photovoltaic Diodes. *Science* **2014**, *343*, 512–516.
- (38) Mort, J.; Machonkin, M.; Chen, I.; Ziolo, R. Charge-Transfer Processes in Buckminsterfullerene Films. *Philos. Mag. Lett.* **1993**, *67*, 77–83.
- (39) Mort, J.; Machonkin, M.; Ziolo, R.; Chen, I. Electronic Carrier Transport and Photogeneration in Buckminsterfullerene Films. *Appl. Phys. Lett.* **1992**, *61*, 1829–1831.
- (40) Kazaoui, S.; Minami, N.; Tanabe, Y.; Byrne, H. J.; Eilmes, A.; Petelenz, P. Comprehensive Analysis of Intermolecular Charge-Transfer Excited States in C₆₀ and C₇₀ Films. *Phys. Rev. B: Condens. Matter Mater. Phys.* **1998**, *58*, 7689–7700.
- (41) Seo, J. H.; Kang, S. J.; Kim, C. Y.; Cho, S. W.; Yoo, K. H.; Whang, C. N. Energy Level Alignment between C₆₀ and Al Using Ultraviolet Photoelectron Spectroscopy. *Appl. Surf. Sci.* **2006**, *252*, 8015–8017.
- (42) Niederhausen, J.; Amsalem, P.; Wilke, A.; Schlesinger, R.; Winkler, S.; Vollmer, A.; Rabe, J. P.; Koch, N. Doping of C₆₀ (Sub)Monolayers by Fermi-Level Pinning Induced Electron Transfer. *Phys. Rev. B: Condens. Matter Mater. Phys.* **2012**, *86*, 081411.
- (43) Akaike, K.; Kanai, K.; Yoshida, H.; Tsutsumi, J.; Nishi, T.; Sato, N.; Ouchi, Y.; Seki, K. Ultraviolet Photoelectron Spectroscopy and Inverse Photoemission Spectroscopy of [6,6]-Phenyl-C₆₁-butyric Acid Methyl Ester in Gas and Solid Phases. *J. Appl. Phys.* **2008**, *104*, 023710.
- (44) Guan, Z. L.; Kim, J. B.; Wang, H.; Jaye, C.; Fischer, D. A.; Loo, Y. L.; Kahn, A. Direct Determination of the Electronic Structure of the Poly(3-hexylthiophene):phenyl-[6,6]-C₆₁ Butyric Acid Methyl Ester Blend. *Org. Electron.* **2010**, *11*, 1779–1785.
- (45) Kalinowski, J.; Giro, G.; Camaioni, N.; Fattori, V.; DiMarco, P. Photoconduction in Solid Films of C₆₀. *Synth. Met.* **1996**, *77*, 181–188.
- (46) Schwarz, C.; Bäessler, H.; Bauer, I.; Koenen, J. M.; Preis, E.; Scherf, U.; Köhler, A. Does Conjugation Help Exciton Dissociation? A Study on Poly(p-phenylene)s in Planar Heterojunctions with C₆₀ or TNF. *Adv. Mater.* **2012**, *24*, 922–925.
- (47) Burkhard, G. F.; Hoke, E. T.; McGehee, M. D. Accounting for Interference, Scattering, and Electrode Absorption to Make Accurate Internal Quantum Efficiency Measurements in Organic and Other Thin Solar Cells. *Adv. Mater.* **2010**, *22*, 3293–3297.
- (48) Pettersson, L. A. A.; Roman, L. S.; Inganäs, O. Modeling Photocurrent Action Spectra of Photovoltaic Devices Based on Organic Thin Films. *J. Appl. Phys.* **1999**, *86*, 487–496.
- (49) Peumans, P.; Yakimov, A.; Forrest, S. R. Small Molecular Weight Organic Thin-Film Photodetectors and Solar Cells. *J. Appl. Phys.* **2003**, *93*, 3693–3723.
- (50) Wynands, D.; Erber, M.; Rentenberger, R.; Levichkova, M.; Walzer, K.; Eichhorn, K. J.; Stamm, M. Spectroscopic Ellipsometry Characterization of Vacuum-Deposited Organic Films for the Application in Organic Solar Cells. *Org. Electron.* **2012**, *13*, 885–893.
- (51) Hahn, T.; Geiger, J.; Blase, X.; Duchemin, I.; Niedzialek, D.; Tscheuschner, S.; Beljonne, D.; Bäessler, H.; Köhler, A. Does Excess Energy Assist Photogeneration in an Organic Low-Bandgap Solar Cell? *Adv. Funct. Mater.* **2015**, *25*, 1287–1295.
- (52) Onsager, L. Initial Recombination of Ions. *Phys. Rev.* **1938**, *54*, 554.
- (53) Pai, D. M.; Enck, R. C. Onsager Mechanism of Photogeneration in Amorphous Selenium. *Phys. Rev. B* **1975**, *11*, 5163–5174.
- (54) Chance, R. R.; Braun, C. L. Temperature-Dependence of Intrinsic Carrier Generation in Anthracene Single-Crystals. *J. Chem. Phys.* **1976**, *64*, 3573–3581.
- (55) Borsenberger, P. M.; Weiss, D. S. *Organic Photoreceptors for Imaging Systems*; Taylor and Francis: London, 1993.
- (56) Shirley, E. L.; Benedict, L. X.; Louie, S. G. Excitons in Solid C₆₀. *Phys. Rev. B: Condens. Matter Mater. Phys.* **1996**, *54*, 10970–10977.
- (57) Steger, H.; Holzapfel, J.; Hielscher, A.; Kamke, W.; Hertel, I. V. Single-Photon Ionization of Higher Fullerenes C₇₀, C₇₈ and C₈₄ - Determination of Ionization-Potentials. *Chem. Phys. Lett.* **1995**, *234*, 455–459.
- (58) Wang, L. S.; Conceicao, J.; Jin, C. M.; Smalley, R. E. Threshold Photodetachment of Cold C₆₀⁻. *Chem. Phys. Lett.* **1991**, *182*, 5–11.
- (59) Chern, G.; Mathias, H.; Testardi, L. R.; Seger, L.; Schlenoff, J. Low-Frequency Dielectric Permittivity of C₆₀. *J. Supercond.* **1995**, *8*, 207–210.
- (60) Leach, S.; Vervloet, M.; Desprès, A.; Bréheret, E.; Hare, J. P.; Dennis, T. J.; Kroto, H. W.; Taylor, R.; Walton, D. R. M. Electronic Spectra and Transitions of the Fullerene C₆₀. *Chem. Phys.* **1992**, *160*, 451–466.
- (61) Kazaoui, S.; Ross, R.; Minami, N. In-Situ Photoconductivity Behavior of C₆₀ Thin-Films - Wavelength, Temperature, Oxygen Effect. *Solid State Commun.* **1994**, *90*, 623–628.
- (62) Pac, B.; Petelenz, P.; Eilmes, A.; Munn, R. W. Charge-Transfer Exciton Band Structure in the Fullerene Crystal-Model Calculations. *J. Chem. Phys.* **1998**, *109*, 7923–7931.
- (63) Weiser, G. Stark-Effect of One-Dimensional Wannier Excitons in Polydiacetylene Single-Crystals. *Phys. Rev. B: Condens. Matter Mater. Phys.* **1992**, *45*, 14076–14085.

Supporting Information:

Role of Intrinsic Photogeneration in Single Layer and Bilayer Solar Cells with C₆₀ and PCBM

Tobias Hahn^{1,+} & Steffen Tscheuschner^{1,+}, Christina Saller², Peter Strohriegl^{2,5}, Puttaraju Boregowda³,
Tushita Mukhopadhyay³, Satish Patil³, Dieter Neher⁴, Heinz Bässler⁵, Anna Köhler^{1,5*}

¹ Experimental Physics II, University of Bayreuth, 95440 Bayreuth, Germany

² Macromolecular Chemistry I, University of Bayreuth, 95440 Bayreuth, Germany

³ Solid State and Structural Chemistry Unit, Indian Institute of Science, Bangalore, 560012

⁴ Institute for Physics and Astronomy, University of Potsdam, 14476 Potsdam-Golm, Germany

⁵ Bayreuth Institute of Macromolecular Science (BIMF), University of Bayreuth, 95440 Bayreuth, Germany

⁺ Both authors contributed equally to this work

* Anna.Koehler@uni-bayreuth.de; Tel: +49 (0)921 55 2600

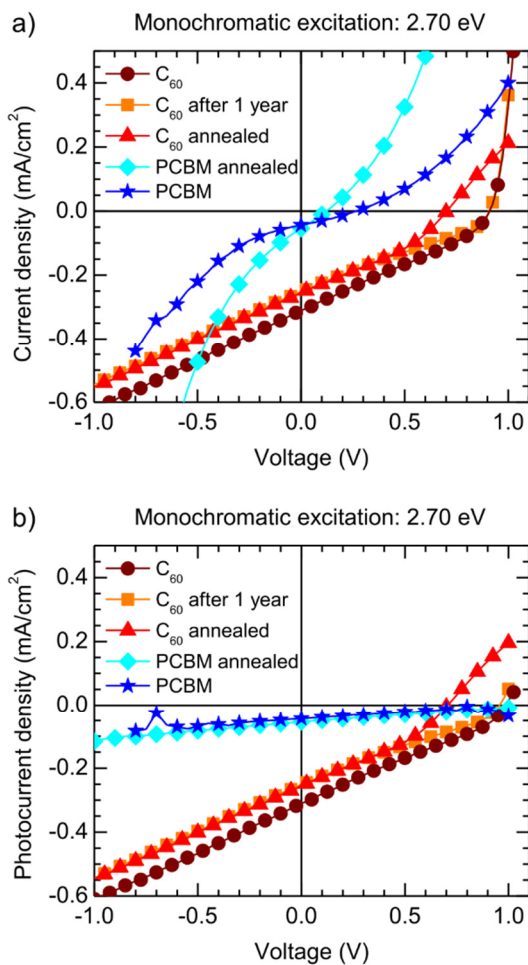
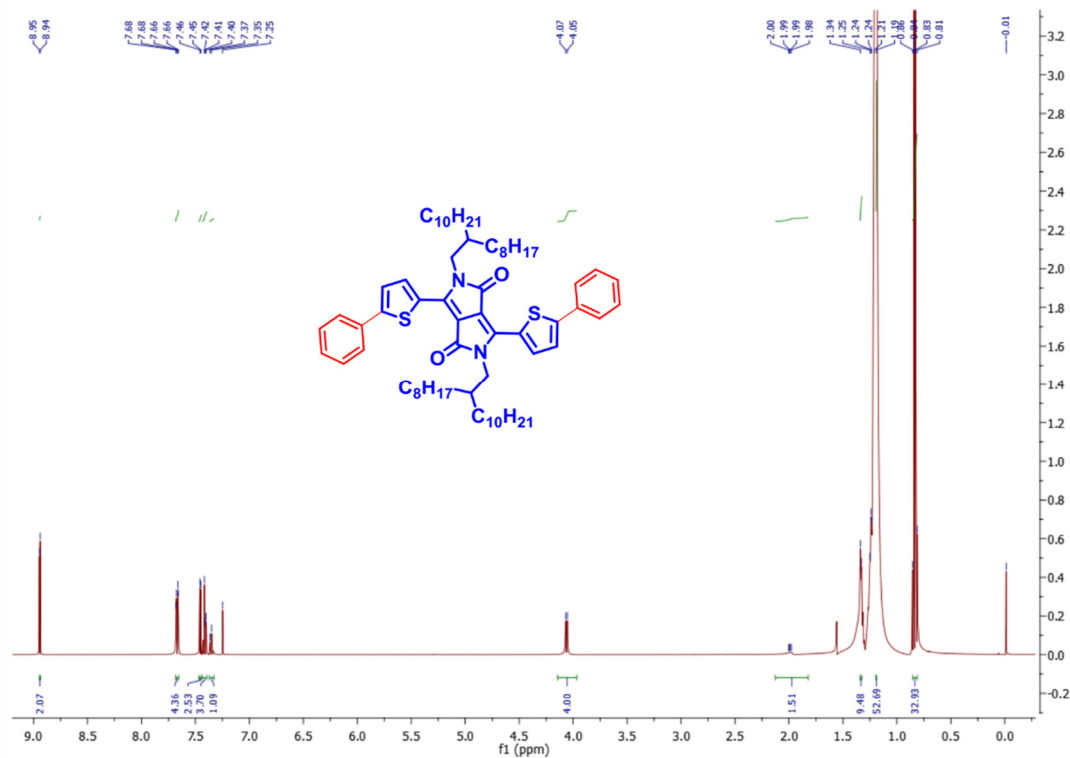
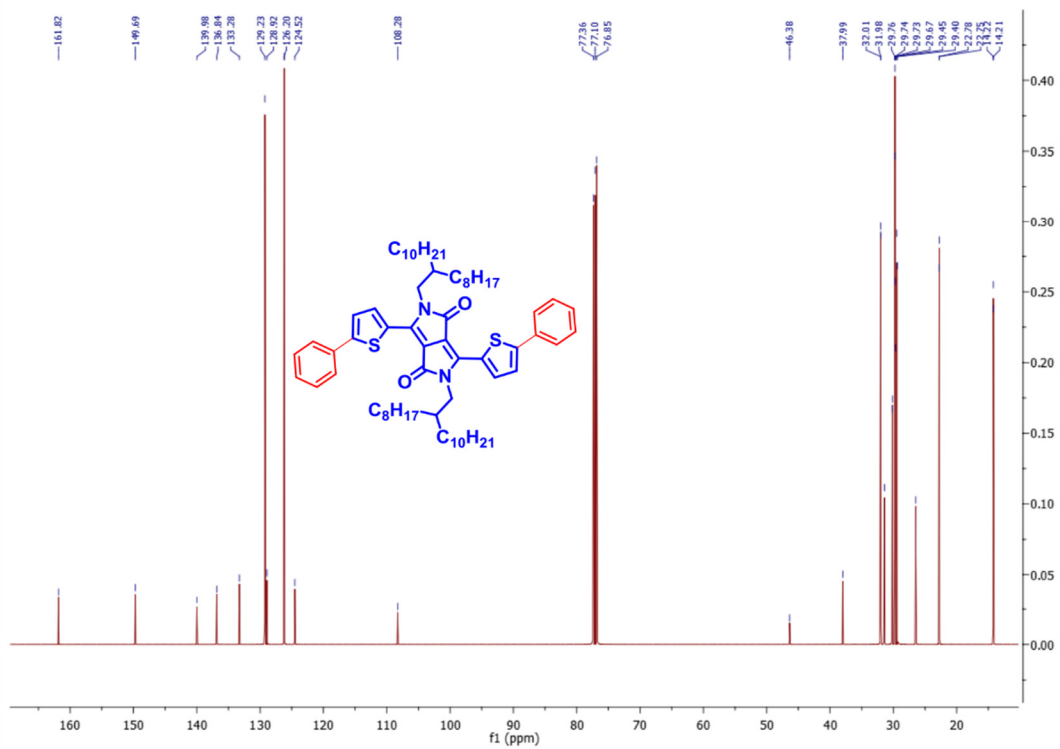


Figure S1: (a) Current and (b) Photocurrent (= Current minus Darkcurrent) for a C₆₀-only device measured immediately (wine circles), a C₆₀-only device stored in a nitrogen glovebox for one year (orange squares), a C₆₀-only device annealed at 140°C for 26 hours under nitrogen (red triangles), a PCBM-only device annealed at 140°C for 30 min and afterwards cooled down to 60°C in a time range of 30 min (cyan diamonds) and for a PCBM-only device which was not annealed and measured as cast (blue stars).

Synthesis of 2,5-bis(2-octyldodecyl)-3,6-bis(5-phenylthiophen-2-yl)pyrrolo[3,4-c]pyrrole-1,4(2H,5H)-dione (Ph-TDPP-Ph)

A mixture of phenylboronic acid (0.079 g, 0.64 mmol) and potassium carbonate (0.089 g, 0.64 mmol) in toluene/ethanol (3:1, 60 mL) was stirred at 50°C for 30 min. Then the compound 3,6-bis(5-bromothiophen-2-yl)-2,5-bis(2-octyldodecyl)pyrrolo[3,4-c]pyrrole-1,4(2H,5H)-dione (0.3 g, 0.29 mmol) was added in one portion, the reaction mixture was heated at 110°C for 12 h and then cooled to room temperature. Dichloromethane (100 mL) and water (200 mL) were added and the layers separated. The organic layer was concentrated *in vacuo*. Further purification was carried out by column chromatography on silica gel eluting with hexane/ethyl acetate (5%) to give the compound Ph-TDPP-Ph as a dark blue solid (0.22 g, 75%). ¹H NMR (400 MHz, CDCl₃), δ = 8.94 (d, *J* = 8 Hz, 2H), 7.67 (dd, *J* = 8.5, 1.3 Hz, 4H), 7.45 (d, *J* = 4.2 Hz, 3H), 7.44 – 7.39 (m, 4H), 7.35 – 7.37 (m, *J* = 7.5 Hz, 1H), 4.06 (d, *J* = 4 Hz, 4H), 1.98 – 2.00 (m, 2H), 1.19 – 1.34 (m, 62H), 0.81 – 0.86 (m, 12H) ppm. ¹³C NMR (100 MHz, CDCl₃) δ 161.82, 149.69, 139.98, 136.84, 133.28, 129.23, 128.92, 126.20, 124.52, 108.28, 46.38, 37.99, 32.01, 31.98, 29.76, 29.74, 29.45, 29.40, 22.78, 22.75, 14.22, 14.21 ppm. ESI-MS calculated for C₆₆H₉₆N₂O₂S₂: *m/z*: 1012.69; found: 1014.12.

Figure S2: ¹H NMR spectrum of Ph-TDPP-PhFigure S3: ¹³C NMR spectrum of Ph-TDPP-Ph

Synthesis of the polymer PCDTBT_{co}

PCDTBT_{co} (poly[(*N*-heptadecan-9'-yl)-2,7-carbazole-*alt*-5,5-(4',7'-bis(thien-2-yl)-2',1',3'-benzothiadiazole)]_{0.7}-*stat*-[*N,N'*-bis(4-methylphenyl)-*N,N'*-diphenylbenzidine-*alt*-5,5-(4',7'-bis(thien-2-yl)-2',1',3'-benzothiadiazole)]_{0.3}) was synthesized via Suzuki coupling according to the following procedure. The molar ratio of the carbazole, the phenyl-substituted benzidine, and the bithienyl-benzothiadiazole units in PCDTBT_{co} is 0.7:0.3:1.

A Schlenk flask was charged with the monomers 2,7-bis-(4',4',5',5'-tetramethyl-1',3',2'-dioxaborolan-2'-yl)-*N*-(heptadecan-9''-yl)-carbazole (0.368 g, 0.560 mmol), *N,N'*-bis(4-methylphenyl)-*N,N'*-bis((4',4',5',5'-tetramethyl-1',3',2'-dioxaborolan-2'-yl)phenyl)-benzidine (0.184 g, 0.239 mmol), 4,7-bis(5'-bromo-thien-2'-yl)-2,1,3-benzothiadiazole (0.367 g, 0.800 mmol) and 12 mL of toluene under argon. One drop of Aliquat 336 and 20 mL of 2 M Na₂CO₃ solution were added and the mixture was degassed by three freeze-thaw cycles. Afterwards, 14 mg of tetrakis(triphenylphosphine)palladium(0) were added and followed by again three freeze-thaw cycles. The reaction mixture was then stirred under reflux in an argon atmosphere for 90 h before bromobenzene (0.126 g, 0.800 mmol) was added. After 2 h, phenylboronic acid (0.098 g, 0.800 mmol) was added and the reaction mixture was again refluxed overnight. The reaction mixture was allowed to cool to room temperature and the polymer was precipitated into methanol/water (10:1). Soxhlet extraction was carried out using acetone and toluene. The reduced toluene fraction was precipitated into methanol/water (10:1) and dried in vacuum overnight, yielding 0.163 g (28 %) of PCDTBT_{co} as a dark-red powder. A molecular weight of 45,000 gmol⁻¹ (*M_w*) and 31,000 gmol⁻¹ (*M_n*) was determined by high temperature polymer size exclusion chromatography in trichlorobenzene at 160°C with a polydispersity index of 1.44.

¹H NMR (300 MHz, C₂D₂Cl₄, 120 °C): δ = 0.66-0.91 (m, CH₃), 0.93 - 1.49 (m, CH₂), 2.08 (br, carbazole-CH₂), 2.22 - 2.48 (m, benzidine-CH₃, carbazole-CH₂), 4.67 (br, CH), 6.76 - 8.27 (m, ar-CH). Broadened and multiple signals are due to atropisomerism. From the integration of the signal for the CH₂ group in the swallow-tail spacer of the carbazole unit (2.08 ppm) and the combined signal for the methyl group in the benzidine units and the other CH₂ group in the carbazole spacer (2.22 - 2.48 ppm), a molar ratio of 0.7:0.3:1 was calculated.

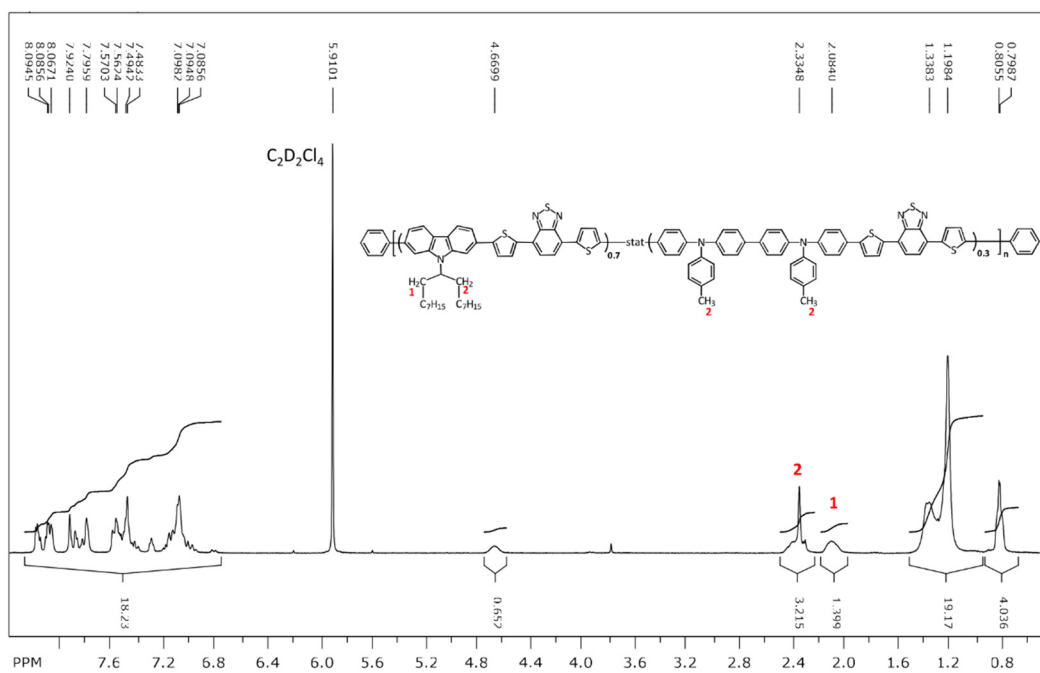
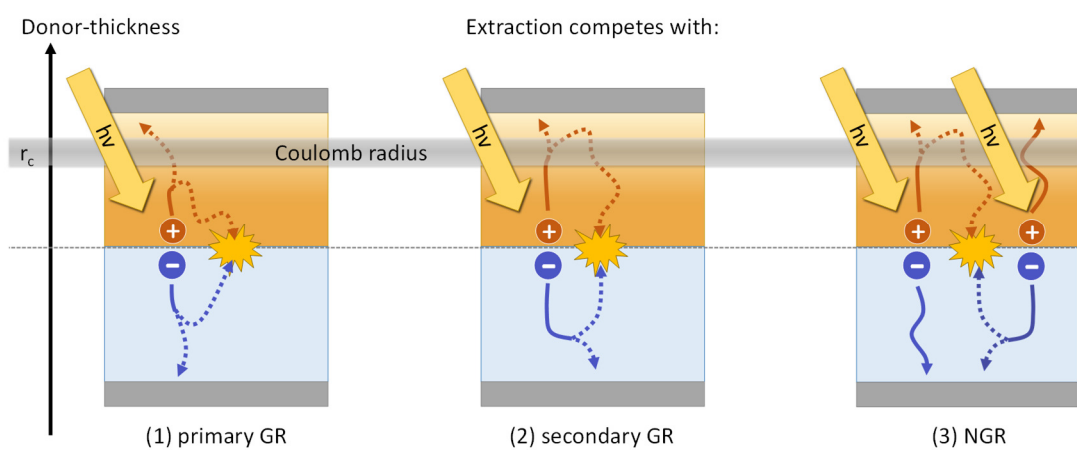


Figure S4: ¹H NMR spectrum of PCDTBT_{co} (300 MHz) in C₂D₂Cl₄ at 120 °C for the calculation of the molar ratio.

7. Monomolecular and bimolecular recombination of electron–hole pairs at the interface of a bilayer organic solar cell

Tobias Hahn, Steffen Tscheuschner, Frank-Julian Kahle, Markus Reichenberger,
Stavros Athanasopoulos, Christina Saller, Guillermo C. Bazan, Thuc-Quyen Nguyen,
Peter Strohriegl, Heinz Bässler, and Anna Köhler



Published in *Advanced Functional Materials*

doi: 10.1002/adfm.201604906

Reprinted with permission from *Advanced Functional Materials* **2017**, 12, 1604906

Copyright © 2016 WILEY-VCH Verlag GmbH & Co. KGaA, Weinheim

Monomolecular and Bimolecular Recombination of Electron–Hole Pairs at the Interface of a Bilayer Organic Solar Cell

Tobias Hahn, Steffen Tscheuschner, Frank-Julian Kahle, Markus Reichenberger, Stavros Athanasopoulos, Christina Saller, Guillermo C. Bazan, Thuc-Quyen Nguyen, Peter Strohriegl, Heinz Bässler, and Anna Köhler*

While it has been argued that field-dependent geminate pair recombination (GR) is important, this process is often disregarded when analyzing the recombination kinetics in bulk heterojunction organic solar cells (OSCs). To differentiate between the contributions of GR and nongeminate recombination (NGR) the authors study bilayer OSCs using either a PCDTBT-type polymer layer with a thickness from 14 to 66 nm or a 60 nm thick p-DTS(FBTTh₂)₂ layer as donor material and C₆₀ as acceptor. The authors measure *JV*-characteristics as a function of intensity and charge-extraction-by-linearly-increasing-voltage-type hole mobilities. The experiments have been complemented by Monte Carlo simulations. The authors find that fill factor (FF) decreases with increasing donor layer thickness (*L_p*) even at the lowest light intensities where geminate recombination dominates. The authors interpret this in terms of thickness dependent back diffusion of holes toward their siblings at the donor–acceptor interface that are already beyond the Langevin capture sphere rather than to charge accumulation at the donor–acceptor interface. This effect is absent in the p-DTS(FBTTh₂)₂ diode in which the hole mobility is by two orders of magnitude higher. At higher light intensities, NGR occurs as evidenced by the evolution of s-shape of the *JV*-curves and the concomitant additional decrease of the FF with increasing layer thickness.

1. Introduction

The power conversion efficiency in organic solar cells (OSCs) depends in a complex way on several parameters, i.e., (i) the fraction of the solar spectrum that is absorbed in the cell, (ii) the probability that an absorbed photon creates a Coulomb-bound pair of charge carriers, (iii) the internal electric field needed to dissociate that electron–hole pair (eh-pair), (iv) the fraction of charge carriers that escapes bimolecular recombination before reaching the electrodes, and (v) the contact resistance that can impede charge extraction at the electrodes.^[1–3] A measure of the fraction of the photo-generated charges that are actually collected at the electrodes is the fill factor (FF).^[4–11] Its value thus directly reflects the mechanism of charge carrier generation, which is a controversially discussed issue in the organic photovoltaic (OPV) community. By definition, the FF gives an indication on the voltage dependence of the photocurrent in the range between zero applied voltage and the open-circuit voltage.

Traditional models for the photogeneration of charges,^[12] and thus also for the photocurrent–voltage (*JV*) curves, have always taken into account that an electric field is needed to dissociate the interfacial eh-pair, be it in bulk heterojunction (BHJ)^[8,13] or in planar heterojunction (PHJ)^[14,15] solar cells. This implies that the inverse process, geminate recombination (GR), plays a role in controlling the shape of the *JV*-curves. The significant influence of electric field assisted dissociation and, conversely, geminate recombination has been well established experimentally for both PHJ cells^[16,17] and BHJ cells.^[18–20] In recent years, however, there has been an increasing number of reports demonstrating that device performance, and concomitantly the FF, is dominated by nongeminate recombination (NGR) processes such as Langevin or Shockley–Read–Hall-type recombination.^[21–26] Moreover, the appearance of an s-shaped kink in the *JV*-curves of PHJ cells has been associated with the prevalence of NGR, provided that injection or extraction barrier effects can be excluded.^[27,28] The NGR is considered to arise from charge accumulation at the heterojunction interface.^[24] What causes a significant

T. Hahn, S. Tscheuschner, F.-J. Kahle, M. Reichenberger,
Dr. S. Athanasopoulos, Prof. A. Köhler
Experimental Physics II
University of Bayreuth
95440 Bayreuth, Germany
E-mail: Anna.Koehler@uni-bayreuth.de



Dr. S. Athanasopoulos
Departamento de Física
Universidad Carlos III de Madrid
Avenida Universidad 30, 28911 Leganés, Madrid, Spain

C. Saller, Prof. P. Strohriegl
Macromolecular Chemistry I
University of Bayreuth
95440 Bayreuth, Germany

Prof. G. C. Bazan, Prof. T.-Q. Nguyen
Department of Chemistry and Biochemistry
Center for Polymers and Organic Solids
University of California
Santa Barbara, CA 93106-9510, USA

Prof. P. Strohriegl, Prof. H. Bässler, Prof. A. Köhler
Bayreuth Institute of Macromolecular Science (BIMF)
University of Bayreuth
95440 Bayreuth, Germany

DOI: 10.1002/adfm.201604906

contribution of either geminate or nongeminate recombination, and which factors determine the relative weight of both recombination pathways has been addressed by a few groups.^[19,29–34] These groups find distinct branching ratios between GR and NGR that change with film morphology, so that it can be influenced by appropriate processing conditions. Nevertheless, a microscopic understanding of what controls these recombination pathways is still lacking.

Here we have analyzed *J*-*V*-curves of PHJ cells made with different donor layer thicknesses (*L*_p) from 14 to 66 nm covered by a 30 nm thick C₆₀ layer as acceptor, sandwiched between ITO/MoO₃ and Al electrodes. The donor material PCZ_{0.3} is a statistical low bandgap copolymer of the PCDTBT family shown in Figure 1. For brevity, we shall refer to it as

PCDTBT_{stat}. The results are compared to PHJ cells employing the molecular donor p-DTS(FBTTh₂)₂. We show that the branching ratio between GR and NGR depends not only on operational parameters such as light intensity and electric field but also on device parameters such as film thickness. Using Monte Carlo (MC) simulations we illustrate how, close to the open-circuit condition, not only nongeminate recombination, but also the rate of geminate recombination depends on the competition between diffusive motion toward the collecting electrode and toward the sibling countercharge. The role of mobility and delocalization of charges is discussed. These results advance our microscopic understanding of the charge generation process which is the basis for the fabrication of efficient solar cells.

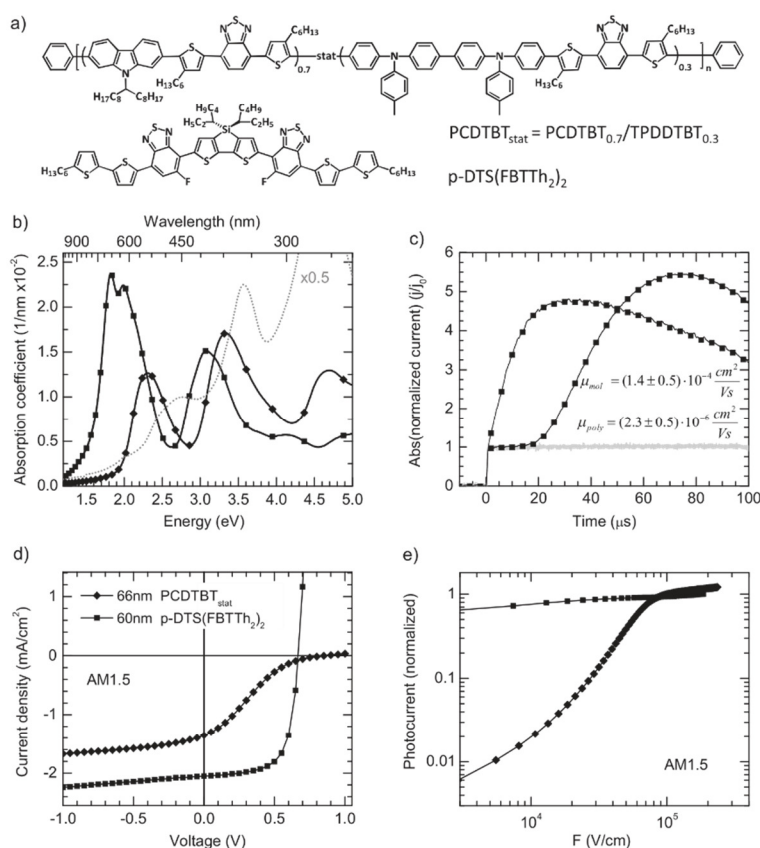


Figure 1. a) Chemical structure of the polymeric PCDTBT_{stat} and the oligomeric p-DTS(FBTTh₂)₂ donor materials and b) the absorption coefficients of PCDTBT_{stat} (gray diamonds), p-DTS(FBTTh₂)₂ (black squares) and C₆₀, measured from a 30 nm thick film. c) The current–response curves obtained in an MIS-CELIV measurement for PCDTBT_{stat} and for p-DTS(FBTTh₂)₂, as well as the response of the samples when no offset is applied (gray line). The extracted mobilities are given in the figure. d) The current as a function of applied voltage under AM1.5 sun light conditions for a bilayer cell with 66 nm of PCDTBT_{stat} donor and for an identical bilayer cell made with 60 nm of p-DTS(FBTTh₂)₂ as donor. e) The photocurrent obtained from (d) replotted as a function of internal field.

2. Results

Tress et al. suggested that mobility imbalance between electron and holes would be a major factor contributing to an s-shape in the JV -characteristics of PHJ cells.^[27] In order to probe this hypothesis and to illustrate its effect we measured the JV -characteristics of two bilayer diodes, each made with a 60–66 nm thick low bandgap donor layer covered by a 30 nm thick C_{60} acceptor layer sandwiched between an ITO/ MoO_3 anode and an Al cathode. The chemical structures and absorption spectra of the donor materials, i.e., the molecule p-DTS(FBTTh₂)₂ and the polymer PCDTBT_{stat}, are shown in Figure 1a,b. Both materials form suitable heterojunctions with C_{60} , since C_{60} has HOMO and LUMO levels of -6.4 and -3.7 eV, while the corresponding values for the donors are -5.12 and -3.34 eV for the p-DTS(FBTTh₂)₂ and -5.2 and -2.9 eV for PCDTBT_{stat}.^[35–40] A key difference between the two materials is their hole mobility. We used the metal–insulator–semiconductor charge-extraction-by-linearly-increasing-voltage (MIS-CELIV) approach to determine specifically the hole mobility in each donor (Figure 1c). For p-DTS(FBTTh₂)₂, we obtain a value of $1.4 \pm 0.5 \times 10^{-4}$ cm² V⁻¹ s⁻¹, while only $2.3 \pm 0.5 \times 10^{-6}$ cm² V⁻¹ s⁻¹ are obtained for the hole mobility in PCDTBT_{stat}. The latter value is about three orders of magnitude lower than the electron mobility in C_{60} , which is in the range of 10^{-3} – 10^{-2} cm² V⁻¹ s⁻¹.^[41] Indeed, under AM1.5 illumination (Figure 1d), the JV -characteristics of the bilayer diode with the PCDTBT_{stat} is s-shaped with a fill-factor of merely 22%, in contrast to the diode with p-DTS(FBTTh₂)₂, that has a fill-factor of 67%. This difference is also evident when replotting the JV -curves as field dependence of the photocurrent (Figure 1e), as described further below. While these data clearly confirm the notion that the magnitude of hole mobility has an important bearing of the diode performance, it is not fully understood how this relates to the underlying microscopic mechanism.

To address the microscopic reason, we consider the JV -curves of the bilayer as a function of the layer thickness of the donor for the PCDTBT_{stat} (Figure 2), in the dark as well as both for broadband excitation at AM1.5 (100 mW cm⁻²) and for monochromatic excitation. The thickness of the C_{60} acceptor layer was kept at 30 nm while the donor layer thickness was varied from 14 to 66 nm. The dark current characteristics for the diodes (Figure 2a) are a superposition of an ohmic leakage current that is symmetric about $V = 0$ V and an injection current that increases steeply with voltage above ≈ 0.6 V and with decreasing thickness of the donor layer. This strong voltage dependence of the forward current on the donor thickness is an indication that it is controlled by the space charge injected from the ohmic ITO/ MoO_3 anode. Thus, the dark JV -curves are perfectly “well-behaved” and they are tractable in terms of drift-diffusion theory developed by Wetzelaer et al.^[42,43]

Under illumination, the highest short circuit current j_{SC} , 2.2 mA cm⁻², is obtained for the thinnest diode using broadband excitation at air mass 1.5 (AM1.5), shown in Figure 2b. Considering that in a bilayer OSC only excitations generated within a 5–10 nm exciton diffusion range to the bilayer contribute to the photocurrent, this is a remarkably high value. The short circuit current decreases slightly when the thickness L_p of the polymer layer increases, approaching a value of

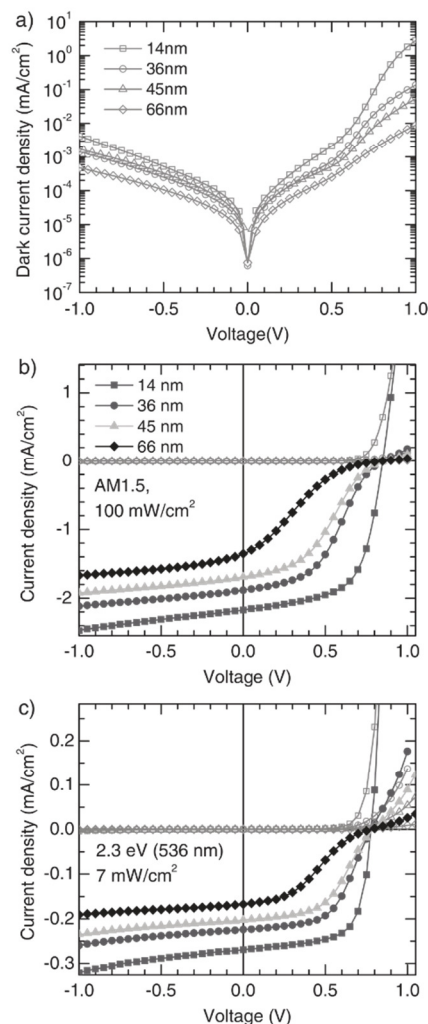


Figure 2. Current–voltage characteristics for different polymer layer thicknesses, i.e., 14 nm (squares), 36 nm (circles), 45 nm (triangles), 66 nm (diamonds), measured a) in the dark, b) under broadband excitation at AM1.5, and c) under monochromatic excitation at 536 nm (2.3 eV) at 7 mW cm⁻². The filled symbols show the total current under illumination and the open symbols the dark current for each polymer layer thickness.

1.5 mA cm⁻² for the diode with $L_p = 66$ nm. More importantly, with increasing thickness of the donor layer the JV -curves acquire an s-shape character. Since the only variable parameter of the diodes is the thickness of the donor layer it appears straightforward to associate the evolution of the s-shape character of the JV -curves upon increasing L_p with charge carrier

7. Monomolecular and bimolecular recombination of electron–hole pairs at the interface of a bilayer organic solar cell

recombination rather than with injection or extraction barriers.^[28] These experimental results at AM1.5 are consistent with reports by Yu et al. for PHJ cells made with SubPc and C₆₀, for donor thicknesses from 10 to 40 nm^[24] and with reports by Petersen et al., for PHJ cells using a merocyanine dye as donor and C₆₀ as acceptor.^[17] It seems that this recombination effect depends on hole mobility since the s-shape of the *JV*-curve is lost when the PCDTBT_{stat} is replaced by the p-DTS(FBTTh₂)₂ that has an almost 100 times higher hole mobility (Figure 1d). A similar thickness-dependence of the s-shape also appears upon monochromatic excitation of 7 mW cm⁻² of predominantly the donor at the maximum of its first absorption band (536 nm, about 2.3 eV), though it sets in at higher voltages.

Similar results are obtained for excitation at 580 nm (2.1 eV, see Figure S2 in the Supporting Information). Since the C₆₀ still absorbs weakly at 2.3 eV, yet it does not absorb at 2.1 eV (see Figure 1), all subsequent monochromatic measurements were carried out at 2.1 eV. The radiant flux of 2.1 eV photons impinging on the sample is 6.7 mW cm⁻².

A straightforward way to check whether or not the evolution of the s-shape PCDTBT_{stat}/C₆₀ diodes is indeed caused by charge carrier recombination is to measure the dependence of the photocurrent as a function of light intensity. Figure 3a shows that the short circuit photocurrents, measured at a photon energy of 2.1 eV (580 nm), are perfectly linear with incident light intensity up to 30 mW cm⁻² and even up to 100 mW cm⁻² broadband

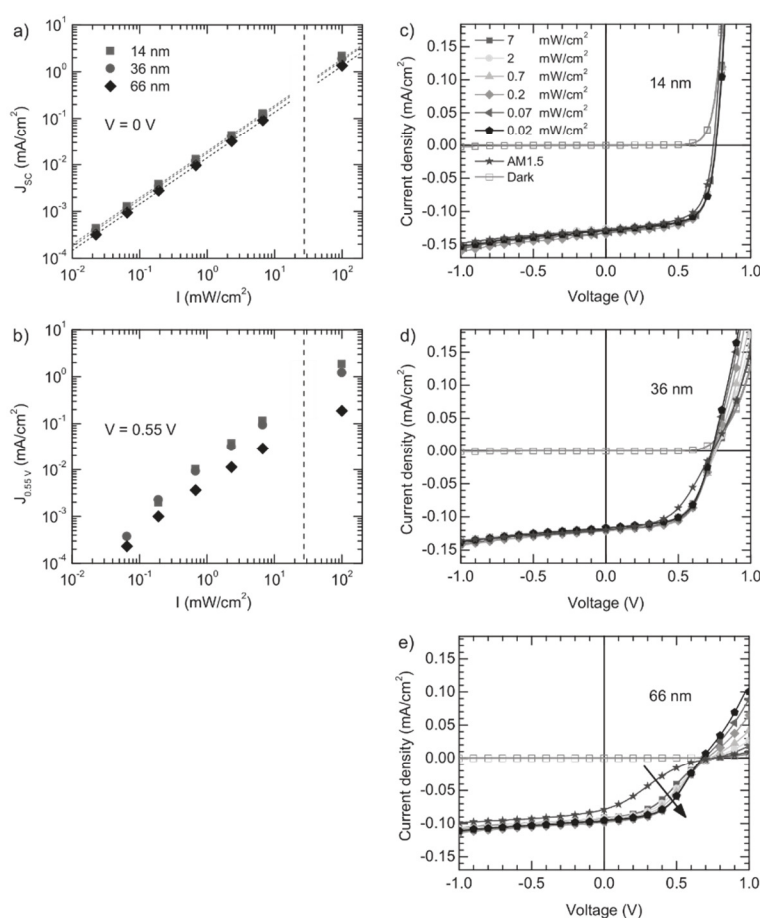


Figure 3. The total current as a function of illumination intensity, measured a) under short-circuit conditions ($V = 0$ V) and b) at $V = 0.55$ V. Values up to 30 mW cm⁻² are for monochromatic illumination at 580 nm (2.1 eV), and values at 100 mW cm⁻² are for broadband excitation at AM1.5. The dotted lines indicate a linear fit of the data points below 30 mW cm⁻². For a c) 14 nm, d) 36 nm, and e) 66 nm thick polymer layer current–voltage characteristics are shown for different light intensities at 580 nm and AM1.5 illumination. The *JV*-characteristics are normalized as described in the text.

excitation (AM1.5), suggesting that virtually no carriers are lost by bimolecular recombination. In contrast, when measuring the photocurrent closer to the open-circuit voltage, e.g., at 0.55 V (Figure 3b), we observe a deviation from linearity that implies that bimolecular processes are now dominant.

We can use the observed linear dependence of j_{SC} to normalize our JV -curves to j_{SC} , such as to compare their shapes. In Figure 3c–e, we thus assess how the light intensity affects the photocurrents as a function of voltage for different film thicknesses. Usually, comparing the JV -curves of solar cells under different high intensity illuminations is straightforward since in each case the dark current characteristic is negligible. A negligible contribution of the dark current is also tacitly assumed when calculating the fill factor, usually defined as the product of current and voltage at the maximum power point divided by the product of short-circuit current and open-circuit voltage.^[1] However, this assumption is no longer valid when the light intensity decreases by up to three orders of magnitude because the dark current stays constant while the photocurrent decreases until the photocurrent eventually becomes comparable or even smaller than the dark current. In order to avoid any artifacts associated with the dark current we subtracted the dark current from the total current, thus obtaining the photocurrent. This photocurrent was then normalized to the light intensity $I_0 = 6.7 \text{ mW cm}^{-2}$ and the dark current was added again. Thus, the normalized current is given by

$$j_{\text{normalized}}(V) = \left[j_{\text{photo}}(V) \cdot \frac{I_0}{I} \right] + j_{\text{dark}} \quad (1)$$

where j_{photo} is the photocurrent obtained under illumination with intensity I , j_{dark} is the dark current, and I_0 is our reference intensity $I_0 = 6.7 \text{ mW cm}^{-2}$. Note that if instead we had normalized the JV -curves of the total current, we would also have implicitly multiplied the dark current by the normalization factor $\frac{I_0}{I}$, thus introducing an artefact, and this is avoided by subtracting the dark current prior to the normalization and then adding it again afterwards.

Figure 3c–e compares the JV -curves obtained for different light intensities, normalized as just described to illumination with $I_0 = 6.7 \text{ mW cm}^{-2}$, for different film thicknesses. We focus on the voltage range between $V = 0 \text{ V}$ and $V = V_{OC}$. It is evident that, as V approaches V_{OC} , the JV -characteristics become more intensity dependent as the donor thickness increases. For diodes with 14 nm, the JV -curve normalized to light intensity are indistinguishable, indicating that bimolecular effects cannot be important. For $L_p = 36 \text{ nm}$ diodes, some deviation is seen upon increasing the intensity (Figure 3d) and, for $L_p = 66 \text{ nm}$, an s-shape develops (Figure 3e). The effect is more pronounced when the data measured under AM1.5 illumination are included. Figure 3 confirms that in the thicker diode bimolecular recombination becomes a loss process for photo-carriers while this is not the case in the thinnest diode.

From Figure 3, we can read out the fill factor as a function of light intensity, shown in Figure 4. We find that for the $L_p = 14 \text{ nm}$ diode, the FF remains constant at about 67% as the illumination intensity changes by four orders of magnitude. For the $L_p = 36 \text{ nm}$ diode, the FF decreases from 61% to 50%

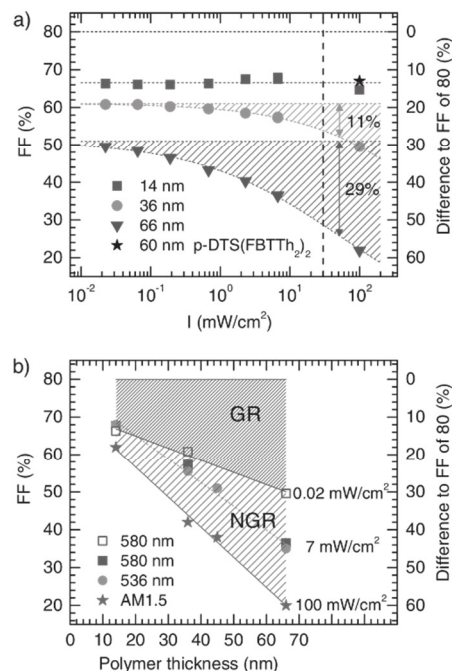


Figure 4. a) Fill factor for a polymer thickness of 14, 36, and 66 nm for different light intensities at an excitation wavelength of 580 nm. Dotted lines serve as guide to the eye. The fill factor obtained with AM1.5 illumination is also shown (on the right side of the dashed vertical line). The FF was calculated using the JV -curves shown in Figure 3. The fill factor for an identical bilayer cell made with 60 nm of the oligomer p-DTS(FBTTh₂)₂ is also shown (black star). On the right axis, the difference to an assumed ideal fill factor of 80% is indicated. The colored horizontal lines indicate the asymptotic value of the data at each thickness for infinitely low illumination, obtained by extrapolation of a fit to the data. The difference between the horizontal lines and 80% is attributed to losses due to geminate recombination, and the difference between the horizontal lines and the data points (shaded area) is attributed to losses by nongeminate recombination. The vertical arrows and associated numbers indicate the NGR losses at AM1.5 (the arrows are slightly offset from 100 mW cm^{-2} for clarity of display). b) Fill factors for different light intensities as a function of polymer layer thickness. The difference in FF between the data obtained at 0.02 mW cm^{-2} to 80% (densely shaded area) is attributed to losses by geminate recombination, and the difference between the data at 0.02 mW cm^{-2} and the data obtained at higher intensities such as 100 mW cm^{-2} is attributed to nongeminate recombination.

while in the 66 nm diode FF drops from 51% to 22% under AM1.5 (Figure 4a). For reference, we also include the FF of the 60 nm p-DTS(FBTTh₂)₂/C₆₀ diode, which is 67%, i.e., the same as in the 14 nm PCDTBT_{stat}/C₆₀ diode at any intensity.

Figure 4a allows to differentiate between the contributions of geminate and nongeminate recombination to the overall reduction in fill factor. Let us assume that, for an ideal cell in the Shockley–Queisser limit, the maximum obtainable fill factor is

80%, in agreement with simulations of Bartesaghi et al.^[5] The difference to the FF actually observed in the limit of the lowest illumination intensity can be assigned to predominantly geminate recombination. In Figure 4a, this value is indicated by a dashed line for each film thickness. The difference to this value that arises with increasing illumination intensity, however, can be attributed to nongeminate recombination losses, indicated by the shaded areas in Figure 4a. Evidently, the FF is reduced by predominantly GR for the thinnest donor layer, while the losses due to GR and NGR are equal at AM1.5 for the thickest layer investigated.

How the fill factor decreases with the thickness of the donor layer is illustrated in Figure 4b. The contributions from GR and from NGR are indicated by the red and green areas. While the FF value for the thin sample is, within the experimental error, independent of intensity, with increasing film thickness a slope arises not only for broadband illumination at AM1.5 but also for monochromatic illumination at 0.02 mW cm⁻², suggesting a thickness dependence of geminate recombination.

For the subsequent analysis it is useful to convert the *JV*-plots into plots of the photocurrent as a function of the internal electric field. We calculated the internal field *F* according to $F = (V_{\text{build-in}} - V)/(L_p + L_{\text{C60}})$, where *L_p* and *L_{C60}* are the thicknesses of the polymer donor layer and the C₆₀ layer, *V* is the voltage applied to the diode and *V_{build-in}* is the voltage at which the photocurrent equals zero. In Figure 5a, we compare the field dependence of the photocurrents for different thicknesses of the donor layer taken under low light intensity and under AM1.5. The arrows indicate the field strengths corresponding to the short-circuit conditions for the OSCs with *L_p* = 14 nm and *L_p* = 66 nm, i.e., corresponding to *V* = 0 V. While the photocurrent is independent of electric field and illumination intensities for high internal fields, (*V* < 0 V), there is a strong field dependence of the photocurrent for low internal fields, even at very low illumination intensity, which reflects the field dependence of the dissociation of eh-pairs at the interface.^[18] For reference, an internal field of 10⁴ V cm⁻¹ translates into a difference of less than 0.1 V to *V_{build-in}*.

This field dependence increases with light intensity and with increasing thickness of the polymer donor layer. The difference between the field dependent photocurrent for low and for high intensity, normalized to the current at AM1.5, is displayed in Figure 5b, from which the strong thickness dependence is particularly evident. Essentially, in Figure 5b, the current is corrected for the field dependence due to the geminate recombination, so that the data reflect the strong field and thickness dependence of the nongeminate recombination pathway. This difference between the photocurrent at high and low illumination intensities vanishes above saturation field *F_{sat}* of the photocurrent. This is the field at which all primarily generated eh-pairs are dissociated and are extracted by the electrodes. For *F* < *F_{sat}* an increasing fraction of eh-pairs execute a diffusive motion inside the coulombic capture sphere. They are thus able to return to their siblings. As their concentration increases due to more intense illumination, they find recombination partners that are not their siblings. Figure 5b shows that this nongeminate recombination is particularly field dependent for thick donor layers.

To further probe the effect of film thickness on the dissociation of CT states, we carried out Monte Carlo simulations. In

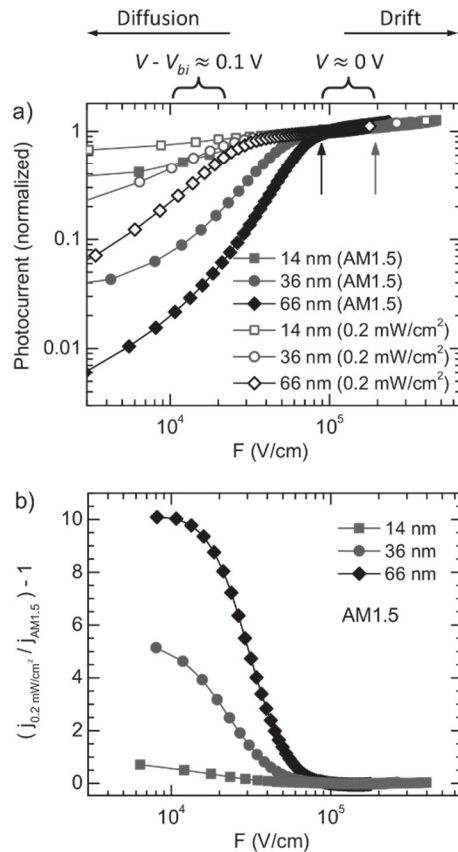


Figure 5. a) Photocurrent as a function of internal field $F = (V_{\text{build-in}} - V)/(L_p + L_{\text{C60}})$ for different polymer layer thicknesses, i.e., 14 nm (squares), 36 nm (circles), 45 nm (triangles), 66 nm (diamonds), taken under 580 nm illumination with an intensity of 0.2 mW cm⁻² (open symbols) and under AM1.5 illumination (filled symbols). The field is calculated using $V_{\text{build-in}} = 0.85$ V for all thicknesses at AM1.5 and $V_{\text{build-in}} = 0.76, 0.74,$ and 0.71 V for $L_p = 14, 36,$ and 66 nm for 580 nm excitation, respectively. The arrows indicate the field strengths corresponding to the internal field under short-circuit conditions for the OSCs with $L_p = 14$ nm (right arrow) and $L_p = 66$ nm (left arrow). b) Difference between photocurrent at 0.2 mW cm⁻² and at AM1.5, normalized to the photocurrent at AM1.5, $(j_{0.2 \text{ mW/cm}^2} - j_{\text{AM1.5}})/j_{\text{AM1.5}}$, as a function of internal field for different film thicknesses.

order to simplify the simulation we considered a bilayer OSC composed of an array of point sites with variable thickness of the donor layer, assuming that the electron remains stationary in the acceptor layer. As detailed in the methodology, the quantum yield $\phi(F)$ for electron–hole separation was calculated by averaging over 10⁶ individual trials. In each trial, we created a single electron–hole pair at the interface. We kept the electron stationary while allowing the hole to execute a random walk in the potential created by the mutual Coulomb attraction

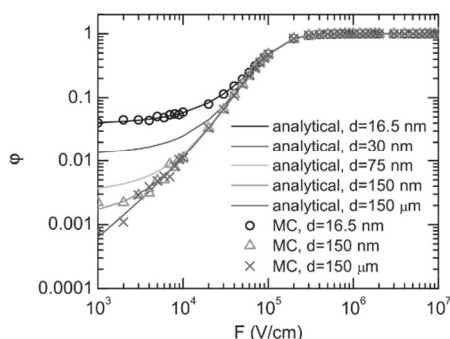


Figure 6. The probability of electron–hole separation as a function of internal field derived by Monte Carlo simulation (symbols) and derived by an analytical model (lines) for different thicknesses L_p of the polymer layer as described in the text.

and the applied field. The trial was over when the hole reached either the collecting electrode or when it recombined with the electron. In this simulation, only monomolecular recombination is taken into account since only one electron–hole pair is considered for each trial. In addition to the MC simulations, we have also used an analytical expression to calculate the field dependent separation efficiency as developed by Rubel et al.^[44] (see Section 5) which is in perfect agreement with the MC simulation. Compared to the experiment displayed in Figure 5, **Figure 6** shows that the simulations predict a qualitatively similar shape of the dissociation yield as a function of field and, moreover, a similar evolution with film thickness as observed experimentally. The simulations do, however, predict a larger saturation field than found in experiment because in the simulation we ignored the effect that a low effective mass of the conjugated polymer has on the dissociation yield.^[45] However, this does not alter the conclusions regarding the thickness dependence of recombination at low fields. In **Figure 6** we see that the photocurrent yield is enhanced when the thickness of the donor transport layer is of the order of the Langevin capture radius (≈ 16 nm) and the yield reduces considerably with thicknesses up to ≈ 150 nm.

3. Discussion

Let us first summarize the essential experimental results. (i) In bilayer solar cells made with two different donors yet the same donor layer thickness of about 60 nm, a s-shape occurs for the donor with the lower hole mobility, yet not for the donor with the higher hole mobility, consistent with Tress et al.^[27] (ii) The short circuit photocurrent in the bilayer diodes is linear with light intensity but when the applied voltage approaches V_{OC} , the JV -curves acquire s-shape character as the thickness of the donor layer increases (Figures 2 and 3). (iii) The fill factors increase and finally saturate at decreasing light intensity, and the saturation values decrease with increasing donor layer thickness (Figure 4). (iv) Losses in FF increase with increasing

film thickness for both, geminate recombination and non-geminate recombination. (v) Above a critical electric field, F_{sat} , the photocurrent is saturated. For $F < F_{sat}$ the photocurrent decreases. This effect is stronger (i.e., the slope dj/dF is steeper) with increasing donor layer thickness and with increasing light intensity (Figure 5). (vi) The Monte Carlo simulations carried out in a strictly monomolecular regime reproduce the field and thickness dependence of the photocurrent that is experimentally observed.

Based upon the present experimental results we shall critically examine the role of monomolecular, i.e., geminate, recombination and of bimolecular, nongeminate recombination in organic solar cells, in particular with a view to the thickness dependence of the JV -curves.

The basic idea to account for the thickness dependence of the JV -curves is to consider the balance between charge extraction at the electrode and recombination of the electron–hole pair.^[17,24] We stress that this is a field-dependent process. Let us first attend to the regime of very low excitation density, represented in the Monte Carlo simulation (Figure 6) and in the JV -curves under monochromatic illumination as displayed in Figures 2 and 5. After generation of an electron–hole pair, its hole diffuses in the combined potential of the Coulomb attraction by the electron and the internal field. If it does not leave the Langevin capture radius before recombining with the electron, i.e., if it has not truly been separated from its sibling electron, this is termed primary geminate recombination according to the IUPAC goldbook definition.^[46] The Coulomb capture radius, i.e., the Langevin radius, is given by $r_{Coul} = \frac{e^2}{4\pi\epsilon k_B T}$, and it is about 16 nm for a material with dielectric constant of 3.5. We note that due to energetic disorder and charge delocalization this is not a well-defined, sharp boundary but rather a blurred out range. Primary geminate recombination does not play a role in the thickness dependence of the photocurrent yield, as in our case the polymer donor layer was always equal or larger than the Langevin capture radius. However, in particular at low internal fields, i.e., close to V_{OC} , it is also possible for the hole to separate from the electron by diffusing out of the Langevin capture radius, yet to enter it again at a later stage in its diffusive motion such as to return to its sibling electron. In chemical kinetics, recombination with the initial sibling countercharge after separation is known as secondary geminate recombination.^[46]

Clearly, the rate of secondary geminate recombination depends on the thickness of the polymer donor layer. The thinner the polymer layer, the more likely it is that the hole in its diffusive motion meets the extracting electrode rather than returning to the electron. This is particularly true close to V_{OC} , i.e., in the low field regime, where the diffusive regime is prominent. The overall efficiency of geminate recombination is then controlled by the competition between a thickness-dependent charge extraction rate and a recombination rate that is independent of thickness. This is analogous to the well-known competition between NGR and extraction of free charges.^[5] We therefore conclude that geminate recombination reduces the photocurrent close to V_{OC} , i.e., for low internal fields (Figure 5a), with this process being particularly important for thicker polymer donor layers. Geminate recombination thus is

also responsible for a reduction in fill factor (Figure 4a) under low light intensities, i.e., in the monomolecular regime.

We shall now discuss the evolution of the shape of the *JV*-curves as well the fill factor at higher light intensities. In addition to the monomolecular, geminate recombination processes, bimolecular processes can occur. The obvious process is nongeminate recombination from charges that, after photoexcitation, diffused out of their Langevin radius and return diffusively to the interface such as to recombine with another opposite charge there. The probability for this process increases with both light intensity and thickness of the donor layer. It will also become more probably for lower fields that enable diffusive return toward the interfacial layer. A further process that is possible is that one geminately bound pair can recombine with another geminately bound pair. While such a recombination of still primarily bound geminate pairs will also depend on intensity and field, it will not depend on film thickness. The ratio in the field dependence of the photocurrent for low and high intensity is displayed in Figure 5b. The stronger sensitivity to field for thick donor layers as compared to thinner donor layers thus directly reflects the increase in nongeminate recombination compared to the geminate recombination channel. For fields exceeding the saturation field, there is no thickness dependence since the charges are free, so that there is neither geminate nor nongeminate recombination.

So far, we have analyzed the *JV*-curve in the framework of considering geminate and nongeminate recombination. The appearance of an s-shape can, however, also be related to other factors. In particular, barriers to charge extraction or injection, as well as low or unbalanced carrier mobilities have been identified as causes for low fill factors and s-shaped *JV*-curves.^[27,28,47,48] In our studies, the only parameter that has been varied was the thickness of the donor layer. The appearance of an s-shaped kink can therefore not be attributed to energy barriers or mobilities, as none of these change with film thickness.

Tress et al. further highlighted the role of low mobility and of imbalanced carrier mobility in reducing the fill factor of organic solar cells. Based on drift-diffusion simulations, Tress concludes that low carrier mobilities as well as imbalanced carrier mobilities lead to a high carrier density at the donor–acceptor interface, thus promoting recombination.^[27] The key point of his argument is thus based on considering the carrier density. An increased recombination due to charge accumulation at the interface is also brought forward by Yu et al. to account for the appearance of an s-shape with donor layer thickness in SubPc/C₇₀ based PHJ cells.^[24] Consistent with their reasoning, we also find that an increased excitation density enhances recombination by adding the NGR channel. However, our key argument goes beyond this and also applies in the limit of vanishing carrier density. Charge accumulation at the interface is not required to reduce the fill factor. This is important as it implies that the carrier density does not need to be high or even in the range of the capacitor charge for the FF to be reduced by recombination losses.^[7]

Clearly, the rate of carrier extraction, which prevents recombination, increases with mobility, even in the limit of considering a single electron–hole pair prone to geminate recombination. In the diffusive regime near V_{OC} , the diffusion range L_p depends

on the diffusivity D by $L_p = \sqrt{D\tau}$, with τ being the carrier lifetime. Diffusivity is directly proportional to the carrier mobility by the Einstein relation $eD = \mu kT$. The probability of a hole to diffuse to the collecting electrode rather than to return to its sibling electron, i.e., the extraction rate, therefore increases with mobility. In this way, increasing mobility increases the photocurrent yield near V_{OC} and improves the fill factor even in the regime of low illumination intensity and in the limit of vanishing carrier density. This microscopic picture accounts for the observation by Proctor et al.,^[31] that changes in morphology reduce both losses due to GR and NGR.

In a similar way, increasing the delocalization of charges should, and in fact does, also improve the extraction rate.^[45,49–51] One factor that contributes to this is that excited states or charges that are well delocalized, i.e., with an extended wavefunction, can diffuse further in a disordered environment than localized charges due to geometric reasons.^[52] A second, and perhaps more important factor relates to the fact that the binding energy of the eh-pair is reduced by an additional energy term when the eh-pair is more delocalized. In the case of on-chain wavefunction delocalization of a hole along a polymer chain, this additional energy arises from the zero-point oscillation of the delocalized hole in the pair potential. Mathematically, it can be expressed via a reduced effective mass of the hole, that can be as low as 0.1 times the electron mass for planarized or well-ordered polymers.^[45,53] A similar effect can arise for crystalline assemblies of donor or acceptor molecules. An additional 200 meV of electrostatic energy has, for example, been reported by Gélinas et al. due to electron delocalization in ordered regions of the fullerene acceptor material.^[50]

4. Conclusions

The stimulant for this work was that we wondered why in a thin bilayer OSC the fill factor can be as high as about 70% but decreases with increasing thickness of the polymeric donor layer (L_p). To this end we measured the *JV*-characteristics of bilayer diodes composed of PCDTBT_{stat} donor layers with thicknesses ranging from 14 nm and 66 nm and a 30 nm thick C₆₀ acceptor layer and light intensities ranging from 0.02 to 100 mW cm⁻². We find that at low light intensities the diode characteristics is strictly linear in intensity but the fill factor decreases from 67% to 50% when the thickness of the donor layer L_p increases from 14 nm to 66 nm. Supported by Monte Carlo simulations we argue that this decrease of FF is a signature of GR of holes that initially escaped from the Langevin capture sphere but can diffuse back toward the interface and can recombine with their siblings. The presence of an exit electrode prevents back diffusion. Therefore the trade-off between GR and charge extraction becomes thickness dependent up to a layer thickness of a multiple of the Langevin capture radius.

Since GR is ultimately limited by the nonradiative decay of the charge transfer states at the donor–acceptor interface, the efficiency of hole extraction should increase with hole diffusivity, i.e., hole mobility. Experiments with a diode in which the polymeric donor has been replaced by a 60 nm thick p-DTS(FBTTh₂)₂ layer that has an about 100 times higher hole mobility confirms this expectation. The FF of a 60 nm

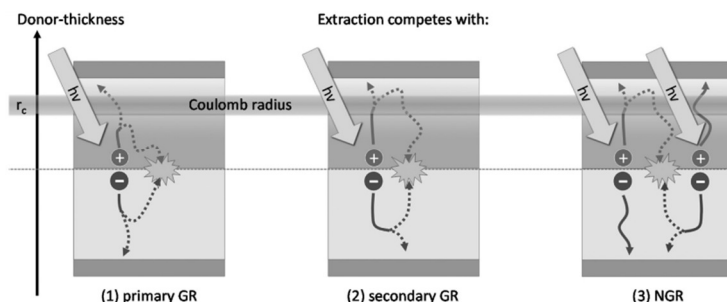


Figure 7. Schematic illustrating the competition between recombination at the donor–acceptor interface and extraction at the electrode for the monomolecular process of geminate recombination and for the bimolecular process of nongeminate recombination. r_c denotes the Coulomb capture radius (Langevin radius).

OSC with p-DTS(FBTTh₂)₂ at AM1.5 has a higher value than the FF of a PCDTBT_{stat} OSC with same thickness at 0.02 mW cm⁻². Hence, the total losses of the p-DTS(FBTTh₂)₂ cell, i.e., GR and NGR, must be lower than the GR of the PCDTBT_{stat} OSC (Figure 4). Thus, our results show that the limitation to the FF that is imposed by GR can be overcome by increasing the charge mobility. However, we stress that this effect is diffusion controlled, and consequently mobility controlled rather than controlled by interfacial charging, as is the case of NGR.^[24]

As the light intensity increases and finally approaches AM1.5 the *JV*-curves acquire an s-shape that becomes more pronounced as the layer thickness increases. This is a signature of the onset of bimolecular, i.e., nongeminate recombination, at the donor–acceptor interface. As is well known, ultimately the diode efficiency is controlled by the trade-off between – the thickness dependent – extraction and NGR. The effect of NGR depends strongly on the internal electric field and film thickness (Figure 5b) due to interfacial charging.^[24] Since the primary dissociation of charge transfer states at the interface is a field-assisted process, at lower electric field more eh-pairs exist near the donor–acceptor interface, so that a back-diffusing charge can easily find a recombination partner other than their siblings.

The overall picture is summarized in Figure 7. At low light intensity, a hole executing a random walk within the Coulomb capture radius of its electron may recombine with its sibling prior to any escape (primary GR). If it diffuses out of the Coulomb capture radius, it may be extracted at the electrode or it may diffuse back into the Coulomb capture radius such as to recombine with its sibling (secondary GR). Both processes are monomolecular. At high intensity, NGR will occur as additional, bimolecular process, as described above. In the framework of this microscopic picture it becomes evident why any process that improves charge carrier mobility, e.g., increasing the degree of (short-range) order in a film by processing, reduces not only losses due to NGR but also losses due to GR through enhancing the extraction rate.^[31]

Our results show that simple *JV*-experiments of bilayer OSCs with variable layer thickness and variable light intensity provide a simple tool to quantify the effect of GR and NGR because the origins of recombination – be it geminate or nongeminate – and charge extraction are spatially separated.

5. Experimental Section

The compound p-DTS(FBTTh₂)₂ was synthesized as described by van der Poll et al.^[35]

Synthesis of the Polymer PCDTBT_{0.7}/TPDDBT_{0.3} (PCDTBT_{stat}): PCDTBT_{stat} (poly[(*N*-heptadecan-9'-yl)-2,7-carbazole-*alt*-5,5-(4',7'-bis-(4-hexylthien-2-yl)-2',1',3'-benzothiadiazole)]_{0.7}-*stat*-[*N,N'*-bis(4-methylphenyl)-*N,N'*-diphenylbenzidine-*alt*-5,5-(4',7''-bis-(4-hexylthien-2-yl)-2',1',3'-benzothiadiazole)]_{0.3}) was synthesized via Suzuki coupling according to the following procedure. The molar ratio of the carbazole, the phenyl-substituted benzidine, and the bisthieryl-benzothiadiazole units in PCDTBT_{stat} was 0.7:0.3:1.

A Schlenk flask was charged with the monomers 2,7-bis-(4',4',5',5'-tetramethyl-1',3',2'-dioxaborolan-2'-yl)-*N*-(heptadecan-9''-yl)-carbazole (0.368 g, 0.560 mmol), *N,N'*-bis(4-methylphenyl)-*N,N'*-bis((4',4',5',5'-tetramethyl-1',3',2'-dioxaborolan-2'-yl)phenyl)-benzidine (0.184 g, 0.239 mmol), 4,7-bis(5'-bromo-4'-hexylthien-2'-yl)-2,1,3-benzothiadiazole (0.501 g, 0.800 mmol) and 12 mL of toluene under argon. One drop of Aliquat 336 and 20 mL of 2 M Na₂CO₃ solution were added and the mixture was degassed by three freeze–thaw cycles. Afterward 14 mg of tetrakis(triphenylphosphine)palladium(0) were added and followed by again three freeze–thaw cycles. The reaction mixture was then stirred under reflux in an argon atmosphere for 90 h before bromobenzene (0.126 g, 0.800 mmol) was added. After 2 h phenylboronic acid (0.098 g, 0.800 mmol) was added and the reaction mixture was again refluxed overnight. The reaction mixture was allowed to cool to room temperature and the polymer was precipitated into methanol/water (10:1). Soxhlet extraction was carried out using acetone and toluene. The reduced toluene fraction was precipitated into methanol/water (10:1) and dried in vacuum overnight, yielding 0.669 g (93%) of PCDTBT_{stat} as a dark-red powder. A molecular weight of 47 000 gmol⁻¹ (M_w) and 18 000 gmol⁻¹ (M_n) was determined by size exclusion chromatography in THF solution with a polydispersity index of 2.56 (polystyrene calibration). The ionization potential was determined by photoelectron spectroscopy to be –5.2 eV. Adding the photon energy at maximum of the first absorption band yields –2.9 eV as a rough estimate for the ionization potential.

¹H NMR (300 MHz, C₂D₂Cl₄, 120 °C): δ = 0.75–0.95 (m, CH₃), 1.05–1.55 (m, CH₂), 1.75 (br, thiophene–CH₂), 2.04 (br, carbazole–CH₂), 2.23–2.44 (m, benzidine–CH₃, carbazole–CH₂), 2.63–2.95 (m, thiophene–CH₂), 4.62 (br, CH), 6.92–8.22 (m, ar–CH). Broadened and multiple signals were due to atropisomerism. From the integration of the signal for the CH₂ group in the swallow-tail spacer of the carbazole unit (2.04 ppm), the combined signal for the methyl group in the benzidine units and the other CH₂ group in the carbazole spacer (2.23–2.44 ppm), and the signal for the CH₂ groups in the hexyl spacer of the thiophene (1.75 ppm), a molar ratio of 0.7:0.3:1 was calculated (for ¹H NMR spectrum see the Supporting Information).

Experiments: To fabricate the bilayer solar cells, ITO-coated substrates were covered with a patterned photoresist as described by Schwarz et al.^[54] A 15 nm thick MoO₃ (Sigma Aldrich) layer was evaporated on top of it. The donor (PCDTBT_{stat} or p-DTS(FBTTh₂)₂) was spun onto this from chlorobenzene solution (7.0 mg mL⁻¹). The thickness of the donor layer was controlled with a Dektak (Veeco) profilometer. The donor was covered by subsequent thermal evaporation of a 30 nm thick C₆₀ layer and a 100 nm thick aluminum cathode. The devices were annealed at 140 °C for 15 min. The complete solar cell fabrication was done in a nitrogen atmosphere using a glovebox with direct access to the evaporation chamber. In Figure S1 in the Supporting Information, additional measurements were also carried out on samples where (i) the annealing step was omitted, or (ii) annealing was omitted and a 5 nm thick BCP layer was evaporated between C₆₀ and aluminum, or (iii) annealing was carried out for 15 min after C₆₀ evaporation, prior to deposition of a 5 nm thick BCP layer and aluminum. Since it turned out that the shape of the JV-curves is in dependent on the diode preparation the authors used annealed samples with the structure ITO/MoO₃/donor/C₆₀/Al since these feature particularly low dark current.

The current–voltage characteristics were measured in vacuum at room temperature under either broad band AM1.5 illumination employing a Newport sun simulator or under monochromatic illumination at 536 nm (2.3 eV) or 580 nm (2.1 eV), provided by a 450 W Xenon lamp (Osram) using a commercial monochromator. In the latter case the incident light intensity was varied by neutral optical density (OD) filters with optical densities of 0.5, 1.0, 1.5, 2.0, and 2.5. The light intensity impinging on the diode was measured using a Hamamatsu S1337-33BQ photodiode. Without OD filter, it was 7.1 mW cm⁻² for 536 nm and 6.7 mW cm⁻² for 580 nm. The photocurrents were measured with a Keithley 236 and 238 source-measure-unit.

To determine the fill factor of the photodiode at variable light intensities, both the dark current $j_{\text{dark}}(V)$ as well as the total current $j(V)$ under illumination were measured. The difference is the photocurrent $j_{\text{photo}}(V) = j(V) - j_{\text{dark}}(V)$. At low light intensities, one needs to take account of the fact that the dark current is independent on intensity while the photocurrent decreases with decreasing intensity. The authors did this by normalizing the photocurrent to the monochromatic light intensity without optical density (OD) filter. To do this, the photocurrent is multiplied by the ratio of the light intensity of monochromatic light without and with OD filters, and the dark current is added subsequently

$$j_{\text{normalized}}(V) = \left[j_{\text{photo}}(V) \frac{I_0}{I_0'} \right] + j_{\text{dark}} \quad (2)$$

When the photocurrent is displayed as a function of internal field, the field was determined according to $F = (V_{\text{build-in}} - V)/(L_p - L_{\text{C60}})$, with L_p being the layer of the polymer donor layer and L_{C60} being the thickness of the C₆₀ acceptor layer (30 nm). The fields in the solar cells were calculated using $V_{\text{build-in}}$ which was approximated by the voltage at which the photocurrent equals zero.

MIS-CELIV measurements were performed according to the procedure described in literature.^[55,56] For both materials the same parameters were used. The layer thickness of p-DTS(FBTTh₂)₂ was 100 nm and for PCDTBT_{stat} 121 nm. A hole injection layer of 6 nm MoO₃ was used. The voltage was supplied by a Rigol DG4102 function generator. The slope of the voltage ramp, the offset voltage, and the length of the voltage pulse were fixed to 0.1 V μs⁻¹, 7 V, and 100 μs, respectively, for all measurements, to make sure that experimental conditions are identical for all compounds and samples. This ensures that observed trends and effects may be attributed to materials. The resulting current response signal was amplified using a Femto DHPCA-100 current amplifier and recorded with a Tektronix TDS3000 digital phosphor oscilloscope. In all the measurements the authors applied a prebias voltage of 7 V for one minute to ensure equilibrium conditions.

Monte Carlo Simulations: The authors performed Monte Carlo simulations to model the extraction efficiency in a bilayer device as a function of the electric field for different donor layer thicknesses. The system consisted of a 1D array of points with a separation distance $a = 1.5$ nm and an interface at origin. At $t = 0$ a hole and an electron

were placed in an adjacent configuration at the interface with a minimal separation. The electron position was fixed while the hole was allowed to move between neighboring points with a hopping rate $\nu_{i,j}$ given by a Miller–Abrahams expression

$$\nu_{i,j} = \begin{cases} \nu_0 e^{-2\alpha r_{ij}} e^{-\left(\frac{\epsilon_j - \epsilon_i}{k_B T}\right)}, & \epsilon_j > \epsilon_i \\ \nu_0 e^{-2\alpha r_{ij}}, & \epsilon_j \leq \epsilon_i \end{cases} \quad (3)$$

where i is the hole residence site and j the target neighboring site, separated by a distance r_{ij} . The site energies ϵ_i and ϵ_j include contributions from the Coulomb potential due to the presence of the electron at the interface and the voltage drop due to the externally applied field. The attempt-to-hop frequency was set to $\nu_0 = 10$ ps⁻¹, the relative permittivity to $\epsilon_r = 4$, and the inverse localization length to $\alpha = 2$ nm⁻¹. At each Monte Carlo step the authors calculate a waiting time for each hopping event: $\tau_{ij} = -\frac{1}{\nu_{i,j}} \ln X$ and a waiting time for recombination between the electron–hole pair: $\tau_r = -\tau \ln X$, where τ is the electron–hole pair lifetime that increases exponentially with electron hole distance r_{eh} as $\tau = \tau_0 e^{2\alpha(r_{\text{eh}} - a)}$ and X is a random number from a box distribution between 0 and 1. The lifetime at close proximity is $\tau_0 = 1000t_0$ with t_0 being the minimum hopping time $t_0 = \frac{1}{\nu_0} e^{2\alpha a}$.

The event with the smallest waiting time is selected and executed. If the accepted event was a hop, then the authors updated the site of the hole and recalculated waiting times. If the chosen event was recombination, the authors removed the charges and started a new trial. Each trial terminated successfully when the electron–hole distance was larger than a given separation distance d , ranging from 16.5 nm to 150 μm. By averaging over 10⁶ trials the authors calculated the quantum yield for separation as: $\varphi(F) = \frac{N_{\text{sep}}(F)}{N_{\text{tot}}(F)}$, where $N_{\text{sep}}(F)$ is the number of successful trials for an applied field F and $N_{\text{tot}}(F)$ the total number of trials.

The authors also used an analytical expression to calculate the field dependent separation efficiency $\varphi(F)$ as developed by Rubel et al.^[44] This is derived from a rate equation model and reads

$$\varphi(F) = 1 - \frac{\sum_{i=1}^{n-1} \nu_{i,i+1}^{-1} e^{-\left(\frac{\epsilon_i - \epsilon_1}{k_B T}\right)}}{\tau_0 + \sum_{i=1}^{n-1} \nu_{i,i+1}^{-1} e^{-\left(\frac{\epsilon_i - \epsilon_1}{k_B T}\right)}} \quad (4)$$

where ϵ_1 is the energy of the initially placed hole site at the interface right next to the electron and the index i runs from 1 to $n - 1$ with n being the site at distance d from the interface at which the authors considered that the hole was separated. The forward, with respect to the field direction, hopping rates $\nu_{i,i+1}$ were given by the Miller–Abrahams expression described above.

Supporting Information

Supporting Information is available from the Wiley Online Library or from the author.

Acknowledgements

The authors acknowledge financial support by the Bavarian State Ministry of Science, Research, and the Arts through the Collaborative Research Network “Solar Technologies go Hybrid”, by the Volkswagen foundation and by the German Science Foundation DFG through the doctoral training center “GRK 1640.” This project further received funding from the Universidad Carlos III de Madrid, the European Union’s Seventh Framework Programme for research, technological development and demonstration under grant agreement no. 600371, el Ministerio de

7. Monomolecular and bimolecular recombination of electron–hole pairs at the interface of a bilayer organic solar cell

Economía y Competitividad (COFUND2014-51509), el Ministerio de Educación, cultura y Deporte (CEI-15-17), and Banco Santander. M.R. additionally acknowledges support from the Hanns Seidel Foundation for a stipend through funds from the German Ministry of Education and Research (BMBF). T.-Q.N. thanks the Office of Naval Research (#N000141410076) for the support. Furthermore, the authors would like to thank the anonymous referees for helpful suggestions.

Received: September 21, 2016
Published online: November 23, 2016

- [1] A. Köhler, H. Bässler, *Electronic Processes in Organic Semiconductors: An Introduction*, Wiley-VCH, Weinheim, Germany, 2015.
- [2] P. Würfel, *Physics of Solar Cells*, Wiley-VCH, Weinheim, Germany, 2005.
- [3] N. C. Giebink, C. P. Wiederrecht, M. R. Wasielewski, S. R. Forrester, *Phys. Rev. B* **2011**, *83*, 195326.
- [4] B. Liu, R. Q. Png, J. K. Tan, P. K. H. Ho, *Adv. Energy Mater.* **2014**, *4*, 1200972.
- [5] D. Bartsaghi, I. D. Perez, J. Kniepert, S. Roland, M. Turbiez, D. Neher, L. J. A. Koster, *Nat. Commun.* **2015**, *6*, 7083.
- [6] M. Stollerfoht, A. Armin, B. Philippa, R. D. White, P. L. Burn, P. Meredith, G. Juska, A. Pivrikas, *Sci. Rep.* **2015**, *5*, 9949.
- [7] M. Stollerfoht, B. Philippa, S. Shoaee, H. Jin, W. Jiang, R. D. White, P. L. Burn, P. Meredith, A. Pivrikas, *J. Phys. Chem. C* **2015**, *119*, 26866.
- [8] L. J. A. Koster, E. C. P. Smits, V. D. Mihailetchi, P. W. M. Blom, *Phys. Rev. B* **2005**, *72*, 085205.
- [9] L. J. A. Koster, V. D. Mihailetchi, P. W. M. Blom, *Appl. Phys. Lett.* **2006**, *88*, 093511.
- [10] P. W. M. Blom, V. D. Mihailetchi, L. J. A. Koster, D. E. Markov, *Adv. Mater.* **2007**, *19*, 1551.
- [11] N. Christ, S. W. Kettlitz, S. Valouch, J. Mescher, M. Nintz, U. Lemmer, *Org. Electron* **2013**, *14*, 973.
- [12] C. L. Braun, *J. Chem. Phys.* **1984**, *80*, 4157.
- [13] V. D. Mihailetchi, L. J. A. Koster, J. C. Hummelen, P. W. M. Blom, *Phys. Rev. Lett.* **2004**, *93*, 216601.
- [14] J. A. Barker, C. M. Ramsdale, N. C. Greenham, *Phys. Rev. B* **2003**, *67*, 075205.
- [15] N. C. Giebink, B. E. Lassiter, G. P. Wiederrecht, M. R. Wasielewski, S. R. Forrester, *Phys. Rev. B* **2010**, *82*, 155306.
- [16] A. Ojala, A. Petersen, A. Fuchs, R. Lovrincic, C. Polking, J. Trollmann, J. Hwang, C. Lennartz, H. Reichelt, H. W. Hoffken, A. Pucci, P. Erk, T. Kirchartz, F. Würthner, *Adv. Funct. Mater.* **2012**, *22*, 86.
- [17] A. Petersen, A. Ojala, T. Kirchartz, T. A. Wagner, F. Würthner, U. Rau, *Phys. Rev. B* **2012**, *85*, 245208.
- [18] R. A. Marsh, J. M. Hodgkiss, R. H. Friend, *Adv. Mater.* **2010**, *22*, 3672.
- [19] S. Albrecht, W. Schindler, J. Kurpiers, J. Kniepert, J. C. Blakesley, I. Dumsch, S. Allard, K. Fostiropoulos, U. Scherf, D. Neher, *J. Phys. Chem. Lett.* **2012**, *3*, 640.
- [20] D. Veldman, O. Ipek, S. C. J. Meskers, J. Sweelssen, M. M. Koetse, S. C. Veenstra, J. M. Kroon, S. S. van Bavel, J. Loos, R. A. J. Janssen, *J. Am. Chem. Soc.* **2008**, *130*, 7721.
- [21] C. G. Shuttle, R. Hamilton, B. C. O'Regan, J. Nelson, J. R. Durrant, *Proc. Natl. Acad. Sci. USA* **2010**, *107*, 16448.
- [22] T. M. Clarke, J. R. Durrant, *Chem. Rev.* **2010**, *110*, 6736.
- [23] M. Gluecker, A. Foertig, V. Dyakonov, C. Deibel, *Phys. Status Solidi RRL* **2012**, *6*, 337.
- [24] H. M. Yu, R. C. Yi, J. W. Zhang, A. R. Yu, H. Peng, J. J. Qin, X. Y. Hou, *J. Phys. D: Appl. Phys.* **2016**, *49*, 205105.
- [25] D. Credgington, Y. Kim, J. Labram, T. D. Anthopoulos, J. R. Durrant, *J. Phys. Chem. Lett.* **2011**, *2*, 2759.
- [26] R. Mauer, I. A. Howard, F. Laquai, *J. Phys. Chem. Lett.* **2010**, *1*, 3500.
- [27] W. Tress, A. Petrich, M. Hummert, M. Hein, K. Leo, M. Riede, *Appl. Phys. Lett.* **2011**, *98*, 063301.
- [28] W. Tress, A. Merten, M. Furno, M. Hein, K. Leo, M. Riede, *Adv. Energy Mater.* **2013**, *3*, 631.
- [29] F. Etzold, I. A. Howard, R. Mauer, M. Meister, T. D. Kim, K. S. Lee, N. S. Baek, F. Laquai, *J. Am. Chem. Soc.* **2011**, *133*, 9469.
- [30] A. Foertig, J. Kniepert, M. Gluecker, T. Brenner, V. Dyakonov, D. Neher, C. Deibel, *Adv. Funct. Mater.* **2014**, *24*, 1306.
- [31] C. M. Proctor, S. Albrecht, M. Kuik, D. Neher, T. Q. Nguyen, *Adv. Energy Mater.* **2014**, *4*, 1400230.
- [32] S. Albrecht, J. R. Tumbleston, S. Janietz, I. Dumsch, S. Allard, U. Scherf, H. Ade, D. Neher, *J. Phys. Chem. Lett.* **2014**, *5*, 1131.
- [33] S. Albrecht, S. Janietz, W. Schindler, J. Frisch, J. Kurpiers, J. Kniepert, S. Inal, P. Pingel, K. Fostiropoulos, N. Koch, D. Neher, *J. Am. Chem. Soc.* **2012**, *134*, 14932.
- [34] F. Gao, J. P. Wang, J. C. Blakesley, I. C. Hwang, Z. Li, N. C. Greenham, *Adv. Energy Mater.* **2012**, *2*, 956.
- [35] T. S. van der Poll, J. A. Love, T. Q. Nguyen, G. C. Bazan, *Adv. Mater.* **2012**, *24*, 3646.
- [36] M. A. Faist, T. Kirchartz, W. Gong, R. S. Ashraf, I. McCulloch, J. C. de Mello, N. J. Ekins-Daukes, D. D. C. Bradley, J. Nelson, *J. Am. Chem. Soc.* **2012**, *134*, 685.
- [37] J. H. Seo, S. J. Kang, C. Y. Kim, S. W. Cho, K. H. Yoo, C. N. Whang, *Appl. Surf. Sci.* **2006**, *252*, 8015.
- [38] J. Niederhausen, P. Amsalem, A. Wilke, R. Schlesinger, S. Winkler, A. Vollmer, J. P. Rabe, N. Koch, *Phys. Rev. B* **2012**, *86*, 081411.
- [39] K. Akaike, K. Kanai, H. Yoshida, J. Tsutsumi, T. Nishi, N. Sato, Y. Ouchi, K. Seki, *J. Appl. Phys.* **2008**, *104*, 023710.
- [40] Z. L. Guan, J. B. Kim, H. Wang, C. Jaye, D. A. Fischer, Y. L. Loo, A. Kahn, *Org. Electron* **2010**, *11*, 1779.
- [41] B. P. Rand, J. G. Xue, S. Uchida, S. R. Forrester, *J. Appl. Phys.* **2005**, *98*, 124902.
- [42] G. A. H. Wetzelaer, M. Kuik, M. Lenes, P. W. M. Blom, *Appl. Phys. Lett.* **2011**, *99*, 153506.
- [43] P. de Bruyn, A. H. P. van Rest, G. A. H. Wetzelaer, D. M. de Leeuw, P. W. M. Blom, *Phys. Rev. Lett.* **2013**, *111*, 186801.
- [44] O. Rubel, S. D. Baranovskii, W. Stolz, F. Gebhard, *Phys. Rev. Lett.* **2008**, *100*, 196602.
- [45] C. Schwarz, S. Tscheuschner, J. Frisch, S. Winkler, N. Koch, H. Bässler, A. Köhler, *Phys. Rev. B* **2013**, *87*, 155205.
- [46] K. J. Laidler, *Pure Appl. Chem.* **1996**, *68*, 149.
- [47] J. Wagner, M. Gruber, A. Wilke, Y. Tanaka, K. Topczak, A. Steindamm, U. Hormann, A. Opitz, Y. Nakayama, H. Ishii, J. Pflaum, N. Koch, W. Brütting, *J. Appl. Phys.* **2012**, *111*, 054509.
- [48] J. Nelson, J. Kirkpatrick, P. Ravirajan, *Phys. Rev. B* **2004**, *69*, 035337.
- [49] S. Tscheuschner, H. Bässler, K. Huber, A. Köhler, *J. Phys. Chem. B* **2015**, *119*, 10359.
- [50] S. Gelinias, A. Rao, A. Kumar, S. L. Smith, A. W. Chin, J. Clark, T. S. van der Poll, G. C. Bazan, R. H. Friend, *Science* **2014**, *343*, 512.
- [51] A. A. Bakulin, A. Rao, V. G. Pavelyev, P. H. M. van Loosdrecht, M. S. Pshenichnikov, D. Niedzialek, J. Cornil, D. Beljonne, R. H. Friend, *Science* **2012**, *335*, 1340.
- [52] S. Athanasopoulos, S. T. Hoffmann, H. Bässler, A. Köhler, D. Beljonne, *J. Phys. Chem. Lett.* **2013**, *4*, 1694.
- [53] B. B. Y. Hsu, C. M. Cheng, C. Luo, S. N. Patel, C. Zhong, H. T. Sun, J. Sherman, B. H. Lee, L. Ying, M. Wang, G. C. Bazan, M. Chabinyc, J. L. Brédas, A. Heeger, *Adv. Mater.* **2015**, *27*, 7759.
- [54] C. Schwarz, H. Bässler, I. Bauer, J. M. Koenen, E. Preis, U. Scherf, A. Köhler, *Adv. Mater.* **2012**, *24*, 922.
- [55] G. Juska, N. Nekrasas, K. Genevicius, *J. Non-Cryst. Solids* **2012**, *358*, 748.
- [56] A. Armin, G. Juska, M. Ullah, M. Velusamy, P. L. Burn, P. Meredith, A. Pivrikas, *Adv. Energy Mater.* **2014**, *4*, 1300954.

ADVANCED FUNCTIONAL MATERIALS

Supporting Information

for *Adv. Funct. Mater.*, DOI: 10.1002/adfm.201604906

Monomolecular and Bimolecular Recombination of Electron-Hole Pairs at the Interface of a Bilayer Organic Solar Cell

*Tobias Hahn, Steffen Tscheuschner, Frank-Julian Kahle,
Markus Reichenberger, Stavros Athanasopoulos, Christina
Saller, Guillermo C. Bazan, Thuc-Quyen Nguyen, Peter
Strohriegl, Heinz Bässler, and Anna Köhler**

Supporting Information to:

Monomolecular and bimolecular recombination of electron-hole pairs at the interface of a bilayer organic solar cell

Tobias Hahn¹, Steffen Tscheuschner¹, Frank-Julian Kahle¹, Markus Reichenberger¹, Stavros Athanasopoulos^{1,2}, Christina Saller³, Guillermo C. Bazan⁴, Thuc-Quyen Nguyen⁴, Peter Strohriegl^{3,5}, Heinz Bässler⁵, Anna Köhler^{1,5*}

¹ Experimental Physics II, University of Bayreuth, 95440 Bayreuth, Germany

² Departamento de Física, Universidad Carlos III de Madrid, Avenida Universidad 30, 28911 Leganés, Madrid, Spain

³ Macromolecular Chemistry I, University of Bayreuth, 95440 Bayreuth, Germany

⁴ Department of Chemistry and Biochemistry, Center for Polymers and Organic Solids, University of California, Santa Barbara, California 93106-9510, United States

⁵ Bayreuth Institute of Macromolecular Science (BIMF), University of Bayreuth, 95440 Bayreuth, Germany

7. Monomolecular and bimolecular recombination of electron-hole pairs at the interface of a bilayer organic solar cell

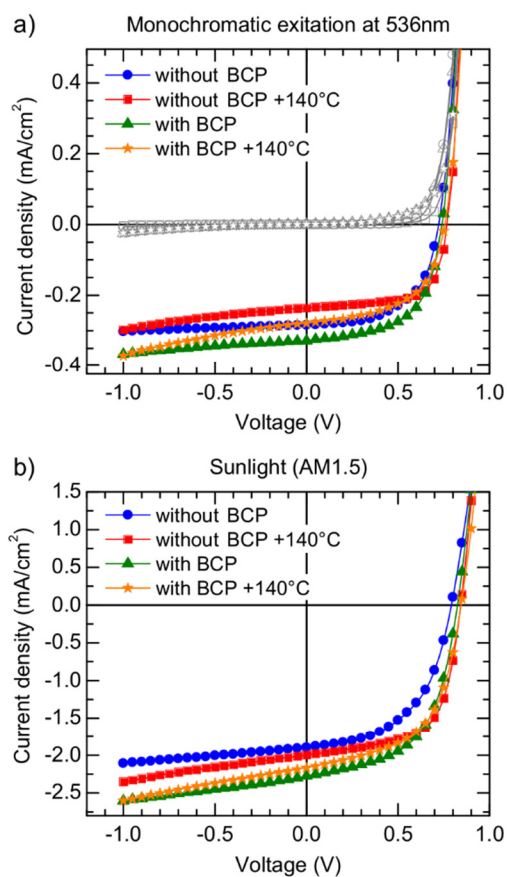


Figure S1: (a) Current-voltage characteristics of ITO/MoO₃/PCDTBT_{stat}/C₆₀/(BCP)/Al bilayer solar cells measured with or without BCP interlayer and with or without annealing step for monochromatic excitation at 536 nm. Open grey symbols indicate the associated dark current. (b) The same for AM1.5 sun light conditions.

7. Monomolecular and bimolecular recombination of electron–hole pairs at the interface of a bilayer organic solar cell

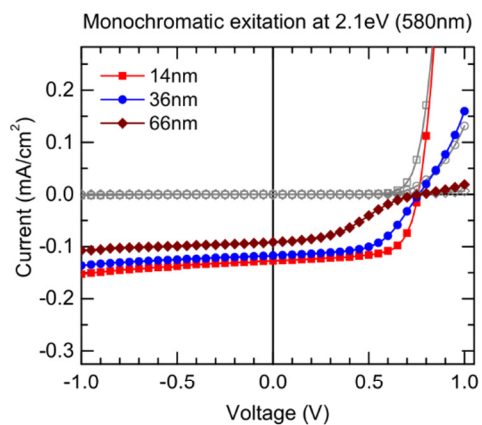


Figure S2: Current-voltage characteristics of ITO/MoO₃/PCDTBT_{stat}/C₆₀/Al bilayer solar cells for different film thicknesses taken for monochromatic excitation at 580 nm (2.1 eV).

7. Monomolecular and bimolecular recombination of electron-hole pairs at the interface of a bilayer organic solar cell

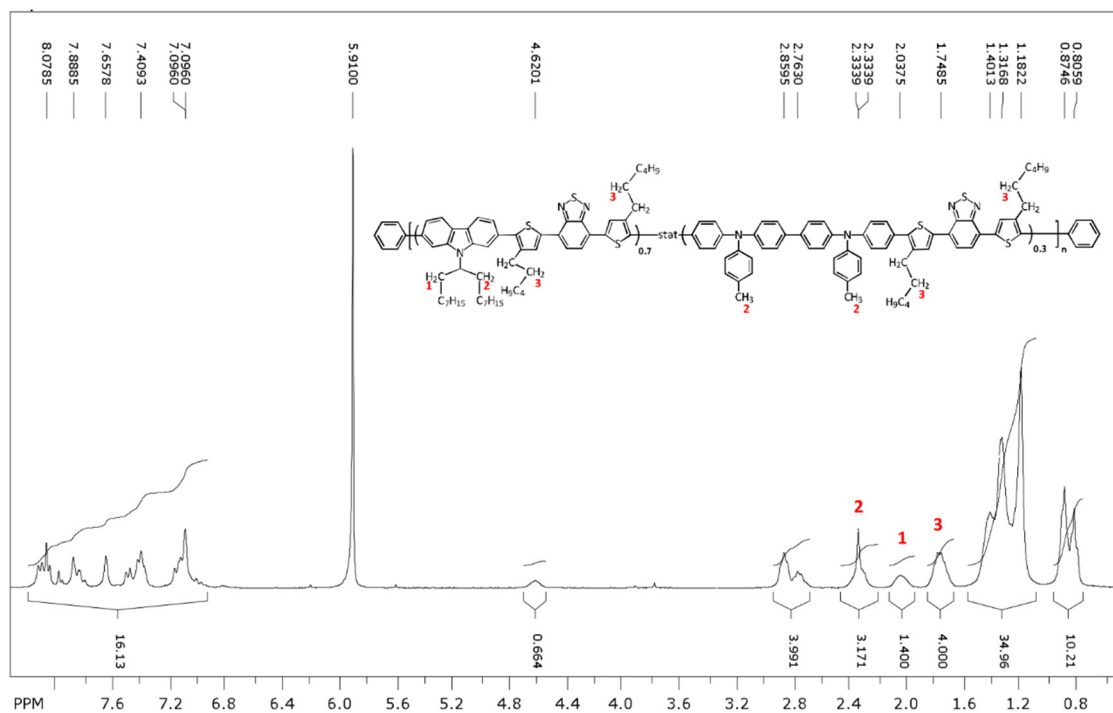
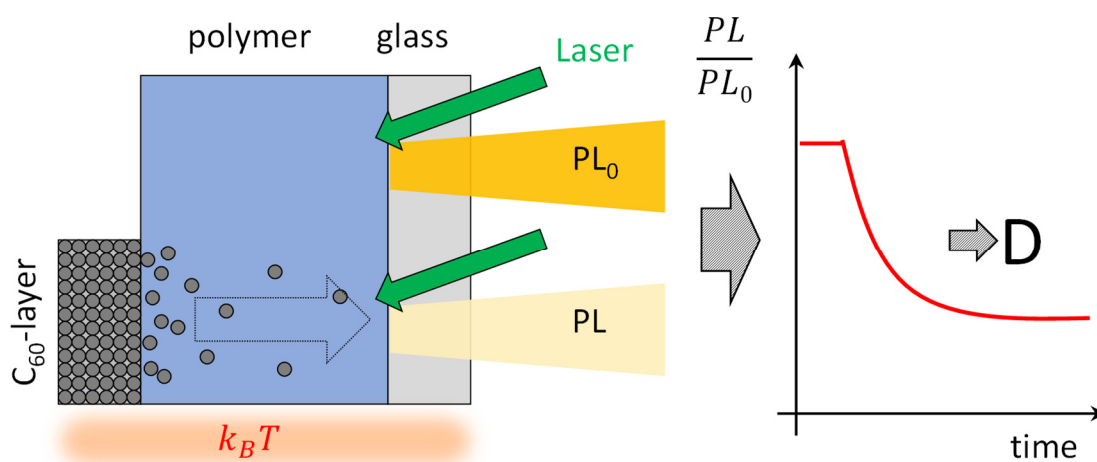


Figure S3: ^1H NMR spectrum of PCDTBT_{0.7}/TPDDTBT_{0.3} (300 MHz) in $\text{C}_2\text{D}_2\text{Cl}_4$ at 120°C . For the calculation of the molar ratio see Experimental Section.

8. Facile method for the investigation of temperature-dependant C_{60} diffusion in conjugated polymers

Christina Saller, Frank-Julian Kahle, Thomas Müller, Tobias Hahn, Steffen Tscheuschner,
Denys Priadko, Peter Strohrriegl, Heinz Bässler, and Anna Köhler



Accepted to be published in *ACS Advanced Materials & Interfaces*

doi: 10.1021/acsami.8b05520

Reprinted with permission from *ACS Advanced Materials & Interfaces* **2018**

Copyright © 2018 American Chemical Society

Facile Method for the Investigation of Temperature-Dependent C₆₀ Diffusion in Conjugated Polymers

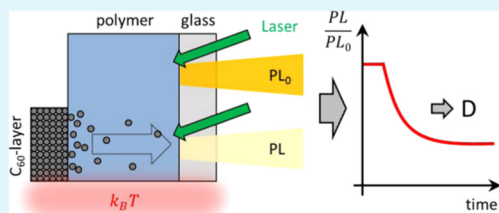
Christina Saller,^{†,‡} Frank-Julian Kahle,^{‡,‡,‡} Thomas Müller,[‡] Tobias Hahn,[‡] Steffen Tscheuschner,[‡] Denys Priadko,[‡] Peter Strohrriegel,^{‡,§,||} Heinz Bässler,[§] and Anna Köhler^{*,‡,§,§}

[†]Macromolecular Chemistry I, [‡]Soft Matter Optoelectronics, [§]Bayreuth Institute of Macromolecular Science (BIMF), and ^{||}Bavarian Polymer Institute (BPI), University of Bayreuth, 95440 Bayreuth, Germany

Supporting Information

ABSTRACT: We developed a novel all-optical method for monitoring the diffusion of a small quencher molecule through a polymer layer in a bilayer architecture. Experimentally, we injected C₆₀ molecules from a C₆₀ layer into the adjacent donor layer by stepwise heating, and we measured how the photoluminescence (PL) of the donor layer becomes gradually quenched by the incoming C₆₀ molecules. By analyzing the temporal evolution of the PL, the diffusion coefficient of C₆₀ can be extracted, as well as its activation energy and an approximate concentration profile in the film. We applied this technique to three carbazole-based low-bandgap polymers with different glass temperatures with a view to study the impact of structural changes of the polymer matrix on the diffusion process. We find that C₆₀ diffusion is thermally activated and not driven by WFL-type collective motion above T_g but rather by local motions mediated by the sidechains. The results are useful as guidance for material design and device engineering, and the approach can be adapted to a wide range of donor and acceptor materials.

KEYWORDS: diffusion, fullerene, low-bandgap polymer, fluorescence quenching, glass transition



1. INTRODUCTION

Molecular diffusion processes and associated changes in film composition and/or morphology are a critical factor in terms of performance, thermal stability, and degradation of organic semiconducting devices.^{1–3} For example, in an organic light-emitting diode (OLED), the active element is a stack of several transport and emitter layers including a large number of interfaces. Those interfaces can be sharp during the initial film preparation but may become more intermixed during the subsequent device operation because of molecular diffusion, which will alter the performance of the OLED.⁴ In fact, if well controlled, the diffusion process may be employed beneficially not only to determine the degree of interfacial intermixing but also to control doping processes in organic semiconductors.³ Similarly, for organic semiconductor devices such as organic solar cells (OSCs) annealing can induce morphological changes that improve the device performance.^{2,5} However, device optimization by annealing is often based on trial and error as too little is known about the temperature-dependent diffusivities of molecular dyes, acceptors, or dopants in the polymer matrix.

The diffusion of ions in inorganic glasses^{6–8} or of tracer molecules in polymers^{9–11} has been studied extensively. The results indicate that ion diffusion in inorganic glasses is a thermally assisted process featuring an Arrhenius-type temperature dependence, whereas molecular diffusion in polymers is usually controlled by Vogel–Fulcher–Tammann (or Wil-

liams–Landel–Ferry, WLF) law, applicable to glass dynamics near or above the glass transition temperature T_g, described by free volume concepts. The pertinent question is to which extent these conclusions apply for the diffusion of more bulky molecules such as C₆₀ in soft organic semiconductors such as conjugated polymers or glasses of organic oligomers. It seems plausible that in this case, molecular diffusion might indeed require free volume of the transporting matrix.^{12–15}

The diffusion of acceptor or dopant molecules in a polymeric or molecular matrix has only been addressed in the organic electronics community over the past decade, with the main concern being the morphological stability of films used in optoelectronic devices at elevated temperatures.^{3,16–18} In recent years, however, there have been an increasing number of studies that addressed molecular diffusion by various methods in a qualitative or quantitative way.^{2–4,14,16,19–27} Approaches employed include dynamic secondary ion-mass spectroscopy (DSIMS),^{2,14,19–21,25} scattering experiments (grazing-incidence small-angle scattering, grazing-incidence wide-angle X-ray scattering, resonant soft X-ray scattering, neutron reflectivity, near edge X-ray absorption fine structure, small-angle neutron scattering, grazing incidence X-ray diffraction),^{2,4,14,16,23,25,26} or spatially resolved optical, electron,

Received: April 5, 2018

Accepted: May 30, 2018

Published: May 30, 2018

7. Monomolecular and bimolecular recombination of electron–hole pairs at the interface of a bilayer organic solar cell

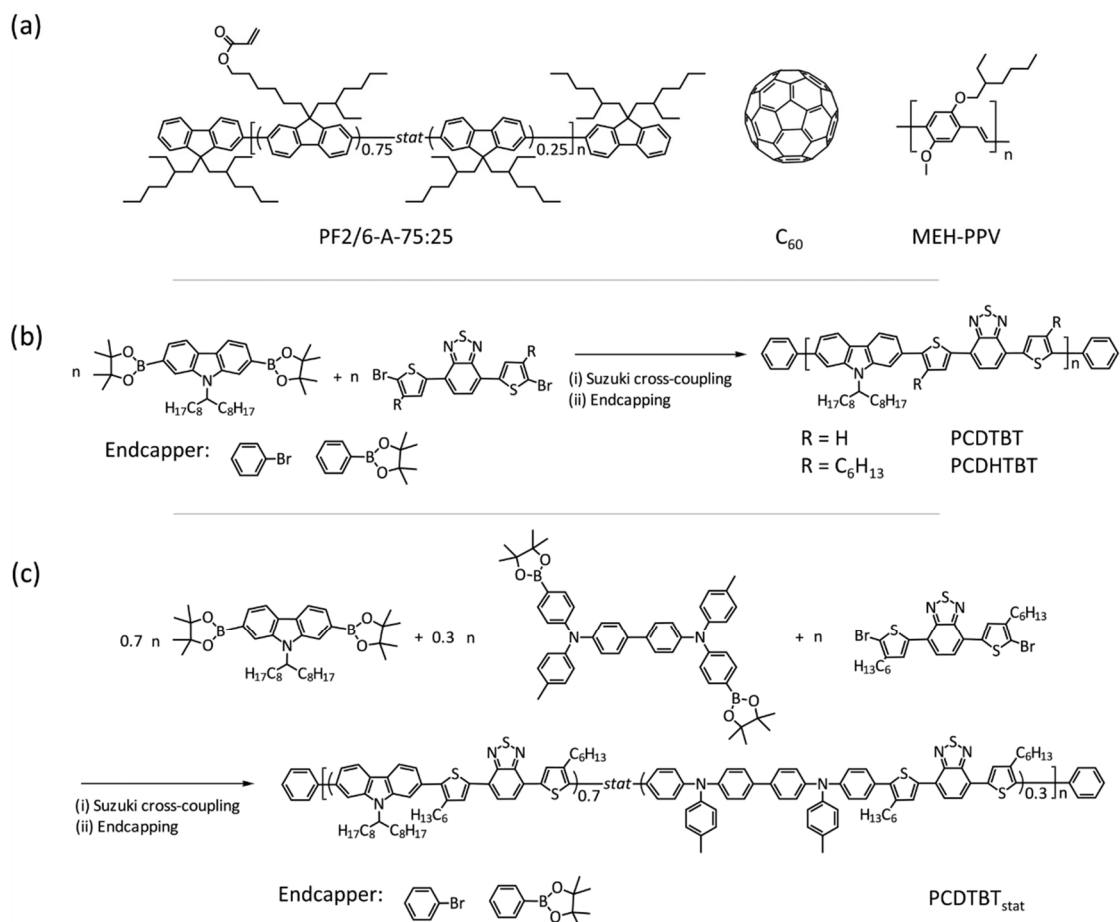


Figure 1. (a) Chemical structures of the PF2/6-A-75:25 polymer with cross-linkable acrylate groups, fullerene C₆₀, and poly(2-methoxy-5-(2-ethylhexyloxy)-1,4-phenylenevinylene) (MEH-PPV). (b) Synthetic route to the two donor–acceptor polymers PCDTBT and PCDHBT: (i) toluene, aqueous NEt₄OH solution (20 wt %), Pd₂dba₃, P(*o*-tolyl)₃, reflux, 72 h, (ii) bromobenzene, reflux, 1 h, phenylboronic acid, reflux, overnight. (c) Synthetic route to the donor–acceptor polymer PCDTBT_{stat}: (i) toluene, aqueous Na₂CO₃ solution (2 M), Aliquat 336, Pd(PPh₃)₄, reflux, 72 h, (ii) bromobenzene, reflux 1 h, phenylboronic acid, reflux, 1 h.

or X-ray microscopy as a tool to monitor diffusion.^{2,4,14,16,23–25,27}

In previous work, we introduced an approach to monitor diffusion and determine diffusion coefficients by comparatively simple photoluminescence (PL) measurements.²⁸ The approach was based on an adaptation of the time-of-flight-time technique, originally used to measure the mobility of charge carriers in organic semiconductor sandwiches between injecting and extracting electrodes.^{29–31} In that work, a polyfluorene derivative was sandwiched between a C₆₀ layer on top and a fluorescent sensor layer at bottom. C₆₀ molecules were “injected” from the C₆₀ layer via stepwise increase of the temperature and diffused through the polymer layer to the sensor, where they accumulate and quench the sensor’s photoluminescence (PL). By recording the time until the PL quenching sets in, the diffusivity of the C₆₀ molecules in the polymer could be derived. The essential result was that C₆₀ diffusion is indeed thermally activated, and that the diffusion coefficient is reduced by 3 orders of magnitude upon cross-

linking the polyfluorene layer. This is a clear manifestation that the morphology of the transport layer is important and gives a guideline toward improved stability of polymer/C₆₀ devices. In our current work, we again apply an all-optical approach to study the diffusion of small quencher molecules, in our case C₆₀, in a polymer matrix but now applying a modified two-layer architecture. The advantage of our new approach is that the investigated material itself acts as a sensor for PL quenching, thus resulting in greater variability of investigable systems. The only requirement is its fluorescing ability.

This article is structured as follows. After introducing the materials in Section 2, Section 3 describes how the experiment is conducted and analyzed, and how it compares to our previous measurements. Section 4 illustrates how the novel approach can be employed to study fullerene diffusion in low-bandgap polymers such as PCDTBT and its derivatives previously spectrally not accessible to us. We show that our new method is capable of quantitatively determining the temperature-dependent diffusion coefficient and the associated

B

DOI: 10.1021/acsami.8b05520
ACS Appl. Mater. Interfaces XXXX, XXX, XXX–XXX

activation energy and equilibrium concentration of small molecules within a polymer matrix, both above and below the glass transition temperature. Interestingly, we find that diffusion is already present well below the glass transition temperature of the polymer backbone, T_g , and that all three PCDTBT derivatives feature similar diffusion coefficients at T_g . This means that below T_g , diffusion of small molecules in these polymers may be governed by local chain motion because of the mobility of the sidechains rather than by the collective motion of the chain backbone. In the end, because of its simplicity, our new approach may provide facile and valuable assistance in the engineering process of organic semiconducting devices.

2. SYNTHESIS AND MATERIALS

For the investigation of the diffusion process of C_{60} in a polymer matrix, we used two different material sets. For the comparison of the novel two-layer and three-layer methods, the cross-linkable polyfluorene PF2/6-A-75:25, already investigated in ref 28, was used. The chemical structures of PF2/6-A-75:25 with pendant acrylate units fullerene C_{60} and poly(2-methoxy-5-(2-ethylhexyloxy)-1,4-phenylenevinylene) (MEH-PPV) are shown in Figure 1a. In PF2/6-A-75:25, 75% of the sidechains contain acrylate moieties that were cross-linked by illumination with UV light at 40 °C for 10 min. In addition, a series of three donor–acceptor polymers including the well-known low-bandgap polymer PCDTBT was chosen (Figure 1b,c). This series exhibits fluorescence at longer wavelengths and allows studying the impact of small changes of the chemical structure on the diffusion behavior. The addition of hexyl spacers to the thiophene groups in the acceptor unit of PCDTBT yielded PCDHTBT. Another modification was the incorporation of a phenyl-substituted benzidine unit in the polymer backbone, resulting in PCDTBT_{stat}.

The synthesis of the three polymers is schematically depicted in Figure 1b,c. The donor monomer 2,7-bis-(4',4',5',5'-tetramethyl-1',3',2'-dioxaborolan-2'-yl)-N-(heptadecan-9'-yl)-carbazole and the acceptor monomers 4,7-bis(5'-bromothien-2'-yl)-2,1,3-benzothiadiazole and 4,7-bis(5'-bromo-4'-hexylthien-2'-yl)-2,1,3-benzothiadiazole are commercially available. For the synthesis of the second donor monomer N,N'-bis(4-methylphenyl)-N,N'-bis((4',4',5',5'-tetramethyl-1',3',2'-dioxaborolan-2'-yl)phenyl)benzidine, the corresponding dibromide is synthesized according to literature³² and converted into the bisborolane monomer via lithiation and reaction with 2-isopropoxy-4,4,5,5-tetramethyl-1,3,2-dioxaborolane, as shown in the Supporting Information.

The polymerizations are performed via Suzuki cross-coupling between bisborolane donor- and dibromide acceptor monomers. PCDTBT and PCDHTBT are synthesized similar to literature procedures.^{33,34} Endcapping of the polymers was carried out by subsequent addition of bromobenzene and phenylboronic acid after the polycondensation was finished. In the case of PCDTBT_{stat}, the donor monomer fraction was divided into a molar ratio of 0.7:0.3 for the carbazole and the phenyl-substituted benzidine monomer.³⁵ The composition was verified by NMR spectroscopy to be 0.7:0.3:1 for the carbazole, the benzidine, and the bithienyl benzothiadiazole moieties. The complete synthetic details are given in the Supporting Information.

Within this series of low-bandgap polymers, the glass transition temperature of the polymers varies. Table 1 includes the glass transition temperatures T_g and the molecular weights for the three polymers, as determined by differential scanning calorimetry (DSC) and (high-temperature) size-exclusion chromatography (SEC), respectively. We find that the reference polymer PCDTBT exhibits a T_g of 112 °C, whereas the glass transition temperature decreases to about 60 °C for PCDHTBT. We attribute this mainly to the addition of hexyl spacers to the thiophene units, which renders the PCDHTBT chains more flexible, and, to a minor extent, to the lower molecular weight of PCDHTBT.¹ In contrast, the incorporation of the bulky phenyl-substituted benzidine units in PCDTBT_{stat} leads to a lower

Table 1. Glass Transition Temperatures T_g and Molecular Weights (Number-Average M_n and Weight-Average M_w) of the Three Polymers, as Determined by DSC and SEC Measurements

polymer	T_g /°C	M_n /g mol ⁻¹	M_w /g mol ⁻¹
PCDTBT	112	16 000 ^a	37 000 ^a
PCDHTBT	60	7000	14 000
PCDTBT _{stat}	110	18 000	47 000

^aHigh-temperature SEC at 150 °C in trichlorobenzene and polystyrene calibration.

flexibility. However, this is balanced by the hexyl spacers in the acceptor units. Thus, the glass transition of PCDTBT_{stat} is almost equal to that of PCDTBT, namely 110 °C. The DSC measurements are included in the Supporting Information. PF2/6-A-75:25 has a T_g of 80 °C,³⁶ which increases upon cross-linking.

3. ALL-OPTICAL MEASUREMENT OF C_{60} DIFFUSION BY A TWO-LAYER SETUP

3.1. Optical Two-Layer Setup. We prepared samples in a nitrogen-filled glovebox by first spin-coating a thin polymer layer onto a 2×2 cm² quartz substrate and then evaporating a 30 nm thick C_{60} layer with a shadow mask onto half of the polymer film. The general structure is shown in Figure 2a. Here, we used 200–270 nm thick films of PF2/6-A-75:25 that were cross-linked by UV-illumination at 40 °C (15 min at 50 W) prior to C_{60} deposition. This allows for a comparison to a previously used three-layer setup in which the same material was used.²⁸ The measurement is based on comparing the photoluminescence obtained from the half that is covered with C_{60} to that from the uncovered reference half after a temperature increase. As illustrated in Figure 2b, the technique is based on the premise that enhanced diffusion of C_{60} into the polymer layer takes place after a sudden temperature increase from T_1 to T_2 , which reduces the observed PL through quenching.

To this end, the polymer layer is excited through the quartz substrate on the C_{60} -covered half and on the reference half, using a continuous-wave diode laser at 405 nm for PF2/6-A-75:25 at an excitation density of ca. 15 mW cm⁻². The photoluminescence is recorded using a fiber-coupled spectrometer connected to a charge-coupled device camera (Andor-Solis). For the measurements, the samples are held under nitrogen in a heatable cryostat. The temperature was controlled with an ITC502 temperature controller. For the temperature rise, a high heating rate of 10 K min⁻¹ was chosen until the final temperature T_2 was reached. To record each data point, the reference half and the C_{60} -covered half of the sample were excited immediately after each other, and shutters were used to limit the exposure time of the sample in between recordings to the minimum. Figure 2c shows how the photoluminescence intensity of the C_{60} -covered half, normalized to that of the reference half, reduces as a function of time upon heating. For reference, the temperature in the cryostat is also indicated.

3.2. Theoretical Model. The diffusion coefficient $D(T_2)$ can be obtained from the photoluminescence transients using a suitable theoretical model. Consider the half that is initially covered with the C_{60} layer. As a result of the C_{60} coverage, we consider there to be an initial, uniformly distributed concentration of C_{60} sites in the film, $c(t=0) = c_0(T_1)$, that may be finite or zero. We presume that photoluminescence (PL) quenching occurs upon contact between the polymer and

C

DOI: 10.1021/acsami.8b05520
ACS Appl. Mater. Interfaces XXXX, XXX, XXX–XXX

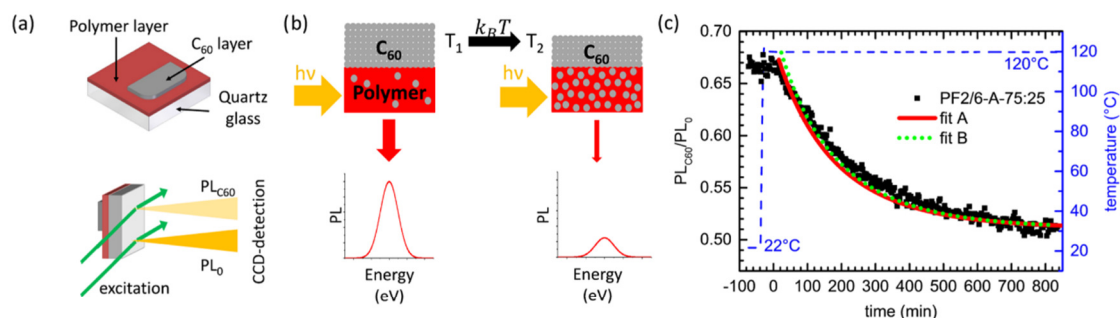


Figure 2. (a) Schematic of the sample and measurement geometry. (b) Schematic illustrating how the experiment is conducted. (c) Time-dependent decrease of the relative PL intensity, $PL_{C_{60}}/PL_0$ (left axis), measured on bilayer samples of cross-linked PF2/6-A-75:25 with C_{60} on top upon increasing the temperature from 22 to 120 °C (right axis). The solid red line and the green dotted lines correspond to different fits.

the C_{60} . Upon increasing the temperature from T_1 to T_2 , a new, larger equilibrium concentration $c_0(T_2) = c_0(T_1) + \Delta c_0(T_1, T_2)$ will establish at long times as a result of increased C_{60} diffusion from the top layer into the film. Concomitantly, the photoluminescence in the polymer film will reduce until a final equilibrium value is obtained at long times.

As the area of the polymer film (400 mm²) is large compared with its thickness (200–270 nm), it suffices to consider one-dimensional diffusion, on the basis of Fick's second law

$$\frac{\partial c(x, t)}{\partial t} = D \cdot \frac{\partial^2 c(x, t)}{\partial x^2} \quad (1)$$

where D is the diffusion coefficient, taken to be constant in time and space. We take $x = 0$ to be on the polymer side of the interface between the C_{60} layer and the polymer layer, and $x = d$ at the polymer-facing interface between the polymer and the quartz substrate, where no further diffusion is possible. For the boundary conditions $c(x = 0, t > 0) = c_0(T_2)$, and $\frac{\partial c(x = d, t)}{\partial x} = 0$, we use the known solution³⁷

$$c(x, t) = c_0(T_1) + \Delta c_0(T_1, T_2) \cdot f_c(x, t, T_2) \quad (2)$$

with $f(x, t, T_2) = \left(1 - \frac{4}{\pi} \sum_{n=0}^{\infty} \frac{(-1)^n}{2n+1} \exp\left(-D(T_2)(2n+1)^2 \pi^2 \frac{t}{4d^2}\right) \cos\left(\frac{(2n+1)\pi(d-x)}{2d}\right)\right)$ and $t \geq 0$ as

well as $0 \leq x \leq d$ and $\Delta c_0(T_1, T_2) = c_0(T_2) - c_0(T_1)$. This concentration of quenching sites leads to luminescence quenching with a rate $k_q(x, t)$. When a film of surface area A and thickness d is excited from the quartz side with a photon rate $k_0 = K_0 \exp(-\alpha(d-x))$, we thus find

$$PL(t) = A \cdot K_0 \int_0^d \exp(-\alpha(d-x)) \cdot \frac{k_r}{k_r + k_{nr} + k_q(x, t)} dx \quad (3)$$

for the film with the C_{60} quenchers, whereas

$$PL_0 = A \cdot K_0 \cdot \frac{k_r}{k_r + k_{nr}} \cdot \frac{1 - \exp(-\alpha d)}{\alpha} \quad (4)$$

applies for the part of the film that is not covered by C_{60} . α denotes the absorption coefficient, k_r the radiative, and k_{nr} the nonradiative decay rate of the excited state. The ratio between eqs 3 and 4 gives the evolution of the recorded normalized photoluminescence, that is,

$$\frac{PL}{PL_0}(t) = \frac{\alpha}{1 - \exp(-\alpha d)} \int_0^d \exp(-\alpha(d-x)) \cdot \left(1 + \frac{k_q(x, t)}{k_r + k_{nr}}\right)^{-1} dx \quad (5)$$

When the quenching rate depends linearly on the concentration of C_{60} molecules, $k_q(x, t) = K_D \cdot c(x, t)$, eq 5 reduces to

$$\frac{PL}{PL_0}(t) = \frac{\alpha}{1 - \exp(-\alpha d)} \int_0^d \exp(-\alpha(d-x)) \cdot (1 + K_D \cdot c(x, t))^{-1} dx \quad (6)$$

where $K_D = K_q/(k_r + k_{nr})$ is the Stern–Volmer constant that describes how strongly the PL of a material is reduced by a certain quencher.³⁸ At long times, a new equilibrium concentration $c_{max}(T_2)$ establishes so that quenching occurs with a constant rate $k_q(c_0(T_2)) = K_q \cdot c_0(T_2)$. This leads to a stationary value for the PL that is expressed by the Stern–Volmer equation

$$\frac{PL}{PL_0}(t \rightarrow \infty, T_2) = (1 + K_D \cdot c_0(T_2))^{-1} dx \quad (7)$$

The key equations to analyze the experimental data by numerical simulation are eqs 6 and 2. A more detailed derivation of eqs 6–5 can be found in the [Supporting Information](#). There are two approaches to obtain the diffusion coefficient from this. A straightforward way (“fit A”) to obtain the diffusion coefficient is therefore to simulate the time-dependent decay of the luminescence using eq 6, with the C_{60} concentration given by eq 2. For this, the initial and final, spatially homogeneous equilibrium concentrations $c_0(T_1)$ and $c_0(T_2)$ are estimated on the basis of the experimental data using eq 7. The required Stern–Volmer constant K_D is taken from steady-state quenching experiments that we carried out as detailed in the [Supporting Information](#). We determined the absorption coefficient, α , required to evaluate the data by measuring the absorption and the thickness of the films. In the simulation, the diffusion coefficient D is adjusted until the numerical simulation agrees with the experimentally observed luminescence decay. [Figure 2c](#) exemplarily illustrates the good agreement between the PL quenching obtained for a 270 nm film of cross-linked PF2/6-A-75:25 and the simulated curve, using a value of $K_D = 4.81$ for the respective Stern–Volmer constant. This fitting procedure results in both a value for the

D

 DOI: 10.1021/acsami.8b05520
 ACS Appl. Mater. Interfaces XXXX, XXX, XXX–XXX

8. Facile method for the investigation of temperature-dependent C_{60} diffusion in conjugated polymers

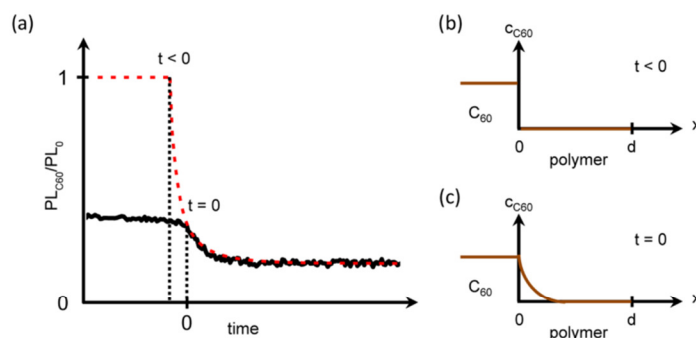


Figure 3. (a) Illustration of the fitting procedure using a self-consistent initial condition as described in the main text (fit B). The black solid line corresponds to experimental data, and the red dashed line is the result of a first simulation round starting nominally before the acceptor was deposited and ending at the final equilibrium concentration. (b) The concentration profiles assumed to prevail just before acceptor deposition at T_1 . This is used as the input to the first fitting round. (c) The concentration profile obtained from the first fitting round, assumed to prevail just before the heating step to T_2 . This is used as the initial condition for the second fitting round to the experimental data.

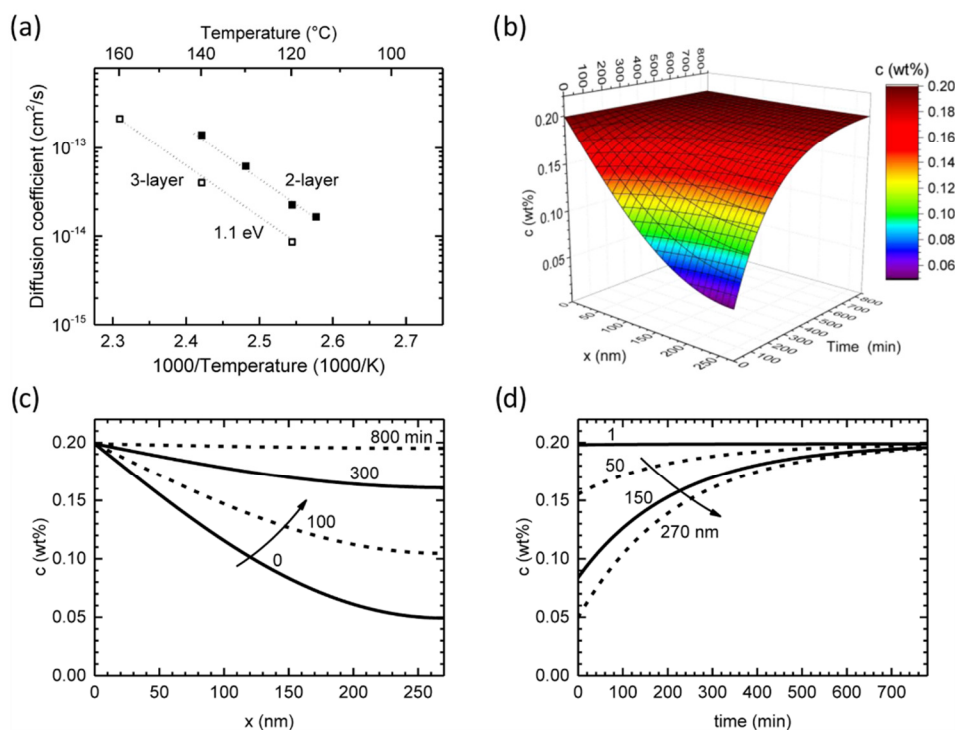


Figure 4. (a) Arrhenius representation of the temperature dependence of the diffusion coefficient for cross-linked PF2/6-A-75:25 measured in a three-layer architecture (open squares) and a two-layer architecture (filled squares). The slope yielding the activation energy, E_A , of diffusion is indicated by dotted lines. (b) Three-dimensional (3D) representation for the calculated time-dependent concentration, $c(x, t)$, of C_{60} . The positions $x = 0$ and 270 nm denote the interface to the C_{60} and the quartz substrate, respectively. (c) Distribution of $c(x, t)$ across the film thickness at different times. (d) Evolution of $c(x, t)$ with time at different positions in the film.

diffusion coefficient as well as a spatial and temporal concentration profile $c(x, t)$ after heating to T_2 .

Although fit A can be implemented easily, it assumes that the initial concentration of C_{60} in the film at T_1 be spatially homogeneous. However, this initial concentration of C_{60} after evaporation is not necessarily constant over the film thickness, and a concentration gradient can prevail. To account for this and to estimate the impact of this approximation, we also

explored an iterative, self-consistent approach (“fit B”). In the first step, we simulate the diffusion with the aim to obtain the approximate initial concentration profile in the experiment. For this, we apply eq 6 with the initial condition that there will be no C_{60} , and thus no PL-quenching in the film at a certain time $t < 0$. The diffusion coefficient, D , is adjusted until a reasonable fit to the experimental data is achieved, in particular at later times, as illustrated in Figure 3. From this simulation, we obtain

E

an initial spatial concentration profile $c(x, t)$. We use this profile at $t = 0$ in the second step as initial input concentration, nominally $c_0(T_1)$, to obtain an improved and more accurate diffusion coefficient. The quality of both fits is illustrated exemplarily in Figure 2c. Across all materials presented in this article, we found that the choice of initial conditions (spatially constant concentration, i.e., fit A, or spatial concentration gradient, i.e., fit B) affects the final value of the diffusion coefficient by less than 20%. This is illustrated and discussed in detail in the Supporting Information. All subsequent data presented in this article are based on fit B, which we consider to represent a more realistic scenario.

Our model has three premises that require discussing. (i) At first sight, the assumption of PL quenching upon C_{60} contact seems to neglect the exciton diffusion. This is, however, implicitly included through the value of the Stern–Volmer constant that was measured for each material in the solid film. (ii) Similarly, surface quenching at the interface to the C_{60} layer is not explicitly considered. This can be included through an additional surface quenching term in eq 6, but it has no significant effect on the diffusion coefficients as detailed in the Supporting Information. (iii) Equation 6 requires a linear dependence of the quenching rate on the quencher concentration. This is no longer warranted when C_{60} forms clusters. In that case, the effective quenching rate is smaller than that predicted on the basis of the Stern–Volmer constant measured for homogeneously distributed molecular C_{60} . In our measurements, the equilibrium concentrations of C_{60} in the cross-linked polyfluorene and the donor–acceptor polymers are 0.5 and 1–2%, respectively, as discussed in Sections 3.3 and 4.2. These low concentrations rule out cluster formation.

3.3. C_{60} Diffusion in Cross-Linked PF2/6. Figure 4 shows the diffusion coefficients and concentration profiles obtained when measuring a 270 nm film of cross-linked PF2/6-A-75:25 with the novel two-layer approach upon heating from $T_1 = 22$ °C to $T_2 = 120$ °C and fitting it as described above using fit B. Further transients and fits obtained when raising the temperature from room temperature up to 140 °C are displayed in the Supporting Information, along with a detailed table of input and output parameters for the simulations. The diffusion coefficients obtained by Fischer et al. for the three-layer approach for a 200 nm film of cross-linked PF2/6-A-75:25 are also indicated in Figure 4a for comparison.²⁸ We focus on the cross-linked PF2/6-A-75:25 as this will allow for a comparison with solution-processable acceptors, such as PCBM and nonfullerene acceptors, in future work. Over the measured temperature range from 100 °C to 160 °C, we observe an Arrhenius-like activation of the diffusion coefficient, as evidenced from the linear slope in the semilogarithmic plot. The activation energy evidently agrees with the observations made previously for the three-layer technique, though the absolute values for the diffusivity obtained by the two-layer technique are about 2–3 times larger than the values measured previously.

The simulations also yield concentration profiles $c(x, t)$ throughout the samples, as shown exemplarily in the 3D plot of Figure 4b for PF2/6-A-75:25 after heating from $T_1 = 22$ °C to $T_2 = 120$ °C. For the clarity of display, 2D slices along the time and thickness axes are shown in Figure 4c,d, respectively. From Figure 4d, we easily see that, for $t = 0$ s, a C_{60} concentration of 0.05 wt % was obtained at $x = 270$ nm, that is, at the quartz interface. The final, mean effective equilibrium concentration that establishes at long times at a temperature of 120 °C is 0.2

wt %. A total of 90% of the equilibrium concentration are reached at the quartz interface after 460 min. From Figure 4c, one can readily read off which effective concentration levels are obtained at certain positions through the film after some time. Obviously, the final equilibrium concentration obtained will depend on the solubility of the diffusing molecule in the polymer matrix at a given temperature.

The low final equilibrium concentration of about 0.2 wt % that we observe for the diffusion of C_{60} in cross-linked polyfluorene can be attributed to the fact that solubility of unsubstituted fullerene in a polymer matrix is generally rather limited,^{39,40} and this is impeded further by the cross-linking network. We point out that the cross-linking effectively suppresses clustering of C_{60} .⁴¹ Consequently, for this system, we can safely assume that the diffusing species is indeed molecular fullerene and that all of the assumptions made in our model in Section 3.2 are well met.

3.4. Evaluation of the Two-Layer Approach vs the Three-Layer Approach. It is worthwhile comparing the C_{60} diffusion coefficients derived from the two-layer and the three-layer measurements of the polyfluorene derivatives (Figure 4a). We briefly recall how the experiment is conducted with a three-layer sample.²⁸ The differences to the two-layer sample layout consist in using a thicker polymer layer, here 200 nm cross-linked PF2/6-A-75:25, and inserting a thin “sensor” layer in between the polymer and the quartz. The optical gap of the sensor material must be energetically lower than that of the polymer, so that it can be excited selectively. We used an 8 nm layer of MEH-PPV for this purpose. The experiment is conducted in the same way as for the two-layer setup, though with an excitation wavelength of 485 nm that excites only the MEH-PPV sensor layer and not the polyfluorene derivative. The sample is then heated to initiate the C_{60} diffusion. When the C_{60} molecules have traversed the PF2/6-A-75:25 layer and arrive at the MEH-PPV, PL intensity of the sample starts to reduce because of quenching. Neglecting exciton diffusion, the diffusion coefficient, D , for C_{60} could simply be evaluated according to $D = \frac{L^2}{2t}$, with L being the thickness of the PF2/6-A-75:25 layer. However, exciton diffusion in MEH-PPV toward the C_{60} quenching sites needs to be taken into account. As a result,²⁸ the diffusion coefficient is derived from fitting the normalized PL intensity using $\phi(t) = (1 + fp(t))^{-1}$, with $p(t) = 1 - \text{erf}(L(2\sqrt{Dt})^{-1})$ being the relative number of particles that diffused across the PF2/6-A-75:25 layer after time t and f being a dimensionless factor.

This three-layer setup is technologically simple, easy to implement, and data analysis is mathematically robust. However, the use of a lower-energy-emitting sensing layer that can be selectively excited limits this approach to higher energy materials that are typically green or blue emitting. To extend the spectral range of this approach, we developed the two-layer-based technique that can be applied to any photoluminescent material. It is satisfactory that two rather different approaches yield results that agree fully in the activation energy and within a factor of 2–3 as far as the absolute value is concerned.

In addition to allowing for using a larger range of materials, the two-layer method has the further advantage to give concentration profiles obtained from the simulations alongside of the diffusion coefficient (Figure 4b–d). They can be used as guidance when aiming to obtain a certain dopant concentration by annealing at a given temperature for a certain

time. Obviously, the approach can be applied to different diffusing molecules in various polymers, as long as the diffusing molecule quenches photoluminescence. It has to be noted though that the initial profiles are still approximations and may differ from the actual concentration gradients present in the samples, especially at short times and close to the dopant layer. Nevertheless, at later times (>1–2 min) and a few nanometer away from the interface, the profiles are increasingly reliable as the actual initial condition becomes less important (cf. SI). Evidently, the two-layer method may, in future work, also be applied to dopants that dissolve better in the polymer matrix, such as functionalized fullerenes or nonfullerene acceptors.

4. TEMPERATURE DEPENDENCE OF C₆₀ DIFFUSION IN PCDTBT DERIVATIVES

4.1. Determining C₆₀ Diffusion in PCDTBT Derivatives.

Having verified that both approaches give compatible results, we can apply the two-layer method to the low-bandgap polymer PCDTBT. It is a well-known and efficient polymer system that is frequently used in organic solar cells in combination with PCBM giving long-term stable devices with estimated lifetimes of up to 7 years while still maintaining an efficiency of about 4.5% after an initial burn-in loss of about 20%.^{42–44} Here, we use three different derivatives (PCDTBT, PCDTBT_{stat}, and PCDHTBT) to study the effect of different glass transition temperatures and small modifications of the chemical structure of the polymer on the C₆₀ diffusion.

We recorded photoluminescence transients when heating the three low-bandgap polymers (PCDTBT, PCDTBT_{stat}, and PCDHTBT) to different temperatures in the range between 60 and 140 °C. For PCDHTBT, this range is entirely above its glass transition temperature, whereas for PCDTBT and PCDTBT_{stat} this temperature range comprises measurements above and below T_g (cf. Table 1). Figure 5 shows the normalized photoluminescence transients with their fits, exemplary for PCDTBT, and the diffusion coefficients resulting from it, together with those obtained for PF2/6-A-75:25. The transients prior to normalization can be found in the Supporting Information, along with a table detailing all fitting parameters for fit A and fit B. Figure 5a illustrates how a higher final equilibrium temperature translates into an increasingly faster and more efficient quenching, which is attributed to an increased diffusion of C₆₀ into the PCDTBT. We determined the absorption coefficients and Stern–Volmer constants for each material and fitted the data using fit B under the assumption that the quenching rate increases linearly with the quencher concentration, $k_q(x, t) = K_q \cdot c(x, t)$, as detailed in Section 3. With the increase in the final temperature, the equilibrium concentrations as well as the diffusion coefficients rise, as illustrated in Figure 5b,c, respectively. From the linear increase of the temperature-dependent diffusion coefficients in the Arrhenius plot, one can see that PCDHTBT features a thermally activated diffusion above its T_g of 60 °C, similar to the cross-linked polyfluorene derivative, yet with a lower activation energy of 0.70 ± 0.05 eV and about 1 order of magnitude lower absolute values. Despite their slightly different chemical structure, PCDTBT and PCDTBT_{stat} show very similar values, which we attribute to their similar molecular weight and T_g and which gives confidence in the reliability of our approach. For both materials, a temperature-activated diffusion process is also observed, yet the slope of the activation energy changes from 0.40 ± 0.05 eV below T_g to 1.00 ± 0.05 eV above T_g . The

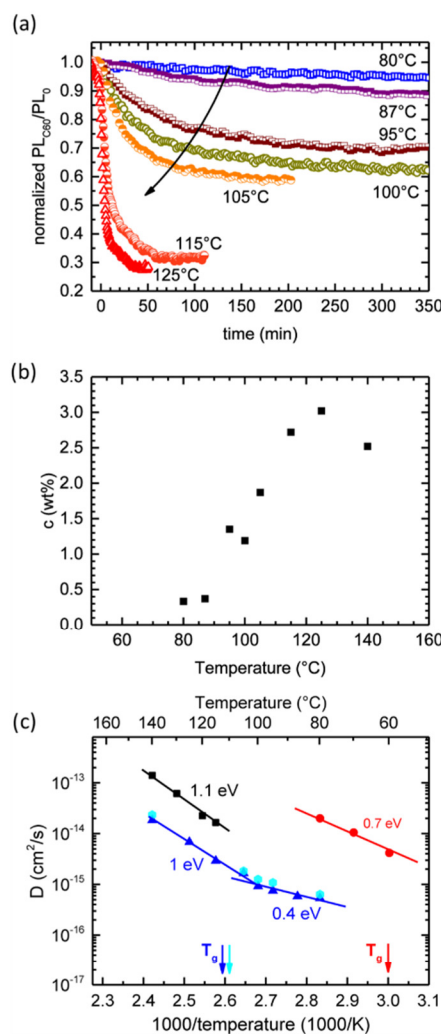


Figure 5. (a) Time dependence of PL_{C₆₀}/PL₀ for PCDTBT for different final temperatures after a one-step temperature increase. (b) Final concentration $c(T_2)$ of C₆₀ in PCDTBT as a function of the final temperature T_2 , obtained from the measurements displayed in (a). (c) Arrhenius representation of the temperature dependence of the diffusion coefficient for cross-linked PF2/6-A-75:25 (black squares), as well as for PCDTBT (blue filled triangles), PCDHTBT (red filled circles), and PCDTBT_{stat} (light blue filled hexagons). The solid lines provide a guide to the eye, and colored arrows indicate the respective T_g .

remarkable feature here is that the diffusion coefficient does not reduce drastically below T_g . The Stokes–Einstein equation that relates diffusion coefficient D , viscosity η , and particle radius r through $D = kT/6\pi\eta r$ would predict such a decrease in D because the viscosity η of polymers is known to strongly increase below T_g . When focussing on the temperature range above T_g , we find diffusion coefficients in the same range as that for PCDHTBT and about 1 order of magnitude below those of the cross-linked PF2/6-A-75:25.

G

DOI: 10.1021/acsami.8b05520
ACS Appl. Mater. Interfaces XXXX, XXX, XXX–XXX

4.2. Analyzing the Temperature Dependence of C_{60} Diffusion in PCDTBT Derivatives. We first assess the values and activation energies we obtain with our facile two-layer approach by comparison to values obtained for dye or dopant diffusion by other methods. To allow for comparison to other compounds despite the strong temperature dependence, we focus on the diffusivity at T_g . We find $D(T_g) = 3 \times 10^{-15} \text{ cm}^2 \text{ s}^{-1}$ for the diffusion of C_{60} in all three PCDTBT derivatives. This diffusivity is about 150 times lower than that determined for polyfluorene using the three-layer method, which extrapolates to $D(T_g = 80 \text{ }^\circ\text{C}) = 5 \times 10^{-13} \text{ cm}^2 \text{ s}^{-1}$,²⁸ and also lower than the values obtained for the cross-linked PF2/6-A-75:25. The equilibrium concentration of C_{60} at T_g was about 1–2 wt %. Our values for the diffusivities and activation energies of PCDTBT derivatives are in a similar range to those determined by rather different methods for other dyes/dopants at low concentrations in a polymer. This agreement is gratifying and supports the appropriateness of our approach.

For example, Ehlich and Sillescu investigated the diffusion of an indigo dye at less than 0.5 wt % in polymers such as polystyrene, poly(methyl methacrylate), and polycarbonate, which have glass transition temperatures of 100, 121, and 150 $^\circ\text{C}$, respectively.¹⁰ They use the holographic grating technique, where the diffusive decay of a photochemically produced grating is monitored by recording the intensity of forced Rayleigh scattering as a function of time, and they obtain values for the diffusion coefficient $D(T_g)$ at the glass transition of 8×10^{-15} , 1×10^{-14} , and $6.3 \times 10^{-12} \text{ cm}^2 \text{ s}^{-1}$, respectively. In a conceptually related way, the group of Moulé¹⁶ uses a confocal microscopy technique, where an acceptor dopant pattern is evaporated through a shadow mask onto a polymer film, and the spatial decay of the polymer luminescence due to the lateral diffusion of the dopant is monitored as a function of time and space before and after a heating step. They determined the diffusion of the acceptor molecules F4TCNQ and F4MCTCNQ in poly(3-hexylthiophene) (P3HT), which has a T_g of 10–14 $^\circ\text{C}$, and report values of $D(25 \text{ }^\circ\text{C}) \approx 5 \times 10^{-14} \text{ cm}^2 \text{ s}^{-1}$ for both compounds. The associated activation energy for an Arrhenius-like temperature dependence is 0.77 and 0.55 eV per molecule for F4TCNQ and F4MCTCNQ, respectively. Dynamic secondary ion-mass spectroscopy (DSIMS) was applied by Treat et al.²⁰ to a terraced bilayer–monolayer structure of PCBM covered with P3HT. Solving Fick's diffusion equation they arrive at D to be about 10^{-11} – $10^{-9} \text{ cm}^2 \text{ s}^{-1}$ for the range from 50 to 110 $^\circ\text{C}$ at a concentration of 1 vol % PCBM and at an activation energy of 0.7 eV per molecule. Extrapolation of their data to a T_g of about 10 $^\circ\text{C}$ gives $D(10 \text{ }^\circ\text{C}) = 1 \times 10^{-12} \text{ cm}^2 \text{ s}^{-1}$. Labram and co-workers²² use a bilayer structure of 40 nm PCBM on top of 8 nm P3HT. This bilayer is on top of a source and drain electrode, a hexamethyldisilazane layer, and a SiO_2 -covered silicon wafer, so as to form an organic field-effect transistor. They analyze the change in electron organic field-effect transistor mobility as a function of time after annealing and deduce $D(130 \text{ }^\circ\text{C}) = 5 \times 10^{-14} \text{ cm}^2 \text{ s}^{-1}$. Given that for very thin layers, T_g tends to be about 20 $^\circ\text{C}$ lower than that in the bulk,¹ this suggests a rather low value at T_g . Thus, overall, it seems that diffusivities for low amounts (≈ 1 wt %) of a diffusing dye/dopant molecule in a polymer at T_g range around 10^{-12} – $10^{-15} \text{ cm}^2 \text{ s}^{-1}$, with activation energies around 0.7 ± 0.3 eV per molecule. By the Stokes–Einstein relation, these variations between polymers even for the same dopant might result from differences in the viscosity of the

polymers, though we argue that they also reflect differences in local polymer motion (vide infra).

We point out that significantly higher diffusivities around 10^{-11} – $10^{-10} \text{ cm}^2 \text{ s}^{-1}$ are reported when the measurements are not concerned with a low dopant amount but rather with a blend of about equal ratios between the molecular and polymeric components, for example, of PCBM and P3HT.^{14,23,24} Although Treat reported only a weak dependence of the diffusivity on concentration,²⁰ results obtained on 1:1 blends are, at this stage, difficult to compare with our measurements as T_g changes, when half of the P3HT ($T_g = 12 \text{ }^\circ\text{C}$) is replaced by PCBM ($T_g = 131 \text{ }^\circ\text{C}$), and as it is not clear whether the diffusing entity then are PCBM molecules or 50 nm clusters, as suggested by Berriman et al.²⁴

We finally comment on the laws governing the observed C_{60} diffusion above and below the glass transition temperature. As mentioned above, according to the classical expectation based on the Stokes–Einstein relation, the diffusion should vanish below T_g ,^{9,45} yet, we observe a continuation of the diffusion process even at lower temperatures. The violation of the Stokes–Einstein relation below T_g has been observed before, for example, by Ehlich and Sillescu in 1990,¹⁰ and seem to occur particularly frequently for polymeric hosts.⁹ The reasons for this are a current subject of research in the area of polymer science.^{45–47} A crucial quantity for describing the dynamics of a glassy material is the free volume of the glass elements that provides motional freedom required for mechanical flow. The temperature dependence of the free volume follows a Williams–Landel–Ferry (WLF) (or, mathematically equivalent, the Vogel–Fulcher–Tammann law), which approaches zero near T_g . It is very different from Arrhenius-type dependence and is incompatible with the temperature dependence we observe. If the C_{60} diffusion was a direct reflection of the dynamics of free volume, it should be frozen out below T_g and the diffusivity should decrease drastically. However, for PCDTBT and PCDTBT_{stat} there is still diffusion well below T_g . On the basis of this observation, we argue that the temperature dependence of C_{60} diffusion is not a direct reflection of collective motion of the glass elements but rather of local and simply activated motion although both have a common origin.

In recent work, Xie et al. used oscillatory shear rheometry to investigate the glass transition temperature in regioregular (rr) and regiorandom (rra) poly(3-hexylthiophene) (P3HT), as well as in poly(bis(octyl)fluorene-dithiophene-benzothiadiazole) (PFTBT), which is structurally identical to PCDTBT, except that the carbazole moiety is exchanged by a fluorene moiety.⁴⁸ They pointed out that there is one glass transition temperature ($T_g = T_a$), for example, at 22 $^\circ\text{C}$ for region-regular P3HT, 6 $^\circ\text{C}$ for region-random P3HT, and 144 $^\circ\text{C}$ for PFTBT, that reflects the motion of the polymer backbone and that is also commonly observed in DSC measurements. In addition, there can be a second transition temperature ($=T_{aPE}$), for example, near $-100 \text{ }^\circ\text{C}$ for P3HT, that is associated with the sidechain. The T_{aPE} that they observe for P3HT is in a temperature range similar to that observed for alkyl sidechain relaxations in other, nonconjugated polymers.⁴⁹ We therefore suggest that it is mainly the mobility of the sidechain that allows for the diffusion of C_{60} below T_g ($=T_a$) in the polymers we investigated and that this diffusion should, in general, be accelerated upon reaching T_g ($=T_a$) by the additional backbone motion. The importance of the sidechains for the diffusivity of the dopant, here the C_{60} molecule, is thus 2-fold. The

H

DOI: 10.1021/acsami.8b05520
ACS Appl. Mater. Interfaces XXXX, XXX, XXX–XXX

sidechains plasticize the backbone and so reduce the T_g ($=T_a$) of the backbone, as detailed in ref 48. In addition, the sidechains themselves enable local motion even below T_g ($=T_a$). As the investigated temperatures are far above the typical transition temperatures for sidechains,¹ as already pointed out above, all sidechains can be regarded to be mobile.

5. CONCLUSIONS

We developed a comparatively simple all-optical technique to monitor diffusion of a quenching dopant in a fluorescent organic layer that is based on monitoring the luminescence decay after inducing the dopant diffusion by heating. We found diffusion coefficients and activation energies that were consistent with earlier work by us and others. The advantage of the here presented two-layer-PL-quenching approach is its versatility. In principle, the method requires only that (i) a bilayer can be made, for example, by evaporation of the top layer, or by lamination¹⁴ and (ii) that the diffusing dopant induces a change in optical properties, for example, photoluminescence quenching. The analysis of the photoluminescence decay gives the diffusivity and its activation energy, as well as an approximation of the time-dependent concentration profile of the dopant. Notably, our approach allows for measurements several tens of degrees below T_g . In the present case, we utilized the extension of the detection range into the red part of the electromagnetic spectrum provided by the new architecture in contrast to the three-layer system to study low-bandgap materials relevant to state-of-the-art organic semiconducting devices, especially solar cells. We used three PCDTBT derivatives to explore the effect of structural variations on the diffusion of small molecules, in our case C₆₀. In these systems, diffusion already takes place well below the glass transition temperature related to the polymer main chain. This and the observation of an Arrhenius-type dependence of the diffusion coefficient on temperature indicate that C₆₀ diffusion is not driven by WFL-type collective motion above T_g but rather by local motions mediated by the sidechains.

The method uses a planar heterojunction layout to determine the diffusion coefficient as well as the maximum soluble equilibrium concentration at a given temperature for a molecular acceptor in a polymer donor matrix. The knowledge of these two parameters is highly relevant for the controlled design as well as for estimations on morphological stability and thus lifetime of bulk heterojunction solar cells. For example, knowing the solubility limit as a function of temperature allows for predictions whether certain compositions will phase separate at room temperature and knowing the temperature-dependent diffusivity will allow estimating on what time scales this should occur. Evidently, knowing the diffusivities and solubilities of the components in binary or ternary blends as a function of temperature will assist the intelligent design of such devices. Our method may, for example, also be applied to the novel nonfullerene acceptor systems that attracted more and more attention in the recent years.⁵⁰ Clearly, for application to OSC materials, acceptors with higher solubility than C₆₀ need to be considered. In future work, our method may be also applied to study the diffusion of dopants in OLED host or transport materials.

Up to now, our method relies on luminescence quenching by the diffusing molecule. Variations of this approach may include measuring changes in photoinduced absorption, charge-transfer-state absorption, electroabsorption, or PL lifetime instead of

PL intensity. In future work, the versatility of our approach should be used to further quantitatively explore the observed diffusion below T_g in device-relevant materials, which might impact the long-term morphological stability of devices.

6. EXPERIMENTAL SECTION

6.1. Sample Preparation. The samples were prepared in a nitrogen-filled glovebox by first spin-coating a thin polymer layer onto a 2×2 cm² quartz substrate from chlorobenzene solution and then evaporating a 30 nm thick C₆₀ layer with a shadow mask onto half of the polymer film. For PF2/6-A-75:2S, we used 200–270 nm thick films that were cross-linked by UV-illumination at 40 °C (15 min at 50 W) prior to C₆₀ deposition. For the low-bandgap polymers, film thicknesses were in the range of 30–70 nm. To ensure that there is no residual solvent in the polymer film anymore, the samples were kept in the evaporation chamber for several hours before depositing C₆₀. It was evacuated down to a pressure of 5×10^{-7} mbar.

■ ASSOCIATED CONTENT

📄 Supporting Information

The Supporting Information is available free of charge on the ACS Publications website at DOI: 10.1021/acsami.8b05520.

Synthetic details of the PCDTBT derivatives; ¹H NMR spectrum of PCDTBT_{stat}; DSC measurements of PCDTBT derivatives; additional experimental details, extensive explanation of the theoretical approach; time-dependent PL ratio decay curves and fits for all investigated polymers; and parameter set used for the simulations (PDF)

■ AUTHOR INFORMATION

✉ Corresponding Author

*E-mail: anna.koehler@uni-bayreuth.de.

ORCID

Frank-Julian Kahle: 0000-0003-3416-0072

Anna Köhler: 0000-0001-5029-4420

Author Contributions

[†]C.S. and F.-J.K. contributed equally.

Notes

The authors declare no competing financial interest.

■ ACKNOWLEDGMENTS

We acknowledge financial support by the German Science Foundation DFG through the doctoral training center “Photophysics of Synthetic and Biological Multichromophoric Systems” (GRK 1640), the Bavarian State Ministry of Education, Science and the Arts through the Collaborative Research Network “Solar Technologies go Hybrid” (SolTech), and by the EU-Marie-Sklodowska-Curie-ITN Network INFORM. Furthermore, F.-J.K. was supported by the Elite Network Bavaria (ENB) in the framework of the Elite Study Program “Macromolecular Science”. We are also very grateful for helpful discussions with W. Köhler.

■ REFERENCES

- (1) Müller, C. On the Glass Transition of Polymer Semiconductors and Its Impact on Polymer Solar Cell Stability. *Chem. Mater.* **2015**, *27*, 2740–2754.
- (2) Chen, D.; Liu, F.; Wang, C.; Nakahara, A.; Russell, T. P. Bulk Heterojunction Photovoltaic Active Layers via Bilayer Interdiffusion. *Nano Lett.* **2011**, *11*, 2071–2078.
- (3) Jacobs, I. E.; Moule, A. J. Controlling Molecular Doping in Organic Semiconductors. *Adv. Mater.* **2017**, *29*, No. 1703063.

- (4) McEwan, J. A.; Clulow, A. J.; Shaw, P. E.; Nelson, A.; Darwish, T. A.; Burn, P. L.; Gentle, I. R. Diffusion at Interfaces in OLEDs Containing a Doped Phosphorescent Emissive Layer. *Adv. Mater. Interfaces* **2016**, *3*, No. 1600184.
- (5) Müller, C.; Ferenczi, T. A. M.; Campoy-Quiles, M.; Frost, J. M.; Bradley, D. D. C.; Smith, P.; Stingelin-Stutzmann, N.; Nelson, J. Binary organic photovoltaic blends: A simple rationale for optimum compositions. *Adv. Mater.* **2008**, *20*, 3510–3515.
- (6) Menezes, P. V.; Martin, J.; Schäfer, M.; Staesche, H.; Roling, B.; Weitzel, K. M. Bombardment induced ion transport-Part II. Experimental potassium ion conductivities in borosilicate glass. *Phys. Chem. Chem. Phys.* **2011**, *13*, 20123–20128.
- (7) Greaves, G. N.; Gurman, S. J.; Catlow, C. R. A.; Chadwick, A. V.; Houdewalter, S.; Henderson, C. M. B.; Dobson, B. R. A Structural Basis for Ionic-Diffusion in Oxide Glasses. *Philos. Mag. A* **1991**, *64*, 1059–1072.
- (8) Smedskjaer, M. M.; Zheng, Q. J.; Mauro, J. C.; Potuzak, M.; Morup, S.; Yue, Y. Z. Sodium diffusion in borosaluminosilicate glasses. *J. Non-Cryst. Solids* **2011**, *357*, 3744–3750.
- (9) Ediger, M. D.; Harrowell, P. Perspective: Supercooled liquids and glasses. *J. Chem. Phys.* **2012**, *137*, No. 080901.
- (10) Ehlich, D.; Sillescu, H. Tracer Diffusion at the Glass-Transition. *Macromolecules* **1990**, *23*, 1600–1610.
- (11) Rössler, E. Indications for a Change of Diffusion Mechanism in Supercooled Liquids. *Phys. Rev. Lett.* **1990**, *65*, 1595–1598.
- (12) Obuchovsky, S.; Levin, M.; Levitsky, A.; Frey, G. L. Morphology visualization of P3HT: Fullerene blends by using subsurface atomic layer deposition. *Org. Electron.* **2017**, *49*, 234–241.
- (13) Maliakal, A. J. Characterization of Dopant Diffusion within Semiconducting Polymer and Small-Molecule Films Using Infrared-Active Vibrational Modes and Attenuated Total Reflectance Infrared Spectroscopy. *ACS Appl. Mater. Interfaces* **2013**, *5*, 8300–8307.
- (14) Treat, N. D.; Brady, M. A.; Smith, G.; Toney, M. F.; Kramer, E. J.; Hawker, C. J.; Chabiny, M. L. Interdiffusion of PCBM and P3HT Reveals Miscibility in a Photovoltaically Active Blend. *Adv. Energy Mater.* **2011**, *1*, 82–89.
- (15) Paternò, G. M.; Skoda, M. W. A.; Dalglish, R.; Cacialli, F.; Sakai, V. G. Tuning Fullerene Intercalation in a Poly (thiophene) derivative by Controlling the Polymer Degree of Self-Organisation. *Sci. Rep.* **2016**, *6*, No. 34609.
- (16) Li, J.; Koshnick, C.; Diallo, S. O.; Ackling, S.; Huang, D. M.; Jacobs, I. E.; Harrelson, T. F.; Hong, K.; Zhang, G.; Beckett, J.; Mascial, M.; Moulé, A. J. Quantitative Measurements of the Temperature-Dependent Microscopic and Macroscopic Dynamics of a Molecular Dopant in a Conjugated Polymer. *Macromolecules* **2017**, *50*, 5476–5489.
- (17) Jung, M. C.; Kojima, H.; Matsumura, I.; Bente, H.; Nakamura, M. Diffusion and influence on photovoltaic characteristics of p-type dopants in organic photovoltaics for energy harvesting from blue-light. *Org. Electron.* **2018**, *52*, 17–21.
- (18) Zhang, L.; Zu, F. S.; Deng, Y. L.; Igbari, F.; Wang, Z. K.; Liao, L. S. Origin of Enhanced Hole Injection in Organic Light-Emitting Diodes with an Electron-Acceptor Doping Layer: p-Type Doping or Interfacial Diffusion? *ACS Appl. Mater. Interfaces* **2015**, *7*, 11965–11971.
- (19) Hartmeier, B. F.; Brady, M. A.; Treat, N. D.; Robb, M. J.; Mates, T. E.; Hexemer, A.; Wang, C.; Hawker, C. J.; Kramer, E. J.; Chabiny, M. L. Significance of Miscibility in Multidonor Bulk Heterojunction Solar Cells. *J. Polym. Sci., Part B: Polym. Phys.* **2016**, *54*, 237–246.
- (20) Treat, N. D.; Mates, T. E.; Hawker, C. J.; Kramer, E. J.; Chabiny, M. L. Temperature Dependence of the Diffusion Coefficient of PCBM in Poly(3-hexylthiophene). *Macromolecules* **2013**, *46*, 1002–1007.
- (21) Dai, A.; Wan, A.; Magee, C.; Zhang, Y. D.; Barlow, S.; Marder, S. R.; Kahn, A. Investigation of p-dopant diffusion in polymer films and bulk heterojunctions: Stable spatially-confined doping for all-solution processed solar cells. *Org. Electron.* **2015**, *23*, 151–157.
- (22) Labram, J. G.; Kirkpatrick, J.; Bradley, D. D. C.; Anthopoulos, T. D. Measurement of the diffusivity of fullerenes in polymers using bilayer organic field effect transistors. *Phys. Rev. B* **2011**, *84*, No. 075344.
- (23) Watts, B.; Belcher, W. J.; Thomsen, L.; Ade, H.; Dastoor, P. C. A Quantitative Study of PCBM Diffusion during Annealing of P3HT:PCBM Blend Films. *Macromolecules* **2009**, *42*, 8392–8397.
- (24) Berriman, G. A.; Holdsworth, J. L.; Zhou, X. J.; Belcher, W. J.; Dastoor, P. C. Molecular versus crystallite PCBM diffusion in P3HT:PCBM blends. *AIP Adv.* **2015**, *5*, No. 097220.
- (25) Collins, B. A.; Gann, E.; Guignard, L.; He, X.; McNeill, C. R.; Ade, H. Molecular Miscibility of Polymer-Fullerene Blends. *J. Phys. Chem. Lett.* **2010**, *1*, 3160–3166.
- (26) Clulow, A. J.; Tao, C.; Lee, K. H.; Velusamy, M.; McEwan, J. A.; Shaw, P. E.; Yamada, N. L.; James, M.; Burn, P. L.; Gentle, I. R.; Meredith, P. Time-Resolved Neutron Reflectometry and Photovoltaic Device Studies on Sequentially Deposited PCDTBT-Fullerene Layers. *Langmuir* **2014**, *30*, 11474–11484.
- (27) Wang, D.; Nakajima, K.; Liu, F.; Shi, S. W.; Russell, T. P. Nanomechanical Imaging of the Diffusion of Fullerene into Conjugated Polymer. *ACS Nano* **2017**, *11*, 8660–8667.
- (28) Fischer, F.; Hahn, T.; Bäessler, H.; Bauer, L.; Strohriegel, P.; Köhler, A. Measuring Reduced C_{60} Diffusion in Crosslinked Polymer Films by Optical Spectroscopy. *Adv. Funct. Mater.* **2014**, *24*, 6172–6177.
- (29) Köhler, A.; Bäessler, H. *Electronic Processes in Organic Semiconductors: An Introduction*; Wiley VCH, 2015.
- (30) Kepler, R. G. Charge Carrier Production and Mobility in Anthracene Crystals. *Phys. Rev.* **1960**, *119*, 1226–1229.
- (31) Leblanc, O. H. Hole and Electron Drift Mobilities in Anthracene. *J. Chem. Phys.* **1960**, *33*, 626.
- (32) Scheler, E.; Strohriegel, P. Three Color Random Fluorene-Based Oligomers for Fast Micrometer-Scale Photopatterning. *Chem. Mater.* **2010**, *22*, 1410–1419.
- (33) Blouin, N.; Michaud, A.; Leclerc, M. A Low-Bandgap Poly(2,7-carbazole) Derivative for Use in High-Performance Solar Cells. *Adv. Mater.* **2007**, *19*, 2295–2300.
- (34) Kim, J.; Kwon, Y. S.; Shin, W. S.; Moon, S. J.; Park, T. Carbazole-Based Copolymers: Effects of Conjugation Breaks and Steric Hindrance. *Macromolecules* **2011**, *44*, 1909–1919.
- (35) Hahn, T.; Tscheuschner, S.; Kahle, F.-J.; Reichenberger, M.; Athanasopoulos, S.; Saller, C.; Bazan, G. C.; Nguyen, T.-Q.; Strohriegel, P.; Bäessler, H.; Köhler, A. Monomolecular and Bimolecular Recombination of Electron–Hole Pairs at the Interface of a Bilayer Organic Solar Cell. *Adv. Funct. Mater.* **2016**, No. 1604906.
- (36) Tanto, B.; Guha, S.; Martin, C. M.; Scherf, U.; Winokur, M. J. Structural and spectroscopic investigations of bulk poly [bis(2-ethyl)hexylfluorene]. *Macromolecules* **2004**, *37*, 9438–9448.
- (37) Crank, J. Methods of Solution When the Diffusion Coefficient is Constant. In *The Mathematics of Diffusion*, 2nd ed., Crank, J., Ed.; Clarendon Press: Oxford, 1975.
- (38) Lakowicz, J. R. *Principles of Fluorescence Spectroscopy*, 3rd ed.; Springer, 2006.
- (39) Dattani, R.; Cabral, J. T. Polymer fullerene solution phase behaviour and film formation pathways. *Soft Matter* **2015**, *11*, 3125–3131.
- (40) Wong, H. C.; Sanz, A.; Douglas, J. F.; Cabral, J. T. Glass formation and stability of polystyrene-fullerene nanocomposites. *J. Mol. Liq.* **2010**, *153*, 79–87.
- (41) Kahle, F. J.; Saller, C.; Köhler, A.; Strohriegel, P. Crosslinked Semiconductor Polymers for Photovoltaic Applications. *Adv. Energy Mater.* **2017**, *7*, No. 1700306.
- (42) Tournebise, A.; Rivaton, A.; Gardette, J. L.; Lombard, C.; Pepinon-Donat, B.; Beaupre, S.; Leclerc, M. How Photoinduced Crosslinking Under Operating Conditions Can Reduce PCDTBT-Based Solar Cell Efficiency and then Stabilize It. *Adv. Energy Mater.* **2014**, *4*, No. 1301530.
- (43) Peters, C. H.; Sachs-Quintana, I. T.; Kastrop, J. P.; Beaupre, S.; Leclerc, M.; McGehee, M. D. High Efficiency Polymer Solar Cells with Long Operating Lifetimes. *Adv. Energy Mater.* **2011**, *1*, 491–494.

8. Facile method for the investigation of temperature-dependent C₆₀ diffusion in conjugated polymers

(44) Peters, C. H.; Sachs-Quintana, I. T.; Mateker, W. R.; Heumueller, T.; Rivnay, J.; Noriega, R.; Beiley, Z. M.; Hoke, E. T.; Salleo, A.; McGehee, M. D. The Mechanism of Burn-in Loss in a High Efficiency Polymer Solar Cell. *Adv. Mater.* **2012**, *24*, 663–668.

(45) Liu, Q.; Huang, S. C.; Suo, Z. G. Brownian Motion of Molecular Probes in Supercooled Liquids. *Phys. Rev. Lett.* **2015**, *114*, No. 224301.

(46) Gotze, W.; Sjogren, L. Relaxation Processes in Supercooled Liquids. *Rep. Prog. Phys.* **1992**, *55*, 241–376.

(47) Berthier, L.; Biroli, G. Theoretical perspective on the glass transition and amorphous materials. *Rev. Mod. Phys.* **2011**, *83*, 587–645.

(48) Xie, R. X.; Lee, Y.; Aplan, M. P.; Caggiano, N. J.; Müller, C.; Colby, R. H.; Gomez, E. D. Glass Transition Temperature of Conjugated Polymers by Oscillatory Shear Rheometry. *Macromolecules* **2017**, *50*, 5146–5154.

(49) Beiner, M.; Huth, H. Nanophase separation and hindered glass transition in side-chain polymers. *Nat. Mater.* **2003**, *2*, 595–599.

(50) Hou, J.; Inganäs, O.; Friend, R. H.; Gao, F. Organic solar cells based on non-fullerene acceptors. *Nat. Mater.* **2018**, *17*, 119–128.

Supporting Information

A Facile Method for the Investigation of Temperature-Dependant C₆₀ Diffusion in Conjugated Polymers

Christina Saller^{1‡}, Frank-Julian Kahle^{2‡}, Thomas Müller², Tobias Hahn², Steffen Tscheuschner², Denys Priadko², Peter Strohriegl^{1,3,4}, Heinz Bässler³, Anna Köhler^{2,3*}

¹ Macromolecular Chemistry I, University of Bayreuth, 95440 Bayreuth, Germany

² Soft Matter Optoelectronics, University of Bayreuth, 95440 Bayreuth, Germany

³ Bayreuth Institute of Macromolecular Science (BIMF), University of Bayreuth, 95440 Bayreuth, Germany

⁴ Bavarian Polymer Institute (BPI), University of Bayreuth, 95440 Bayreuth, Germany

[‡] Both authors contributed equally

*anna.koehler@uni-bayreuth.de

8. Facile method for the investigation of temperature-dependent C₆₀ diffusion in conjugated polymers

Full synthetic details:

Materials

All chemicals and anhydrous THF were used as received from commercial suppliers. For purification, solvents were distilled prior to use. Argon inert gas atmosphere was used for air-sensitive and moisture-sensitive reactions. The monomers 2,7-bis(4',4',5',5'-tetramethyl-1',3',2'-dioxaborolan-2'-yl)-*N*-(heptadecan-9''-yl)carbazole, 4,7-bis(5'-bromothiophen-2'-yl)-2,1,3-benzothiadiazole, and 4,7-bis(5'-bromo-4'-hexylthien-2'-yl)-2,1,3-benzothiadiazole were delivered by SunaTech Inc. and used without further purification. The synthesis of *N,N'*-bis(4-bromophenyl)-*N,N'*-bis(4-methylphenyl)benzidine was carried out as reported in literature.¹ C₆₀ was purchased by American Dye Source and used as received. Poly(2-methoxy-5-(2-ethylhexyloxy)-1,4-phenylenevinylene) (MEH-PPV) was purchased by Aldrich and also used as received. ¹H NMR spectra were recorded on a Bruker Avance 300 spectrometer in CDCl₃ at 300 MHz operated at room temperature. High temperature ¹H NMR spectra were obtained with a Varian INOVA 300 spectrometer at 120 °C in 1,1,2,2-tetrachloroethane as solvent. The residual solvent peaks were used as internal reference. Deuterated solvents were purchased from Deutero. Mass spectra were measured with a Finnigan MAT 8500. Size exclusion chromatography (SEC) was carried out with a Waters 515 pump with UV detector (UV WAT 2489) and refractive index detector (RI WAT 410) equipped with two Resipore columns (3 μm). As eluent, tetrahydrofuran was used at a flow rate of 0.5 mlmin⁻¹ and *o*-dichlorobenzene was used as internal standard. High temperature SEC was performed at PSS Polymer Standards Service GmbH. Differential scanning calorimetry (DSC) was performed on a Mettler Toledo DSC 2 with a temperature rate of 40 Kmin⁻¹ under nitrogen atmosphere. The absorption coefficient α required to evaluate the diffusion data was determined by measuring the absorption spectra using a Cary 5000 spectrometer.

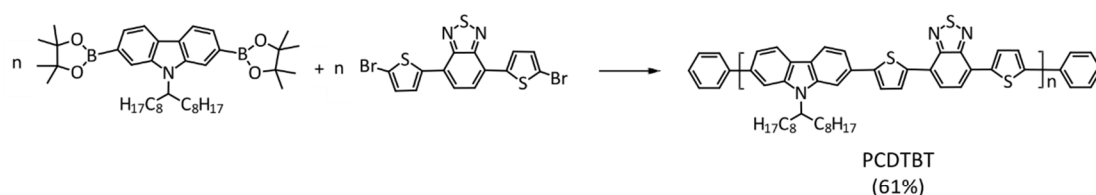


Figure S1: Synthesis scheme for Poly-(*N*-heptadecan-9'-yl)-2,7-carbazole-alt-5,5-(4',7'-bis(thien-2-yl)-2',1',3'-benzothia diazole): PCDTBT

Poly-(*N*-heptadecan-9'-yl)-2,7-carbazole-alt-5,5-(4',7'-bis(thien-2-yl)-2',1',3'-benzothiadiazole): PCDTBT was synthesized similar to the procedure described by Leclerc.² In a Schlenk flask, 0.723 g (1.10 mmol) of

7. Monomolecular and bimolecular recombination of electron–hole pairs at the interface of a bilayer organic solar cell

2,7-bis(4',4',5',5'-tetramethyl1',3',2'-dioxaborolan-2'-yl)-*N*-(heptadecan-9''-yl)carbazole, 0.504 g (1.10 mmol) of 4,7-bis(5'-bromothien-2'-yl)-2,1,3-benzothiadiazole, 14 mL of toluene and 3.7 mL of an aqueous tetraethylammonium hydroxide solution (20 wt%) were mixed under argon. After degassing by three freeze-thaw cycles, 5.0 mg of tris(dibenzylideneacetone)dipalladium(0) and 6.7 mg of tri(*o*-tolyl)-phosphine were added and again three freeze-thaw cycles were conducted before stirring the mixture under reflux for 72 h. Endcapping was performed by addition of 0.173 g (1.1 mmol) of bromobenzene, stirring for 1 h at reflux temperature and addition of 0.134 g (1.10 mmol) of phenylboronic acid. The mixture was allowed to cool to room temperature. After precipitation in methanol/water (10:1), the polymer was fractionated via Soxhlet extraction using acetone, hexane, and toluene. The reduced toluene fraction was precipitated in methanol/water (10:1) and dried in vacuum overnight. Yield: 0.468 g (61%) of a violet powder. A molecular weight of 37,000 gmol⁻¹ (*M_w*) and 16,000 gmol⁻¹ (*M_n*) was determined by high temperature polymer size exclusion chromatography in trichlorobenzene at 150 °C with a polydispersity index of 2.25 (polystyrene calibration). ¹H NMR (300 MHz, C₂D₂Cl₄, 120 °C): δ = 0.68-0.92 (m, CH₃), 1.07-1.59 (m, CH₂), 2.10 (br, carbazole-CH₂), 2.38 (br, carbazole-CH₂), 4.68 (br, CH), 7.04-8.37 (m, ar-CH).

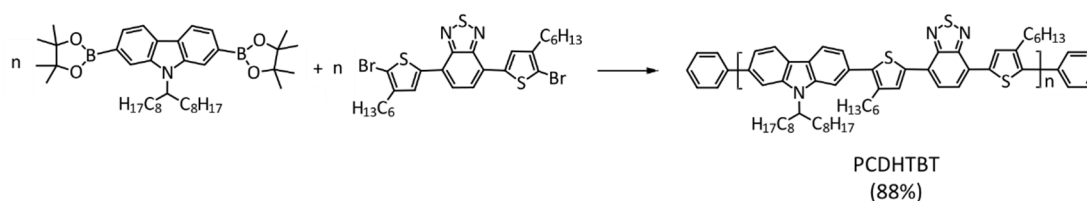


Figure S2: Synthesis scheme for Poly-(*N*-heptadecan-9'-yl)-2,7-carbazole-alt-5,5-(4',7'-bis(4-hexylthien-2-yl)-2',1',3'-benzothiadiazole): PCDHTBT

Poly-(*N*-heptadecan-9'-yl)-2,7-carbazole-alt-5,5-(4',7'-bis(4-hexylthien-2-yl)-2',1',3'-benzothiadiazole):
The synthesis of PCDHTBT was carried out similar to the procedure described in literature, but with a different catalyst system.³ In a Schlenk flask, a mixture of 0.526 g (0.80 mmol) of 2,7-bis(4',4',5',5'-tetramethyl1',3',2'-dioxaborolan-2'-yl)-*N*-(heptadecan-9''-yl)carbazole, 0.501 g (0.80 mmol) of 4,7-bis(5'-bromo-4'-hexylthien-2'-yl)-2,1,3-benzothiadiazole, 8 mL of toluene and 2.7 mL of an aqueous tetraethylammonium hydroxide solution (20 wt%) was degassed by three freeze-thaw cycles. After addition of 3.7 mg of tris(dibenzylideneacetone)dipalladium(0) and 4.9 mg of tri(*o*-tolyl)phosphine, the resulting mixture was degassed again by three freeze-thaw cycles and stirred at reflux temperature under argon for 72 h. 0.126 g (0.80 mmol) of bromobenzene were added and the mixture refluxed for 1 h under argon. Endcapping was finished by the addition of 0.098 g (0.80 mmol) of phenylboronic acid and stirring

8. Facile method for the investigation of temperature-dependent C₆₀ diffusion in conjugated polymers

overnight at reflux temperature. Cooled to room temperature, the polymer was precipitated into methanol/water (10:1) and purified via Soxhlet extraction with acetone and hexane. The reduced hexane fraction was precipitated into methanol/water (10:1) and the polymer was dried in vacuum overnight. Yield: 0.611 g (88%) of a dark-red powder. Size exclusion chromatography in THF solution at room temperature exhibits a molecular weight of 14,000 gmol⁻¹ (M_w) and 7,000 gmol⁻¹ (M_n) with a polydispersity index of 2.09 (polystyrene calibration). ¹H NMR (300 MHz, C₂D₂Cl₄, 120 °C): δ = 0.75-0.94 (m, CH₃), 1.05-1.50 (m, CH₂), 1.75 (br, thiophene-CH₂), 2.04 (br, carbazole-CH₂), 2.32 (br, carbazole-CH₂), 2.67-2.93 (m, thiophene-CH₂), 4.62 (br, CH), 7.02-8.19 (m, ar-CH).

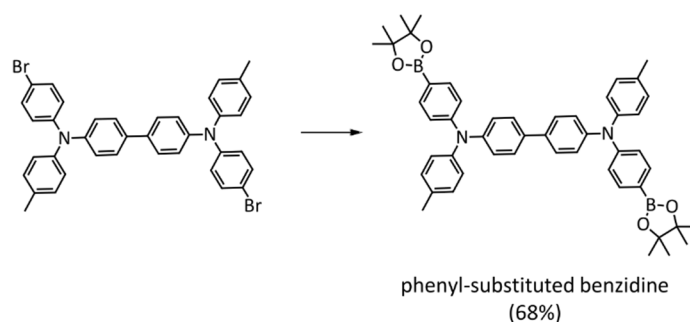


Figure S3: Synthesis scheme for *N,N'*-bis(4-methylphenyl)-*N,N'*-bis((4',4',5',5'-tetramethyl-1',3',2'-dioxaborolan-2'-yl)phenyl)benzidine

N,N'-bis(4-methylphenyl)-*N,N'*-bis((4',4',5',5'-tetramethyl-1',3',2'-dioxaborolan-2'-yl)phenyl)benzidine:

In a three neck flask, 1.246 g (1.85 mmol) of *N,N'*-bis(4-bromophenyl)-*N,N'*-bis(4-methylphenyl)benzidine was dissolved in 18 mL of anhydrous THF under argon. The solution was cooled to -78 °C and 2.54 mL (4.06 mmol) of *n*-butyllithium (1.6 M in hexane) were added dropwise. After stirring for 30 min at -78 °C, 0.91 mL (4.43 mmol) of 2-isopropoxy-4,4,5,5-tetramethyl-1,3,2-dioxaborolane were added rapidly and stirred for 1 h. The reaction mixture was allowed to warm to room temperature and stirred overnight before it was poured into water. After extraction with diethyl ether, the organic phase was washed with brine, dried over Na₂SO₄, and the solvent was evaporated. The crude product was purified via recrystallization in hot ethanol. Yield: 0.962 g (1.25 mmol, 68%) of a white solid. ¹H NMR (300 MHz, CDCl₃, 20 °C): δ (ppm) = 1.33 (s, borolane-CH₃), 2.33 (s, phenyl-CH₃), 7.01-7.16 (m, 16 H, ArH), 7.44 (d, 8.6 Hz, 4 H, ArH benzidine), 7.66 (d, 8.5 Hz, 4 H, ArH borolane). EI MS: m/z (%) = 768 (M⁺, 48), 642 (62) 516 (100), 384 (5), 321 (7), 258 (19).

7. Monomolecular and bimolecular recombination of electron–hole pairs at the interface of a bilayer organic solar cell

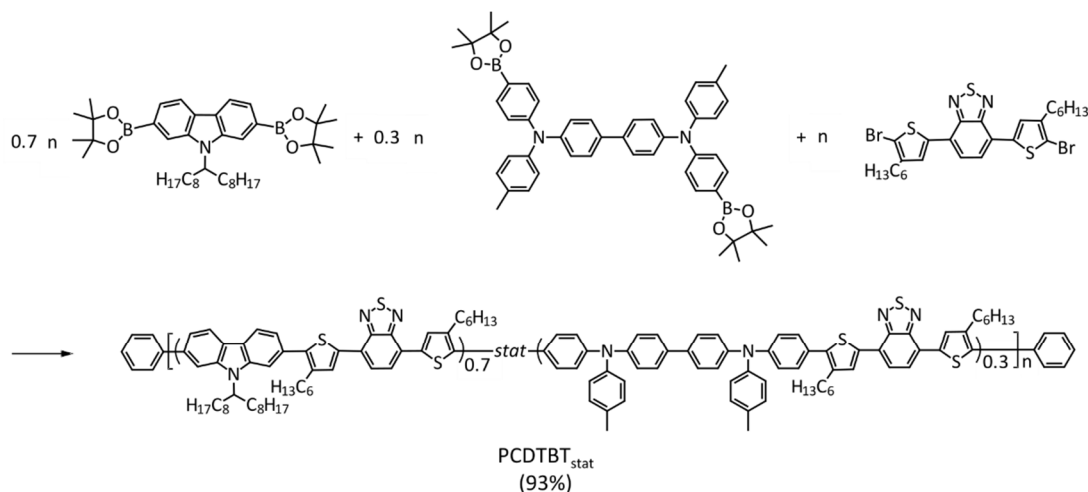


Figure S4: Synthesis scheme for Poly[(*N*-heptadecan-9'-yl)-2,7-carbazole-alt-5,5-(4',7'-bis(4-hexylthien-2-yl)-2',1',3'-benzothiadiazole)]_{0.7}-stat-[*N,N'*-bis(4-methylphenyl)-*N,N'*-diphenylbenzidine-alt-5,5-(4',7'-bis(4-hexylthien-2-yl)-2',1',3'-benzothiadiazole)]_{0.3}: PCDTBT_{stat}

Poly[(*N*-heptadecan-9'-yl)-2,7-carbazole-alt-5,5-(4',7'-bis(4-hexylthien-2-yl)-2',1',3'-benzothiadiazole)]_{0.7}-stat-[*N,N'*-bis(4-methylphenyl)-*N,N'*-diphenylbenzidine-alt-5,5-(4',7'-bis(4-hexylthien-2-yl)-2',1',3'-benzothiadiazole)]_{0.3}: PCDTBT_{stat} was synthesized via Suzuki coupling according to the following procedure:⁴ The molar ratio of the carbazole, the phenyl-substituted benzidine, and the bithienyl benzothiadiazole units in PCDTBT_{stat} is 0.7:0.3:1. A Schlenk flask was charged 0.368 g (0.56 mmol) of 2,7-bis-(4',4',5',5'-tetramethyl-1',3',2'-dioxaborolan-2'-yl)-*N*-(heptadecan-9''-yl)carbazole, 0.184 g (0.24 mmol) of *N,N'*-bis(4-methylphenyl)-*N,N'*-bis((4',4',5',5'-tetramethyl-1',3',2'-dioxaborolan-2'-yl)phenyl)-benzidine, 0.501 g (0.80 mmol) of 4,7-bis(5'-bromo-4'-hexylthien-2'-yl)-2,1,3-benzothiadiazole and 12 mL of toluene under argon. One drop of Aliquat 336 and 20 mL of 2 M Na₂CO₃ solution were added and the mixture was degassed by three freeze-thaw cycles. Afterwards, 14 mg of tetrakis(triphenylphosphine)palladium(0) were added and followed by again three freeze-thaw cycles. The reaction mixture was then stirred under reflux in an argon atmosphere for 90 h before 0.126 g (0.80 mmol) of bromobenzene was added. After stirring at reflux temperature for 2 h, 0.098 g (0.80 mmol) of phenylboronic acid was added and the reaction mixture was refluxed overnight before allowed to cool to room temperature. The polymer was precipitated into methanol/water (10:1). Soxhlet extraction was carried out using acetone and toluene. The reduced toluene fraction was precipitated into methanol/water (10:1) and dried in vacuum overnight. Yield: 0.669 g (93%) of a dark-red powder. A molecular weight of 47,000 gmol⁻¹ (*M_w*) and 18,000 gmol⁻¹ (*M_n*) was determined by size exclusion

8. Facile method for the investigation of temperature-dependent C₆₀ diffusion in conjugated polymers

chromatography in THF solution with a polydispersity index of 2.56 (polystyrene calibration). ¹H NMR (300 MHz, C₂D₂Cl₄, 120 °C): δ = 0.75-0.95 (m, CH₃), 1.05-1.55 (m, CH₂), 1.75 (br, thiophene-CH₂), 2.04 (br, carbazole-CH₂), 2.23-2.44 (m, benzidine-CH₃, carbazole-CH₂), 2.63-2.95 (m, thiophene-CH₂), 4.62 (br, CH), 6.92-8.22 (m, ar-CH). From the integration of the signal for the CH₂ group in the swallow-tail spacer of the carbazole unit (2.04 ppm), the combined signal for the methyl group in the benzidine units and the other CH₂ group in the carbazole spacer (2.23-2.44 ppm), and the signal for the CH₂ groups in the hexyl spacer of the thiophene (1.75 ppm), a molar ratio of 0.7:0.3:1 was calculated (**Figure S5**).

7. Monomolecular and bimolecular recombination of electron-hole pairs at the interface of a bilayer organic solar cell

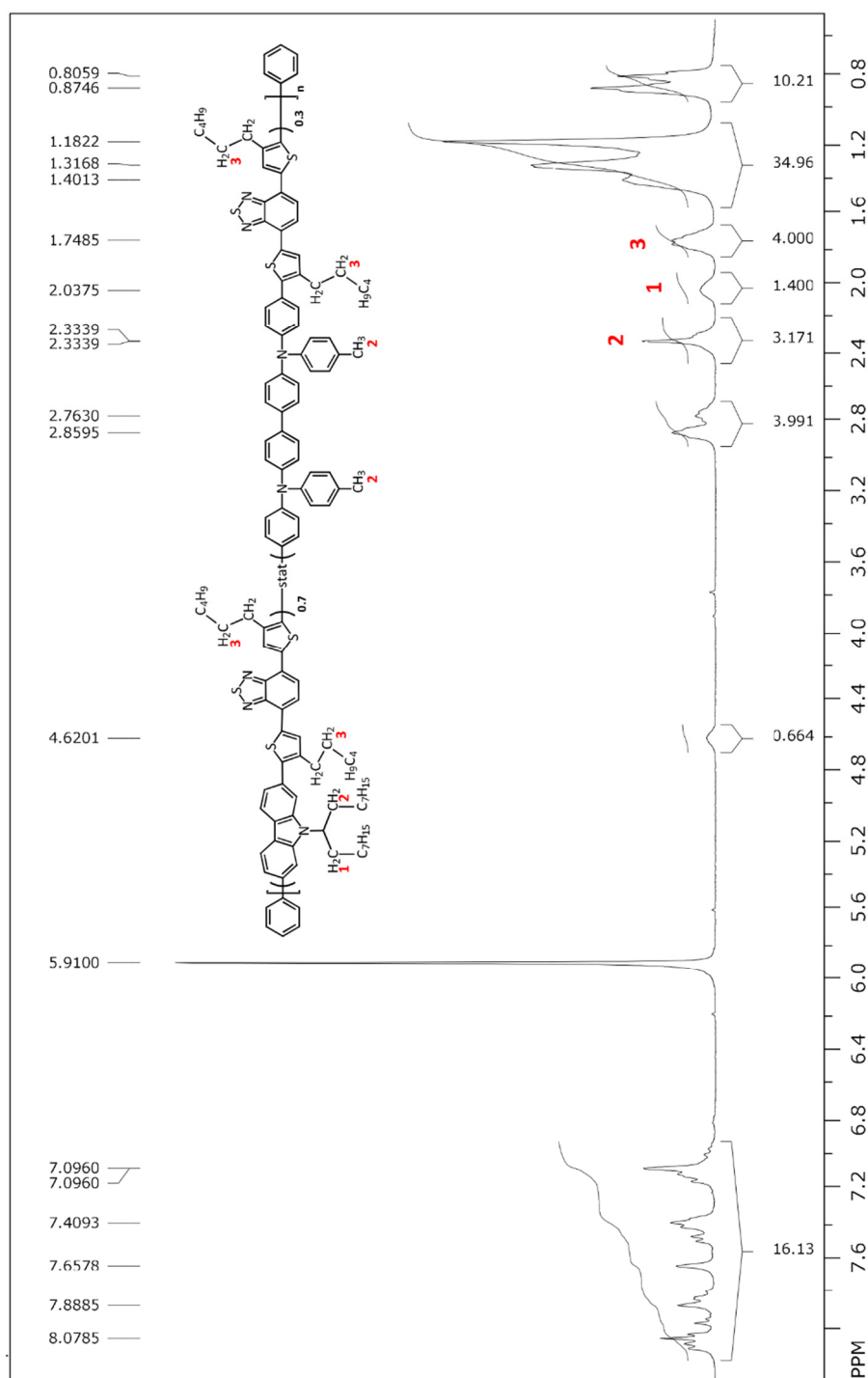


Figure S5: ^1H NMR spectrum of PCDTBT_{stat} (300 MHz) in $\text{C}_2\text{D}_2\text{Cl}_4$ at 120°C . For the calculation of the molar ratio see text.

8. Facile method for the investigation of temperature-dependent C₆₀ diffusion in conjugated polymers

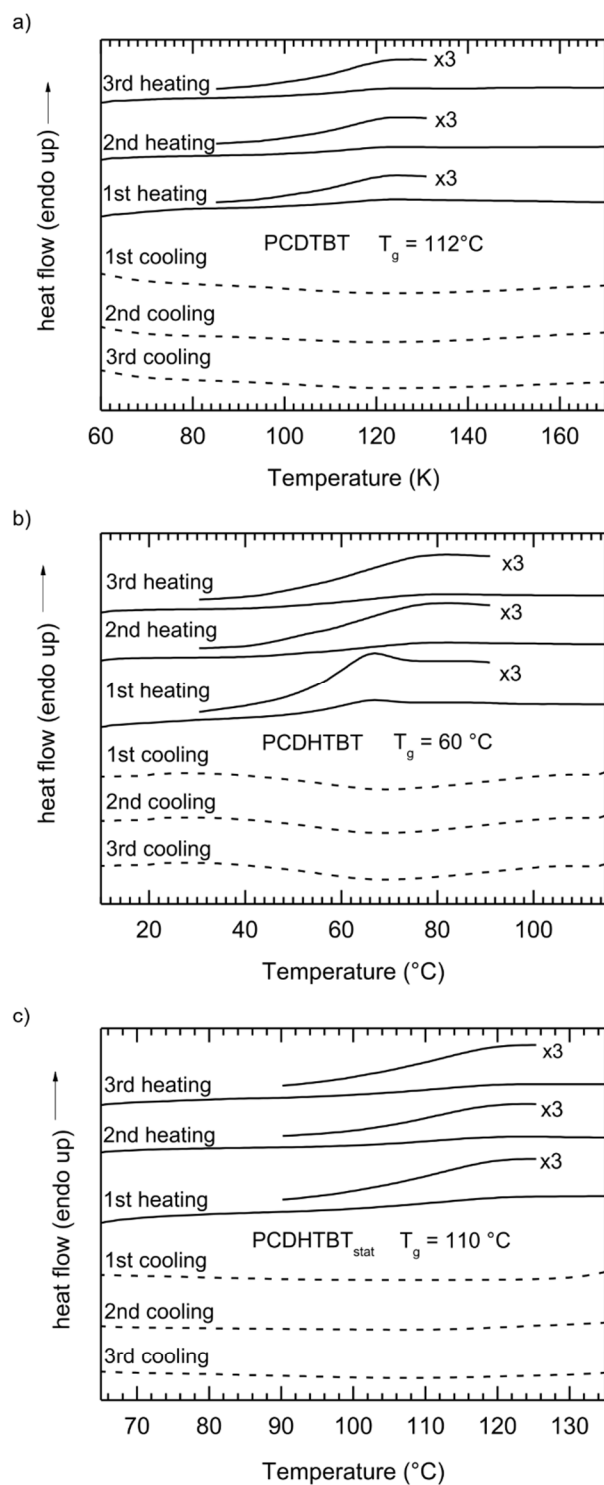


Figure S6: DSC measurements of a) PCDTBT, b) PCDHTBT, and c) PCDTBT_{stat}. A heating and cooling rate of 40 Kmin⁻¹ under nitrogen atmosphere was used.

7. Monomolecular and bimolecular recombination of electron–hole pairs at the interface of a bilayer organic solar cell

Determination of the Stern-Volmer constant K_d :

In order to determine the Stern-Volmer constant K_d we prepared i) neat films of the polymers PF2/6-A-25:75, PCDHTBT, PCDTBT and PCDTBT_{stat} and ii) blend films of the respective polymers with 2 wt% content of PC₆₀BM. PC₆₀BM was chosen to ensure proper solubility in the polymer solution from which the films were cast via spin-coating. To achieve a homogenous distribution of the fullerene within the polymer matrix we used only 2 wt% of PCBM.⁵⁻⁶ For each of the films we then carried out steady-state PL measurements. From the observed quenching in the PCBM containing samples as compared to the neat films we extracted the value of K_d for each polymer according to equation 7 from the main text. The resulting K_d values are given in **Table S1**.

Detailed derivation of equations (3)-(5):

In the following derivation, we assume a film of thickness d consisting of one fluorophore type. This layer will be denoted as sensor layer. The fluorophores shall have only one possible excited electronic state that decays either radiatively or non-radiatively in a film. The PL of a fluorophore is therefore given by

$$PL = \frac{k_0 \cdot k_r}{k_r + k_{nr}} \quad (1')$$

with k_0 being the excitation rate and k_r and k_{nr} being their radiative and non-radiative decay rate of the excited state, respectively. When exciting from the glass side of a sample, the excitation rate is

$$k_0(x) = K_0 \cdot \exp(-\alpha(d - x)) \quad (2')$$

Now we consider a fluorophore film that additionally features a concentration $c(x, t)$ of quenchers, e.g. C₆₀. For the PL of a fluorophore at position x in the sensor layer in the presence of quencher molecules, equation (1') changes to

$$PL(x, t) = \frac{k_0(x) \cdot k_r}{k_r + k_{nr} + k_q(x, t)} \quad (3')$$

k_q denotes the additional quenching rate caused by the presence of C₆₀. Self-absorption within the sensor layer as well as reflexions at the polymer/C₆₀-interface are neglected.

8. Facile method for the investigation of temperature-dependent C₆₀ diffusion in conjugated polymers

For the calculation of the fluorescence of the whole sensor layer consisting of several fluorophores, equation (3') is regarded as a PL density by assuming the rates k to be rate densities ($[k] = \text{m}^{-3}\text{s}^{-1}$). Thus, the photoluminescence of the sensor layer PL_{total} with the area A and the thickness d at a time t can be calculated by inserting (2') into (3') and integrating over the layer volume:

$$PL_{\text{total}}(t) = A \int_0^d PL(x, t) dx = A \cdot K_0 \int_0^d \exp(-\alpha(d-x)) \cdot \frac{k_r}{k_r + k_{\text{nr}} + k_q(x, t)} dx \quad (4')$$

This is equation (3) of the main text.

If there is no quencher present in the sensor layer ($c = 0, k_q = 0$), PL_{total} is given by:

$$PL_{\text{total}}(c = 0) = A \cdot K_0 \cdot \frac{k_r}{k_r + k_{\text{nr}}} \cdot \frac{1 - \exp(-\alpha d)}{\alpha} \quad (5')$$

This is equation (4) of the main text.

Finally, the ratio of the PL from the sample half with C₆₀ in relation to the PL from the reference half without C₆₀ is then given by:

$$\frac{PL_{\text{C}_{60}}(t)}{PL_0} = \frac{PL_{\text{total}}(t)}{PL_{\text{total}}(c = 0)} = \frac{\alpha}{1 - \exp(-\alpha d)} \int_0^d \exp(-\alpha(d-x)) \cdot \left(1 + \frac{k_q(x, t)}{k_r + k_{\text{nr}}}\right)^{-1} dx \quad (6')$$

This is equation (5) of the main text.

Detailed explanation of the self-consistent approach (cf. section 3.2 in the main text):

To account for a possible concentration gradient at the beginning of the experiment, we took an iterative, self-consistent approach ("fit B", red dashed line in **Figure S7a**). In a first step, we simulate the diffusion with the aim to obtain the approximate initial concentration profile in the experiment. For this, we apply equation 6 with the initial condition that there will be no C₆₀, and thus no PL-quenching ($R_0 = 1$) at a certain time $t < 0$ (**Figure S7b**). The diffusion coefficient D is adjusted until a reasonable fit to the experimental data is achieved, in particular at later times, as illustrated in **Figure S7a**. From this simulation, we obtain an initial spatial concentration profile $c(x, t = 0)$ (**Figure S7c**). This is used in a

7. Monomolecular and bimolecular recombination of electron–hole pairs at the interface of a bilayer organic solar cell

second step as initial input concentration, nominally $c_0(T_1)$, to obtain an improved and more accurate diffusion coefficient.

Including surface quenching

To account for a possible influence of exciton quenching at the polymer/C₆₀ interface without the presence of C₆₀ in the polymer bulk we applied a slightly modified approach that is based on the self-consistent procedure discussed above. In this case we added another term in equation 6 of the main text:

$$\frac{PL}{PL_0}(t) = \frac{\alpha}{1-\exp(-\alpha d)} \int_0^d \exp(-\alpha(d-x)) \cdot (1 + K_D \cdot c(x,t) + s(x,t) \cdot y_s)^{-1} dx. \quad (1^*)$$

where y_s is a measure of the initial quenching at the polymer/C₆₀ interface when no dopant is presented within the polymer bulk. This accounts for the fact that excitons may diffuse over a certain distance before they get finally quenched at said interface. s is defined as

$$s(x,t) = \exp\left(-\frac{x}{x_d} \cdot \exp\left(\frac{c(x,t)}{c_{char}}\right)\right) \quad (2^*)$$

Where x_d denotes the exciton diffusion length (typically in the order of 10 nm) and c_{char} defines the characteristic concentration at which the distance to the next interface has decayed to 1/e of the initial value of x_d (here assumed to be 1 wt%). From this concentration on the quenching is regarded to be dominated by the bulk effect characterized by $K_D \cdot c(x,t)$. The second exponential factor accounts for the fact that the distance to the next interface decreases with increasing concentration, effectively reducing the diffusion length of the exciton.

The value for y_s is determined from a quick calculation in which we take equation (1*) at $t = 0$ s and with no quencher molecules present in the bulk of the polymer. y_s is systematically varied until the calculated quenching level is equivalent to the expected quenching level for a given exciton diffusion length x_d , e.g. about 20 % for a film of thickness 70 nm.⁷ Apart from this modification, the fitting procedure is identical to the self-consistent approach discussed above and in the main text (see figure S7).

8. Facile method for the investigation of temperature-dependent C_{60} diffusion in conjugated polymers

An exemplary comparison of all three approaches (effective concentration, self-consistent approach without initial quenching, self-consistent approach with initial surface quenching) is shown in **figure S8** for the case of crosslinked PF2/6-A-75:25. We find good agreement of all three fits with the experimental data and only small to no differences in the extracted diffusion coefficient (cf. **Table S1**). This again illustrates that in our case, an exact knowledge of the initial concentration profile is not required to obtain a reasonable value for the diffusion coefficient of a dopant in a polymer matrix.

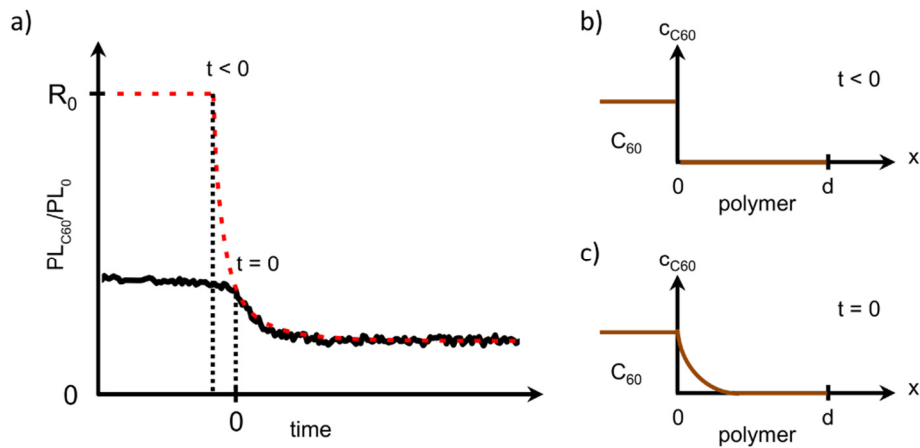


Figure S7: (a) Illustration of the fitting procedure using a self consistent initial condition as described in the main text. The black solid line corresponds to experimental data, the red dashed line is the result of a first simulation starting at zero initial concentration (i.e. right before evaporation) and ending at an equilibrium concentration corresponding to the experimentally observed final quenching level. (b) The concentration profiles assumed to prevail just before acceptor deposition at T_1 . This is used as input to the first fitting round. (c) The concentration profile obtained from the first fitting round, assumed to prevail just before the heating step to T_2 . This is used as initial condition for the second fitting round to the experimental data.

7. Monomolecular and bimolecular recombination of electron–hole pairs at the interface of a bilayer organic solar cell

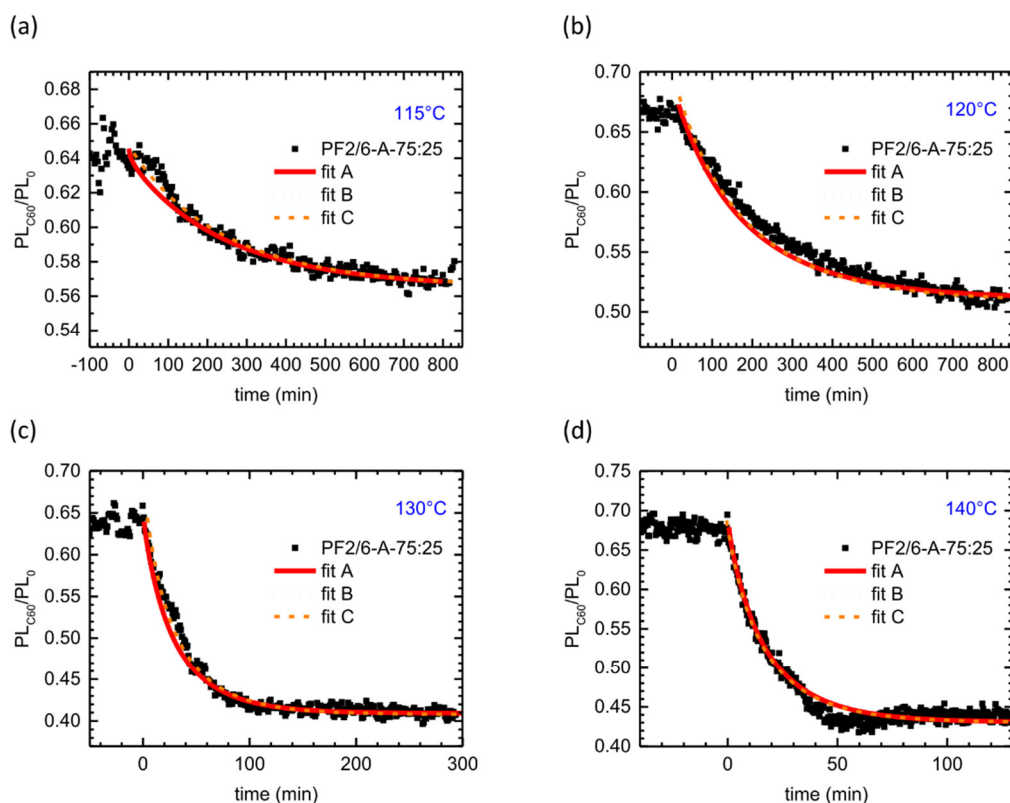


Figure S8: Time-dependence of $PL_{C_{60}}/PL_0$ measured on bilayer samples using crosslinked PF2/6-A-75:25 with C_{60} on top when increasing temperature to (a) 115°C, (b) 120°C, (c) 130°C and (d) 140°C. The red solid lines correspond to a fit according to eq. 6 of the main text using an effective homogeneous concentration as initial condition to extract the diffusion coefficient for C_{60} in PF2/6-A-75:25 as a function of temperature (fit A). The green dotted (fit B) and dashed orange lines (fit C) correspond to fits using a self-consistent initial concentration profile instead, as detailed in section 3.2 of the main text as well as the explanation given here in the supporting information.

8. Facile method for the investigation of temperature-dependent C_{60} diffusion in conjugated polymers

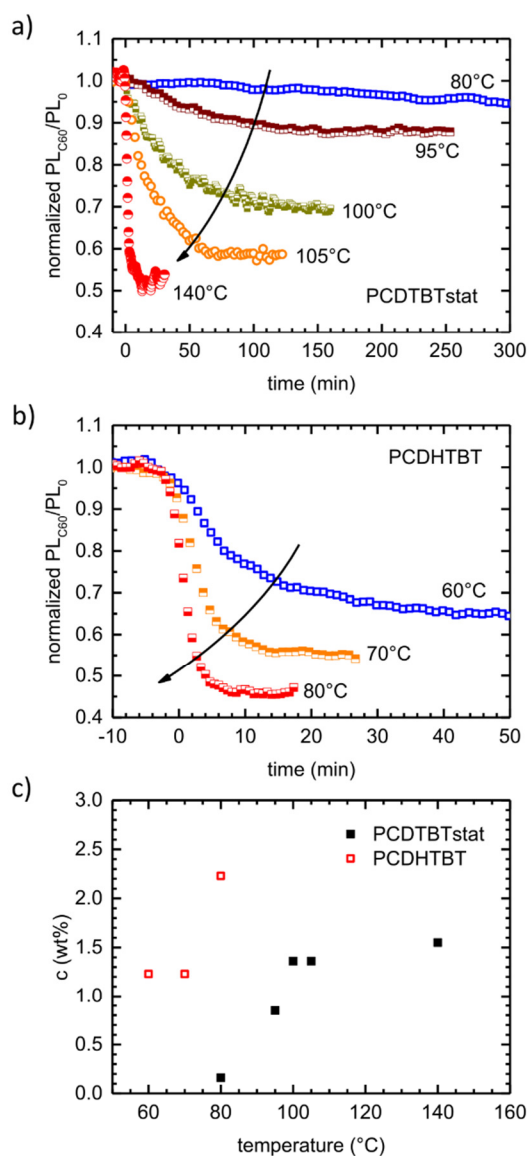
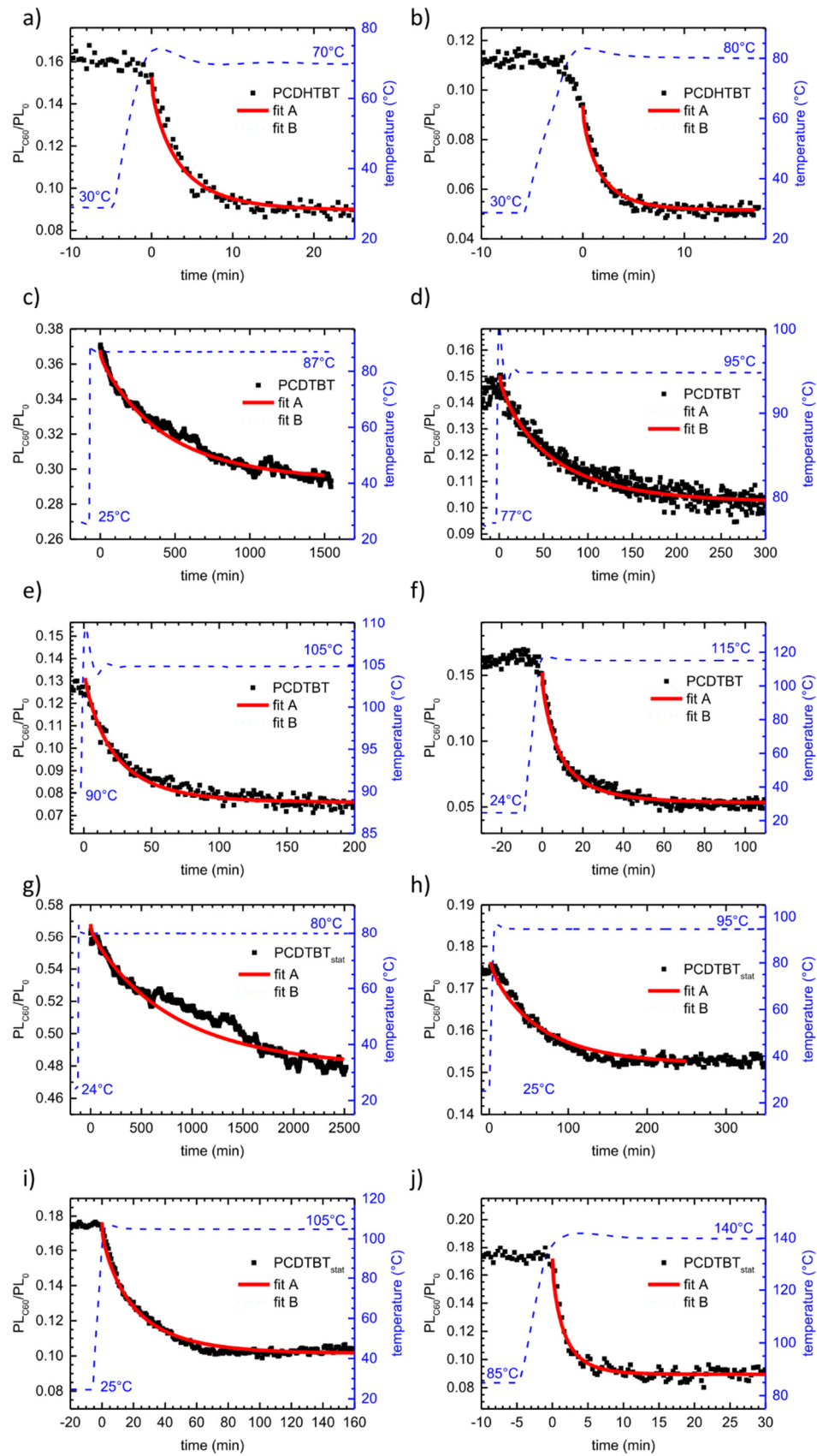


Figure S9: Time-dependence of $PL_{C_{60}}/PL_0$ for different final temperatures after a temperature increase for (a) PCDTBT_{stat} and (b) PCDHTBT. The data are normalized to the initial plateau value of $PL_{C_{60}}/PL_0$ in order to better visualize differences in decay dynamics. (c) Final concentration $c(T_2)$ as a function of the final temperature T_2 for PCDTBT_{stat} (filled symbols) and PCDHTBT (open symbols).

7. Monomolecular and bimolecular recombination of electron–hole pairs at the interface of a bilayer organic solar cell



8. Facile method for the investigation of temperature-dependent C_{60} diffusion in conjugated polymers

Figure S10: Time-dependence of $PL_{C_{60}}/PL_0$ (left axis) measured on bilayer samples using (a,b) PCDHTBT, (c-f) PCDTBT and (g-j) PCDTBT_{stat} with C_{60} on top when applying a heating ramp as indicated by the dashed blue curve (right axis). The red solid and green dotted lines correspond to fits according to eq. 6 of the main text using an effective homogenous concentration (fit A) and a self-consistent initial condition (fit B) to extract the diffusion coefficient for C_{60} (cf. figure 5c in the main text). The decay curves displayed here are the original data corresponding to some of the normalized data displayed in figure 5a in the main text and figure S9 above.

7. Monomolecular and bimolecular recombination of electron–hole pairs at the interface of a bilayer organic solar cell

Table S1: Input and output parameters for the simulated PL decay due to quenching according to the model described in section 3.2 of the main text. T_1 and T_2 correspond to the initial and final temperature of the experimentally applied heating ramp, respectively. α denotes the absorption coefficient of the respective material at the indicated excitation wavelength. K_D is the Stern-Volmer constant as determined from steady state PL quenching experiments as detailed above. $c_0(T_1)$ denotes an effective homogenous initial concentration when evaluating the data according to the first approach outlined in section 3.2 of the main text (“fit A”). $c_0(T_2)$ corresponds to the final equilibrium concentration after the temperature has been raised from T_1 to T_2 . $D_A(T_2)$ refers to the diffusion coefficient for C_{60} diffusion at T_2 assuming an effective initial concentration. $D_B(T_2)$ denotes the diffusion coefficient for C_{60} diffusion at T_2 using a self-consistent initial condition and assuming no initial quenching. $D_C(T_2)$ is deduced from a self-consistent approach with the consideration of surface quenching.

Polymer	input				output				
	T_1 in °C	T_2 in °C	α in nm ⁻¹	K_D in wt% ⁻¹	$c_0(T_1)$ in wt%	$c_0(T_2)$ in wt%	$D_A(T_2)$ in cm ² s ⁻¹	$D_B(T_2)$ in cm ² s ⁻¹	$D_C(T_2)$ in cm ² s ⁻¹
PCDTBT	22	80	0.0157 ^a	6.51	0.28	0.33	5.50·10 ⁻¹⁶	5.33·10 ⁻¹⁶	5.37·10 ⁻¹⁶
	25	87	0.0157 ^a	6.51	0.26	0.37	6.33·10 ⁻¹⁶	5.83·10 ⁻¹⁶	6.17·10 ⁻¹⁶
	77	95	0.0157 ^a	6.51	0.85	1.35	7.50·10 ⁻¹⁶	7.50·10 ⁻¹⁶	7.83·10 ⁻¹⁶
	85	100	0.0157 ^a	6.51	0.72	1.19	9.17·10 ⁻¹⁶	9.17·10 ⁻¹⁶	9.17·10 ⁻¹⁶
	90	105	0.0157 ^a	6.51	0.95	1.87	1.66·10 ⁻¹⁵	1.66·10 ⁻¹⁵	1.75·10 ⁻¹⁵
	25	115	0.0157 ^a	6.51	0.85	2.72	2.83·10 ⁻¹⁵	2.92·10 ⁻¹⁵	2.92·10 ⁻¹⁵
	27	125	0.0157 ^a	6.51	1.00	3.02	7.00·10 ⁻¹⁵	6.83·10 ⁻¹⁵	6.92·10 ⁻¹⁵
	97	140	0.0157 ^a	6.51	1.12	2.52	1.83·10 ⁻¹⁴	1.83·10 ⁻¹⁴	1.87·10 ⁻¹⁴
PCDHTBT	32	60	0.0139 ^a	8.26	0.76	1.23	4.67·10 ⁻¹⁵	4.16·10 ⁻¹⁵	4.16·10 ⁻¹⁵
	30	70	0.0139 ^a	8.26	0.67	1.23	1.12·10 ⁻¹⁴	1.05·10 ⁻¹⁴	1.08·10 ⁻¹⁴
	30	80	0.0139 ^a	8.26	1.17	2.23	2.08·10 ⁻¹⁴	2.00·10 ⁻¹⁴	2.05·10 ⁻¹⁴
PCDTBT _{stat}	25	80	0.0117 ^a	6.56	0.12	0.16	5.83·10 ⁻¹⁶	6.33·10 ⁻¹⁶	5.83·10 ⁻¹⁶
	25	95	0.0117 ^a	6.56	0.70	0.85	8.66·10 ⁻¹⁶	1.08·10 ⁻¹⁵	1.03·10 ⁻¹⁵
	77	100	0.0117 ^a	6.56	0.90	1.36	1.25·10 ⁻¹⁵	1.25·10 ⁻¹⁵	1.33·10 ⁻¹⁵
	87	105	0.0117 ^a	6.56	0.78	1.36	1.83·10 ⁻¹⁵	1.83·10 ⁻¹⁵	1.92·10 ⁻¹⁵
	85	140	0.0117 ^a	6.56	0.73	1.55	2.00·10 ⁻¹⁴	2.33·10 ⁻¹⁴	2.17·10 ⁻¹⁴
PF2/6- A-75:25	32	115	0.00357 ^b	4.81	0.11	0.16	1.62·10 ⁻¹⁴	1.65·10 ⁻¹⁴	1.65·10 ⁻¹⁴
	22	120	0.00357 ^b	4.81	0.09	0.20	2.25·10 ⁻¹⁴	2.25·10 ⁻¹⁴	2.21·10 ⁻¹⁴
	25	130	0.00357 ^b	4.81	0.11	0.30	6.33·10 ⁻¹⁴	6.17·10 ⁻¹⁴	6.17·10 ⁻¹⁴
	35	140	0.00357 ^b	4.81	0.09	0.27	1.38·10 ⁻¹³	1.40·10 ⁻¹³	1.38·10 ⁻¹³

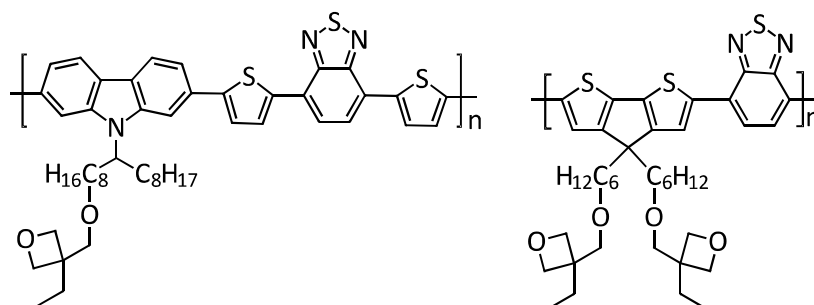
^a at 520 nm

^b at 405 nm

References

- (1) Scheler, E.; Strohriegl, P., Three Color Random Fluorene-Based Oligomers for Fast Micrometer-Scale Photopatterning. *Chem Mater* **2010**, *22*, 1410-1419.
- (2) Blouin, N.; Michaud, A.; Leclerc, M., A Low-Bandgap Poly(2,7-carbazole) Derivative for Use in High-Performance Solar Cells. *Adv Mater* **2007**, *19*, 2295–2300.
- (3) Kim, J.; Kwon, Y. S.; Shin, W. S.; Moon, S. J.; Park, T., Carbazole-Based Copolymers: Effects of Conjugation Breaks and Steric Hindrance. *Macromolecules* **2011**, *44*, 1909-1919.
- (4) Hahn, T.; Tscheuschner, S.; Kahle, F.-J.; Reichenberger, M.; Athanasopoulos, S.; Saller, C.; Bazan, G. C.; Nguyen, T.-Q.; Strohriegl, P.; Bässler, H.; Köhler, A., Monomolecular and Bimolecular Recombination of Electron–Hole Pairs at the Interface of a Bilayer Organic Solar Cell. *Adv Funct Mater* **2016**, 1604906.
- (5) Wong, H. C.; Sanz, A.; Douglas, J. F.; Cabral, J. T., Glass formation and stability of polystyrene-fullerene nanocomposites. *J Mol Liq* **2010**, *153*, 79-87.
- (6) Dattani, R.; Cabral, J. T., Polymer fullerene solution phase behaviour and film formation pathways. *Soft Matter* **2015**, *11*, 3125-3131.
- (7) Lin, J. D. A.; Mikhnenko, O. V.; Chen, J. R.; Masri, Z.; Ruseckas, A.; Mikhailovsky, A.; Raab, R. P.; Liu, J. H.; Blom, P. W. M.; Loi, M. A.; Garcia-Cervera, C. J.; Samuel, I. D. W.; Nguyen, T. Q., Systematic study of exciton diffusion length in organic semiconductors by six experimental methods. *Mater Horizons* **2014**, *1*, 280-285.

Appendix A: Optimized synthetic procedures for PCDTBTOx and PCPDTBTOx

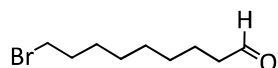


The synthesis of PCDTBTOx and PCPDTBTOx is described in Chapter 4.1.2.

Materials and methods

All chemicals and anhydrous solvents were purchased from commercial suppliers and used as received. Solvents needed for extraction and purification were distilled prior to use. The monomer 4,7-bis(4,4,5,5-tetramethyl-1,3,2-dioxaborolan-2-yl)-2,1,3-benzothiadiazole was delivered by SunaTech Inc. and used without further purification. Reactions comprising air-sensitive and moisture-sensitive substances were conducted under argon inert gas atmosphere. For reaction control and verification of the purity of substances, thin layer chromatography was performed on Polygram SIL G/UV₂₅₄ ready-to-use foil from Macherey-Nagel. Detection was conducted with UV light at 254 nm or 366 nm or staining with phosphomolybdic acid solution (20 wt% in ethanol). Column chromatography was carried out with silica gel 60 (0.063-0,200 mm) from Macherey-Nagel. ¹H NMR spectra at room temperature were recorded on a Bruker Avance 300 spectrometer in deuterated solvents at 300 MHz. High temperature ¹H NMR spectra were measured at 120 °C with a Varian INOVA 300 spectrometer in 1,1,2,2-tetrachloroethane as solvent. As internal references, the residual solvent peaks were used. Chemical shifts δ are denoted in ppm and coupling constants J in Hz. Multiplicities are abbreviated with s (singlet), d (doublet), t (triplet), q (quartet), qui (quintet), m (multiplet), and br (broadened). Deuterated solvents were ordered from Deutero. Mass spectra were recorded on a Finnigan MAT 8500 via electron ionization.

9-Bromononanal



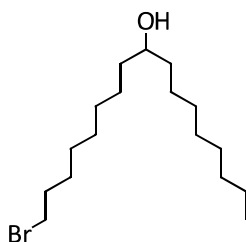
Oxalyl chloride (4.24 mL, 49.29 mmol) was dissolved in anhydrous dichloromethane (100 mL) and cooled to -78 °C under argon. A solution of anhydrous dimethyl sulfoxide (6.99 mL, 98.59 mmol) and anhydrous dichloromethane (20 mL) was added dropwise. After stirring for 5 min, a solution of 9-bromononanol (10.000 g, 44.81 mmol) in anhydrous dichloromethane (45 mL) was added dropwise over a short time and the reaction mixture was stirred for 30 min at -78 °C before triethylamine (31,23 mL, 224.06 mmol) was added dropwise. The reaction mixture was again stirred for 15 min at -78 °C, allowed to warm to room temperature and poured into water. After extraction with dichloromethane, the organic phase was washed twice with HCl solution (2%), twice with deionised water, twice with NaHCO₃ solution (5%) and again twice with deionised water. The organic phase was dried over Na₂SO₄ and the solvent was evaporated. Drying in vacuum overnight yielded 9-bromononanal (9.500 g, 42.96 mmol, 96%) as a colourless oil.

Characterization:

EI-MS: m/z (%) = 221 (M^+ , 4), 204 ($M^+ - O$, 23), 192 ($M^+ - HCO$, 17), 176 ($M^+ - CH_2HCO$, 100), 163 ($M^+ - (CH_2)_2HCO$, 5), 149 ($M^+ - (CH_2)_3HCO$, 7), 135 ($M^+ - (CH_2)_4HCO$, 22).

1H NMR (300 MHz, $CDCl_3$): δ (ppm) = 1.18-1.49 (m, 8H, CH_2), 1.50-1.70 (m, 2H, $HCO-CH_2-CH_2$), 1.75-1.92 (m, 2H, CH_2-CH_2-Br), 2.33-2.48 (m, 2H, $HCO-CH_2$), 3.40 (t, $J = 6.8$ Hz, 2H, CH_2-Br), 9.67-9.76 (t, $J = 1.8$ Hz, 1H, HCO).

1-Bromoheptadecan-9-ol

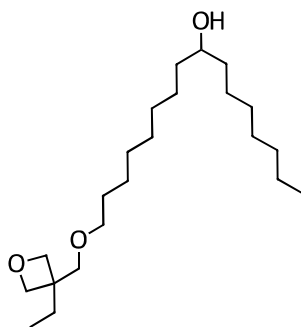


Bromooctane (8.39 mL, 48.57 mmol) was dissolved in anhydrous THF (24 mL) and added slowly to magnesium chips (1.476 g, 60.71 mmol) under argon atmosphere. When the exothermic reaction has started, the remaining solution is added dropwise under stirring and cooling if necessary. The reaction mixture is heated to reflux and stirred for 1 h. After cooling to room temperature, anhydrous THF (8 mL) was added for dilution of the reaction mixture. A solution of 9-bromononanal (8.950 g, 221.13 mmol) in anhydrous THF (15 mL) was added slowly under intermittent cooling. The reaction mixture was stirred at room temperature overnight, poured into water and extracted with diethyl ether. After washing twice with saturated $NaHCO_3$ solution, twice with deionised water and twice with brine, the organic phase was dried over Na_2SO_4 and the solvent was evaporated. After purification via column chromatography (hexanes:ethyl acetate = 5:1), 1-bromoheptadecan-9-ol (9.318 g, 27.78 mmol, 69%) was obtained as a colourless solid.

Characterization:

EI-MS: m/z (%) = 334 (M^+ , 1), 318 ($M^+ - OH$, 19), 221 ($M^+ - (CH_2)_7CH_3$, 73), 143 ($M^+ - (CH_2)_8Br$, 59).

1H NMR (300 MHz, $CDCl_3$): δ (ppm) = 0.88 (t, $J = 6.5$ Hz, 3H, CH_3), 1.19-1.52 (m, 26H, CH_2), 1.85 (qui, $J = 7.3$ Hz, 2H, CH_2-CH_2-Br), 3.41 (t, $J = 6.8$ Hz, 2H, CH_2-Br), 3.52-3.64 (br, $CH-OH$).

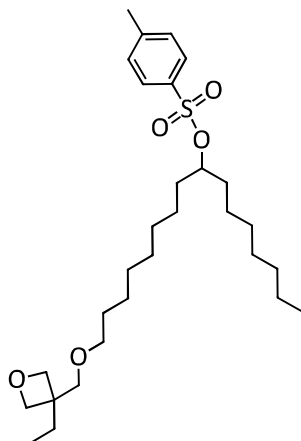
1-((3'-Ethyloxetan-3'-yl)-methoxy)-heptadecan-9-ol

Tetrabutylammonium bromide (0.448 g, 1.39 mmol) was dissolved in aqueous NaOH solution (48.624 g, 45 wt%). A solution of 1-bromoheptadecan-9-ol (9.318 g, 27.79 mmol) and (3-ethyl-oxetan-3-yl)-methanol (5.54 mL, 48.63 mmol) in distilled hexanes (160 mL) was added. The reaction mixture was stirred overnight under reflux. After cooling to room temperature, the reaction mixture was extracted with deionised water and hexanes. The organic phase was dried over Na₂SO₄ and the solvent was evaporated. 1-((3'-Ethyloxetan-3'-yl)-methoxy)-heptadecan-9-ol (6.530 g, 17.62 mmol, 63%) was obtained as a colourless oil after column chromatography (hexanes:ethylacetate = 5:1).

Characterization:

EI-MS: m/z (%) = 371 (M^+ , 1), 353 ($M^+ - OH$, 3), 340 ($M^+ - OCH_2$, 10), 322 ($M^+ - OCH_2 - OH$, 8), 257 ($M^+ - OCH_2O(CH_2)_2CCH_2CH_3$, 22), 227 ($M^+ - (CH_2)_2OCH_2O(CH_2)_2CCH_2CH_3$, 8).

¹H NMR (300 MHz, CDCl₃): δ (ppm) = 0.88 (t, J = 7.5 Hz, 6H, CH₃), 1.16-1.49 (m, 26H, CH₂), 1.50-1.62 (m, 2H, CH₂-CH₂-O), 1.74 (q, J = 7.5 Hz, 2H, oxetane-CH₂-CH₃), 3.44 (t, J = 6.5 Hz, 2H, CH₂-O), 3.52 (s, 2H, O-CH₂-oxetane), 3.53-3.63 (br, CH), 4.41 (q, J = 5.8 Hz, 4H, oxetane).

(1'-((3''-Ethyloxetan-3''-yl)-methoxy)-heptadecan-9'-yl)-4-toluenesulfonate

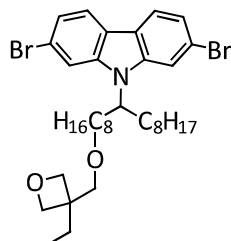
A solution of 1-((3'-ethyloxetan-3'-yl)-methoxy)-heptadecan-9-ol (3.400 g, 9.17 mmol), triethylamine (2.312 g, 22.84 mmol), and trimethylammonium hydrochloride (0.877 g, 9.17 mmol) in anhydrous dichloromethane (20 mL) was cooled to 0 °C. Tosyl chloride (2.169 g, 11.38 mmol) was dissolved in anhydrous dichloromethane (20 mL) and added to the reaction mixture in a time range of 10 min. After stirring for 90 min at 0 °C, the reaction mixture was allowed to warm to room temperature and stirred overnight. Extraction was carried out with dichloromethane and water. The organic phase was washed with deionised water, dried over Na₂SO₄ and the solvent was evaporated. Column chromatography (hexanes:ethyl acetate = 5:1) yielded the spacer molecule (1'-((3''-ethyloxetan-3''-yl)-methoxy)-heptadecan-9'-yl)-4-toluene-sulfonate (3.820 g, 7.28 mmol, 79%) as a colourless oil.

Characterization:

EI-MS: m/z (%) = 524 (M⁺, 1), 494 (M⁺ – OCH₂, 15), 353 (M⁺ – O-tosylate, 37), 322 (M⁺ – O-tosylate – OCH₂, 23), 255 (M⁺ – O-tosylate – CH₂O(CH₂)₂CCH₂CH₃, 78).

¹H NMR (300 MHz, CDCl₃): δ (ppm) = 0.80-0.93 (m, 6H, CH₃), 1.06-1.37 (m, 26H, CH₂), 1.44-1.65 (m, 2H, CH₂-CH₂-O), 1.74 (q, J = 7.5 Hz, 2H, oxetane-CH₂-CH₃), 2.44 (s, 3H, tosylate-CH₃), 3.44 (t, J = 6.5 Hz, 2H, CH₂-O), 3.52 (s, 2H, O-CH₂-oxetane), 4.41 (q, J = 5.8 Hz, 4H, oxetane), 4.53 (qui, J = 6.0 Hz, 1H, CH), 7.19 (d, J = 8.0 Hz, 2H, tosylate), 7.79 (d, J = 8.3 Hz, 2H, tosylate).

2,7-Dibromo-N-(1'-((3''-ethyloxetan-3''-yl)-methoxy)-heptadecan-9'-yl)-carbazole



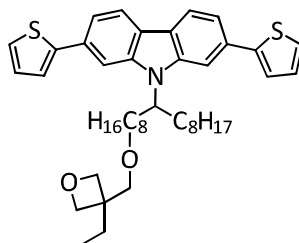
In an argon atmosphere, 2,7-dibromocarbazole (0.991 g, 3.05 mmol) and KOH (0.855 g, 15.24 mmol) were stirred in dimethyl sulfoxide (8 mL) at room temperature. A solution of (1'-((3''-ethyloxetan-3''-yl)-methoxy)-heptadecan-9'-yl)-4-toluenesulfonate (2.400 g, 4.57 mmol) in dimethyl sulfoxide (6 mL) was added slowly over a time range of 1 h. The reaction mixture was stirred at room temperature overnight and extracted with water and diethyl ether. After the organic phase was washed twice with deionised water and dried over Na₂SO₄, the solvent was evaporated. Purification was carried out via column chromatography (hexanes:toluene = 1:2). 2,7-dibromo-N-(1'-((3''-ethyloxetan-3''-yl)-methoxy)-heptadecan-9'-yl)-carbazole (1.400 g, 2.07 mmol, 68%) was obtained as a colourless oil.

Characterization:

EI-MS: m/z (%) = 677 (M^+ , 100), 647 ($M^+ - OCH_2$, 9), 450 ($M^+ - (CH_2)_8OCH_2O(CH_2)_2CCH_2CH_3$, 42), 322 ($M^+ - CH(CH_2)_7CH_3 - (CH_2)_7OCH_2O(CH_2)_2CCH_2CH_3$, 12).

1H NMR (300 MHz, $CDCl_3$): δ (ppm) = 0.77-0.91 (m, 6H, CH_3), 0.92-1.37 (m, 22H, CH_2), 1.42-1.56 (m, 2H, $\underline{CH_2-CH_2-O}$), 1.72 (q, $J = 7.5$ Hz, 2H, oxetane- $\underline{CH_2-CH_3}$), 1.77-1.97 (br, 2H, carbazole- $\underline{CH-CH_2}$), 2.10-2.28 (br, 2H, carbazole- $\underline{CH-CH_2}$), 3.39 (t, $J = 6.6$ Hz, 2H, CH_2-O), 3.49 (s, 2H, $O-\underline{CH_2}$ -oxetane), 4.40 (q, $J = 5.8$ Hz, 4H, oxetane), 4.33-4.47 (br, 1H, CH), 7.28-7.37 (br, 2H, carbazole), 7.49-7.57 (br, 1H, carbazole), 7.64-7.73 (br, 1H, carbazole), 7.84-7.96 (br, 2H, carbazole). Broadened and multiple signals are due to atropisomerism.

2,7-Di(thiophen-2'-yl)-N-(1''-((3'''-ethyloxetan-3'''-yl)-methoxy)-heptadecan-9''-yl)-carbazole



2,7-dibromo-N-(1''-((3'''-ethyloxetan-3'''-yl)-methoxy)-heptadecan-9''-yl)-carbazole (0.500 g, 0.74 mmol) and 2-(4',4',5',5'-tetramethyl-1',3',2'-dioxaborolan-2'-yl)-thiophene (0.465 g, 2.21 mmol) were dissolved in toluene (20 mL). After addition of four drops of Aliquat 336 and aqueous Na_2CO_3 solution (24.95 mL, 2M), the reaction mixture was degassed by three freeze-thaw cycles. Tetrakis(triphenylphosphine)palladium(0) (0.028 g, 0.02 mmol) was added and the reaction mixture was again degassed by three freeze-thaw cycles before stirred under reflux for 90 h. The reaction mixture was poured into water and extracted with dichloromethane. The organic phase was washed twice with deionised water and dried over Na_2SO_4 . After evaporation of the solvent, column chromatography (hexanes:THF = 10:1) was performed to remove the catalyst. 2,7-di(thiophen-2'-yl)-N-(1''-((3'''-ethyloxetan-3'''-yl)-methoxy)-heptadecan-9''-yl)-carbazole (0.485 g, 0.71 mmol, 96%) was yielded as a slightly yellowish oil.

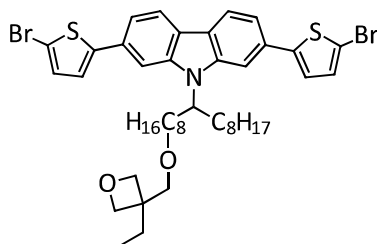
Characterization:

EI-MS: m/z (%) = 684 (M^+ , 98), 654 ($M^+ - OCH_2$, 10), 568 ($M^+ - OCH_2O(CH_2)_2CCH_2CH_3$, 4), 457 ($M^+ - (CH_2)_8OCH_2O(CH_2)_2CCH_2CH_3$, 40), 345 ($M^+ - (CH_2)_7CH_3 - (CH_2)_8OCH_2O(CH_2)_2CCH_2CH_3$, 38), 332 ($M^+ - CH(CH_2)_7CH_3 - (CH_2)_8OCH_2O(CH_2)_2CCH_2CH_3$, 28).

1H NMR (300 MHz, $CDCl_3$): δ (ppm) = 0.74-0.89 (m, 6H, CH_3), 0.97-1.36 (m, 22H, CH_2), 1.38-1.51 (m, 2H, $\underline{CH_2-CH_2-O}$), 1.70 (q, $J = 7.5$ Hz, 2H, oxetane- $\underline{CH_2-CH_3}$), 1.88-2.04 (br, 2H, carbazole- $\underline{CH-CH_2}$), 2.24-2.42 (br, 2H, carbazole- $\underline{CH-CH_2}$), 3.34 (t, $J = 6.6$ Hz, 2H, CH_2-O), 3.46 (s, 2H, $O-\underline{CH_2}$ -

oxetane), 4.38 (q, $J = 5.8$ Hz, 4H, oxetane), 4.54-4.67 (br, 1H, CH), 7.13 (dd, $J = 5.1$ Hz, $J = 3.7$ Hz, 2H, thiophene), 7.31 (dd, $J = 5.1$ Hz, $J = 1.1$ Hz, 2H, thiophene), 7.37-7.44 (br, 2H, carbazole), 7.50 (d, $J = 8.0$ Hz, 2H, thiophene), 7.56-7.62 (br, 1H, carbazole), 7.74-7.81 (br, 1H, carbazole), 8.01-8.11 (br, 2H, carbazole). Broadened and multiple signals are due to atropisomerism.

2,7-Bis(5'-bromothiophen-2'-yl)-N-(1''-((3'''-ethyloxetan-3'''-yl)-methoxy)-heptadecan-9''-yl)-carbazole



A solution of 2,7-di(thiophen-2'-yl)-N-(1''-((3'''-ethyloxetan-3'''-yl)-methoxy)-heptadecan-9''-yl)-carbazole (0.280 g, 0.41 mmol) in anhydrous chloroform (10 mL) was cooled to 0 °C. In the dark, *N*-bromosuccinimide (0.146 g, 0.82 mmol) was added in portions. The reaction mixture was stirred at room temperature for 1 h in the dark, allowed to cool to room temperature and stirred overnight in the dark. NMR spectroscopy was used for reaction control and if required NBS is added to the reaction mixture. After the reaction was completed, the reaction mixture was extracted with water and dichloromethane and the organic phase was washed twice with deionised water. The organic phase was dried over Na₂SO₄ before the solvent was evaporated. After column chromatography (hexanes:THF = 20:1), 2,7-bis(5'-bromothiophen-2'-yl)-N-(1''-((3'''-ethyloxetan-3'''-yl)-methoxy)-heptadecan-9''-yl)-carbazole (0.230 g, 0.27 mmol, 67%) was obtained as a yellowish oil.

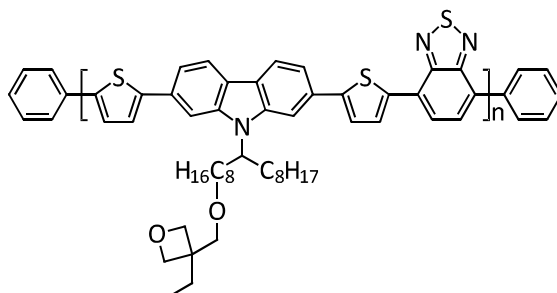
Characterization:

EI-MS: m/z (%) = 841 (M^+ , 100), 811 ($M^+ - OCH_2$, 9), 763 ($M^+ - Br$, 13), 725 ($M^+ - OCH_2O(CH_2)_2CCH_2CH_3$, 4), 647 ($M^+ - Br - OCH_2O(CH_2)_2CCH_2CH_3$, 11), 614 ($M^+ - (CH_2)_8OCH_2O(CH_2)_2CCH_2CH_3$, 23), 502 ($M^+ - (CH_2)_7CH_3 - (CH_2)_8OCH_2O(CH_2)_2CCH_2CH_3$, 19), 488 ($M^+ - CH(CH_2)_7CH_3 - (CH_2)_8OCH_2O(CH_2)_2CCH_2CH_3$, 12), 422 ($M^+ - Br - (CH_2)_7CH_3 - (CH_2)_8OCH_2O(CH_2)_2CCH_2CH_3$, 6), 408 ($M^+ - Br - CH(CH_2)_7CH_3 - (CH_2)_8OCH_2O(CH_2)_2CCH_2CH_3$, 5).

¹H NMR (300 MHz, CDCl₃): δ (ppm) = 0.76-0.93 (m, 6H, CH₃), 0.94-1.37 (m, 22H, CH₂), 1.39-1.53 (m, 2H, CH₂-CH₂-O), 1.71 (q, $J = 7.4$ Hz, 2H, oxetane-CH₂-CH₃), 1.89-2.03 (br, 2H, carbazole-CH-CH₂), 2.21-2.40 (br, 2H, carbazole-CH-CH₂), 3.35 (t, $J = 6.6$ Hz, 2H, CH₂-O), 3.47 (s, 2H, O-CH₂-oxetane), 4.39 (q, $J = 5.8$ Hz, 4H, oxetane), 4.50-4.64 (br, 1H, CH), 7.08 (d, $J = 3.8$ Hz, 2H, thiophene), 7.11-7.19 (br, 2H, carbazole), 7.39 (d, $J = 8.0$ Hz, 2H, thiophene), 7.45-7.55 (br, 1H,

carbazole), 7.62-7.72 (br, 1H, carbazole), 7.98-8.11 (br, 2H, carbazole). Broadened and multiple signals are due to atropisomerism.

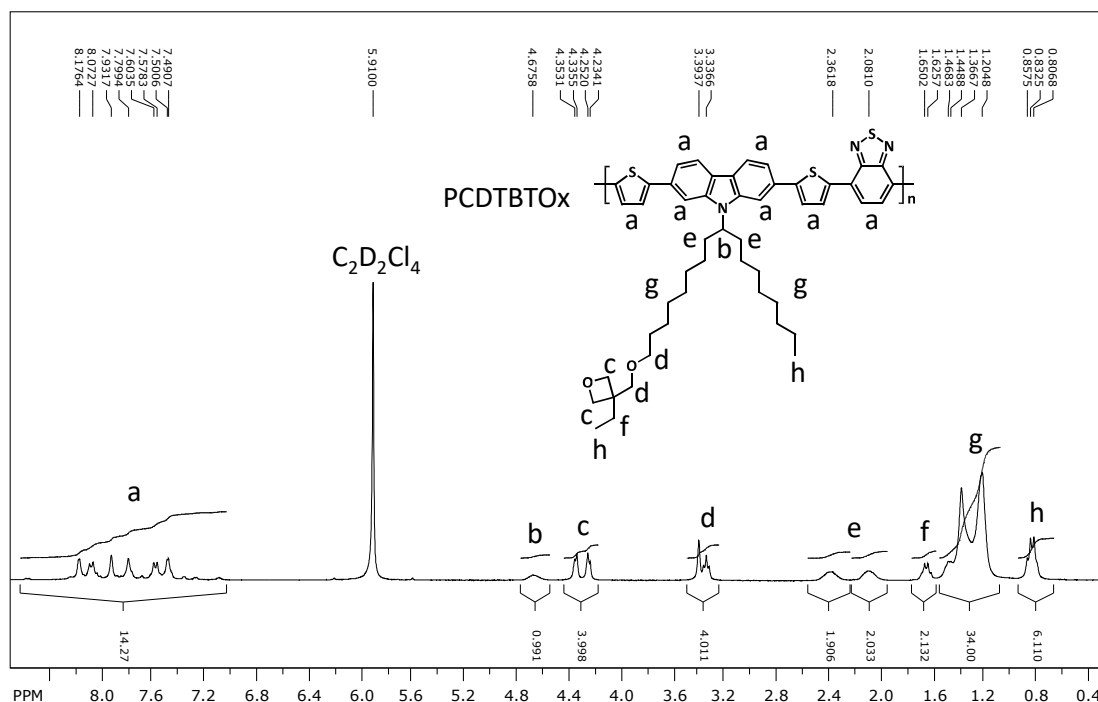
Poly-[(*N*-1'-((3''-ethyloxetan-3''-yl)methoxy)-heptadecan-9'-yl)-2,7-carbazole-*alt*-5,5-(4',7'-bis(thien-2-yl)-2',1',3'-benzothiadiazole)] PCDTBTOx



The monomers 2,7-bis(5'-bromothien-2'-yl)-*N*-(1''-((3'''-ethyloxetan-3'''-yl)methoxy)-heptadecan-9''-yl)carbazole (0.137 g, 0.16 mmol) and 4,7-bis(4',4',5',5'-tetramethyl-1',3',2'-dioxaborolan-2'-yl)-2,1,3-benzothiadiazole (0.063 g, 0.16 mmol) were dissolved in toluene (7 mL) under argon. Four drops of Aliquat 336 and aqueous Na₂CO₃ solution (7.5 mL, 2 M) were added before degassing the reaction mixture by three freeze-thaw cycles. After adding tetrakis(triphenylphosphine)palladium(0) (0.003 g, 0.002 mmol), again three freeze-thaw cycles were conducted. The reaction mixture was stirred under reflux in an argon atmosphere for 90 h. Bromobenzene (0.017 g, 0.16 mmol) was added and the reaction mixture was stirred under reflux for 1 h. Subsequently, phenylboronic acid (0.020 g, 0.16 mmol) was added and the endcapping reaction was completed by stirring the reaction mixture under reflux overnight. After cooling to room temperature, the polymer was extracted with toluene and washed with water. The organic phase was reduced and the polymer was precipitated into cold methanol. Soxhlet extraction was carried out with acetone, hexanes and toluene as solvents. The toluene fraction was evaporated to dryness, the polymer was dissolved in chlorobenzene and precipitated into cold methanol. Drying in vacuum overnight yielded PCDTBTOx (0.084 g, 0.10 mmol, 60%) as a dark-red powder.

Characterization:

¹H NMR (300 MHz, C₂D₂Cl₄, 120 °C): δ (ppm) = 0.72-0.93 (m, 6H, CH₃), 1.09-1.56 (m, 26H, CH₂, CH₂-CH₂-O), 1.57-1.79 (m, 2H, oxetane-CH₂-CH₃), 1.96-2.22 (br, 2H, carbazole-CH-CH₂), 2.25-2.56 (br, 2H, carbazole-CH-CH₂), 3.24-3.54 (m, 4H, CH₂-O, -O-CH₂-oxetane), 4.17-4.45 (m, 4H, oxetane), 4.54-4.77 (br, 1H, CH), 7.04 - 8.61 (m, 12H, ar-CH). Broadened and multiple signals are due to atropisomerism.

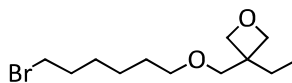


MALDI-ToF (DCTB): 1502.8 ($[M_2 - \text{benzothiadiazole}]$), 1636.0 ($[M_2]$), 1768.8 ($[M_2 + \text{benzothiadiazole}]$), 2315.8 ($[M_3 - \text{benzothiadiazole}]$), 2449.1 ($[M_3]$), 2583.2 ($[M_3 + \text{benzothiadiazole}]$), 3130.3 ($[M_4 - \text{benzothiadiazole}]$), 3265.2 ($[M_4]$), 3397.6 ($[M_4 + \text{benzothiadiazole}]$), 3947.3 ($[M_5 - \text{benzothiadiazole}]$), 4079.5 ($[M_5]$), 4218.2 ($[M_5 + \text{benzothiadiazole}]$), 4759.7 ($[M_6 - \text{benzothiadiazole}]$), 4897.6 ($[M_6]$), 5029.6 ($[M_6 + \text{benzothiadiazole}]$).

UV/Vis (film, 135 nm): $\lambda_{\text{max}} = 392 \text{ nm}, 561 \text{ nm}$.

Fluorescence (film, 135 nm): $\lambda_{\text{max}} = 680 \text{ nm}$ ($\lambda_{\text{ex}} = 390 \text{ nm}, 560 \text{ nm}$).

3-((6'-Bromohexyl)-oxymethyl)-3-ethyloxetane



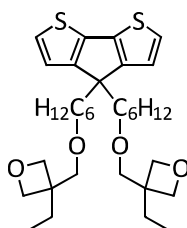
A solution of 1,6-dibromohexane (19.86 mL, 129.13 mmol) and (3-ethyloxetan-3-yl)-methanol (4.91 mL, 48.63 mmol) in distilled hexanes (172 mL) was added to tetrabutylammonium bromide (0.694 g, 2.15 mmol) dissolved in aqueous NaOH solution (43.044 g, 45 wt%). The reaction mixture was stirred overnight under reflux, allowed to cool to room temperature and extracted with deionised water and hexanes. The organic phase was dried over Na_2SO_4 . After evaporation of the solvent, column chromatography (hexanes for eluting of the starting material, THF for eluting of the product) was performed obtaining 3-((6'-Bromohexyl)-oxymethyl)-3-ethyloxetane (10.700 g, 38.32 mmol, 89%) as a colourless oil.

Characterization:

EI-MS: m/z (%) = 248 ($M^+ - OCH_2$, 7), 219 ($M^+ - OCH_2 - CH_2CH_3$, 17), 193 ($M^+ - O(CH_2)_2CCH_2CH_3$, 4), 163 ($M^+ - OCH_2O(CH_2)_2CCH_2CH_3$, 28).

1H NMR (300 MHz, $CDCl_3$): δ (ppm) = 0.88 (t, $J = 7.5$ Hz, 3H, CH_3), 1.29-1.52 (m, 4H, CH_2), 1.53-1.65 (m, 2H, $\underline{CH_2}$ - CH_2 -O), 1.74 (q, $J = 7.5$ Hz, 2H, oxetane- $\underline{CH_2}$ - CH_3), 1.80-1.92 (m, 2H, $\underline{CH_2}$ - CH_2 -Br), 3.35-3.47 (m, 4H, Br- $\underline{CH_2}$, CH_2 -O), 3.52 (s, 2H, O- $\underline{CH_2}$ -oxetane), 4.41 (q, $J = 5.8$ Hz, 4H, oxetane).

4,4-Bis(1'-((3''-ethyloxetan-3''-yl)-methoxy)-hexan-6'-yl)-cyclopenta[2,1-b;3,4-b']dithiophene



4*H*-Cyclopenta[2,1-b;3,4-b']dithiophene (1.366 g, 7.66 mmol) and 3-((6'-Bromohexyl)-oxymethyl)-3-ethyloxetane (4.279 g, 15.33 mmol) were dissolved in dimethyl sulfoxide (33 mL) in an argon atmosphere and KI (0.034 g, 0.21 mmol) was added. After the solution was cooled to 0 °C, KOH (1.364 g, 24.31 mmol) was added in portions and the reaction mixture was stirred for 10 min at 0 °C. The reaction mixture was allowed to warm to room temperature and stirred overnight before it was cooled again to 0 °C and poured in water. Extraction was carried out with dichloromethane and water. The organic phase was washed with deionised water, dried over Na_2SO_4 and the solvent was evaporated. 4,4-Bis(1'-((3''-ethyloxetan-3''-yl)-methoxy)-hexan-6'-yl)-cyclopenta[2,1-b;3,4-b']dithiophene (2.150 g, 3.74 mmol, 49%) was obtained after column chromatography (hexanes: ethyl acetate = 3:1) as a brownish oil.

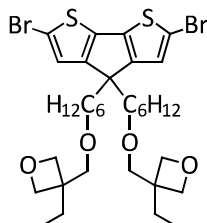
Characterization:

EI-MS: m/z (%) = 574 (M^+ , 100), 544 ($M^+ - OCH_2$, 35), 475 ($M^+ - CH_2O(CH_2)_2CCH_2CH_3$, 3), 460 ($M^+ - OCH_2O(CH_2)_2CCH_2CH_3$, 5), 389 ($M^+ - (CH_2)_5OCH_2O(CH_2)_2CCH_2CH_3$, 7), 375 ($M^+ - (CH_2)_6OCH_2 - O(CH_2)_2CCH_2CH_3$, 5), 261 ($M^+ - OCH_2O(CH_2)_2CCH_2CH_3 - (CH_2)_6OCH_2O(CH_2)_2CCH_2CH_3$, 7), 218 ($M^+ - (CH_2)_3OCH_2O(CH_2)_2CCH_2CH_3 - (CH_2)_6OCH_2O(CH_2)_2CCH_2CH_3$, 7), 203 ($M^+ - (CH_2)_4OCH_2O(CH_2)_2 - CCH_2CH_3 - (CH_2)_6OCH_2O(CH_2)_2CCH_2CH_3$, 48), 191 ($M^+ - (CH_2)_5OCH_2O(CH_2)_2CCH_2CH_3 - (CH_2)_6 - OCH_2O(CH_2)_2CCH_2CH_3$, 23), 178 ($M^+ - (CH_2)_6OCH_2O(CH_2)_2CCH_2CH_3 - (CH_2)_6OCH_2O(CH_2)_2 - CCH_2CH_3$, 11).

1H NMR (300 MHz, $CDCl_3$): δ (ppm) = 0.86 (t, $J = 7.5$ Hz, 6H, CH_3), 0.81-1.29 (m, 12H, CH_2), 1.38-1.51 (m, 2H, $\underline{CH_2}$ - CH_2 -O), 1.71 (q, $J = 7.5$ Hz, 4H, oxetane- $\underline{CH_2}$ - CH_3), 1.77-1.87 (m, 4H, cyclopentadithiophene- $\underline{CH_2}$), 3.36 (t, $J = 6.6$ Hz, 4H, CH_2 -O), 3.47 (s, 4H, O- $\underline{CH_2}$ -oxetane), 4.39 (q,

$J = 5.8$ Hz, 8H, oxetane), 6.92 (d, $J = 4.9$ Hz, 2H, cyclopentadithiophene), 7.15 (d, $J = 4.9$ Hz, 2H, cyclopentadithiophene).

2,6-Dibromo-4,4-bis(1'-((3''-ethyloxetan-3''-yl)-methoxy)-hexan-6'-yl)-cyclopenta[2,1-b;3,4-b']dithiophene



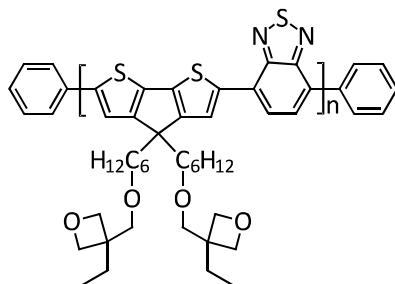
4,4-Bis(1'-((3''-ethyloxetan-3''-yl)-methoxy)-hexan-6'-yl)-cyclopenta[2,1-b;3,4b']dithiophene (0.500 g, 0.87 mmol) was dissolved in anhydrous DMF (10 mL). The solution was cooled to 0 °C and stirred for 10 min at 0 °C before *N*-bromosuccinimide (0.310 g, 1.74 mmol) was added in portions in the dark. After stirring for 1 h at 0 °C, the reaction mixture was allowed to warm to room temperature and stirred overnight in the dark. The reaction mixture was again cooled to 0 °C, poured into water and extracted with water and dichloromethane. The organic phase was washed with deionised water until DMF was removed completely and dried over Na₂SO₄. The solvent was evaporated and column chromatography (hexanes:THF = 3:1) was performed yielding 2,6-dibromo-4,4-bis(1'-((3''-ethyloxetan-3''-yl)-methoxy)-hexan-6'-yl)-cyclopenta[2,1-b;3,4-b']dithiophene (0.285 g, 0.39 mmol, 45%) as a brownish oil.

Characterization:

EI-MS: m/z (%) = 732 (M^+ , 100), 702 ($M^+ - OCH_2$, 11), 652 ($M^+ - Br$, 3), 634 ($M^+ - CH_2O(CH_2)_2CCH_2 - CH_3$, 2), 572 ($M^+ - Br_2$, 2), 543 ($M^+ - Br_2 - OCH_2$, 4), 361 ($M^+ - (CH_2)_4OCH_2O(CH_2)_2CCH_2CH_3 - (CH_2)_6OCH_2O(CH_2)_2CCH_2CH_3$, 6), 348 ($M^+ - (CH_2)_5OCH_2O(CH_2)_2CCH_2CH_3 - (CH_2)_6OCH_2O(CH_2)_2 - CCH_2CH_3$, 3), 339 ($M^+ - Br - OCH_2O(CH_2)_2CCH_2CH_3 - (CH_2)_6OCH_2O(CH_2)_2CCH_2CH_3$, 2), 283 ($M^+ - Br - (CH_2)_4OCH_2O(CH_2)_2CCH_2CH_3 - (CH_2)_6OCH_2O(CH_2)_2CCH_2CH_3$, 7), 258 ($M^+ - Br_2 - OCH_2O(CH_2)_2 - CCH_2CH_3 - (CH_2)_6OCH_2O(CH_2)_2CCH_2CH_3$, 2), 203 ($M^+ - Br_2 - (CH_2)_4OCH_2O(CH_2)_2CCH_2CH_3 - (CH_2)_6 - OCH_2O(CH_2)_2CCH_2CH_3$, 3).

¹H NMR (300 MHz, CDCl₃): δ (ppm) = 0.86 (t, $J = 7.5$ Hz, 6H, CH₃), 0.81-1.28 (m, 12H, CH₂), 1.40-1.52 (m, 2H, CH₂-CH₂-O), 1.64-1.81 (m, 8H, oxetane-CH₂-CH₃, cyclopentadithiophene-CH₂), 3.38 (t, $J = 6.5$ Hz, 4H, CH₂-O), 3.49 (s, 4H, O-CH₂-oxetane), 4.40 (q, $J = 5.8$ Hz, 8H, oxetane), 6.92 (s, 2H, cyclopentadithiophene).

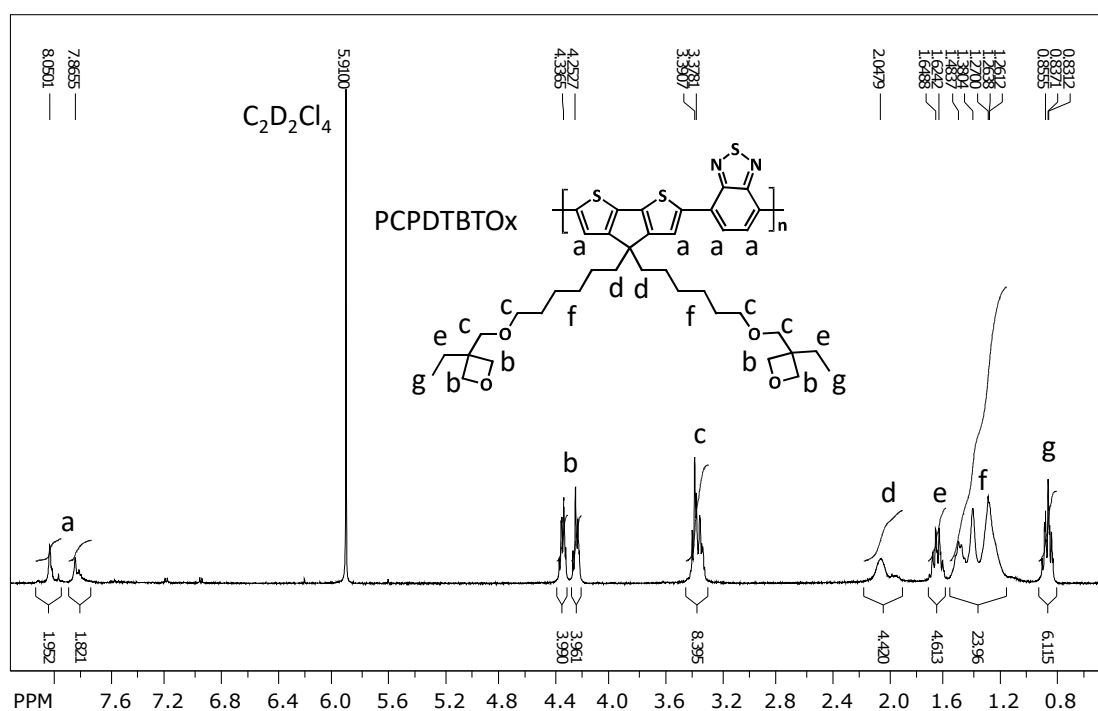
Poly-[2,6-(4',4'-bis-(1'-((3''-ethyloxetan-3''-yl)-methoxy)-hexan-6'-yl)-cyclopenta[2,1-b;3,4-b']dithiophene)-*alt*-4,7-(2,1,3-benzothiadiazole)] PCPDTBTOx



Under argon, the monomers 2,6-dibromo-4,4-bis(1'-((3''-ethyloxetan-3''-yl)-methoxy)-hexan-6'-yl)-cyclopenta[2,1-b;3,4-b']dithiophene (0.181 g, 0.25 mmol) and 4,7-bis(4,4,5,5-tetramethyl-1,3,2-dioxaborolan-2-yl)-2,1,3-benzothiadiazole (0.096 g, 0.25 mmol) were dissolved in toluene (10 mL) before four drops of Aliquat 336 and aqueous Na₂CO₃ solution (12 mL, 2 M) were added. The reaction mixture was degassed by three freeze-thaw cycles and tetrakis(triphenylphosphine)palladium(0) (0.004 g, 0.004 mmol) was added, followed by again three-thaw cycles. After stirring the reaction mixture under reflux in an argon atmosphere for 90 h, bromobenzene (0.026 mL, 0.25 mmol) was added. The reaction mixture was stirred under reflux for 1 h and phenylboronic acid (0.030 g, 0.25 mmol) was added. The reaction mixture was stirred under reflux overnight for completing the endcapping reaction and allowed to cool to room temperature. After extraction of the polymer with toluene and washing with water, the organic phase was reduced. The polymer was precipitated into cold methanol and Soxhlet extraction was performed using acetone, hexanes, butanone, and toluene as solvents. The butanone fraction was reduced before the polymer was precipitated into cold methanol. PCPDTBTOx (0.145 g, 0.21 mmol, 48%) was obtained after drying in vacuum overnight as a brown powder.

Characterization:

¹H NMR (300 MHz, C₂D₂Cl₄, 120 °C): δ (ppm) = 0.75-0.93 (m, 6H, CH₃), 1.01-1.56 (m, 16H, CH₂, CH₂-CH₂-O), 1.57-1.71 (m, 4H, oxetane-CH₂-CH₃), 1.85-2.14 (br, 4H, cyclopentadithiophene-CH₂), 3.26-3.47 (m, 8H, CH₂-O, O-CH₂-oxetane), 4.19-4.41 (m, 8H, oxetane), 7.76-7.92 (m, 2H, ar-H), 7.95-8.14 (m, 2H, ar-H).



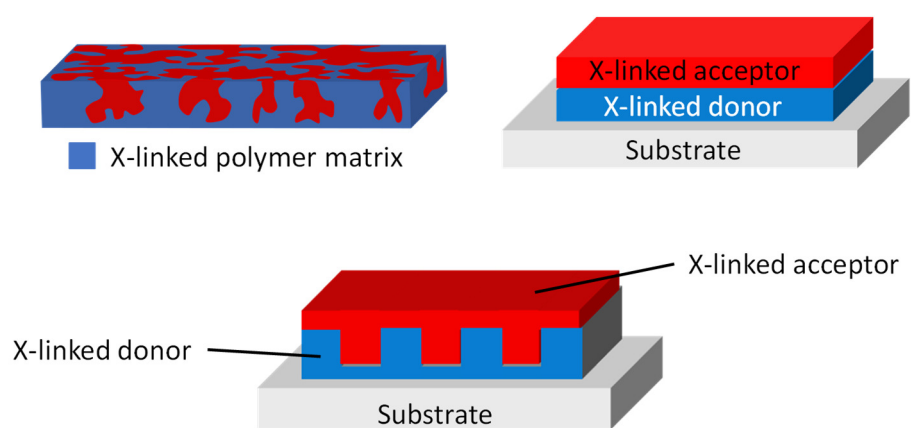
MALDI-ToF (DCTB): 3668.0 ($[M_5 + \text{benzothiadiazole}]$), 4236.7 ($[M_6]$), 4372.2 ($[M_6 + \text{benzothiadiazole}]$), 4151.1 ($[M_6 + 2 \text{ benzothiadiazole}]$), 4814.4 ($[M_7 - \text{benzothiadiazole}]$), 4946.0 ($[M_7]$), 5082.4 ($[M_7 + \text{benzothiadiazole}]$), 5518.5 ($[M_8 - \text{benzothiadiazole}]$), 5654.1 ($[M_8]$), 5788.9 ($[M_8 + \text{benzothiadiazole}]$), 6225.9 ($[M_9 - \text{benzothiadiazole}]$), 6363.1 ($[M_9]$), 6492.8 ($[M_9 + \text{benzothiadiazole}]$), 6933.8 ($[M_{10} - \text{benzothiadiazole}]$), 7066.8 ($[M_{10}]$), 7636.4 ($[M_{11} - \text{benzothiadiazole}]$), 7776.3 ($[M_{11}]$), 8479.3 ($[M_{12}]$).

SEC (butanone fraction, THF, polystyrene calibration, rt): $M_n = 6800 \text{ gmol}^{-1}$, $M_w = 14000 \text{ gmol}^{-1}$, PDI = 2.08.

UV/Vis (film, 90 nm): $\lambda_{\text{max}} = 419 \text{ nm}$, 732 nm.

Appendix B: Patternable conjugated polymers for organic solar cells

Peter Strohriegel, Philipp Knauer, Christina Saller, and Esther Scheler



Published in *Proceedings of SPIE*

doi: 10.1117/12.2023899

Reprinted with permission from *Proceedings of SPIE 8830, Organic Photovoltaics XIV, 2013, 88300P*

Copyright © 2013 Society of Photo Optical Instrumentation Engineers

Patternable Conjugated Polymers for Organic Solar Cells

Peter Strohriegl*, Philipp Knauer, Christina Saller, Esther Scheler

Macromolecular Chemistry I, University of Bayreuth, 95440 Bayreuth, Germany

ABSTRACT

Photocrosslinking is known as a suitable method for patterning organic semiconductors in organic light emitting diodes. We extend this concept to the field of organic solar cells using conjugated polymers bearing sidechains with photocrosslinkable oxetane units. By UV irradiation in the presence of a photo acid generator the oxetane groups polymerize, leading to the formation of a densely crosslinked, and thus insoluble, network of a low-bandgap polymer. In this paper we present the synthesis of two novel photocrosslinkable low-bandgap polymers **PFDTBTOx** and **PCDTBTOx** and discuss several strategies for the fabrication of organic solar cells taking advantage of the novel crosslinkable materials.

Keywords: Photocrosslinking, low-bandgap polymer, oxetane, organic solar cell, PFDTBT, PCDTBT

1. INTRODUCTION

In recent years the scientific and commercial interest in organic photovoltaics has been steadily growing. Organic solar cells (OSCs) are considered one promising option for producing electricity in an environmental friendly way. There are several concepts for the set-up of organic solar cells. One approach is the bulk heterojunction (BHJ) concept, first proposed by Heeger in 1995.¹ In a BHJ solar cell, the active layer comprises a blend of a donor with an acceptor material. Ideally, these two materials form an interpenetrating network by phase separation. This leads to an increased donor-acceptor interface, more efficient exciton dissociation and thus improved device efficiency. In state of the art BHJ devices, low-bandgap polymers are used as light absorbing donor material. Fullerenes, such as C₆₀ and soluble derivatives as PCBM, serve as acceptors. The efficiencies of BHJ devices reported in the literature reach 7.7%.² Optimized solar cells developed by industrial research groups have reached efficiencies up to 10.7%.³ Even higher efficiencies are achieved by complex tandem architectures. In 2013 Heliatek reported a world record cell of 12.0 % efficiency.⁴ This cell is made from more than ten layers of different materials vacuum evaporated on top of each other. Up to now, such complex architectures can only be realized by evaporation of small molecules and not from solution. If a polymer layer is spin coated on top of another polymer, the underlying layer is usually washed away. This can be overcome by either using orthogonal solvents or by crosslinking the polymer layer. Photocrosslinking has been successfully used to create multilayer OLEDs. Müller developed a series of oxetane functionalized conjugated materials to prepare a patterned multilayer OLED from polymers.⁵ The work on photocrosslinkable polymers for OLEDs has been summarized recently.⁶

In the field of organic solar cells only a few reports exist on photocrosslinking of the active layers. The use of sterically hindered bis(fluorophenyl azide)s which act as crosslinking agents and can be mixed into conjugated polymers has been developed in the groups of Friend and Ho.⁷ Upon exposure to ultraviolet light, the azides form nitrenes which undergo a variety of reactions, e. g. insertion into CH bonds. This finally leads to crosslinking and renders the polymer layer insoluble. An organic solar cell consisting of OC₁C₁₀-PPV crosslinked and backinfiltrated with PCBM achieved a power conversion efficiency (PCE) of 2%. Photocrosslinkable hexabenzocoronenes were used by Hesse et al. with regard to the fabrication of patterned OSCs.⁸ The authors utilized microcontact printing to fabricate 90 nm sized hexabenzocoronene patterns which are stabilized by subsequent crosslinking. Organic solar cells have not yet been described by the authors.

* peter.strohriegl@uni-bayreuth.de; <http://www.chemie.uni-bayreuth.de/mci>; Phone: +49-921 55 3296

Recently, Carlé et al. synthesized four crosslinkable derivatives of the low-bandgap polymer TQ1 by attaching bromine, azide, vinyl or oxetane groups to the side chains. By exposure to UV light, the polymer films crosslink and become insoluble. It could be shown that BHJ solar cells made from the crosslinked TQ1 derivatives and PCBM degraded much more slowly at 100 °C if azides or especially oxetanes are used as crosslinkable units.⁹

We have synthesized one fluorene based and one carbazole based low-bandgap polymer which both have photocrosslinkable oxetane groups in the spacer. In this paper we present the synthesis of the two new polymers **PFDTBTOx** and **PCDTBTOx** and several strategies for their incorporation into organic solar cells.

1.1 Previous Work on Polyfluorenes

In the past we have synthesized conjugated organic polymers with pendant photocrosslinkable groups.^{10,11} We started from polyfluorenes bearing acrylate sidechains (**PFAc**).¹² Besides the fluorene homopolymers, a number of crosslinkable copolymers bearing donor and acceptor type comonomers have been synthesized.^{13,14} Figure 1 shows the structures of **PFAc**, **PFTPDAc**, **PFBTAc**, **PFDTAc**, with TPD, benzothiadiazole and bithiophene as comonomers. Molecular weights of the homopolymers and the copolymers were limited to 5000 g/mol by endcapping.

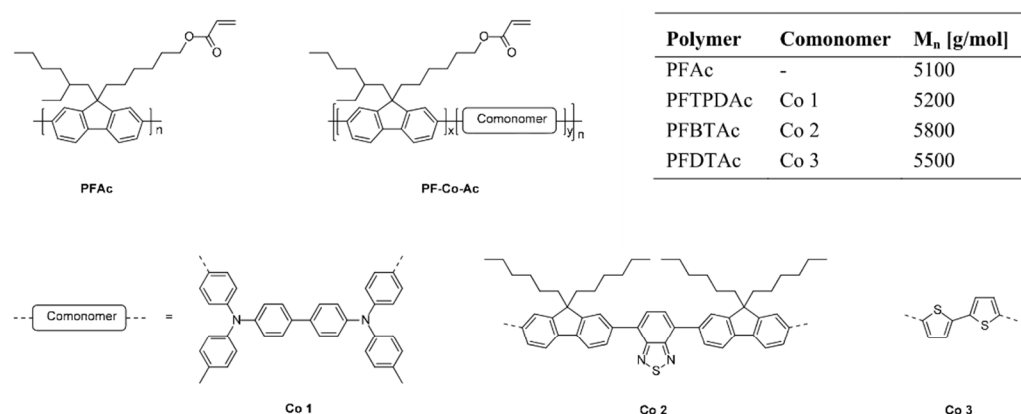


Figure 1: Chemical structures of the patternable fluorene polymers. Molecular weights were determined by gel permeation chromatography (GPC) and calculated using an oligofluorene calibration.¹⁵

The polyfluorenes shown in Figure 1 have reactive acrylate units and can be photocrosslinked using a radical photoinitiator. Exposure of a thin layer of the polyfluorenes to UV light leads to crosslinking and renders the layer insoluble. If a photomask is used during illumination, patterns are formed since the material behaves like a negative photoresist. The photolithographic patterning is schematically displayed in Figure 2. In the first step, the polymer along with a radical photoinitiator is spincoated on top of a substrate. Subsequently, the light exposure is carried out in a vacuum chamber on a hot stage (Figure 2 b). An inert atmosphere is vital for the photocrosslinking, as it prevents the conjugated polymer from photochemical degradation. In the last step, the pattern is developed by dissolving the polymer in the non-irradiated areas. Fluorescence microscope (Fig. 2 c) and SEM (Fig. 2 d) images of the copolymer **PFDTAc** show that by this process resolutions down to 1 μm have already been achieved.

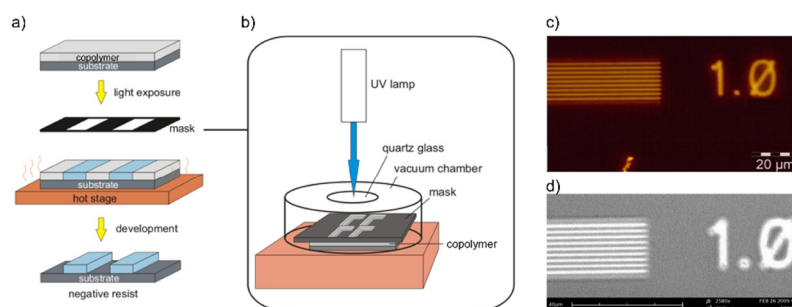


Figure 2: Photolithographic process for the patterning of polyfluoreneacrylates (a,b) and microscopic images of patterns from **PFDTAc** (c: fluorescence microscope, d: SEM). The numbers denote the width of the stripes in μm .¹³

2. SYNTHESIS OF PHOTOCROSSLINKABLE LOW-BANDGAP POLYMERS

We synthesized two different donor-acceptor polymers with oxetane sidechains, **PFDTBTOx** and **PCDTBTOx**. The basic idea behind the synthesis is to use well known low-bandgap polymers and modify them with photocrosslinkable units. In the past we have used acrylates as photocrosslinkable moieties. Crosslinking of acrylates is achieved by free radical polymerization, which is known to be quenched by fullerenes as strong electron acceptors.¹⁶ For this reason, we choose oxetanes as photocrosslinkable units. The crosslinking thereby proceeds by a cationic ring opening polymerization (CROP) in the presence of a photoacid generator (PAG). The mechanism of crosslinking has recently been investigated by Feser et al.¹⁷ An important aspect for the choice of oxetanes is their compatibility with the strongly basic conditions of transition metal catalyzed C-C bond forming reactions like Suzuki cross-coupling. Furthermore, there is evidence in the literature that oxetane crosslinking is possible in the presence of fullerenes.¹⁸

The first low-bandgap polymer we have chosen is poly(2,7-(9-(2'-ethylhexyl)-9-hexylfluorene)-*alt*-5,5-(4',7'-di-3-hexylthien-2-yl-2',1',3'-benzothiadiazole) **PFDTBT** first synthesized by Svensson et al. in 2003.¹⁹ The high mobility and stability of polyfluorene in combination with the benzothiadiazole comonomer DTBT that lowers the bandgap of the polymer render **PFDTBT** suitable for the use in organic solar cells and lead to a device efficiency of 2.2%. We have developed a method to introduce polymerizable oxetane units into **PFDTBT**. The synthetic steps towards the crosslinkable derivative **PFDTBTOx** are displayed in Figure 3.

The synthesis of the oxetane spacer **3** is shown in the first line. We have chosen a C₇ aliphatic spacer which provides good solubility during the monomer and especially the polymer synthesis. Thus, an etherification of 3-ethyl-3-oxetanemethanol **1** with 2,7-dibromoheptane **2** is the first step, affording 3-(7'-bromoheptyloxy)methyl-3-ethyloxetane **3** in a yield of 90%. 2,7-dibromofluorene **4** is dialkylated with the oxetane spacer **3** at the 9-position, whereby **5** is obtained. The yield for this step is 79%. Subsequently, boronic esters are introduced by treating the dibromofluorene **5** with isopropoxyboronic acid pinacol ester **6**. The yield for the fluorene comonomer **7** is 73%.

The synthesis of the dithiophenebenzothiadiazole comonomer **11** starts from 4,7-dibromo-2,1,3-benzothiadiazole **8**, which is reacted with two equivalents of the 3-hexylthiophene-2-boronic acid pinacol ester **9** in a Suzuki cross-coupling. Dithiophenebenzothiadiazole **10** is obtained in a yield of 86%. Finally, **10** is selectively brominated under mild conditions with *N*-bromosuccinimide, yielding 93% of the dithiophenebenzothiadiazole monomer **11**.

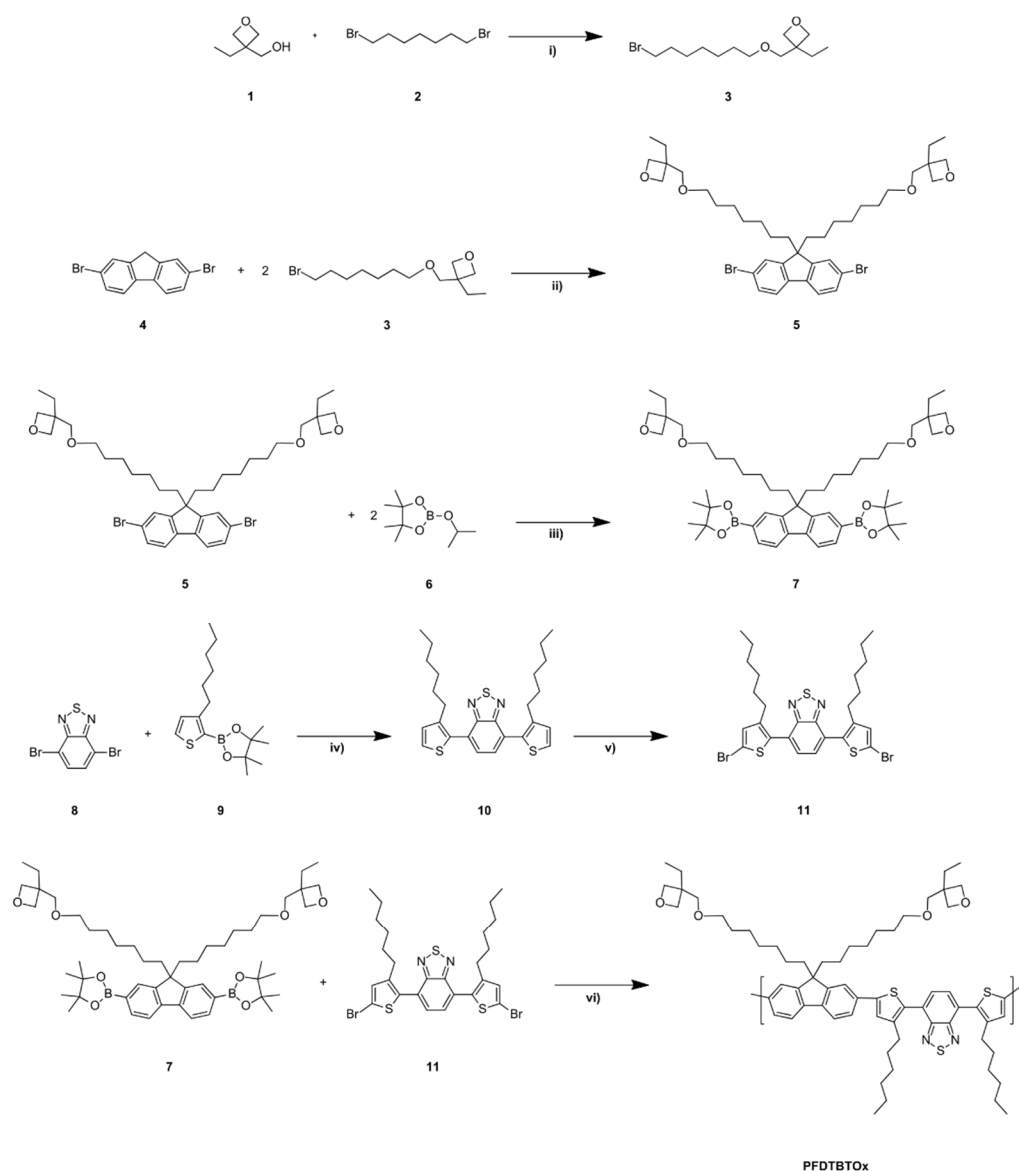


Figure 3: Synthetic route towards **PFDTBTOx**. Reagents and conditions: i) Hexane, NaOH (aq), (Bu)₄NBr; RF, 6 h; 90%; ii) DMSO, NaOH (aq), Ph(Et)₃NCl; RF, 20 h; 79%; iii) THF, n-BuLi; - 78 °C; 36%; iv) Pd₂(dba)₃, PCy₃, K₃PO₄ (aq), Dioxane:Toluene; 90 °C, 20 h, 86%; v) NBS, CHCl₃; RT, 20 h; 93%; vi) Pd[PPh₃]₄, Aliq. 336, Na₂CO₃ (aq):Toluene; RF, 96 h; 86%.

The polymerization is carried out by a palladium catalyzed Suzuki polycondensation of the comonomers **7** and **11**. Thus, the polymer **PFDTBTOx** is obtained as a dark red solid, readily soluble in organic solvents like chloroform and THF. It was characterized by ^1H - and ^{13}C -NMR spectroscopy, GPC, TGA and UV-Vis spectroscopy. Figure 4 shows the GPC-trace and the UV-Vis and fluorescence spectra. The analytical data are summarized in Table 1.

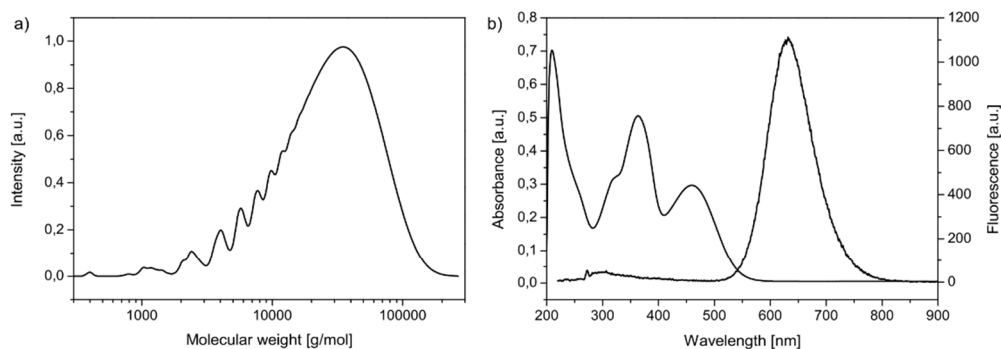


Figure 4: GPC trace (a) and absorption and fluorescence spectra (b) of **PFDTBTOx** (GPC: THF, polystyrene calibration, both spectra taken from THF solutions, fluorescence excitation wavelength 210 nm).

Table 1: Analytical data of **PFDTBTOx**.

SEC			UV-Vis	Fluorescence	TGA
M_n [g/mol]	M_w [g/mol]	D	$\lambda_{\text{abs,max}}$ [nm]	$\lambda_{\text{fl,max}}$ [nm]	1% wt loss
14,000	34,000	2.3	460, 363, 325 (sh), 210	626	346 °C

The molecular weight of **PFDTBTOx** is 34,000 g/mol (M_w) and 14,000 g/mol (M_n) according to the GPC measurements. Absorption maxima are at 460, 363 and 210 nm, additionally a shoulder is observed at 325 nm. The fluorescence spectrum exhibits only one strong maximum at 626 nm. Thermal decomposition starts at 346 °C which is sufficient for solar cell applications.

As a second low-bandgap polymer we chose poly(*N*-9'-heptadecanyl-2,7-carbazole-*alt*-5,5-(4',7'-dithien-2-yl-2',1',3'-benzothiadiazole)) PCDTBT which was first synthesized by Blouin et al. in 2007 and exhibits a high glass transition temperature and good solubility.²⁰ In combination with PCBM, a first bulk heterojunction solar cell achieved a power conversion efficiency of 3.6%. Further optimization by the group of Heeger enhanced this efficiency to 6.1% by modifications like exchanging the acceptor PC₆₀BM by PC₇₀BM and insertion of a thin layer of titanium dioxide as optical spacer.²¹

Figure 4 shows the synthetic strategy for **PCDTBTOx**. In the first step, the novel spacer **14** is synthesized. Conversion of the oxetane containing bromide **3** into the corresponding Grignard reagent and subsequent reaction with 1,2-epoxydecane **12** affords the swallow tailed spacer **13** in 55% yield. Tosylation of the secondary alcohol in **13** leads to **14** in 76% yield, adding a better leaving group.

2,7-dibromocarbazole **17** is achieved by nitration of the starting material 4,4'-dibromobiphenyl **15** affording 80% of 4,4'-dibromo-2-nitrobiphenyl **16** which is converted into the carbazole via a reductive Cadogan ring closure in 56% yield. Alkylation of the 2,7-dibromocarbazole **17** with the spacer molecule **14** yields 50% of the carbazole derivative **18**, which is borylated receiving the carbazole monomer 2,7-bis-(4',4',5',5'-tetramethyl-1',3',2'-dioxaborolan-2'-yl)-*N*-(1'-((3''-ethylxetan-3''-yl)-methoxy)heptadecan-9'-yl)carbazole **19** in 40% yield.

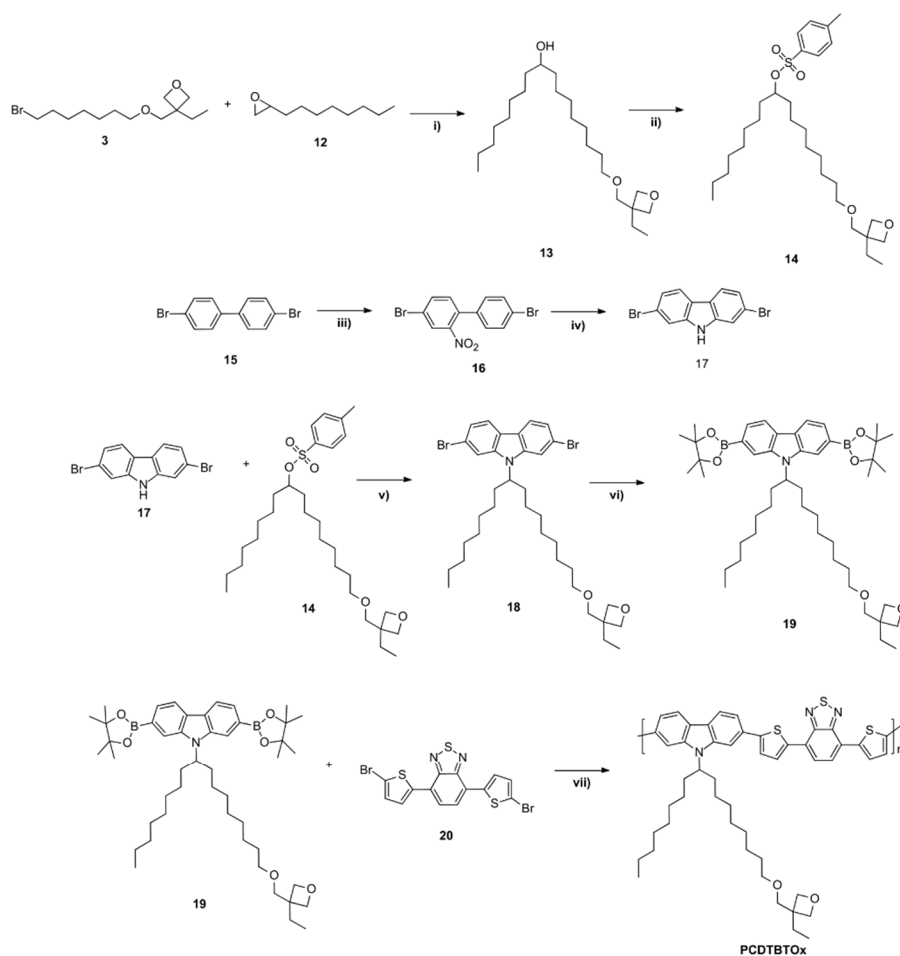


Figure 4. Synthetic route towards **PCDTBTOx**. Reagents and conditions: i) 1. Mg, THF, reflux, 2. **12**, 0 °C, CuI, 3. RT, 10 h, 4. NH₄Cl solution, 55%; ii) tosylchloride, DCM, Et₃N, Me₃N·HCl, 0 °C, 90 min, RT, overnight, 76%; iii) AcOH, HNO₃ + H₂O, 100 °C, 30 min, 80%; iv) P(OEt)₃, reflux, 18 h, 56%; v) 1. KOH, DMSO, 2. **14** over 1 h, 3. RT, overnight, 50%; vi) 1. n-BuLi, THF, -78 °C, 1 h, 2. 2'-Isopropoxy-4,4,5,5-tetramethyl-1,3,2-dioxaborolane, -78 °C, 1 h, 3. RT, overnight, 40%; vii) 1. Pd2(dba)₃, P(o-Tol)₃, toluene, Et₄NOH (aq), reflux, 72 h, 2. bromobenzene, reflux, 1 h, 3. phenylboronic acid, reflux, overnight; 71%.

The photocrosslinkable polymer poly-(*N*-(1'-((3''-ethyloxetan-3''-yl)methoxy)heptadecan-9'-yl)-2,7-carbazole-*alt*-5,5-(4',7'-bis-thien-2'-yl)-2',1',3'-benzothiadiazole) **PCDTBTOx** is synthesized via a palladium-catalyzed Suzuki cross-coupling. This polymerization method provides a strictly alternating arrangement of the two different monomers. At the end of the cross-coupling an endcapping reaction is carried out to stabilize the chain ends of the polymer. **PCDTBTOx** is obtained in 71% yield as a dark red solid which is soluble in chloroform and THF. The characterization includes ¹H- and ¹³C-NMR spectroscopy, size exclusion chromatography, TGA and DSC measurements as well as UV-Vis and fluorescence spectroscopy. The absorption and fluorescence spectra are shown in Figure 6, all results are summarized in Table 2.

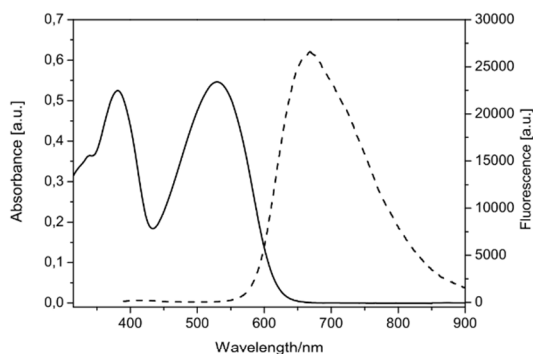


Figure 6. UV-Vis (solid line) and fluorescence spectra (dashed line) of **PCDTBTOx**. Measurements were taken in solution (0.02 mg/ml) in *o*-dichlorobenzene, excitation wavelength for the fluorescence measurement 530 nm.

Table 2. Analytical data of **PCDTBTOx**

SEC			UV-Vis	Fluorescence
M_n [g/mol]	M_w [g/mol]	D	$\lambda_{abs,max}$ [nm]	$\lambda_{fl,max}$ [nm]
970	2,500	2.6	530, 382, 339 (sh)	668

The polymer has a low molecular weight, as can be seen from the SEC data. The value of M_w is 2,500 g/mol and M_n is 970 g/mol. The molecular weight has to be increased in further polymerization runs. The much higher molecular weight obtained for **PFDTBTOx** shows that the oxetane group has no negative influence on the Suzuki cross-coupling. Thermogravimetric analysis demonstrates that the polymer is stable up to ca. 300 °C. The absorption maxima at 530 nm and 382 nm and can be ascribed to the S_0 - S_1 and the S_0 - S_2 transition, respectively.²² The fluorescence spectrum has a maximum at 668 nm.

3. CONCLUSIONS AND OUTLOOK

We have extended the concept of photocrosslinkable conjugated polymers towards donor-acceptor copolymers for organic solar cells and developed the synthesis of two novel crosslinkable low-bandgap polymers **PFDTBTOx** and **PCDTBTOx**. In the next step we will carefully investigate the photocrosslinking process and use the novel materials in organic solar cells.

In bulk heterojunction OSCs diffusion of the low molar mass fullerenes in the polymer matrix is concerned as a problem for the long-term stability. Carlé et al. showed that annealing at 100 °C for 50 hours leads to a strong decrease of the efficiency of BHJ-devices from the low-bandgap polymer TQ1 and PCBM. Crosslinking of the polymer matrix is expected to slow down the diffusion of the fullerenes.⁹ This strategy is shown in Figure 7.

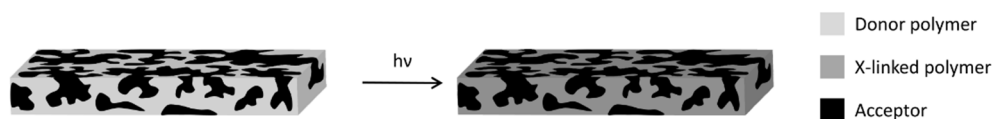


Figure 7. Photocrosslinking of the donor polymer in bulk heterojunction organic solar cells.

The morphology of BHJ cells incorporating an interpenetrating network of the donor and acceptor material is known to give high efficiencies in organic solar cells. Nevertheless, analyzing the morphology in detail shows that it contains areas in which carriers are trapped and have to diffuse against the electric field in order to escape. Photocrosslinking allows the design of comb-like structures, shown in Figure 8. Such patterns can in principle be realized by photolithography like discussed in the chapter on polyfluorenes. Nevertheless, it will be difficult to obtain large area sub-100 nm patterns for organic solar cells by means of photolithography. We intend to realize such patterns by microcontact printing. In the first step the crosslinkable polymer is spin cast and subjected to microcontact printing. The patterns are subsequently stabilized by crosslinking the low-bandgap polymer. In the next step, the fullerene acceptor layer can be applied by both thermal evaporation of C₆₀ and from PCBM solutions.

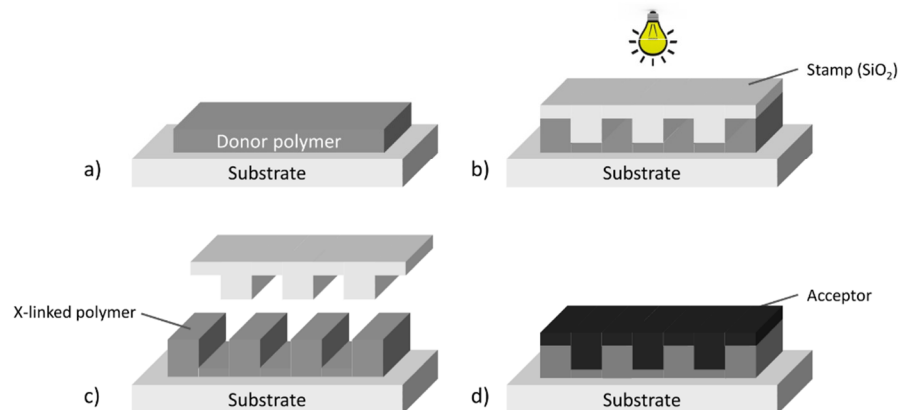


Figure 8. Patterning of the donor-acceptor interface by microcontact printing.

Photocrosslinking also allows the fabrication of multilayer organic solar cells from solution like shown in Figure 9. Here, the low-bandgap polymer is cast on top of the electrode and subsequently photocrosslinked. This renders the layer insoluble and allows to coat a second layer on top without dissolving the first layer. If the second layer is also photocrosslinkable, this concept can be extended to multilayer OSCs. This procedure avoids the use of orthogonal solvents which is often difficult to realize with chemically similar polymers.

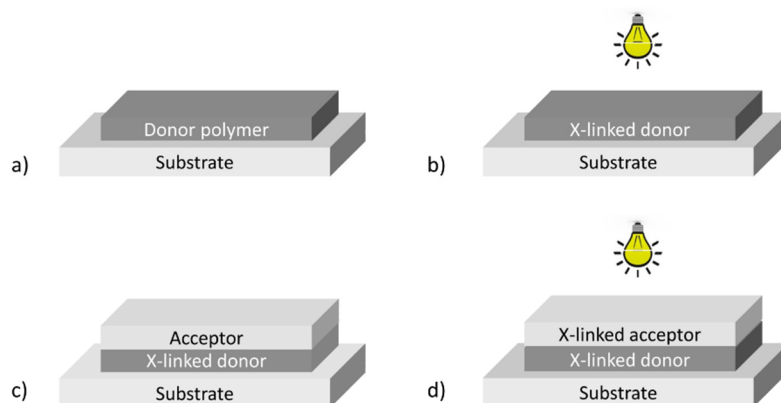


Figure 9. The use of photocrosslinking in the solution processing of multilayer organic solar cells.

Acknowledgments

We thank A. Köhler, C. Schwarz, T. Hahn und T. Müller for stimulating discussions and I. Bauer for technical assistance.

Financial support from the German Science Foundation (DFG/ GRK 1640) and the Bavarian State Ministry of Science, Research, and the Arts for the Collaborative Research Network "Solar Technologies go Hybrid" is gratefully acknowledged.

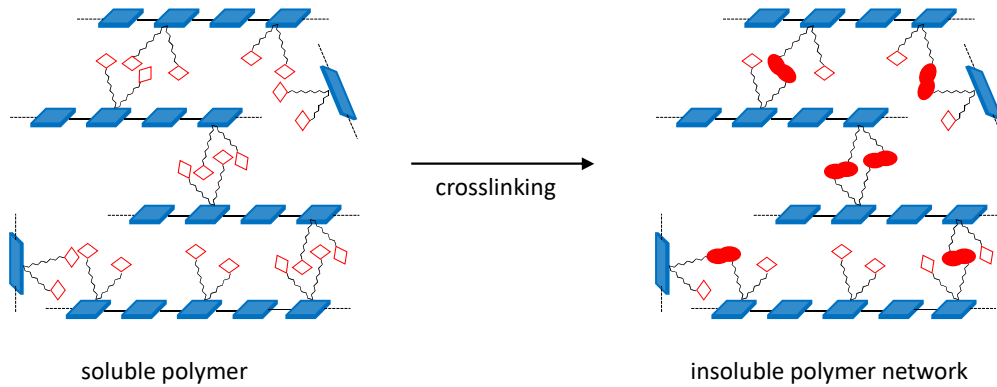
REFERENCES

- [1] Yu, G., Gao, J., Hummelen, J. C., Wudl, F. and Heeger, A. J., "Polymer Photovoltaic Cells: Enhanced Efficiencies via a Network of Internal Donor-Acceptor Heterojunctions," *Science* 270, 1789–1791 (1995).
- [2] Chen, H.-Y., Hou, J., Zhang, S., Liang, Y., Yang, G., Yang, Y., Yu, L., Wu, Y. and Li, G., "Polymer solar cells with enhanced open-circuit voltage and efficiency," *Nature Photonics* 3, 649–653 (2009).
- [3] Green, M. A., Emery, K., Hishikawa, Y., Warta, W. and Dunlop, E. D., "Solar cell efficiency tables (version 41)," *Prog. Photovolt: Res. Appl.* 21, 1–11 (2013).
- [4] Heliatek consolidates its technology leadership by establishing a new world record for organic solar technology with a cell efficiency of 12%, 16 January 2013, www.heliatek.com.
- [5] Müller, C. D., Falcou, A., Reckefuss, N., Rojahn, M., Wiederhorn, V., Rudati, P., Frohne, H., Nuyken, O., Becker, H., Meerholz, K., "Multi-colour organic light-emitting displays by solution processing," *Nature* 421, 829–833 (2003).
- [6] Scheler, E. and Strohriegl, P., "Organic Light Emitting Diodes (OLEDs) with Polarized Emission," in Bushby, R. J., Kelly, S. M. and O'Neill, M. (Eds), "Liquid crystalline semiconductors," Springer (2013), p. 197–218.
- [7] Png, R.-Q., Chia, P.-J., Tang, J.-C., Liu, B., Sivaramakrishnan, S., Zhou, M., Khong, S.-H., Chan, H. S. O., Burroughes, J. H., Chua, L.-L., Friend, R. H. and Ho, P. K. H., "High-performance polymer semiconducting heterostructure devices by nitrene-mediated photocrosslinking of alkyl side chains," *Nat Mater* 9, 152–158 (2009).
- [8] Hesse, H. C., Lembke, D., Dössel, L., Feng, X., Müllen, K. and Schmidt-Mende, L., "Nanostructuring discotic molecules on ITO support," *Nanotechnology* 22, 55303 (2011).
- [9] Carlé, J. E., Andreasen, B., Tromholt, T., Madsen, M. V., Norrman, K., Jørgensen, M. and Krebs, F. C., "Comparative studies of photochemical cross-linking methods for stabilizing the bulk hetero-junction morphology in polymer solar cells," *J. Mater. Chem.* 22, 24417–24423 (2012).
- [10] Jandke, M., Hanft, D., Strohriegl, P., Whitehead, K. S., Grell, M., and Bradley, D. D. C., "Polarized electroluminescence from photocrosslinkable nematic fluorene bisacrylates," *SPIE Proceedings* 4105, 338–347 (2001).
- [11] Thiem, H., Jandke, M., Hanft, D. and Strohriegl, P., "Synthesis and Orientation of Fluorene Containing Reactive Mesogens," *Macromol. Chem. Phys.* 207, 370–381 (2006).
- [12] Scheler, E. and Strohriegl, P., "Tailoring fluorene-based oligomers for fast photopatterning," *J. Mater. Chem.* 19, 3207–3212 (2009).
- [13] Scheler, E. and Strohriegl, P., "Three Color Random Fluorene-Based Oligomers for Fast Micrometer-Scale Photopatterning," *Chem. Mater.* 22, 1410–1419 (2010).
- [14] Scheler, E., Betthausen, E. and Strohriegl, P., "Synthesis and Properties of Alternating Fluorene-Based Oligomers for Sub- μm Photopatterning," *Macromol. Chem. Phys.* 211, 2081–2089 (2010).
- [15] Scheler, E. and Strohriegl, P., "Synthesis of oligofluorenes by endcapping," *Liquid Crystals* 34, 667–672 (2007).
- [16] Mehrotra, S., Nigam, A. and Malhotra, R., "Effect of [60]fullerene on the radical polymerization of alkenes," *Chem. Commun.* 5, 463–464 (1997).
- [17] Feser, S. and Meerholz, K., "Investigation of the Photocross-linking Mechanism in Oxetane-Functionalized Semiconductors," *Chem. Mater.* 23, 5001–5005 (2011).
- [18] Cheng, Y.-J., Cao, F.-Y., Lin, W.-C., Chen, C.-H. and Hsieh, C.-H., "Self-Assembled and Cross-Linked Fullerene Interlayer on Titanium Oxide for Highly Efficient Inverted Polymer Solar Cells," *Chem. Mater.* 23, 1512–1518 (2011).
- [19] Svensson, M., Zhang, F., Inganäs, O. and Andersson, M., "Synthesis and properties of alternating polyfluorene copolymers with redshifted absorption for use in solar cells," *Synthetic Metals* 135–136, 137–138 (2003).

- [20] Blouin, N., Michaud, A. and Leclerc, M., "A Low-Bandgap Poly(2,7-Carbazole) Derivative for Use in High-Performance Solar Cells," *Adv. Mater.* 19, 2295–2300 (2007).
- [21] Park, S. H., Roy, A., Beaupré, S., Cho, S., Coates, N., Moon, J. S., Moses, D., Leclerc, M., Lee, K. and Heeger, A. J., "Bulk heterojunction solar cells with internal quantum efficiency approaching 100%," *Nature Photonics* 3, 297–302 (2009).
- [22] Banerji, N., Cowan, S., Leclerc, M., Vauthey, E. and Heeger, A. J., "Exciton Formation, Relaxation, and Decay in PCDTBT," *J. Am. Chem. Soc.* 132, 17459–17470 (2010).

Appendix C: Crosslinkable low bandgap polymers for organic solar cells

Peter Strohriegel, Christina Saller, Philipp Knauer, Anna Köhler, Tobias Hahn,
Florian Fischer, and Frank-Julian Kahle



Published in *Proceedings of SPIE*

doi: 10.1117/12.2239400

Reprinted with permission from *Proceedings of SPIE 9942, Organic Photovoltaics XVII, 2016*,
994200

Copyright © 2016 Society of Photo Optical Instrumentation Engineers

Crosslinkable low bandgap polymers for organic solar cells

Peter Strohriegl*^a, Christina Saller^a, Philipp Knauer^a, Anna Köhler^b, Tobias Hahn^b,
Florian Fischer^b, Frank-Julian Kahle^b

^aUniversity of Bayreuth, Macromolecular Chemistry I; ^bUniversity of Bayreuth, Experimental
Physics II, Universitätsstraße 30, 95440 Bayreuth, Germany

ABSTRACT

We present a number of polyfluorene based conjugated polymers with crosslinkable acrylate and oxetane units. These polymers can be crosslinked by free radical polymerization in the case of acrylates and by cationic ring opening polymerization for oxetanes. Upon polymerization densely crosslinked networks are formed which are completely insoluble. We show that the diffusion coefficient of C₆₀ in polyfluorene is reduced by a factor of 1000 by crosslinking. MIS-CELIV measurements are used to monitor changes in the charge carrier mobility upon crosslinking. It shows that using appropriate conditions, e.g. low initiator concentrations or thermal crosslinking, the charge carrier mobility is not reduced by crosslinking. Solution processed three layer organic solar cells were realized with a crosslinkable fluorene based copolymer containing acrylate groups. The efficiency is increased from 1.4% for the reference to 1.8% in the three layer cell with a crosslinked exciton blocking layer. A critical issue of BHJ cells is the instability of the morphology of the polymer:fullerene blend over long operation times at elevated temperature. We present a crosslinkable derivative of the low bandgap polymer PFDTBT which contains oxetane units. BHJ cells with the crosslinked PFDTBT derivative and PCBM were tested in accelerated aging experiments at 100 °C for times up to 100 h. Stabilization was clearly observed in crosslinked BHJ cells compared to the non-crosslinked reference. We show for the first time that oxetane containing polymers can be thermally crosslinked without any added initiator. Initiator free crosslinking is particularly attractive as it avoids the formation of decomposition products, and thus potential electron traps and quenching sites from the initiator.

Keywords: organic solar cells, crosslinking, polyfluorene, low bandgap polymer, C₆₀ diffusion, MIS-CELIV, carrier mobility, OSC stabilization

1. INTRODUCTION

The bulk heterojunction (BHJ) is the most popular concept for the active layer of organic solar cells based on conjugated polymers.¹ Typically, a conjugated polymer and a low-molar mass fullerene derivative, such as PCBM, are mixed together. However, such a donor acceptor blend only achieves its best solar cell performance if the morphology meets certain requirements: Domains in the range of the exciton diffusion length of about 10 nm ensure that excitons can reach a donor-acceptor interface within their lifetime and separate into electrons and holes. Nanometer sized domains also result in an increased donor-acceptor interface area. Furthermore, an ideal morphology comprises a bicontinuous network of donor and acceptor material. This provides paths for both kinds of charge carriers towards the electrodes.

Obviously, controlling the morphology is the crucial point of the BHJ approach.² Different strategies to control the blend morphology during device fabrication are known: The choice of solvent, solvent additives, thermal annealing or solvent vapor annealing can help achieving an optimum morphology. However, this complex morphology is thermodynamically

*peter.strohriegl@uni-bayreuth.de; www.chemie.uni-bayreuth.de/mci; phone +49 921 553296

Organic Photovoltaics XVII, edited by Zakya H. Kafafi, Paul A. Lane, Ifor D. W. Samuel,
Proc. of SPIE Vol. 9942, 99420O · © 2016 SPIE · CCC code: 0277-786X/16/\$18
doi: 10.1117/12.2239400

Proc. of SPIE Vol. 9942 99420O-1

Downloaded From: <http://proceedings.spiedigitallibrary.org/> on 10/19/2016 Terms of Use: <http://spiedigitallibrary.org/ss/TermsOfUse.aspx>

unstable and prone to macro phase separation on a long timescale.³ This effect is even enhanced if one component tends to crystallize. Once degradation of the nanoscale morphology occurs, the overall performance of an organic solar cell will drop significantly.³

In recent years, crosslinking emerged as an approach to freeze the morphology of a donor-acceptor blend and thus improve its long term stability.^{4,5} Basically, three concepts for crosslinking bulk heterojunction materials are known: Crosslinking the donor polymer,^{6,7,8,9} crosslinking the acceptor,¹⁰ and crosslinking donor and acceptor.¹¹ In most cases crosslinking proceeds via functional groups attached to the side chains of the organic semiconducting materials. Bromide,¹² vinyl,¹³ acrylate,¹⁴ azide,¹⁵ and oxetane¹⁶ are popular crosslinkable groups. In this paper we describe a number of studies on crosslinked conjugated polymers including our recent work to stabilize BHJ solar cells by crosslinking. In contrast to earlier studies with crosslinkable acrylate units,^{17,18,19} oxetane was chosen as crosslinkable moiety. In this case crosslinking takes place by a cationic ring opening polymerization (CROP).²⁰ The cationic mechanism is suitable for crosslinking the donor polymer in a BHJ cell in contrast to any radical based reaction, since the strongly electron accepting fullerene derivatives will prevent free radical crosslinking.

2. MATERIALS

Usually, crosslinking is applied to a film after it was cast from solution. The key point of crosslinking is the transformation of a soluble material into an insoluble network. One approach is crosslinking via functional groups. In the field of conjugated polymers, crosslinkable groups are usually attached to the ends of the solubilizing alkyl chains. The formation of an insoluble polymer network is illustrated in Figure 1.

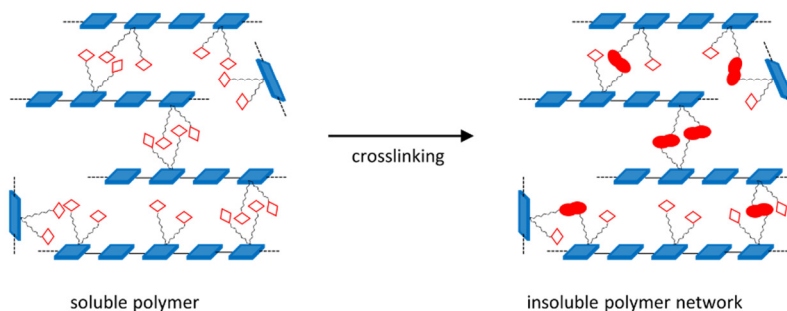
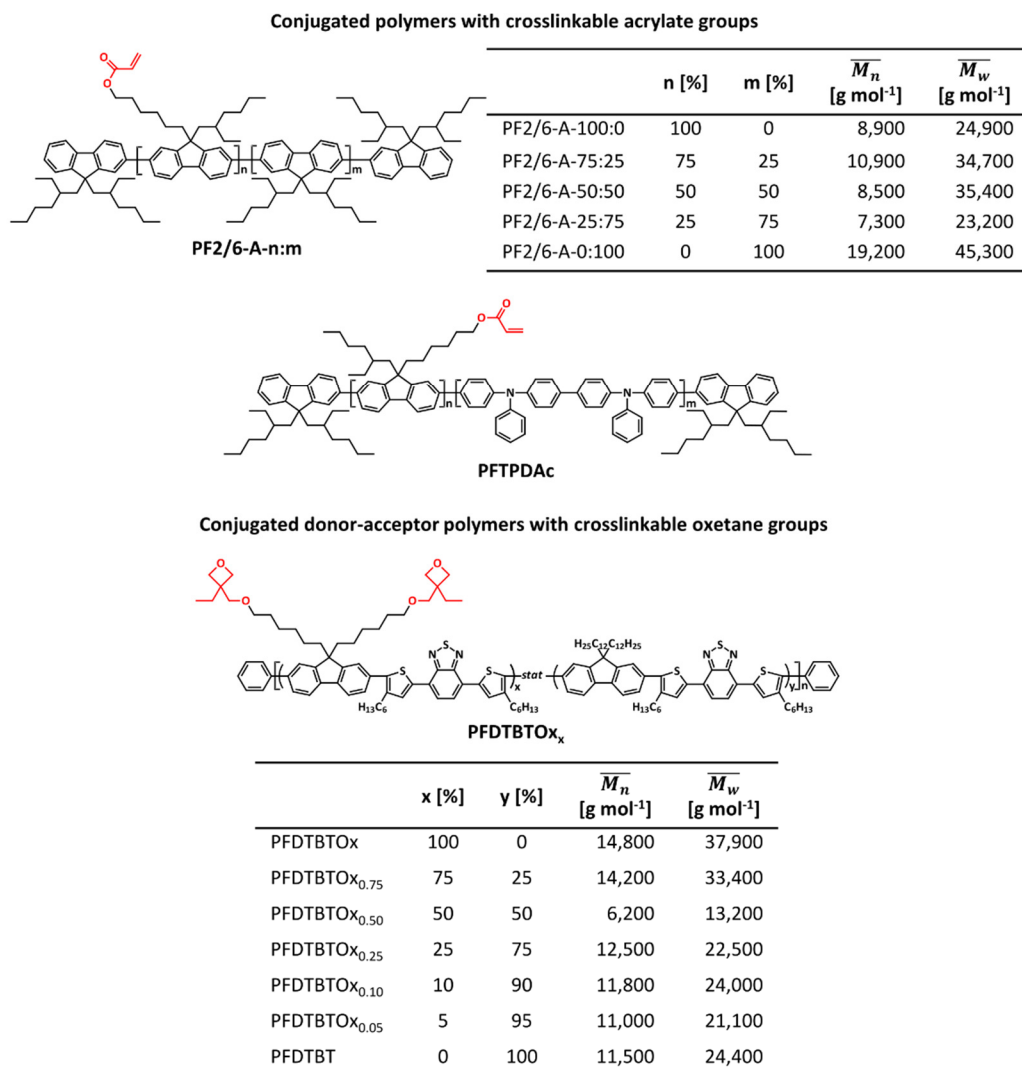


Figure 1. Schematic drawing of the formation of an insoluble network by crosslinking chains of a conjugated polymers.

Over the years, we have prepared a number of oligo- and polyfluorenes with reactive acrylate groups and studied crosslinking in detail.^{17,18,19} The chemical structures of two examples are shown in Figure 2. More recently, we extended our work to donor-acceptor type polymers containing oxetane units.²¹ The structure of a series of oxetane modified low bandgap polymers based on the well-known poly(2,7-(9,9-dialkylfluorene)-*alt*-(5,5-(4',7'-di-2-thienyl-2',1',3'-benzothiadiazole) PFDTBT is also shown in Figure 2.


 Figure 2. Conjugated polymers with crosslinkable acrylate^{17,18,19} and oxetane groups.²¹

The crosslinking of PFDTBTOx by cationic ring opening polymerization was carefully investigated.²¹ Solubility tests were performed as a measure for the success of the crosslinking reaction. This experiment compares the optical density of PFDTBTOx films before and after crosslinking and after rinsing with solvent. Film retention of 100% indicates that every polymer chain of the sample has become a part of an insoluble network. A schematic representation of the solubility test is shown in Figure 3a.

A very efficient initiator for the CROP is trifluoroacetic acid (TFA).⁷ This strategy combines a number of advantages compared to commonly used photoinitiators: The samples are prepared from plain polymer solutions without any photolabile component, which needs to be taken care of during processing. The low boiling point of 78 °C and TFA's high vapor pressure help saturating the thin sample with protons even at comparably low temperatures. Thus, residual TFA can easily be removed from the films by a simple vacuum treatment. Treating PFDTBTOx with TFA vapor at 100 °C for five minutes resulted in the formation of insoluble films. The same results were achieved after reducing the temperature to 80 °C. After experiencing that TFA vapor rapidly leads to the formation of insoluble films of PFDTBTOx, we studied the kinetics of crosslinking in detail. Therefore, crosslinking experiments with copolymers with a decreasing number of oxetane groups were performed. Polymer films were exposed to TFA vapor at 80 °C for 2, 5, 10, 20, and 30 minutes. The kinetics are shown in Figure 3b. Polymers with high density of oxetane groups, PFDTBTOx and PFDTBTOx_{0.75}, almost immediately form insoluble networks upon exposure to TFA. With PFDTBTOx_{0.50} 90% film retention is achieved after 20 min. In PFDTBTOx_{0.25} exposure times of 10 minutes and below do not result in any significant crosslinking. In this case a longer exposure time to TFA vapor helps to crosslink at least parts of the films, resulting in 50% film retention after 30 minutes.

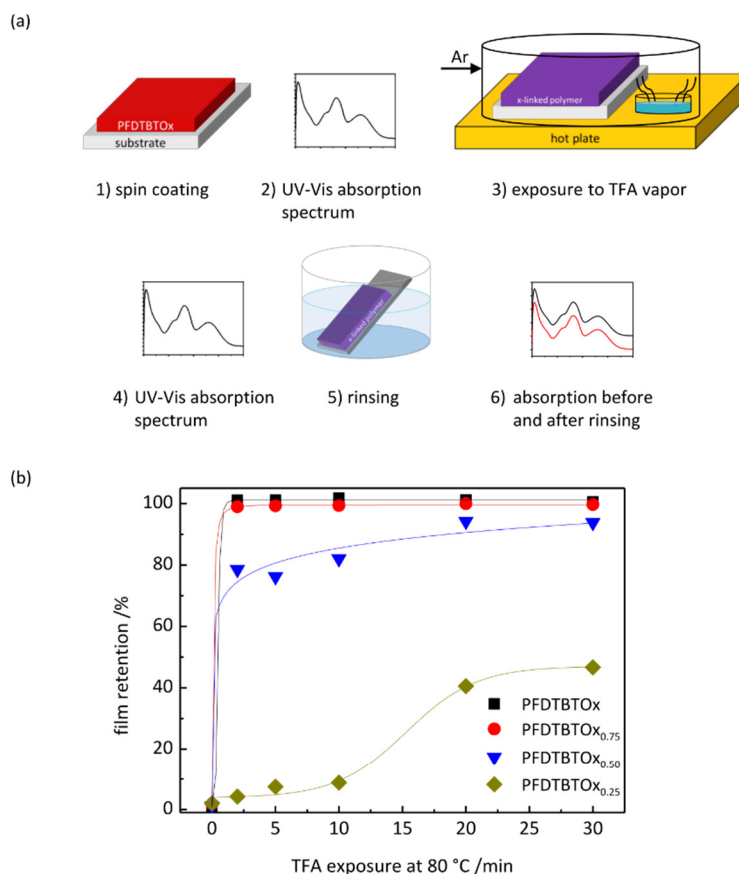


Figure 3. (a) Solubility test for the crosslinking of PFDTBTOx initiated by trifluoroacetic acid. (b) Kinetics of crosslinking from solubility tests. Film retention was calculated from the optical density before and after rinsing with THF.

With respect to the application in BHJ solar cells the crosslinking of PFDTBTOx in blends with PCBM was also investigated. As described for the neat polymer solubility tests were conducted. Already after short exposure times (5 minutes at 80 °C) to TFA vapor an insoluble polymer network is formed. PCBM is not involved in the crosslinking reaction and is washed off during solvent rinsing.

3. APPLICATIONS

The crosslinkable polymers described in chapter 2 have been used in a number of studies which can be divided into more fundamental studies on the influence of crosslinking on the diffusion of small molecules in a polymer matrix and on carrier mobility. In addition, the application of crosslinked polymers in multilayer organic solar cells and for the stabilization of BHJ cells was investigated.

3.1 Measuring the diffusion coefficient of C₆₀ in conjugated polymers

We developed a new method for diffusion measurements of small molecules like C₆₀ in a polymer matrix.²² The setup for the diffusion measurements (Figure 4a) includes a sensor layer of MEH-PPV and a polyfluorene transport layer on top. C₆₀ was vacuum evaporated on half of the sample. The C₆₀ free cell acted as control. The sensor layers of both cells were excited by a diode laser and the photoluminescence was recorded. At 140 °C the diffusion can be monitored by the quenching of the photoluminescence of MEH-PPV. From the time-dependent decrease of the photoluminescence a diffusion coefficient of $1.5 \cdot 10^{-11}$ cm²s⁻¹ for C₆₀ in polyfluorene can be derived. In this study we investigated a series of polyfluorene copolymers in which the amount of crosslinkable acrylate units was varied systematically (Figure 2 top). The diffusion coefficient could be decreased by three orders of magnitude upon crosslinking what means that the diffusion is drastically decelerated by crosslinking.

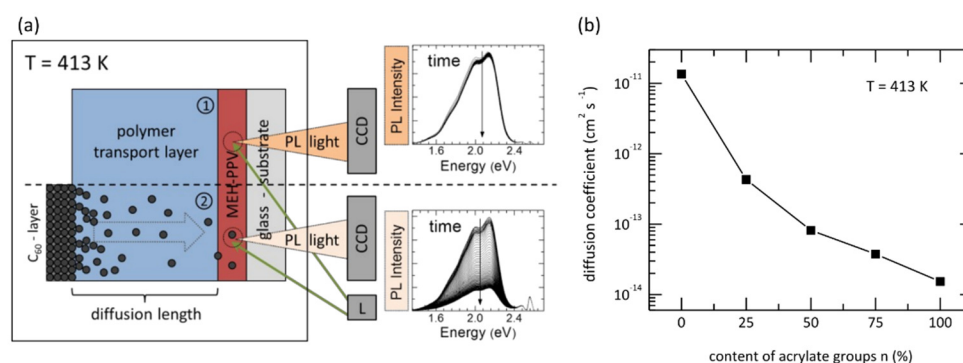


Figure 4. (a) Experimental procedure for measuring the diffusion coefficient of C₆₀ in polyfluorene. In the control cell (1) and the probe cell (2) the fluorescence of the MEH-PPV sensor layer, excited by a diode laser-shutter unit (L-S) (485 nm), is separately recorded by a CCD camera. After heating up the sample within a time interval of 5-10 min to a operation temperature of 413 K, C₆₀ molecules begin to diffuse. (b) Diffusion coefficient of C₆₀ as a function of the fraction of crosslinked polymer repeat units for PF2/6-A-n:m (ref. Figure 2) at 413 K.

3.2 Influence of crosslinking on charge carrier mobility in crosslinkable polyfluorene derivatives

Carrier mobility is a key parameter for the application of conjugated polymers in all fields of organic electronics. We have investigated the same series of polyfluorenes used for the diffusion studies to monitor the influence of crosslinking on carrier mobility (Figure 5).²³ For the regime of low to medium charge carrier density, relevant for OPVs and OLEDs, we used MIS-CELIV measurements (MIS: Metal-Insulator-Semiconductor, CELIV: Charge Extraction by Linearly Increasing Voltage).

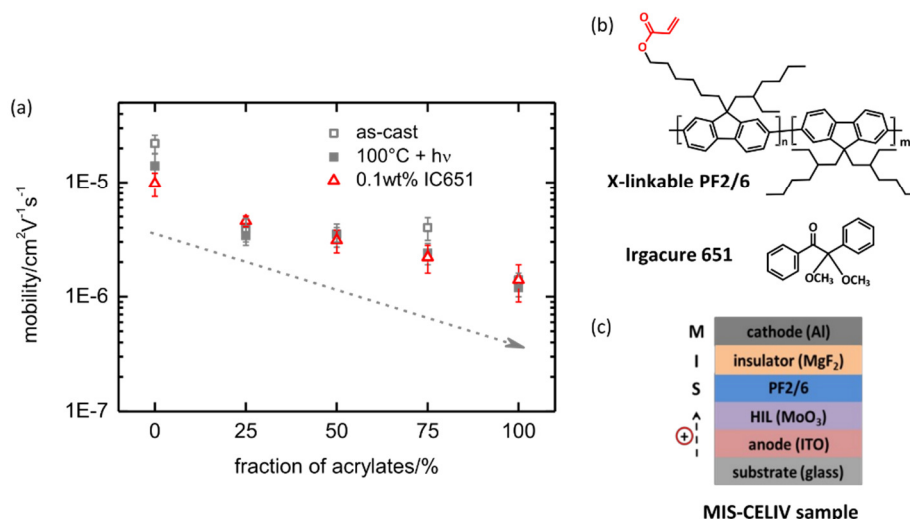


Figure 5. (a) Hole mobility as a function of the fraction of acrylate containing repeat units for different sample treatments, i.e. as cast without photoinitiator (open squares), crosslinked without photoinitiator (full grey squares), crosslinked with 0.1wt% of organic photoinitiator (Irg. 651, red open triangles). The grey dotted arrow indicates the mobility trend for increasing acrylate content. (b) Chemical structure of the crosslinkable polyfluorenes and the photoinitiator. (c) Experimental setup for MIS-CELIV measurements.

The results of the MIS-CELIV measurements are shown in Figure 5a, where the mobility is plotted as a function of acrylate contents. For untreated as-cast films of PF2/6-A-0:100, we find a mobility of about $2 \cdot 10^{-5} \text{ cm}^2\text{V}^{-1}\text{s}^{-1}$. Heating this sample at 100°C for 50 min under UV illumination only induces a small mobility reduction. We also find no significant difference in the mobility for PF2/6-A-0:100 samples with 0.1 wt% of the organic photoinitiator Irgacure 651. The mobility reduces, however, from about $2 \cdot 10^{-5} \text{ cm}^2\text{V}^{-1}\text{s}^{-1}$ to $2 \cdot 4 \cdot 10^{-6} \text{ cm}^2\text{V}^{-1}\text{s}^{-1}$ by introducing acrylate groups into the polymer structure, as indicated by the dashed grey arrow in Figure 5a. This is independent on whether the polymer is used as cast, thermally crosslinked without initiator or crosslinked with 0.1 wt% of photoinitiator. This means that *crosslinking itself* does not reduce mobility. The decrease in mobility by about one order of magnitude when introducing acrylate groups into PF2/6 can be attributed to changes in the microstructure of the amorphous film resulting in slightly enhanced chain torsions.²³

3.3 Three layer organic solar cell with a crosslinked exciton blocking layer

In the previous chapters we have described diffusion and mobility measurements on crosslinked polyfluorene derivatives. Recently, we have extended the synthesis to crosslinkable fluorene copolymers and used these materials in three layer solar cells.²⁴ For this purpose we synthesized a polyfluorene copolymer containing phenyl-substituted benzidine units (Figure 6c). The organic solar cell (Figure 6a) consists of a MoO_3 layer on top of which a 8 nm thick

layer of PFTPDAc was coated and subsequently crosslinked by UV irradiation. By this the PFTPDAc layer becomes completely insoluble and a second layer of the well-known low bandgap polymer PCDTBT can be spincoated on top without dissolving the PFTPDAc layer. The cell was completed by evaporating C₆₀ and an aluminum electrode on top. From current-voltage measurements a power conversion efficiency of 1.8% is determined for the three layer cell. In a reference cell without the PFTPDAc layer the efficiency drops to 1.4%. Photoluminescence measurements show that the increase of solar cell performance can be attributed to exciton blocking by the crosslinked PFTPDAc interlayer.

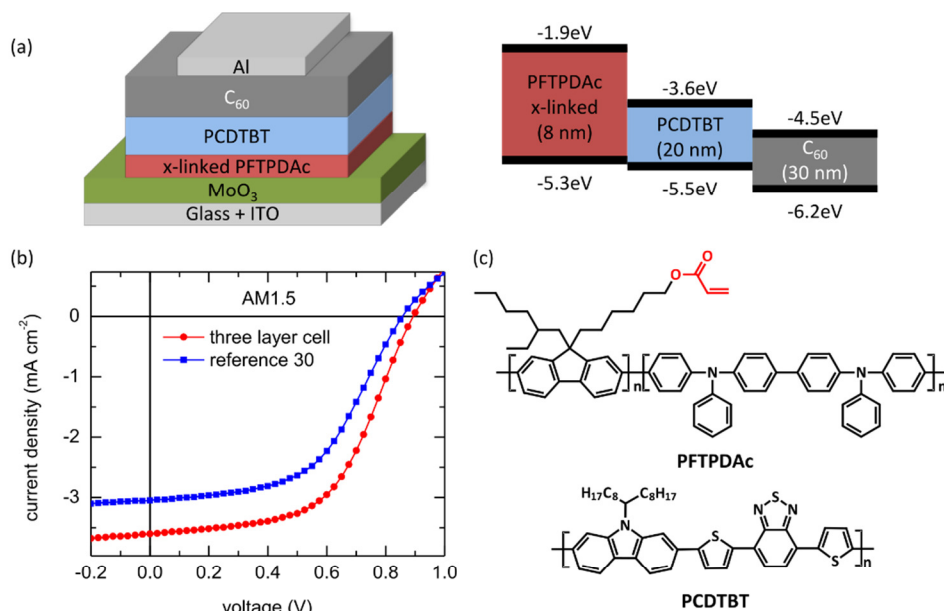


Figure 6. (a) Device structure of the three layer solar cell (left) and cascading energy levels of the different materials in the device (right). (b) Current-voltage characteristics for the three layer cell (red circles) and the reference cell with a 30 nm thick PCDTBT layer (blue squares). (c) Chemical structures of PFTPDAc and PCDTBT.

3.4 Stabilization of bulk heterojunction solar cells by crosslinking

BHJ solar cells usually consist of a blend of an electron donating low bandgap polymer and a soluble, electron accepting fullerene derivative like PCBM. Such donor acceptor blends achieve their best solar cell performance only if the morphology meets certain requirements. Domains in the range of the exciton diffusion length (ca. 10 nm) ensure that excitons can reach a donor acceptor interface within their lifetime and separate into electrons and holes. Such domain sizes also result in a large donor acceptor interface area. Furthermore, an ideal morphology comprises a bicontinuous network of donor and acceptor material. This provides paths for both kinds of charge carriers towards the electrodes. However, this complex morphology is thermodynamically unstable and prone to macrophase separation on a long timescale. This effect is even enhanced if one component tends to crystallize. Once degradation of the nanoscale morphology occurs, the overall performance of an organic solar cell will drop significantly.

For investigating the influence of crosslinking on the stabilization of BHJ solar cells at elevated temperature, we have synthesized a low bandgap polymer based on the structure of PFDTBT (Figure 7b).²¹ The novel polymer PFDTBTOx contains oxetane units that can be crosslinked by cationic ring opening polymerization (CROP). Oxetane units were

chosen because CROP can be carried out in BHJ cells with strongly electron accepting fullerenes. In order to investigate if crosslinking can slow down the formation of large aggregates of the electron acceptor PCBM in BHJ cells, accelerated aging tests were performed. In such an experiment the change of the device characteristics after long operation times is simulated. As described above, the morphology is the crucial point for BHJ solar cells. For a polymer:PCBM blend the morphology is likely to be hampered by diffusion of the low-molar mass fullerene. However, PCBM diffusion is rather slow at room temperature. In an accelerated aging experiment diffusion is increased by annealing the samples at elevated temperatures. Thus, the behavior of solar cells at long operation times can be simulated in a reasonable time. In this work, 100 °C was chosen as the temperature for the annealing process. This temperature is high enough to accelerate PCBM diffusion on the one hand and low enough to prevent thermal degradation of the active materials on the other.

For the accelerated aging experiments BHJ solar cells of PFDTBTOx crosslinked with trifluoroacetic acid were compared with the neat PFDTBTOx and with the reference polymer PFDTBT. Polymer:PCBM ratios of 1:2 were investigated. This means that the BHJ consists of 66 wt% of low molar mass PCBM in the polymer matrix. The steps of the accelerated aging experiment are illustrated in Figure 7a. To monitor the development of the device performance during annealing, they were characterized after 15 minutes, 60 minutes, 8 hours, 30 hours, and 100 hours of thermal treatment at 100 °C. Solar cell characterization was executed under inert atmosphere. For each material combination four solar cells were measured. From the current-voltage characteristics the PCEs were calculated for every time step.

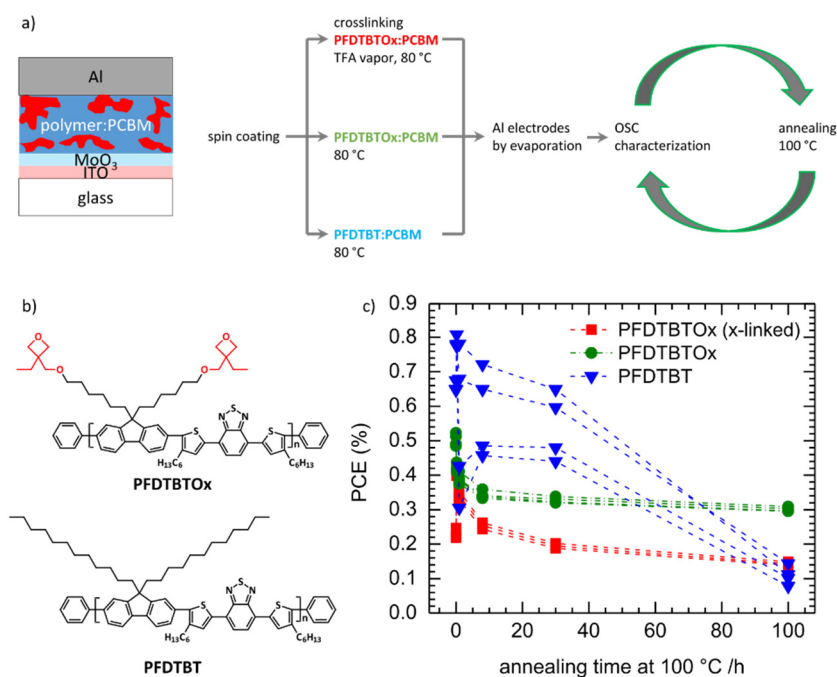


Figure 7. (a) Accelerated aging experiment. The layer structure of the BHJ cell. Sequence of steps for device fabrication, characterization and annealing. After spin-coating, the blends were heated to 80 °C and, in one case, the blend of PFDTBTOx:PCBM was exposed to TFA vapor. For the second PFDTBTOx:PCBM blend and the PFDTBT:PCBM reference TFA treatment was omitted. The aluminum electrodes were evaporated in the final step. The organic solar cells were then measured, annealed at 100°C for a certain time, and remeasured. For all three types of organic solar cells a polymer:PCBM blend ratio of 1:2 was investigated. (b) Chemical structures of PFDTBT and PFDTBTOx. (c) Development of the PCE for the TFA crosslinked PFDTBTOx, thermally crosslinked PFDTBTOx and non-crosslinkable PFDTBT in a 1:2 blend ratio with PCBM. For each system four different cells were measured.

It can be seen that for the 1:2-blends of PFDTBT:PCBM and PFDTBTOx:PCBM the initial efficiencies are different. PFDTBT shows the highest efficiency of 0.65% followed by the non-crosslinked PFDTBTOx blend with 0.50%. We attribute this difference to the incorporation of the crosslinkable oxetane groups. We are aware of reports in the literature that the incorporation of a large number of crosslinkable groups might be detrimental for device performance.^{7,25} For the TFA-crosslinked PFDTBTOx blend the initial efficiency is lower (0.25%) but increases to the value of the non-crosslinked PFDTBTOx sample within 15 minutes of annealing. Looking at the development over the entire annealing time of 100 hours, the PCEs of the crosslinked devices reach their maxima after 15 minutes and start to decrease afterwards. The initial PCE is reached after approximately 18 hours. After 100 hours of annealing at 100 °C, the efficiency of the crosslinked devices drops to 0.16% which corresponds to 65% of their initial efficiency.

Moreover, we observed that crosslinking can be obtained not only by exposure to trifluoroacetic acid vapor but also thermally by heating to 100 °C without any added initiator. In the case of the thermally crosslinked PFDTBTOx devices (green dots), the most significant loss of efficiency happens within the first eight hours of annealing. At longer times the decay is slowed down, and the PCE saturates at around 65% of the starting value.

Compared with the PFDTBTOx based devices, the solar cells comprising the PFDTBT reference polymer without crosslinkable oxetane groups behave differently. The PCE of the 1:2 blend device decays stepwise and no saturation is observed. Between 30 and 100 hours of annealing the most significant loss of efficiency is visible. Additionally, the values of the four investigated solar cells scatter severely within the first 30 hours of the accelerated aging experiment. After 100 hours of annealing, the PCE has dropped to approximately 20% of the starting value. The scattering observed for single devices of PFDTBT 1:2 blends can be attributed to arbitrary PCBM aggregation in the not stabilized devices. In summary, the PCEs of PFDTBT and PFDTBTOx blends behave differently upon annealing at 100 °C. While the efficiencies of the PFDTBT reference blends decays significantly to low efficiencies, the PCEs of PFDTBTOx blends stabilize after 30 hours. For longer annealing times up to 100 hours only small changes can be observed for both PFDTBTOx samples. This behavior can be attributed to stabilization by crosslinking the polymer in the blend. Thermal crosslinking by annealing for longer times seems to be an interesting possibility to stabilize blend solar cells without reducing the efficiency by the crosslinking process itself.

4. SUMMARY

We present a number of polyfluorene based conjugated polymers with crosslinkable acrylate and oxetane units. These polymers can be crosslinked by free radical polymerization in the case of acrylates and by cationic ring opening polymerization for oxetanes. Upon polymerization densely crosslinked networks are formed which are completely insoluble. Crosslinking of oxetanes by CROP is also possible in BHJ cells containing strongly electron accepting fullerene derivatives like PCBM.

Using the novel crosslinkable polymers we have carried out a number of studies. In a simple experimental setup based on fluorescence quenching we could show that the diffusion coefficient of C_{60} in polyfluorene at 140 °C can be reduced by a factor of 1000 by crosslinking the polymer matrix. With the same set of crosslinkable polyfluorenes we studied the influence of crosslinking on the charge carrier mobility. MIS-CELIV measurements show that the charge carrier mobility remains almost constant during crosslinking if proper conditions, e.g. thermal crosslinking or small amount of photoinitiator, are chosen.

Crosslinkable fluorene based copolymers have been tested in organic solar cells. We realized a three layer solar cell which contains a crosslinked PFTPDAC interlayer and layers of the low bandgap polymer PCDTBT and C_{60} . From current-voltage measurements an increase of the power conversion efficiency from 1.4% for a reference cell to 1.8% for the three layer cell is determined. PL measurements show that this increase can be attributed to exciton blocking of the PFTPDAC interlayer.

A critical issue of BHJ cells is the instability of the morphology of the polymer:fullerene blend over long operation times at elevated temperature. We present a crosslinkable derivative of the low bandgap polymer PFDTBT which contains oxetane units. During crosslinking via cationic ring opening polymerization the oxetane containing polymer rapidly forms insoluble networks in the presence of fullerenes. We investigated the device stability upon annealing at 100 °C for

times up to 100 h in accelerated aging experiments. Stabilization was clearly observed in crosslinked BHJ cells compared to the non-crosslinked reference. Moreover, we find that crosslinking can be obtained not only by exposure to trifluoroacetic acid vapor but also thermally by heating to 100 °C without any added initiator. Initiator free crosslinking is particularly attractive as it avoids the formation of decomposition products, and thus potential electron traps and quenching sites from the initiator.

Crosslinking of conjugated polymers with reactive groups in the side chains allows the preparation of multilayer solar cells from solution. Upon crosslinking, the underlying layer becomes insoluble and enables the deposition of a second layer from solution on top. Crosslinking also leads to a stabilization of BHJ solar cells. Due to a decrease in mobility of low molar mass acceptors like PCBM the morphology of BHJ cells is stabilized and hence the long term stability at elevated temperatures is improved.

5. ACKNOWLEDGEMENTS

We thank Irene Bauer and Frank Schirmer for technical assistance and Heinz Bässler and Thomas Unger for stimulating discussions. Financial support by the Bavarian State Ministry of Science, Research, and the Arts through the Collaborative Research Network “Solar Technologies go Hybrid” and by the German Science Foundation DFG through the doctoral training center “GRK 1640” is acknowledged.

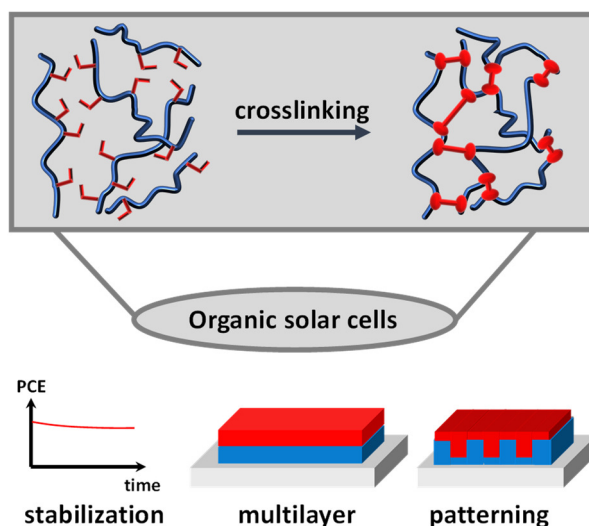
REFERENCES

- [1] Heeger, A. J., “Bulk Heterojunction Solar Cells: Understanding the Mechanism of Operation,” *Adv. Mater.* 26, 10-28 (2014).
- [2] Brabec, C. J., Sariciftci N. S. and Hummelen J. C., “Plastic Solar Cells,” *Adv. Funct. Mater.* 11, 15-26 (2001).
- [3] Jørgensen, M., Norrman, K., Gevorgyan, S. A., Tromholt, T., Andreasen, B. and Krebs, F. C., “Stability of Polymer Solar Cells,” *Adv. Mater.* 24, 580-612 (2012).
- [4] Wantz, G., Derue, L., Dautel, O., Rivaton, A., Hudhomme P. and Dagrón-Lartigau, C., “Stabilizing polymer-based bulk heterojunction solar cells via crosslinking,” *Polym. Int.* 63, 1346-1361 (2014).
- [5] Rumer, J. W. and McCulloch, I., “Organic photovoltaics: Crosslinking for optimal morphology and stability,” *Materials Today*, 18, 425-435 (2015).
- [6] Carlé, J. E., Andreasen, B., Tromholt, T., Madsen, M. V., Norrman, K., Jørgensen M. and Krebs, F. C., “Comparative studies of photochemical cross-linking methods for stabilizing the bulk hetero-junction morphology in polymer solar cells,” *J. Mater. Chem.* 22, 24417-24423 (2012).
- [7] Yau, C. P., Wang, S., Treat, N. D., Fei, Z., Tremolet de Villers, B. J., Chabinc M. L. and Heeney M., “Investigation of Radical and Cationic Cross-Linking in High-Efficiency, Low Band Gap Solar Cell Polymers,” *Adv. Energy Mater.* 5, 1401228 (2015).
- [8] Brotas, G., Farinhas, J., Ferreira, Q., Rodrigues, R., Martins, I. L., Morgado, J. and Charas, A., “Synthesis, characterization, and applications in photovoltaic cells of oxetane-functionalized P3HT derivatives,” *J. Polym. Sci. Part A: Polym. Chem.* 52, 652-663 (2015).
- [9] Griffini, G., Douglas, J. D., Piliago, C., Holcombe, T. W., Turri, S., Fréchet, J. M. J. and Mynar, J. L., “Long-Term Thermal Stability of High-Efficiency Polymer Solar Cells Based on Photocrosslinkable Donor-Acceptor Conjugated Polymers,” *Adv. Mater.* 23, 1660-1664 (2011).
- [10] Li, C.-Z., Yip, H.-L. and Jen, A. K.-Y., “Functional fullerenes for organic photovoltaics,” *J. Mater. Chem.* 22, 4161-4177 (2012).
- [11] Ryu, M. S. and Jang, J., “Improvement of conversion efficiency of bulk heterojunction organic solar cells using photo-curable crosslinker,” *Solar Energy Materials and Solar Cells* 94, 1384-1388 (2010).
- [12] Kim, B. J., Miyamoto, Y., Ma, B. and Fréchet, J. M. J., “Photocrosslinkable Polythiophenes for Efficient, Thermally Stable, Organic Photovoltaics,” *Adv. Funct. Mater.* 19, 2273-2281 (2009).

- [13] Lee, U. R., Lee, T. W., Hoang, M. H., Kang, N. S., Yu, J.W., Kim, K. H., Lim, K.-G., Lee, T.-W., Jin, J.-I. and Choi, D. H., "Photoreactive low-bandgap 4H-cyclopenta[2,1-b:3,4-b']dithiophene and 4,7-di(thiophen-2-yl)benzo[c][1,2,5]thiadiazole-based alternating copolymer for polymer solar cell," *Organic Electronics* 12, 269-278 (2011).
- [14] Penterman, R., Klink, S. I., de Koning, H., Nisato, G. and Broer, D. J., "Single-substrate liquid-crystal displays by photo-enforced stratification," *Nature* 417, 55-58 (2002).
- [15] Gholamkhash, B. and Holdcroft, S., "Toward Stabilization of Domains in Polymer Bulk Heterojunction Films," *Chem. Mater.* 22, 5371-5376 (2010).
- [16] Müller, C. D., Falcou, A., Reckefuss, N., Rojahn, M., Wiederhorn, V., Rudati, P., Frohne, H., Nuyken, O., Becker, H. and Meerholz, K., "Multi-colour organic light-emitting displays by solution processing," *Nature* 421, 829-833 (2003).
- [17] Jandke, M., Hanft, D., Strohriegl, P., Whitehead, K., Grell, M. and Bradley, D. D. C., "Polarized electroluminescence from photocrosslinkable nematic fluorene bisacrylates," *Proc. SPIE* 4105, 338 (2001).
- [18] Scheler, E. and Strohriegl, P., "Three color random fluorene-based oligomers for fast micron-scale photopatterning," *Chem. Mater.* 22, 1410-1419 (2010).
- [19] Scheler, E., Betthausen, E. and Strohriegl, P., "Synthesis and properties of alternating fluorene-based oligomers for sub-micron photopatterning," *Macromol. Chem. Phys.* 211, 2081-2089 (2010).
- [20] Feser, S. and Meerholz, K., "Investigation of the Photocross-Linking Mechanism in Oxetane-Functionalized Semiconductors," *Chem. Mater.* 23, 5001-5005 (2011).
- [21] Knauer, P., Hahn, T., Köhler, A. and Strohriegl, P., "Initiator free crosslinking of oxetane functionalized low bandgap polymers: An approach towards stabilized bulk heterojunction solar cells," submitted.
- [22] Fischer, F., Hahn, T., Bässler, H., Bauer, I., Strohriegl, P. and Köhler, A., "Measuring reduced C60 diffusion in crosslinked polymer films by optical spectroscopy," *Adv. Funct. Mater.* 24, 6172-6177 (2014).
- [23] Kahle, F.-J., Bauer, I., Köhler, A. and Strohriegl, P., "Influence of Crosslinking on Charge Carrier Mobility in Crosslinkable PF2/6 Derivatives," submitted.
- [24] Hahn, T., Saller, C., Weigl, M., Bauer, I., Unger, T., Köhler, A. and Strohriegl, P., "Organic solar cells with crosslinked polymeric exciton blocking layer," *Phys. Stat. Solidi A* 212, 2162-2168 (2015).
- [25] Chen, X.-Q., Yao, X., Xiang, X., Liang, L., Shao, W., Zhao, F.-G., Lu, Z., Wang, W., Li, J. and Li, W.-S., "Long-term thermally stable organic solar cells based on cross-linkable donor-acceptor conjugated polymers," *J. Mater. Chem. A* 4, 9286-9292, (2016).

Appendix D: Crosslinked semiconductor polymers for photovoltaic applications

Frank-Julian Kahle, Christina Saller, Anna Köhler, and Peter Strohrriegl



Published in *Advanced Energy Materials*

doi: 10.1002/aenm.201700306

Reprinted with permission from *Advanced Energy Materials* **2017** 7, 1700306

Copyright © 2017 WILEY-VCH Verlag GmbH & Co. KGaA, Weinheim

Crosslinked Semiconductor Polymers for Photovoltaic Applications

Frank-Julian Kahle, Christina Saller, Anna Köhler, and Peter Strohriegl*

Organic solar cells (OSCs) have achieved much attention and meanwhile reach efficiencies above 10%. One problem yet to be solved is the lack of long term stability. Crosslinking is presented as a tool to increase the stability of OSCs. A number of materials used for the crosslinking of bulk heterojunction cells are presented. These include the crosslinking of low bandgap polymers used as donors in bulk heterojunction cells, as well as the crosslinking of fullerene acceptors and crosslinking between donor and acceptor. External crosslinkers often based on multifunctional azides are also discussed. In the second part, some work either leading to OSCs with high efficiencies or giving insight into the chemistry and physics of crosslinking are highlighted. The diffusion of low molar mass fullerenes in a crosslinked matrix of a conjugated polymer and the influence of crosslinking on the carrier mobility is discussed. Finally, the use of crosslinking to make stable interlayers and the solution processing of multilayer OSCs are discussed in addition to presentation of a novel approach to stabilize nanoimprinted patterns for OSCs by crosslinking.

1. Introduction

In recent years, the research on solar cells from organic semiconducting materials has made fast progress.^[1] Organic solar cells (OSCs) are an interesting alternative to the widely used silicon solar cells because of their unique properties. These include low weight, cost-efficient fabrication via solution processing, and the ability for application on flexible substrates.^[2] The active layer of an OSC is composed of an electron donor and an electron acceptor. The most promising approach is the bulk heterojunction (BHJ) solar cell that is composed of a blend of the two materials. In many cases, electron-donating polymers and electron-accepting fullerenes are applied.^[1b] Using different low bandgap polymers like NT812/PC₇₁BM^[3] and

PTB7-Th/PC₇₁BM,^[4] high efficiencies of 10.33% and 10.95% could be achieved, respectively.

Most BHJ solar cells containing a donor polymer and a fullerene acceptor are realized by solution processing. In contrast, vacuum evaporation allows the fabrication of solar cells with a large number of layers by subsequent deposition of different small molecules. Using this technique, BHJ as well as planar heterojunction (PHJ) solar cells, multilayer solar cells, and tandem solar cells can be fabricated. The advantage of this method is the possibility to optimize the properties of the different layers separately. The highest reported efficiency of a polymer tandem solar cell made under laboratory conditions is 11.3%.^[5] Companies announced multilayer OSCs with efficiencies up to 13.2%.^[6]

As the exciton diffusion length in OSCs is about 10 nm, a controlled morphology of the active layer in combination with direct charge percolation paths towards the electrodes is of vital importance for the performance of organic solar cells. One possible solution for that issue are nanostructured active layers, for example realized by nanoimprinting.^[7] By means of this method, an efficiency of 4.4% could be achieved with a nanostructured poly-3-hexylthiophene (P3HT) layer and [6,6]-phenyl-C61-butyric acid methyl ester (PCBM).^[8] In this case, the nanoimprinting additionally enforces a favorable chain alignment of the polymer.

However, a major disadvantage of OSCs is their lack of stability. Device instability arises from different reasons such as thermal, chemical or mechanical stress, and light exposure.^[9] Encapsulation of the device can prevent degradation by water or oxygen.^[10] One major issue regarding thermal degradation of BHJ solar cells is the diffusion of low molecular weight fullerenes and subsequent formation of large fullerene aggregates. This results in a decreased device performance.^[11]

Extending the concept of multilayer structures from evaporated low molar mass compounds to polymers is difficult as they are solution processed. The underlying polymer layer would be dissolved by the deposition of a second polymer solution on top. This can be prevented by the use of orthogonal solvents^[12] or the introduction of inorganic interlayers, especially in the field of tandem devices.^[5a,13] Orthogonal solvents are also used to prevent nanoimprinted patterns from dissolution.^[7,8]

One approach to overcome the problems mentioned above is the application of crosslinkable materials.^[14] The basic advantage applying crosslinkable materials is the “freezing”

F.-J. Kahle, Prof. A. Köhler
Experimental Physics II
University of Bayreuth
95440 Bayreuth, Germany

C. Saller, Prof. P. Strohriegl
Macromolecular Chemistry I
University of Bayreuth
95440 Bayreuth, Germany

E-mail: peter.strohriegl@uni-bayreuth.de

Prof. A. Köhler, Prof. P. Strohriegl
Bayreuth Institute of Macromolecular Science (BIMF)
University of Bayreuth
95440 Bayreuth, Germany

DOI: 10.1002/aenm.201700306

of the initial morphology. This principle is illustrated using the example of a crosslinkable polymer in **Figure 1a**. Before crosslinking, the conjugated polymer is soluble and can be solution processed. Upon crosslinking, covalent bonds, which

connect the polymer chains, are formed. The resulting densely crosslinked conjugated polymer network is insoluble and its morphology is frozen. Initiation of the crosslinking process is possible via a (photo)initiator, exposure to UV-light or heat.

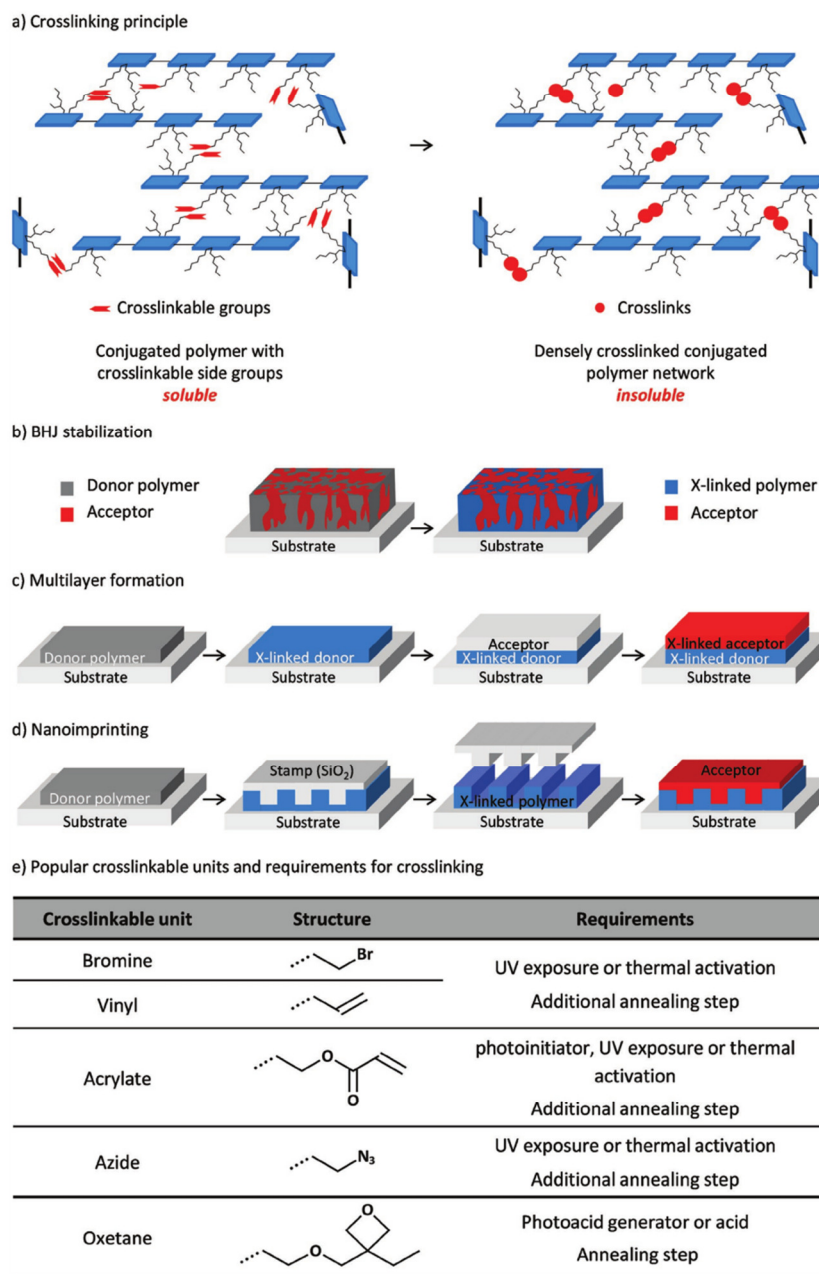


Figure 1. a) Schematic drawing of the formation of an insoluble network by crosslinking chains of a conjugated polymer. b) Stabilization of a BHJ morphology by crosslinking of the donor polymer. c) Multilayer formation by application of a crosslinkable donor and a crosslinkable acceptor. d) Patterning via nanoimprinting of a crosslinkable donor polymer. e) Popular crosslinkable units and requirements for crosslinking.

Crosslinking enables the realization of different concepts regarding organic solar cells. The first one is the stabilization of BHJ morphologies and is shown in Figure 1b. In this example, the blend is made up of a crosslinkable donor polymer. After crosslinking, the donor polymer has become insoluble and the morphology is locked. Thus, the migration of low molecular mass acceptors such as PCBM is reduced, leading to a stabilization of the OSC. A second concept concerns the multilayer formation from solution-processed materials. Figure 1c depicts the process applying two crosslinkable materials. First, the crosslinkable donor polymer is spin-coated onto a substrate. Subsequent crosslinking in presence of an initiator renders the donor polymer insoluble. This allows the spin-coating of an acceptor solution on top of the donor layer without damaging or dissolving the underlying layer. More complex stacks can also be realized by applying further crosslinkable functional materials. Finally, the realization of patterned structures by nanoimprinting is presented in Figure 1d. The first step in this process is the deposition of a crosslinkable donor polymer on a substrate. The pattern is transferred to the polymer layer with a stamp. Subsequent crosslinking of the donor polymer leads to a pattern that is stabilized and completely insoluble. After removal of the stamp, an acceptor can be deposited via solution processing or vacuum evaporation on top of the pattern without damaging it.

In the following, the design strategies for crosslinkable materials as well as the most popular crosslinking units are presented.

2. Overview of the Chemistry of Crosslinkable Materials

Three approaches can be discriminated for the crosslinking of active layers. These include the crosslinking of the donor material or the acceptor material as well as crosslinking both the donor and acceptor.

A lot of research effort has been put into crosslinkable donor materials over the last years. In organic solar cells, polymers are frequently used as electron donor. The general approach is to attach crosslinkable units to the solubilizing side chains of the polymers. Bromine, vinyl, acrylate, azide, and oxetane groups are commonly used. Their molecular structure and requirements for the crosslinking procedure are summarized in Figure 1e.^[14b] Bromine, vinyl, acrylate, and azide functionalities are activated upon UV-light exposure or thermally and the crosslinking procedure can additionally implement an annealing step to ensure complete crosslinking. In addition to its benefits, crosslinking may cause some problems that differ between the functional units. Remaining bromine groups can negatively influence device properties such as the charge carrier mobility. For the crosslinking of acrylates, photoinitiators are often used. The residues of the photoinitiator decomposition remain in the polymer layer. The activation of azides results in the release of nitrogen and very reactive nitrene species are formed. Because of the high reactivity, the nitrenes may not only attack the polymer side chains, but also insert into the conjugated backbone. Oxetane crosslinking requires the presence of an acid source or prolonged thermal activation.^[15] An

annealing step is necessary to ensure complete crosslinking. The problems with acid activated crosslinking are acid residues or the counterions of the photoacid generators. In contrast to the radical crosslinking process applying for bromine, vinyl and acrylate, the cationic mechanism of oxetane allows crosslinking in the presence of radical scavenging materials such as fullerene.

The crosslinking groups shown in Figure 1e have been attached to a number of polymers. P3HT, a widely used conjugated donor polymer, has been modified with several crosslinkable units. Kim et al. presented the derivative P3HT-Br containing up to 20% of bromine units that can be photo-crosslinked via UV-exposure.^[16] The chemical structure is shown in Figure 2. Both planar heterojunction (PHJ) and BHJ solar cells were prepared. An efficiency of 2.2% was reached for a polymer with 10% bromine in a PHJ geometry and 3.4% efficiency for the 5% bromine derivative in a BHJ geometry. Stability tests at 150 °C showed that the efficiency is stable upon crosslinking for PHJ solar cells for up to three days and for BHJ solar cells for up to two days. Vinyl functionalized P3HT that can be crosslinked thermally was used to realize BHJ cells and the stability was tested by annealing at 150 °C for 10 h (Figure 2).^[17] The crosslinked devices showed a better thermal stability than the non-crosslinked reference devices. This is confirmed by optical microscopy yet the formation of PCBM crystals could not be fully suppressed. A P3HT diblock copolymer consisting of a P3HT block and a polythiophene block with pendent acrylate units was synthesized by Ouhib et al. and crosslinked thermally (Figure 2).^[18] BHJ cells with the crosslinked polymer retained 85% of their initial efficiency after 165 h at 110 °C. In contrast, the P3HT reference devices exhibited a decrease to 65%. Kim et al. demonstrated the synthesis of a photo-crosslinkable P3HT-azide copolymer (Figure 2).^[19] Annealing at 150 °C for 40 h yielded thermally stable BHJ solar cells with 3.3% efficiency. Another crosslinking chemistry was presented by Brotas et al. who synthesized a P3HT copolymer with 10% oxetane functionalization (P3HT-oxetane, Figure 2).^[20] The oxetane group was crosslinked using UV-light in presence of a photoacid generator and a subsequent annealing step. The incorporation of the oxetane unit decreased the performance of BHJ cells to 1.1% compared to 1.9% for the non-functionalized P3HT cell. Crosslinking of the blend led to a further drop to 0.2%. However, this is balanced by an improved stability of the cells during illumination for 40 min.

Recently, the interest shifted from P3HT to low bandgap polymers that can harvest a large part of the sun's spectrum. Griffini et al. presented a crosslinkable PBDTTPD derivative with 16% and 33% bromine in the side chains, respectively (Figure 2).^[21] This was the first crosslinkable low bandgap polymer applied in BHJ solar cells. The devices composed of the polymer with 16% bromine containing repeat units were annealed for 72 h at 150 °C and finally exhibited a remarkably high efficiency of 4.6%, while the efficiency of the reference cell dropped from 5.2% to 3.9%. In 2012, the Krebs group presented a study in which the performances of OSCs from the low bandgap polymers TQ-x (Figure 2) with different crosslinkable groups were compared.^[22] TQ1 was modified either with an alkyl chain, a bromine, a vinyl, or an oxetane functionality. This work is discussed in more detail in the next

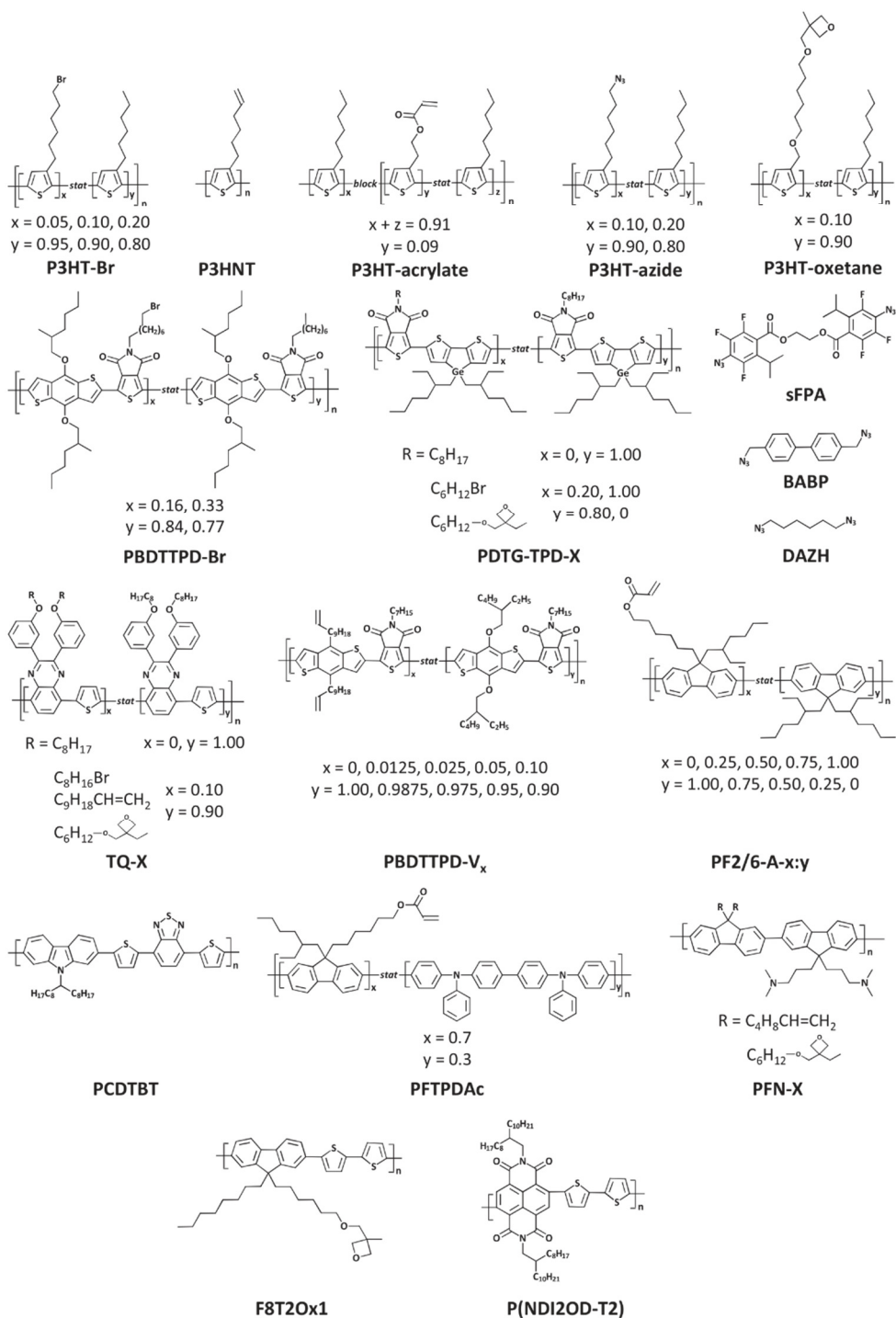


Figure 2. Crosslinkable semiconducting polymers and low molar mass crosslinkers. The chemical structures of the copolymers are drawn according to the IUPAC nomenclature, where -stat- means statistical and -block- denotes block copolymers.

section. Further work was performed on bromine containing low bandgap polymers,^[23] azide functionalized copolymers^[24] as well as on a series of PBT derivatives including bromine, azide, and vinyl units.^[25]

In the polymers discussed above, the crosslinkable groups are attached to the polymer side chain. Another option for the incorporation of a crosslinkable unit is the backbone itself. Bui et al. reported three different copolymers containing triple bonds in the polymer backbone.^[26] Two of them were tested as buffer layers in inverted OSCs for the interface modification of zinc oxide. Thereby, the crosslinking was performed by exposure of the polymer layers to UV-light. The increase of the hydrophobicity of the zinc oxide layer due to the crosslinked interlayer resulted in an improved efficiency of 3.1% compared to 2.7% for the reference cell.

A versatile approach for crosslinking without the need of functional groups is the use of small molecule crosslinkers. A prominent example was presented by Friend and co-workers. They added the reactive bis-nitrene crosslinker sFPA (Figure 2) to non-functionalized conjugated polymers.^[27] With this method, a PHJ solar cell with three polymer layers on top of each other was realized.^[28] The materials featured cascaded energy levels achieving an efficiency of 0.45%. In addition, P3HT was also crosslinked by the use of sFPA. Bilayer cells with PCBM as acceptor yielded 3.0% efficiency in comparison to 3.3% efficiency for the non-crosslinked reference.^[29] Derue et al. studied the crosslinking of fullerenes in blends with different donor polymers under mild conditions using the bis-azide BABP (Figure 2).^[30] 3.3% efficiency was achieved for a cell with P3HT. After 120 days at 85 °C, 90% of the initial efficiency could be retained. Regarding PTB7, an efficiency decrease from 5.8% to 4.6% was observed upon annealing for 16 h at 150 °C. PDPPTBT^[30] exhibited an initial value of 4.5%, which dropped to 3.0% when the cell was annealed for 15 h at 150 °C. In the group of McCulloch, SiIDT-BT was crosslinked using the bis-azide DAZH (Figure 2), which improves the efficiency from 6.0% to 7.0%.^[31] Thermal aging for 130 h at 85 °C resulted in an efficiency of 4.1% for the crosslinked cell compared to 3.5% for the reference cell.

In addition to the crosslinking of donor polymers, crosslinkable fullerene derivatives were also investigated in the last years and are discussed in the reviews of Wantz et al. and Rumer et al.^[14]

3. Application of Crosslinking in Organic Photovoltaics

In the preceding section a number of polymers and different reactive groups used to make OSCs with crosslinked layers were presented. In a short review, however, it is not possible to cover all the work on crosslinked OSCs.^[14] Instead, we decided to highlight work that leads to efficient OSCs or that we believe is important for the understanding and the development of crosslinked solar cells. We begin with work on the stabilization of BHJ solar cells followed by a section on the use of crosslinked layers and multilayer OSCs and end with a short section on patterning.

As discussed above, there are several approaches of crosslinking in organic solar cells: donor to donor, acceptor

to acceptor, or donor to acceptor. In principal, all of the three approaches are capable of stabilizing the blend morphology in BHJ solar cells. Crosslinking of the donor is often used, as it is relatively easy and versatile and may be applied to a variety of material classes.^[14,18,22,25]

In an attempt to systematically assess the relation between different functional groups and the stability of the crosslinked OSCs, comparative studies were performed by several groups.^[22,25,32] Krebs and co-workers^[22] compared bromine-, azide-, vinyl-, and oxetane- functionalized derivatives of the low bandgap polymer TQ1 (Figure 2). Crosslinking via UV-illumination resulted in solvent resistant films and did not change the optical absorption spectra, therefore excluding damage to the π -conjugated polymer backbone. Photochemical and thermal stability was investigated using different experimental conditions for aging: dark versus illumination under 1 sun and ambient versus inert atmosphere. The observed stability enhancement was attributed to the suppression of morphological changes, that is fullerene aggregation, as confirmed by optical microscopy. Yet, the analysis of stability under the different experimental conditions did not result in a consistent correlation between polymer stability and the different functional groups used for crosslinking.

Heeney and co-workers^[32] compared derivatives of the low bandgap polymer PDTG-TPD with both bromine and oxetane functional groups (Figure 2). The pure polymers can both readily be crosslinked. Yet, in blends with fullerenes, crosslinking was only successful for the oxetane-containing PDTG-TPD derivative. This might be attributed to the radical scavenging ability of fullerenes^[33] preventing radical polymerization in the case of bromine. Moreover, efficiencies as high as 5.02% could be obtained with a relatively small number of oxetane units (20%). Finally, Heeney and co-workers found an increased thermal stability of the crosslinked BHJ cells on the timescale of 30 min.

Similar observations with regard to small amounts of functional groups were also made by several other groups.^[16,21,22,24,34] A noteworthy example is the work by Chen et al., who obtained a PCE of 6.06% using only 2.5% of crosslinkable vinyl-groups in PBDTTPD-V_x (Figure 2) combined with PC₇₁BM, still retaining 91% of the efficiency after 40 h of annealing at 150 °C. This is among the highest PCEs reported for OPVs using crosslinked active layers.^[34]

In the context of oxetane functionalization, it is noteworthy that, although it is generally assumed that this mechanism requires the exposure to an acid,^[14,35] Knauer et al.^[15] showed that crosslinking via oxetane groups can be achieved by prolonged heating, yielding a fully crosslinked and long-term stable BHJ cell.

In general, this possibility of crosslinking without crosslinking additives is a great benefit, as possible remnant by-products, which could be detrimental for device performance, are avoided.^[14b,36] This issue was addressed by Kahle et al., who investigated the effect of crosslinking on the charge carrier mobility of acrylate functionalized PF2/6-A-x:y (Figure 2) using MIS-CELIV measurements.^[36b] They showed that an amount of photoinitiator of 1 wt% could deteriorate charge transport in a PF2/6 polymer layer. This effect was especially pronounced in the case of a Ti-based initiator, leading to a reduction of hole

mobility by over two orders of magnitude due to the introduction of traps. On the other hand, when choosing appropriate conditions such as a small amount of Ti-free photoinitiator (0.1 wt%) or even purely thermal crosslinking, no reduction in mobility compared to the respective non-crosslinked reference was observed.

In addition, Kahle et al. found a reduction of the mobility with increasing content of functional groups because of steric effects, implying that a smaller amount of functional groups may be advantageous for devices. This is in agreement with the results of Heeney and co-workers^[32] discussed above, who have shown that just 20% of crosslinkable groups result in sufficient device stabilization.

Apart from creating a 3D network of the donor polymer as a stable matrix for the fullerene acceptor, one can also follow the approach of directly crosslinking donor to acceptor. In this case, there are only a limited number of functional groups^[14a] available due to the electron scavenging properties of fullerene. The most suitable and common pathway to perform a controlled reaction between the donor and the acceptor is thermal crosslinking using azide-functionalized donor polymers.^[19,37]

A remarkable exception is the work of Tournebize and co-workers,^[38] who managed to link donor and acceptor without any additional functionalization using a blend of PCDTBT (Figure 2) and PC₇₁BM. The underlying mechanism was identified to be of photochemical origin and studied via accelerated artificial photoaging. It proceeds via scission of the bond between the N-atom of the carbazole units of PCDTBT and the alkyl side chain followed by reaction of the macroradicals with the fullerene. The formation of the covalent crosslinks first results in a decrease in PCE ("burn-in") of about 25% of the initial value,^[39] but then leads to an impressive long-term stability and an expected average lifetime of PCDTBT/PCBM solar cells of about seven years, as reported by McGehee and co-workers (Figure 3).^[39] To the best of our knowledge this is the best long-term stability of polymer:fullerene blends reported to date. By performing additional thermal annealing and measuring

(light-induced) electron paramagnetic resonance ([L]EPR), it was shown that the crosslinking is mainly related to polymer crosslinking and not only due to a thermally reversible PCBM oligomerization.^[38]

The last possibility to suppress fullerene crystallization in a blend morphology is to directly crosslink functionalized fullerene derivatives.^[40] Yet, due to the electron scavenging properties of fullerenes and their ability to terminate radical reactions, only a limited number of functional groups may be used, and this approach is only rarely applied in BHJ stabilization.^[14a] In the emerging class of non-fullerene acceptors,^[41] no crosslinkable materials have been reported yet. We believe that such materials would be an interesting perspective for further research.

Instead of being a component of the BHJ layer, functionalized fullerenes are more often used as thin self-assembled layers at an electrode for passivating interfacial trap states and lowering the contact resistance,^[42] which leads to another possible application of crosslinking in organic photovoltaics: the formation of stable, insoluble interlayers. In general, this approach allows the fabrication of multilayer devices or even tandem or triple junction solar cells from solution without the use of orthogonal solvents^[43] or relying on materials that have to be evaporated. More specifically, crosslinked layers may be used as exciton blocking or transport layers at the electrodes allowing for subsequent deposition of further layers from solution or preventing materials from diffusing into each other.^[27,28,44]

However, to date, to best of our knowledge there is no report about advanced multilayer organic solar cell devices that are fully processed from solution using several crosslinked layers. Well-known examples such as the work by Janssen and co-workers^[13a] or Leo and co-workers^[45] still rely on solution-processed inorganic interlayers or vacuum-deposited small molecules. Nevertheless, there is some recent work demonstrating the successful application of polymeric interlayers in multilayer devices.^[27,28,44c,d,g-i] Hahn et al. were able to improve the efficiency of a PCDTBT/C₆₀ bilayer cell by introducing an additional

layer of crosslinked PFTPDAC (Figure 2) that reduced exciton quenching at the donor-anode interface leading to an increase of 25% in efficiency.^[44c] Wang et al. demonstrated an efficiency improvement of 195% using PFN-V (Figure 2) as an additional interlayer at the cathode of an inverted PTB7-Th/PC₇₁BM solar cell reaching a remarkable PCE of 9.18%. The improvement was attributed to enhanced vertical phase separation due to a favorable surface energy of the polymer interlayer.^[46] A 204% increase of the efficiency to 9.28% was achieved with a crosslinked interlayer of PFN-Ox in an inverted PTB7/PC₇₁BM cell.^[44]

The general ability of crosslinking to slow down or suppress the diffusion of fullerenes in BHJ cells is commonly accepted, but rather difficult to address experimentally. Therefore, this topic has only rarely been dealt with in the literature up to now.^[11,47] Recently an experimentally simple approach

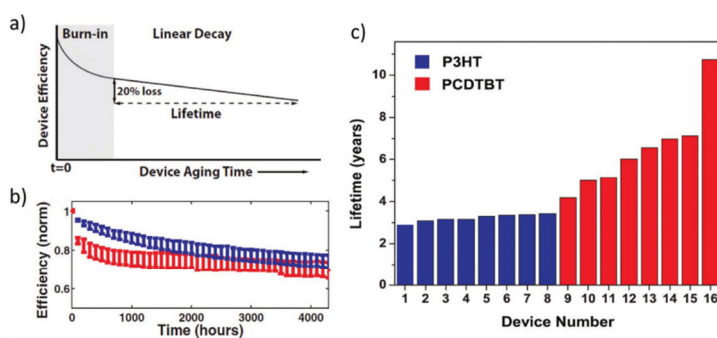


Figure 3. a) Definition of the OSC lifetime according to McGehee and co-workers. It is defined as the point at which the efficiency has dropped to 80% of the value at the start of the linear decay period. Both axes are linear. b) Normalized device efficiency for PCDTBT (red) and P3HT (blue) solar cells over a time span of 4400 h of continuous testing. Each point is the average of the efficiency for 8 individual solar cells of each type. c) Estimated lifetimes of eight P3HT and eight PCDTBT devices. The latter show, on average, significantly longer lifetimes. The wider spread of the PCDTBT data compared to P3HT is attributed to less experience with the PCDTBT system. Reproduced with permission.^[39a] Copyright 2011, John Wiley Sons, Inc.

to assess diffusivity of fullerenes in a polymer matrix by optical means was presented by Fischer et al.^[44] The method is based on photoluminescence quenching in a sensing layer (here: MEH-PPV) induced by electron transfer from the excited singlet exciton of the sensor to the fullerene after the fullerene has diffused through a polymer matrix starting from the top of the polymer layer (Figure 4a–c). In the accompanying work, Fischer et al. demonstrated a reduction of three orders of magnitude in the diffusion coefficient of C_{60} at 140 °C when using a densely crosslinked polyfluorene derivative (PF2/6-A-x:y) compared to a non-crosslinked reference sample (Figure 4d).

Finally, the stability and insolubility of crosslinked layers may be exploited in a third possible application: nanostructuring of layers and interfaces in optoelectronic devices. Structuring allows controlled tuning of donor–acceptor interfaces, phase intercalation, and percolation pathways and therefore is an approach to achieve an optimal spatial morphology on a nanometer scale.^[7,48] In addition to conventional photopatterning^[49] using crosslinkable conjugated polymers as negative photoresists, it is also

possible to apply nanotemplating to a blend mixture^[35,50] or even to use mold-assisted mechanical imprinting techniques.^[51] The latter even allows resolution beyond the limits imposed by light diffraction or beam scattering, that is even sub-10 nm accuracy,^[7] which is on the order of the exciton diffusion length. The templating approach was used, for example, by Farinhas et al., who processed a mixture of F8T2Ox1 (Figure 2), a conjugated polymer, and polystyrene, utilizing the tendency of both polymers to demix. After crosslinking F8T2Ox, polystyrene was removed, leading to columnar structures of F8T2Ox, which were then filled with PCBM. Unfortunately, the resulting PCEs were smaller than 1%.^[50b] A promising approach to get a spatially very well-defined interface morphology, allowing the systematic study of the influence of the interface on device performance, was presented by Schmidt-Mende and co-workers.^[51b] They applied nanoimprinting lithography (NIL)^[52] to process a comb-like bilayer all-polymer structure from the non-fullerene acceptor P(NDI2OD-T2) (Figure 2) and P3HT with exact control over spacing, dimensions and pattern of the

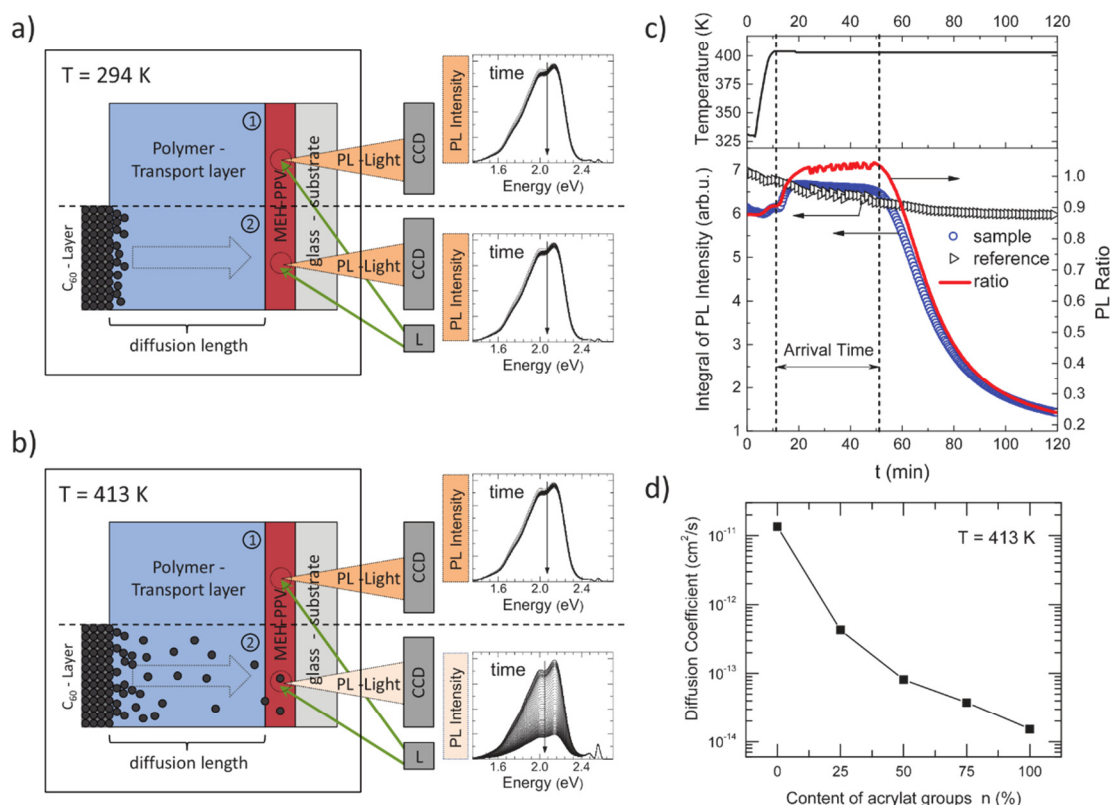


Figure 4. Illustration of the diffusion experiment from ref. [44]. a) In the reference cell (1) and the sample cell (2) the fluorescence of the sensor layer (MEH-PPV), excited by a laser-shutter unit (L-S), is recorded using a charge-coupled detector (CCD) camera. At 294 K the fluorescence is almost constant with time. b,c) After heating the sample to 413 K, C_{60} molecules diffuse leading to a decrease in the fluorescence of the sample cell at a certain time (blue circles). The corresponding kink is assigned to the arrival time of C_{60} in the sensor layer. The red solid line gives the temporal evolution of the sensor fluorescence in the sample cell (blue circles) normalized to that of the reference cell (black triangles). d) Diffusion coefficient of C_{60} as a function of the fraction of crosslinked polymer repeat units for PF2/6-A-x:y at 413 K. The structure formula of PF2/6-A-x:y is shown in Figure 2. Reproduced with permission.^[44] Copyright 2014, John Wiley Sons, Inc.

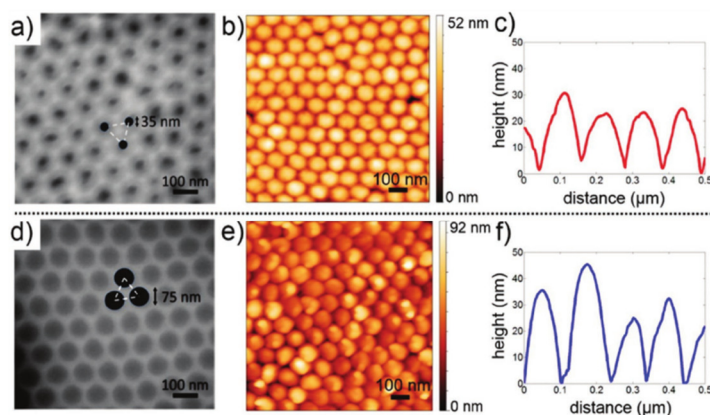


Figure 5. Comparison of nanoimprinting topographies with pore parameters of 35 nm (first row) and 75 nm (second row). The honeycomb lattice has a periodicity of 100 nm. a,d) SEM images of the master mold structures used in the NIL process. b,e) AFM height profiles of imprinted P(NDI2OD-T2) films. c,f) Exemplary AFM line sections. Adapted with permission.^[51b] Copyright 2014, American Chemical Society.

structure and therefore the resulting donor-acceptor interface (Figure 5). Photoinduced crosslinking of the P(NDI2OD-T2) layer was used to additionally stabilize the printed template and allow for the subsequent deposition of P3HT from solution. Schmidt-Mende and co-workers found that the enhanced harvesting of photoexcitations due to a larger interfacial area is outbalanced by increased polaron recombination losses. This results in efficiencies smaller than 1%. Consequently, morphology must be spatially and energetically optimized to achieve good efficiencies.

4. Conclusion and Outlook

One major problem concerned with OSCs is the lack of long-term stability. An important issue regarding the degradation in particular of BHJ solar cells is the diffusion of low molecular weight electron acceptors, for example fullerenes, followed by the formation of aggregates accompanied with a decrease in performance. In this article, crosslinking of the organic layers in OSCs is presented as a tool to overcome problems concerned with diffusion. According to the chosen synthetic strategy, crosslinking can take place within the donor polymer, between donor and acceptor, and within the acceptor. Until now, crosslinking the donor polymer is the most popular strategy. Nevertheless, the two other options will lead to an even stronger decrease in the diffusion of the acceptors and should be investigated intensively in the future. Different reactive groups such as bromine, vinyl, acrylate, azide, and oxetane have been used to crosslink OSC materials. As discussed in detail in Section 2, all reactive groups have certain advantages and disadvantages, for example with respect to their crosslinking ability in the presence of fullerenes. Consequently, up to now no final decision can be made as to which reactive unit is best suited to crosslink certain OSC materials. Here, some fundamental studies to clarify how the process of crosslinking influences the

basic properties of the crosslinked layers and finally the OSCs have already been carried out by several groups. Apart from comparing different functional groups concerning device stability, lifetime, and efficiency, such studies include investigations on the influence of crosslinking on the charge carrier mobility and on the diffusion coefficient of low molar mass electron acceptors in a crosslinked polymer matrix, including the effect of the resulting crosslink density on both charge carrier mobility and diffusion.

In the crosslinked materials mentioned above the reactive group is part of the low bandgap polymers or of a low molar mass molecule, normally the electron acceptor. An alternative concept uses external crosslinkers that are added to an existing low bandgap polymer and lead to crosslinking upon UV-irradiation or heating. The most popular materials from this class are bis-nitrenes.

For both crosslinkable polymers and low molar mass crosslinkers, the following design rules can be established. In general, it is important that crosslinking is carried out in a way that minimizes changes in the conjugated material. Therefore, the functional groups must be situated in the solubilizing spacer group or flexible low molar mass crosslinkers must be used. The chemistry of crosslinking has to be selective, meaning that crosslinking has to take place solely in the side chains and the conjugated system should not be affected. In the case that initiators are used, fragments of the initiating species remain in the polymer. By the choice of appropriate initiators, one has to make sure that these fragments do not negatively influence the material properties such as the charge carrier mobility. If possible, crosslinkable groups such as acrylates that can be crosslinked thermally or by UV-light without any initiator should be used.

Crosslinking of the active layer in BHJ solar cells has become rather popular and it has to be mentioned that unintentional crosslinking of PCDTBT/PCBM layers resulted in OSCs with the, to our knowledge, best long term stability.^[39a] Nevertheless, crosslinking can be used not only in BHJ solar cells but also to get crosslinked, insoluble layers of a single material, which are used as interlayers or to obtain multilayer OSCs by solution processing. This concept has been successfully used in the solution processing of OLEDs^[43] and, to our opinion, is a promising concept also in the field of OSCs.

Recently, crosslinking has been used for the stabilization of nanoscale polymer structures obtained by imprinting. Such small structures are prone to degradation and crosslinking seems to be a promising way to stable nanostructures.^[51b]

Acknowledgements

F.-J.K. and C.S. contributed equally to this work. Financial support by the Bavarian State Ministry of Science, Research, and the Arts through the Collaborative Research Network "Solar Technologies go Hybrid" and by the German Science Foundation DFG through the doctoral training center "GRK 1640" is acknowledged.

Conflict of Interest

The authors declare no conflict of interest.

Keywords

bulk heterojunctions, cross-linking, multilayer materials organic solar cells, stability

Received: February 3, 2017
Revised: February 27, 2017
Published online: May 23, 2017

- [1] a) H. Bente, D. Mori, H. Ohkita, S. Ito, *J. Mater. Chem. A* **2016**, *4*, 5340; b) J. W. Jung, J. W. Jo, E. H. Jung, W. H. Jo, *Org. Electron.* **2016**, *37*, 149.
- [2] H. Kang, G. Kim, J. Kim, S. Kwon, H. Kim, K. Lee, *Adv. Mater.* **2016**, *28*, 7821.
- [3] Y. Jin, Z. Chen, S. Dong, N. Zheng, L. Ying, X.-F. Jiang, F. Liu, F. Huang, Y. Cao, *Adv. Mater.* **2016**, *28*, 9811.
- [4] J. Huang, J. H. Carpenter, C. Z. Li, J. S. Yu, H. Ade, A. K. Y. Jen, *Adv. Mater.* **2016**, *28*, 967.
- [5] a) H. Q. Zhou, Y. Zhang, C. K. Mai, S. D. Collins, G. C. Bazan, T. Q. Nguyen, A. J. Heeger, *Adv. Mater.* **2015**, *27*, 1767; b) X. Z. Che, X. Xiao, J. D. Zimmerman, D. J. Fan, S. R. Forrest, *Adv. Energy Mater.* **2014**, *4*, 1400568.
- [6] heliatek, *Technical Data*, <http://www.heliatek.com/de/heliatekfilm/technische-daten> (accessed December 2016).
- [7] J. Weickert, R. B. Dunbar, H. C. Hesse, W. Wiedemann, L. Schmidt-Mende, *Adv. Mater.* **2011**, *23*, 1810.
- [8] Y. Yang, K. Mielczarek, A. Zakhidov, W. Hu, *ACS Appl. Mater. Interfaces* **2016**, *8*, 7300.
- [9] P. Cheng, X. W. Zhan, *Chem. Soc. Rev.* **2016**, *45*, 2544.
- [10] D. Yu, Y. Q. Yang, Z. Chen, Y. Tao, Y. F. Liu, *Opt. Commun.* **2016**, *362*, 43.
- [11] a) N. D. Treat, T. E. Mates, C. J. Hawker, E. J. Kramer, M. L. Chabiny, *Macromolecules* **2013**, *46*, 1002; b) N. D. Treat, M. A. Brady, G. Smith, M. F. Toney, E. J. Kramer, C. J. Hawker, M. L. Chabiny, *Adv. Energy Mater.* **2011**, *1*, 82; c) B. A. Collins, E. Gann, L. Guignard, X. He, C. R. McNeill, H. Ade, *J. Phys. Chem. Lett.* **2010**, *1*, 3160.
- [12] H. Kong, J. Sinha, D. Hoef, S. B. Kirschner, D. H. Reich, H. E. Katz, *Org. Electron.* **2013**, *14*, 703.
- [13] a) W. W. Li, A. Furlan, K. H. Hendriks, M. M. Wien, R. A. J. Janssen, *J. Am. Chem. Soc.* **2013**, *135*, 5529; b) A. Puetz, F. Steiner, J. Mescher, M. Reinhard, N. Christ, D. Kutsarov, H. Kalt, U. Lemmer, A. Colmann, *Org. Electron.* **2012**, *13*, 2696.
- [14] a) G. Wantz, L. Derue, O. Dautel, A. Rivaton, P. Hudhomme, C. Dagron-Lartigau, *Polym. Int.* **2014**, *63*, 1346; b) J. W. Rumer, I. McCulloch, *Mater. Today* **2015**, *18*, 425.
- [15] P. Knauer, T. Hahn, A. Köhler, P. Strohhriegl, *J. Mater. Chem. C* **2016**, *4*, 10347.
- [16] B. J. Kim, Y. Miyamoto, B. W. Ma, J. M. J. Fréchet, *Adv. Funct. Mater.* **2009**, *19*, 2273.
- [17] S. Miyayoshi, K. Tajima, K. Hashimoto, *Macromolecules* **2009**, *42*, 1610.
- [18] F. Ouhib, M. Tomassetti, J. Manca, F. Piersimoni, D. Spoltore, S. Bertho, H. Moons, R. Lazzaroni, S. Desbief, C. Jerome, C. Detrembleur, *Macromolecules* **2013**, *46*, 785.
- [19] H. J. Kim, A. R. Han, C. H. Cho, H. Kang, H. H. Cho, M. Y. Lee, J. M. J. Fréchet, J. H. Oh, B. J. Kim, *Chem. Mater.* **2012**, *24*, 215.
- [20] G. Brotas, J. Farinhas, Q. Ferreira, J. Morgado, A. Charas, *Synth. Met.* **2012**, *162*, 2052.
- [21] G. Griffini, J. D. Douglas, C. Pilego, T. W. Holcombe, S. Turri, J. M. J. Fréchet, J. L. Mynar, *Adv. Mater.* **2011**, *23*, 1660.
- [22] J. E. Carlé, B. Andreasen, T. Tromholt, M. V. Madsen, K. Norrman, M. Jorgensen, F. C. Krebs, *J. Mater. Chem.* **2012**, *22*, 24417.
- [23] a) D. P. Qian, Q. Xu, X. L. Hou, F. Z. Wang, J. J. Hou, Z. A. Tan, *J. Polym. Sci. Pol. Chem.* **2013**, *51*, 3123; b) K. Yao, L. Chen, T. Hu, Y. W. Chen, *Org. Electron.* **2012**, *13*, 1443.
- [24] C. J. Mueller, T. Klein, E. Gann, C. R. McNeill, M. Thelakkat, *Macromolecules* **2016**, *49*, 3749.
- [25] X. Chen, L. Chen, Y. W. Chen, *J. Polym. Sci. Pol. Chem.* **2013**, *51*, 4156.
- [26] T. T. T. Bui, S. Park, M. Jahandar, C. E. Song, S. K. Lee, J. C. Lee, S. J. Moon, W. S. Shin, *RSC Adv.* **2016**, *6*, 61284.
- [27] R. Q. Png, P. J. Chia, J. C. Tang, B. Liu, S. Sivaramakrishnan, M. Zhou, S. H. Khong, H. S. O. Chan, J. H. Burroughes, L. L. Chua, R. H. Friend, P. K. H. Ho, *Nat. Mater.* **2010**, *9*, 152.
- [28] Z. K. Tan, K. Johnson, Y. Vaynzof, A. A. Bakulin, L. L. Chua, P. K. H. Ho, R. H. Friend, *Adv. Mater.* **2013**, *25*, 4131.
- [29] C. Tao, M. Aljada, P. E. Shaw, K. H. Lee, H. Cavaye, M. N. Balfour, R. J. Borthwick, M. James, P. L. Burn, I. R. Gentle, P. Meredith, *Adv. Energy Mater.* **2013**, *3*, 105.
- [30] L. Derue, O. Dautel, A. Tournebize, M. Drees, H. L. Pan, S. Berthumeyrie, B. Pavageau, E. Cloutet, S. Chambon, L. Hirsch, A. Rivaton, P. Hudhomme, A. Facchetti, G. Wantz, *Adv. Mater.* **2014**, *26*, 5831.
- [31] J. W. Rumer, R. S. Ashraf, N. D. Eisenmenger, Z. G. Huang, I. Meager, C. B. Nielsen, B. C. Schroeder, M. L. Chabiny, I. McCulloch, *Adv. Energy Mater.* **2015**, *5*, 1401426.
- [32] C. P. Yau, S. Wang, N. D. Treat, Z. P. Fei, B. J. T. de Villers, M. L. Chabiny, M. Heaney, *Adv. Energy Mater.* **2015**, *5*, 1401228.
- [33] a) Y. Chen, K. C. Lin, *J. Polym. Sci. Pol. Chem.* **1999**, *37*, 2969; b) S. Chambon, A. Rivaton, J. L. Gardette, M. Firon, *Sol. Energy Mater. Sol. Cells* **2007**, *91*, 394; c) S. Chambon, A. Rivaton, J. L. Gardette, M. Firon, *Sol. Energy Mater. Sol. Cells* **2008**, *92*, 785; d) M. Manceau, S. Chambon, A. Rivaton, J. L. Gardette, S. Guillerez, N. Lemaître, *Sol. Energy Mater. Sol. Cells* **2010**, *94*, 1572.
- [34] X. Q. Chen, X. Yao, X. Xiang, L. Liang, W. Shao, F. G. Zhao, Z. Q. Lu, W. W. Wang, J. J. Lic, W. S. Li, *J. Mater. Chem. A* **2016**, *4*, 9286.
- [35] A. Charas, Q. Ferreira, J. Farinhas, M. Matos, L. Alcácer, J. Morgado, *Macromolecules* **2009**, *42*, 7903.
- [36] a) S. Feser, K. Meerholz, *Chem. Mater.* **2011**, *23*, 5001; b) F.-J. Kahle, I. Bauer, P. Strohhriegl, A. Köhler, *J. Polym. Sci. B Polym. Phys.* **2017**, *55*, 112.
- [37] a) B. Gholamkhash, S. Holdcroft, *Chem. Mater.* **2010**, *22*, 5371; b) C. Y. Nam, Y. Qin, Y. S. Park, H. Hlaing, X. H. Lu, B. M. Ocko, C. T. Black, R. B. Grubbs, *Macromolecules* **2012**, *45*, 2338.
- [38] A. Tournebize, A. Rivaton, J. L. Gardette, C. Lombard, B. Pépin-Donat, S. Beaupré, M. Leclerc, *Adv. Energy Mater.* **2014**, *4*, 1301530.
- [39] a) C. H. Peters, I. T. Sachs-Quintana, J. P. Kastrop, S. Beaupré, M. Leclerc, M. D. McGehee, *Adv. Energy Mater.* **2011**, *1*, 491; b) C. H. Peters, I. T. Sachs-Quintana, W. R. Mateker, T. Heumüller, J. Rivnay, R. Noriega, Z. M. Beiley, E. T. Hoke, A. Salleo, M. D. McGehee, *Adv. Mater.* **2012**, *24*, 663.
- [40] a) C. P. Chen, C. Y. Huang, S. C. Chuang, *Adv. Funct. Mater.* **2015**, *25*, 207; b) N. Deb, R. R. Dasari, K. Moudgil, J. L. Hernandez, S. R. Marder, Y. Sun, A. Karim, D. G. Bucknall, *J. Mater. Chem. A* **2015**, *3*, 21856; c) C. Z. Li, H. L. Yip, A. K. Y. Jen, *J. Mater. Chem.* **2012**, *22*, 4161; d) J. F. Nierengarten, S. Setayesh, *New J. Chem.* **2006**, *30*, 313; e) Y. J. Cheng, C. H. Hsieh, P. J. Li, C. S. Hsu, *Adv. Funct. Mater.* **2011**, *21*, 1723; f) M. Drees, H. Hoppe, C. Winder, H. Neugebauer, N. S. Sariciftci, W. Schwinger, F. Schaffler, C. Topf, M. C. Scharber, Z. G. Zhu, R. Gaudiana, *J. Mater. Chem.* **2005**, *15*, 5158.
- [41] C. B. Nielsen, S. Holliday, H. Y. Chen, S. J. Cryer, I. McCulloch, *Acc. Chem. Res.* **2015**, *48*, 2803.
- [42] a) Y. J. Cheng, F. Y. Cao, W. C. Lin, C. H. Chen, C. H. Hsieh, *Chem. Mater.* **2011**, *23*, 1512; b) W. W. Liang, C. Y. Chang, Y. Y. Lai,

- S. W. Cheng, H. H. Chang, Y. Y. Lai, Y. J. Cheng, C. L. Wang, C. S. Hsu, *Macromolecules* **2013**, *46*, 4781.
- [43] K. Meerholz, *Nature* **2005**, *437*, 327.
- [44] a) N. Cho, H. L. Yip, J. A. Davies, P. D. Kazarinoff, D. F. Zeigler, M. M. Durban, Y. Segawa, K. M. O'Malley, C. K. Luscombe, A. K. Y. Jen, *Adv. Energy Mater.* **2011**, *1*, 1148; b) C. E. Tsai, M. H. Liao, Y. L. Chen, S. W. Cheng, Y. Y. Lai, Y. J. Cheng, C. S. Hsu, *J. Mater. Chem. C* **2015**, *3*, 6158; c) T. Hahn, C. Saller, M. Weigl, I. Bauer, T. Unger, A. Köhler, P. Strohriegel, *Phys. Status Solidi A* **2015**, *212*, 2162; d) B. Meng, Z. Y. Xie, J. Liu, L. X. Wang, *Chem.-Asian J.* **2016**, *11*, 1218; e) Y. J. Cheng, C. H. Hsieh, Y. J. He, C. S. Hsu, Y. F. Li, *J. Am. Chem. Soc.* **2010**, *132*, 17381; f) C. H. Hsieh, Y. J. Cheng, P. J. Li, C. H. Chen, M. Dubosc, R. M. Liang, C. S. Hsu, *J. Am. Chem. Soc.* **2010**, *132*, 4887; g) Y. Sun, S. C. Chien, H. L. Yip, Y. Zhang, K. S. Chen, D. F. Zeigler, F. C. Chen, B. P. Lin, A. K. Y. Jen, *Chem. Mater.* **2011**, *23*, 5006; h) Q. Xu, F. Z. Wang, D. P. Qian, Z. A. Tan, L. J. Li, S. S. Li, X. H. Tu, G. Sun, X. L. Hou, J. H. Hou, Y. F. Li, *ACS Appl. Mater. Interfaces* **2013**, *5*, 6591; i) K. Zhang, C. M. Zhong, S. J. Liu, C. Mu, Z. K. Li, H. Yan, F. Huang, Y. Cao, *ACS Appl. Mater. Interfaces* **2014**, *6*, 10429; j) F. Fischer, T. Hahn, H. Bässler, I. Bauer, P. Strohriegel, A. Köhler, *Adv. Funct. Mater.* **2014**, *24*, 6172.
- [45] R. Meerheim, C. Körner, B. Oesen, K. Leo, *Appl. Phys. Lett.* **2016**, *108*, 103302.
- [46] J. Wang, K. Lin, K. Zhang, X. F. Jiang, K. Mahmood, L. Ying, F. Huang, Y. Cao, *Adv. Energy Mater.* **2016**, *6*, 1502563.
- [47] D. Chen, F. Liu, C. Wang, A. Nakahara, T. P. Russell, *Nano Lett.* **2011**, *11*, 2071.
- [48] a) P. K. Watkins, A. B. Walker, G. L. B. Verschoor, *Nano Lett.* **2005**, *5*, 1814; b) K. M. Coakley, M. D. McGehee, *Chem. Mater.* **2004**, *16*, 4533.
- [49] a) E. Scheler, P. Strohriegel, *J. Mater. Chem.* **2009**, *19*, 3207; b) E. Scheler, P. Strohriegel, *Chem. Mater.* **2010**, *22*, 1410.
- [50] a) B. Liu, R. Q. Png, L. H. Zhao, L. L. Chua, R. H. Friend, P. K. H. Ho, *Nat. Commun.* **2012**, *3*, 1321; b) J. Farinhas, Q. Ferreira, R. E. Di Paolo, L. Alcacer, J. Morgado, A. Charas, *J. Mater. Chem.* **2011**, *21*, 12511.
- [51] a) H. C. Hesse, D. Lembke, L. Dossel, X. Feng, K. Müllen, L. Schmidt-Mende, *Nanotechnology* **2011**, *22*, 055303; b) T. Pfadler, M. Coric, C. M. Palumbiny, A. C. Jakowetz, K. P. Strunk, J. A. Dorman, P. Ehrenreich, C. Wang, A. Hexemer, R. Q. Png, P. K. H. Ho, P. Müller-Buschbaum, J. Weickert, L. Schmidt-Mende, *ACS Nano* **2014**, *8*, 12397; c) C. Y. Chang, C. E. Wu, S. Y. Chen, C. H. Cui, Y. J. Cheng, C. S. Hsu, Y. L. Wang, Y. F. Li, *Angew. Chem. Int. Ed.* **2011**, *50*, 9386; d) X. M. He, F. Gao, G. L. Tu, D. Hasko, S. Hüttner, U. Steiner, N. C. Greenham, R. H. Friend, W. T. S. Huck, *Nano Lett.* **2010**, *10*, 1302; e) N. Haberkorn, J. S. Gutmann, P. Theato, *ACS Nano* **2009**, *3*, 1415; f) R. Bai, M. Ouyang, R. J. Zhou, M. M. Shi, M. Wang, H. Z. Chen, *Nanotechnology* **2008**, *19*, 055604.
- [52] L. J. Guo, *Adv. Mater.* **2007**, *19*, 495.

List of publications

- 1) Tobias Hahn, Christina Saller, Marlene Weigl, Irene Bauer, Thomas Unger, Anna Köhler, Peter Strohriegl
Organic solar cells with crosslinked exciton blocking layer
Physica Status Solidi A, **2015**, 212, 2162-2168
doi: 10.1002/pssa.201532040
- 2) Tobias Hahn, Steffen Tscheuschner, Christina Saller, Peter Strohriegl, Puttaraju Boregowda, Tushita Mukhopadhyay, Satish Patil, Dieter Neher, Heinz Bäessler, Anna Köhler
Role of intrinsic photogeneration in single layer and bilayer solar cells with C₆₀ and PCBM
The Journal of Physical Chemistry C **2016**, 120, 25083-25091
doi: 10.1021/acs.jpcc.6b08471
- 3) Tobias Hahn, Steffen Tscheuschner, Frank-Julian Kahle, Markus Reichenberger, Stavros Athanasopoulos, Christina Saller, Guillermo C. Bazan, Thuc-Quyen Nguyen, Peter Strohriegl, Heinz Bäessler, Anna Köhler
Monomolecular and bimolecular recombination of electron-hole pairs at the interface of a bilayer organic solar cell
Advanced Functional Materials **2017**, 12, 1604906
doi: 10.1002/adfm.201604906
- 4) Christina Saller, Frank-Julian Kahle, Thomas Müller, Tobias Hahn, Steffen Tscheuschner, Denys Priadko, Peter Strohriegl, Heinz Bäessler, Anna Köhler
Facile method for the investigation of temperature-dependant C₆₀ diffusion in conjugated polymers
ACS Applied Materials & Interfaces **2018**, doi: 10.1021/acsami.8b05520
doi: 10.1021/acsami.8b05520
- 5) Peter Strohriegl, Philipp Knauer, Christina Saller, Esther Scheler
Patternable conjugated polymers for organic solar cells
Proceedings of SPIE 8830, Organic Photovoltaics XIV, **2013**, 88300P
doi: 10.1117/12.2023899
- 6) Peter Strohriegl, Christina Saller, Philipp Knauer, Anna Köhler, Tobias Hahn, Florian Fischer, Frank-Julian Kahle
Crosslinkable low bandgap polymers for organic solar cells
Proceedings of SPIE 9942, Organic Photovoltaics XVII, **2016**, 994200
doi: 10.1117/12.2239400

- 7) Frank-Julian Kahle, Christina Saller, Anna Köhler, Peter Strohrigl
Crosslinked semiconductor polymers for photovoltaic applications
Advanced Energy Materials **2017** 7, 1700306
doi: 10.1002/aenm.201700306

Danksagung

An dieser Stelle möchte ich meinen Dank all denjenigen widmen, die auf verschiedenste Art und Weise zur Entstehung dieser Doktorarbeit beigetragen haben und ohne die diese Arbeit nicht möglich gewesen wäre.

Allen voran möchte ich Prof. Dr. Peter Strohrriegl für die Betreuung meiner Promotion und die Bereitstellung dieses interessanten und anwendungsbezogenen Themas danken. Besonders bedanke ich mich für Ihr stets offenes Ohr und die jederzeitige Hilfsbereitschaft. Herzlichen Dank möchte ich auch für die Möglichkeit der Teilnahme an internationalen Konferenzen mit eigenem Beitrag aussprechen, was eine große Bereicherung für meine Arbeit war.

Bei Prof. Dr. Hans-Werner Schmidt möchte ich mich für die Bereitstellung eines gut ausgestatteten Laborplatzes bedanken.

Dem Graduiertenkolleg 1640 „Photophysik synthetischer und biologischer multichromophorer Systeme“, dem bayerischen Verbundprojekt „Solar Technologies go Hybrid“ sowie der Graduate School der Universität Bayreuth danke ich für die finanzielle Unterstützung und die zahlreichen Seminare zu unterschiedlichsten Themen. Dankeschön auch an alle Mitglieder des Graduiertenkollegs 1640. Die interdisziplinäre Zusammenarbeit während meiner Promotion sorgte stets für einen Blick über den Tellerrand.

Vielen Dank an Prof. Dr. Mukundan Thelakkat für seine Tätigkeit als Mentor im Rahmen des Graduiertenkollegs 1640.

Herzlich bedanken möchte ich mich bei Prof. Dr. Anna Köhler vom Lehrstuhl Experimentalphysik II für die erfolgreiche Zusammenarbeit zwischen Chemie und Physik, die lehrreichen Diskussionen sowie die Unterstützung als Mentor. Mein Dank gilt auch Prof. Dr. Heinz Bässler für seine Hilfe bei der Interpretation der Ergebnisse.

Bei Tobias Hahn, Steffen Tscheuschner und Julian Kahle bedanke ich mich für die gelungene Kooperation bei unseren gemeinsamen Projekten. Vielen Dank für die hilfreichen Ideen, die unzähligen Messungen, den fachlichen Austausch und euren unermüdlichen Einsatz zu allen Tages- und Nachtzeiten – die Arbeit mit euch hat sehr viel Spaß gemacht. Julian danke ich für das Korrekturlesen dieser Arbeit. Danke an die gesamte Arbeitsgruppe für die vielfältige Hilfe und hilfreichen Gespräche. Für die Herstellung der vielen Solarzellensubstrate, die Hilfe beim Plasmaätzen und Aufdampfen und allen weiteren Arbeiten im Physikkeller möchte ich mich besonders bei Irene Bauer und Frank Schirmer bedanken.

Ein ganz großes Dankeschön geht an meine Laborkollegen aus 595, Dr. Andreas Ringk, Dr. Daniel Wagner, Dr. Philipp Knauer, Julia Wollmann und Irene Bauer. Ganz lieben Dank für die tolle Zusammenarbeit, die angenehme Atmosphäre, eure Hilfe im Laboralltag, den netten Austausch auch abseits der Chemie und die vielen aufmunternden Worte, wenn die Synthesen mal wieder nicht funktionieren wollten – es war eine tolle Zeit mit euch. Danke an Daniel und Julia für das

Korrekturlesen dieser Arbeit. Julia möchte ich besonders danken für die jederzeitige Hilfsbereitschaft, die vielen Gespräche und die lustigen Stunden im Labor. Irene, herzlichen Dank für deine Unterstützung bei allen kleineren und größeren Problemen und deine unermüdliche Hilfe bei den unzähligen Synthesen.

Vielen Dank an meine Praktikanten Minde Jin, Julia Wollmann, Andreas Rösch und Kevin Winter für die tatkräftige Mithilfe im Labor und der Charakterisierung. Einen besonderen Dank möchte ich hier an Sonja Dziejwior aussprechen, die mich während ihrer Bachelorarbeit und diverser Praktika immer engagiert bei den Synthesen unterstützt hat.

Weiterhin geht mein Dank an alle Mitarbeiter des Lehrstuhls Makromolekulare Chemie I für die gute Arbeitsatmosphäre, Unterstützung und jederzeitige Diskussionsbereitschaft. Bei Dr. Anne Neubig, Dr. Andreas Bernet und Dr. Christian David Heinrich möchte ich mich für ihre produktiven Ratschläge bei vielfältigen Syntheseproblemen bedanken. Danke an die Gerätebetreuer und Techniker für ihre stete Hilfsbereitschaft. Dr. Katharina Neumann, Dr. Klaus Kreger, Paul Reichstein, Tina Weller und Philip Schmode danke ich für die Messungen meiner GPC-Proben. Für die MALDI-Messungen möchte ich mich bei Alexander Krimalowski bedanken. Besonderer Dank gilt meinen Kollegen vom NMR-Team, Dr. Andreas Haedler, Christian Bartz, Jannik Mechau und Markus Drummer, mit denen ich viele Stunden am NMR-Gerät verbracht habe. Dankeschön auch an Alexander Kern und Jonas Mayer für die Hilfestellung bei technischen Angelegenheiten.

Für die großartige Unterstützung bei sämtlichen organisatorischen Themen bedanke ich mich herzlich bei Petra Weiß, Christina Wunderlich und Claudia Geier.

An meine Freunde daheim geht ebenfalls ein riesiges Dankeschön für den Beistand während meiner Zeit in Bayreuth. Danke, dass ihr mich unterstützt, motiviert und aufgeheitert habt sowie für die notwendige Ablenkung und den Ausgleich zur Arbeit gesorgt habt. Dank euch hat es auch andere Themen als die Chemie gegeben und ihr habt mich auch in stressigen Momenten auf andere Gedanken gebracht. Ihr seid immer für mich da gewesen, auch wenn ich oft wenig Zeit hatte – ganz lieben Dank dafür.

Der größte Dank gebührt meiner Familie, die mir immer bedingungslos den Rücken gestärkt und an mich geglaubt hat. Ganz lieben Dank an meine Eltern Brigitte und Wolfgang, meinen Bruder Reinhard sowie meine Oma Anni – ohne euch wäre dies alles nicht möglich gewesen. Herzlichen Dank auch an Regina und Werner für die Unterstützung. Ganz besonders möchte ich Sven für sein Verständnis, seine Geduld, sowie den unermüdlichen Beistand und den grenzenlosen Rückhalt in den letzten Jahren danken. Danke, dass du immer für mich da bist.

Danke!

Erklärung

nach der Promotionsordnung der Bayreuther Graduiertenschule für Mathematik und Naturwissenschaften (BayNAT) vom 15.09.2017

(§ 9 S. 2 Nr. 3)

Hiermit versichere ich an Eides statt, dass ich die vorliegende Arbeit selbstständig verfasst und keine anderen als die von mir angegebenen Quellen und Hilfsmittel verwendet habe. Ich habe die Dissertation nicht bereits zur Erlangung eines akademischen Grades eingereicht und habe nicht bereits diese oder eine gleichartige Doktorprüfung endgültig nicht bestanden.

(§ 9 S. 2 Nr. 4)

Hiermit erkläre ich, dass ich die Hilfe von gewerblichen Promotionsberatern bzw. -vermittlern oder ähnlichen Dienstleistern weder bisher in Anspruch genommen habe noch künftig in Anspruch nehmen werde.

(§ 9 S. 2 Nr. 7)

Hiermit erkläre ich mich einverstanden, dass die elektronische Fassung meiner Dissertation unter Wahrung meiner Urheberrechte und des Datenschutzes einer gesonderten Überprüfung unterzogen werden kann.

(§ 9 S. 2 Nr. 8)

Hiermit erkläre ich mich einverstanden, dass bei Verdacht wissenschaftlichen Fehlverhaltens Ermittlungen durch universitätsinterne Organe der wissenschaftlichen Selbstkontrolle stattfinden können.

Bayreuth, den 27.06.2018

Christina Saller